XI ICOLD BENCHMARK WORKSHOP ON NUMERICAL ANALYSIS OF DAMS

Valencia, October 20-21, 2011

THEME A

Effect of concrete swelling on the equilibrium and displacements of an arch dam

FORMULATION

Dr Christine Noret

Mr Xavier Molin

CONTACT
Coyne et Bellier – Tractebel Engineering, rue du 19 mars 1962, 92622 Gennevilliers Cedex, France

1. Objective of the Problem

During the last ICOLD Congress in Brasilia, a common meeting between the technical committee on concrete and the technical committee on numerical methods for dams took place, during which the attention was called upon consequences of AAR on the structural behaviour of hyperstatic structures, and the question was raised on how to evaluate the different existing methods and software which have the ability to consider concrete swelling. The question was again put on the table at a workshop held in Gennevilliers in September 2009, just before the 10th ICOLD Benchmark Workshop on numerical methods of analysis of dams.

The numerical problem now proposed in the frame of Theme A of the 11th Benchmark Workshop is very representative of those raised to engineers by swelling due to AAR. The example selected is that of Kariba dam, a large arch dam built on the Zambezi River between Zambia and Zimbabwe in the late fifties, which has shown evident signs of swelling soon after the starting of its operation. Thanks to the careful and efficient surveillance made along years by the Zambezi River Authority who operates the dam, thanks also to the progressive implementation of additional instruments, the specific behavior of the structure could be monitored, modeled and interpreted, which allows today to conclude that in spite of this swelling process, the dam behaves well as a whole and remains safe.

Photo 1: Kariba dam on Zambezi River

A very specific feature to Kariba dam case is the apparently strong anisotropy which exists between vertical and horizontal swelling rates, well reported by measurements of horizontal (topographic and pendulums) movements on one side, leveling measurements on the other. This has been interpreted as being due to the stress dependence of the swelling process, since major stresses are mainly developed in the direction of horizontal arches, while vertical stresses are only due to the dead weight and therefore much smaller.

The exercise proposed to participants to the 11th Benchmark Workshop consists in determining the adequate swelling law and parameters which allow the best identification with both horizontal and vertical movements of the dam vs time. Water level and monitoring results will be provided during the 1963-1995 period to allow this identification, then only water level will be given to allow the prediction of further movements during the 1995-2010 period of time.

Participants are free to select the more or less sophisticated swelling law they will use for the exercise.

In order to keep the exercise within reasonable limits of difficulty, some strong simplifications have been adopted, especially in

- the construction, joint grouting and impounding sequence,
- the thermal effects, made negligible by adequate selection of monitoring readings.

Additionally participants are strongly encouraged to adopt a simplified reservoir level curve with several successive periods during which the water level will be supposed constant.

2. General Information

2.1. KARIBA arch dam

The Kariba dam is a long double curvature arch dam built across the Zambezi River between 1956 and 1959. It creates the World's largest artificial lake (181 km^3).

The dam shape is shown on photos 1 and 2 and its crown section is presented in Figure 1.

The leading features of the dam are:

- Structural height above foundation (H) 128 m
- Developed crest length (L) 617 m
- Length/height ratio (L/H) 4.8
- Crest thickness 13 m
- Total concrete volume, approx. 1 million m^3

Photo 2: Kariba dam from Right Bank

The temperature at site has only small variations through the year around 27°C.

The foundation rock is excellent gneiss on the left bank and in the river channel. The top of the right bank is affected by mica seams and jointed quartzite overlying a more weathered gneiss. These poor rock conditions led, at the end of the construction period, to add a gravity thrust block, and to reinforce the foundation with four concrete underground buttresses penetrating the weathered/altered material and transmitting the dam thrust to the underlying sound gneiss. As a result of this treatment, the foundation rigidity can be considered uniform.

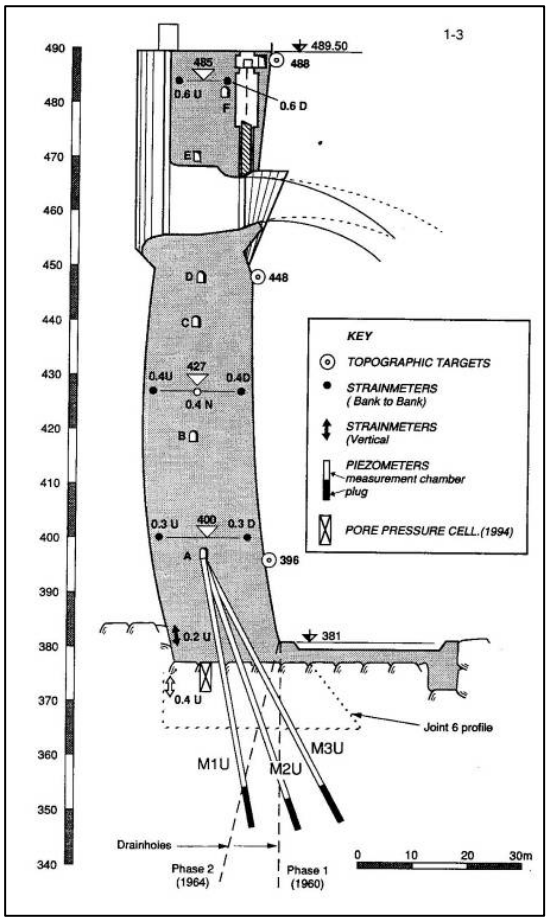

Figure 1: Kariba dam crown cantilever

2.2. History of construction and operation of the dam

The history of reservoir level is shown on Figure 2. More on the very interesting history of Kariba dam can be found in Appendix 1 and in many papers listed in the bibliography at the end of this document.

The dam has been built between 1957 and mid-1959, with 41 independent blocks, each approx. 14 m wide. Vertical contraction joints between adjacent blocks have been cement grouted in 1959-1960, at a time when the average concrete temperature can be considered equal to 25°C. The impoundment of the lake started in early 1959 and was completed in late 1963.

For the purpose of the exercise, it will be supposed that the dam concrete blocks have been erected first, then the contraction joints have been grouted, then the impounding of the reservoir started, all at a uniform and constant temperature of 27°C.

During the 1963-1994 operation period, the fluctuations of the reservoir level are generally limited, mainly due to the exceptional size of the reservoir. One can identify 3 successive periods:

(1) 1963-73: high level (average 483.80),
(2) 1974-81: very high (average 486.10),
(3) 1982-94: low level (average 479.90)

From 1995 (which will be the start of the prediction period of the exercise), the water level has been substantially more variable.

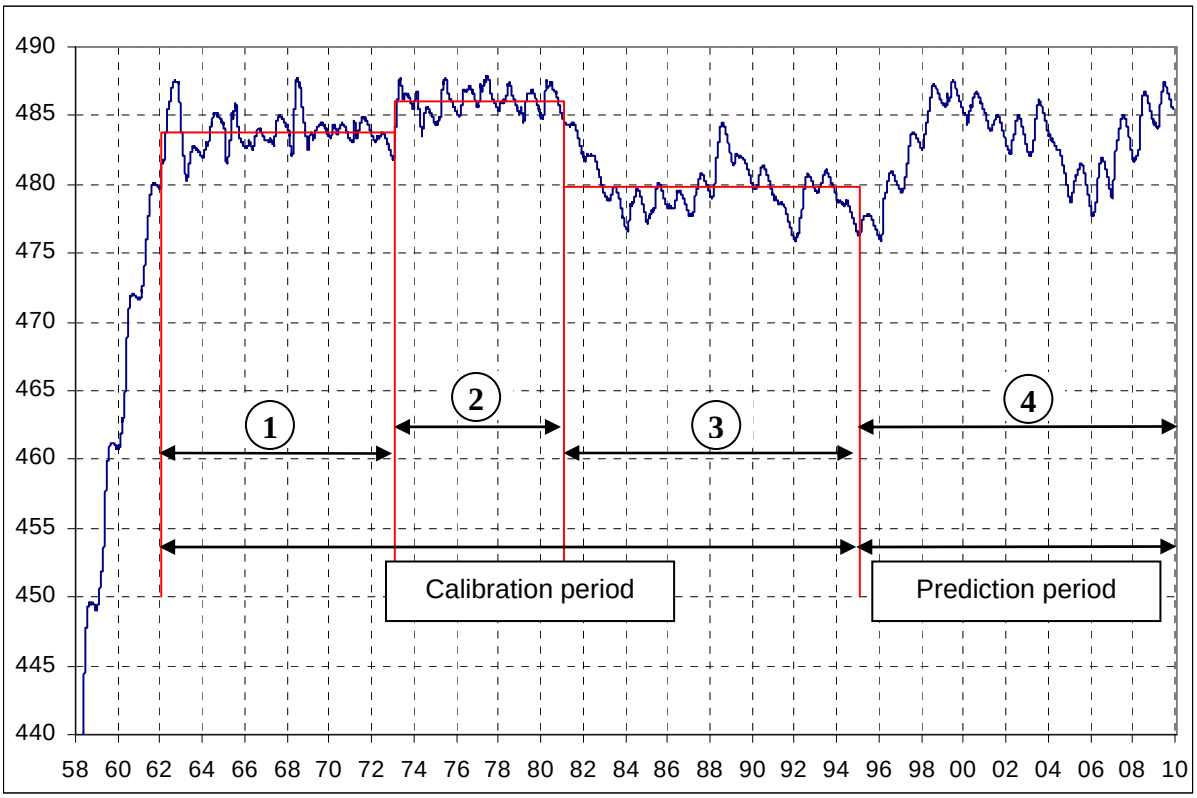

Figure 2: History of Kariba dam lake level

2.3. Monitoring system of the dam

The monitoring system for the dam and foundation is described in detail in Santa Clara (ICOLD, 1985, Q 56 R 54) and Goguel & Mpala (WPDC, June 1992). The initial monitoring system was based on topographic survey of a number of targets placed on the dam downstream face, and vibrating wire extensometers embedded into the dam concrete, combined with the "special test" (see next section).

The monitoring system of the dam has been progressively complemented, especially as regards movements: 6 lines of pendulums, and precise leveling along inspection galleries have been installed and measured from 1989.

The location of the main instruments is shown on Figure 3.

For the purpose of the exercise, only those instruments readings which are clearly related to the swelling phenomenon are provided, and data have been substantially summarized, with only one carefully selected value being given each year.

2.4. Swelling of the dam concrete

From the beginning, the dam monitoring system incorporated a "special test" system, which consisted in a set of correction vibrating wire sensors which allowed, in principle, correct determination of stresses inside the dam, with correction from thermal, creep effects and others. This specific device indeed indicated very soon that something unusual was happening, namely a discrepancy between measured stresses and deformations, which strongly deviated from elasticity. This phenomenon was identified in the eighties as being due to AAR expansion.

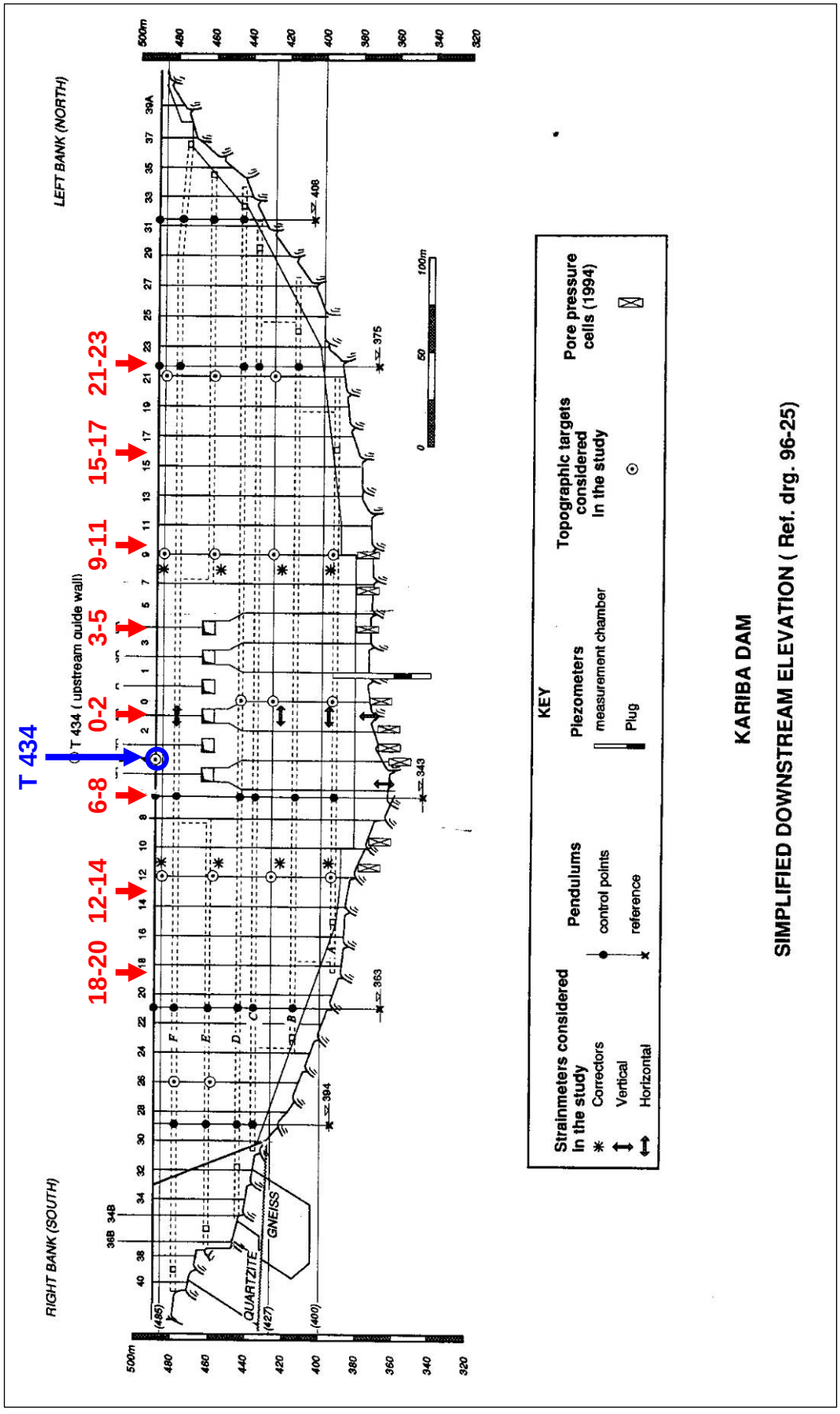

Figure 3: Developed elevation and location of the main instruments

Careful long-term laboratory tests had been already carried out in the seventies, which made the demonstration, as soon as 1975 that a relationship does exist between the local stress tensor and the anisotropic swelling rate tensor. Long-term monitoring of horizontal and vertical movements of the dam confirms that swelling inside the dam body is neither uniform nor isotropic.

3. Data provided to participants

3.1. Dam geometry and model mesh

Details of the dam shape are provided in Appendix 2.
Two meshes of the dam and its foundation are provided to participants in the files named BW11A_Model1.mesh and BW11A_Model2.mesh included in the Theme 11A package. The meshes only differ by the modelling of the arch/foundation contact with or without joint elements. The files format is detailed in Appendix 3. This global mesh and the cross section of the key block are shown on Figure 4.

Intentionally the proposed mesh does not incorporate the spillway structure, which does not influence the overall deformation of the arch and only affects local reactions.

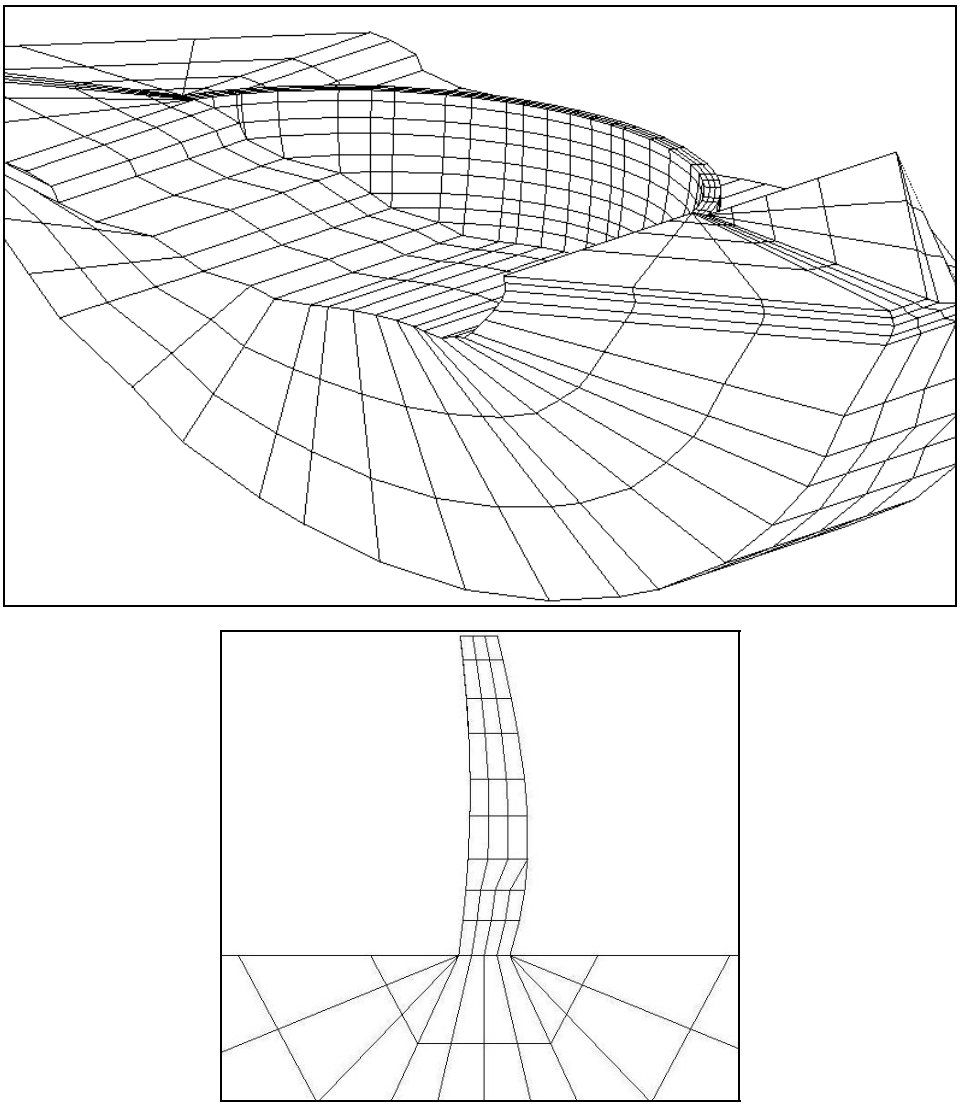

Figure 4: Proposed mesh for Kariba dam

3.2. Mechanical properties of materials

For the exercise, the materials mechanical properties shall be taken as follows:

Property	Material Unit	Foundation rock	Dam concrete
Modulus of elasticity	GPa	10.0	22.0
Poisson's ratio	/	0.2	0.20
Unit weight	kN/m^3	*Not considered*	2350
Swelling properties		*Not considered*	**To be determined**

Table 1: Properties of materials

3.3. Construction and operation of the dam

The dam construction shall be supposed to be built with independent cantilevers and joint grouted at the end of concreting, at a uniform temperature equal to the average ambient air temperature. The dam will be considered completed and ready for loading on April 30, 1959.

Impounding and operation of the dam between 1959 and 2010 will be as shown on Figure 5 and detailed in the file BW11A_Monitoring_data.XLS, sheet 'Data', column C.

The yearly average temperature at site is 27°C, and seasonal variations are very low. Considering that the temperature of the dam concrete at the time of joint grouting was close to this nearly constant value, and since the problem to be analyzed is a long-term one, all thermal effects are to be neglected for the present exercise.

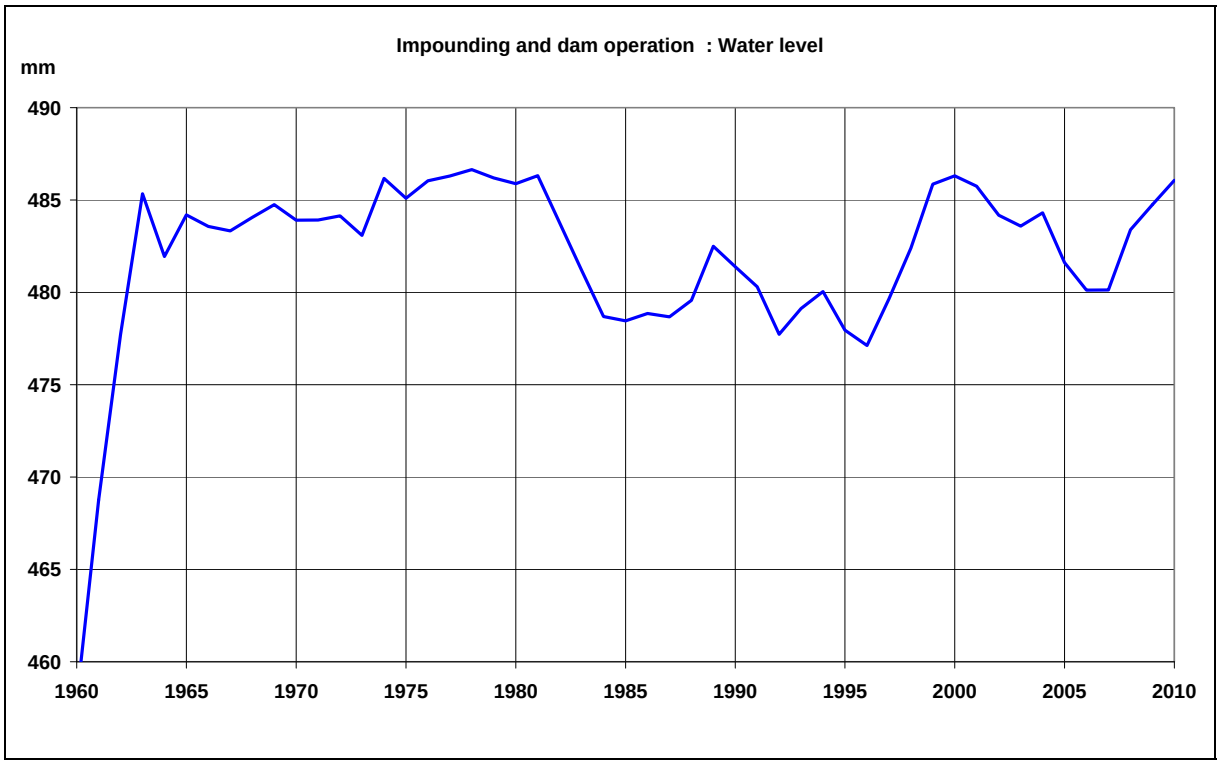

Figure 5: Water level during impounding and operation of the reservoir

3.4. Results of monitoring

The location of instruments whose readings are to be used is shown on Figure 3. The correspondence with the specific nodes of the model mesh is also indicated below.

3.4.1. Radial displacements from topographical survey

Target T434 is located on the dam crest at the crown cantilever. It corresponds to node n° 3127 and n° 3275 of the proposed meshes N°1 and 2 respectively. Its movements are supposed not to be influenced by the neighborhood of the spillway structure.

Readings of target T434 are given in the data file BW11A_Monitoring_data.XLS, sheet 'Data', column E.

Figure 6 shows the variations of the radial displacements vs time.

It should be noticed that the zero value of this series of readings cannot be considered reliable, therefore it cannot be used for calibration during the first impounding.

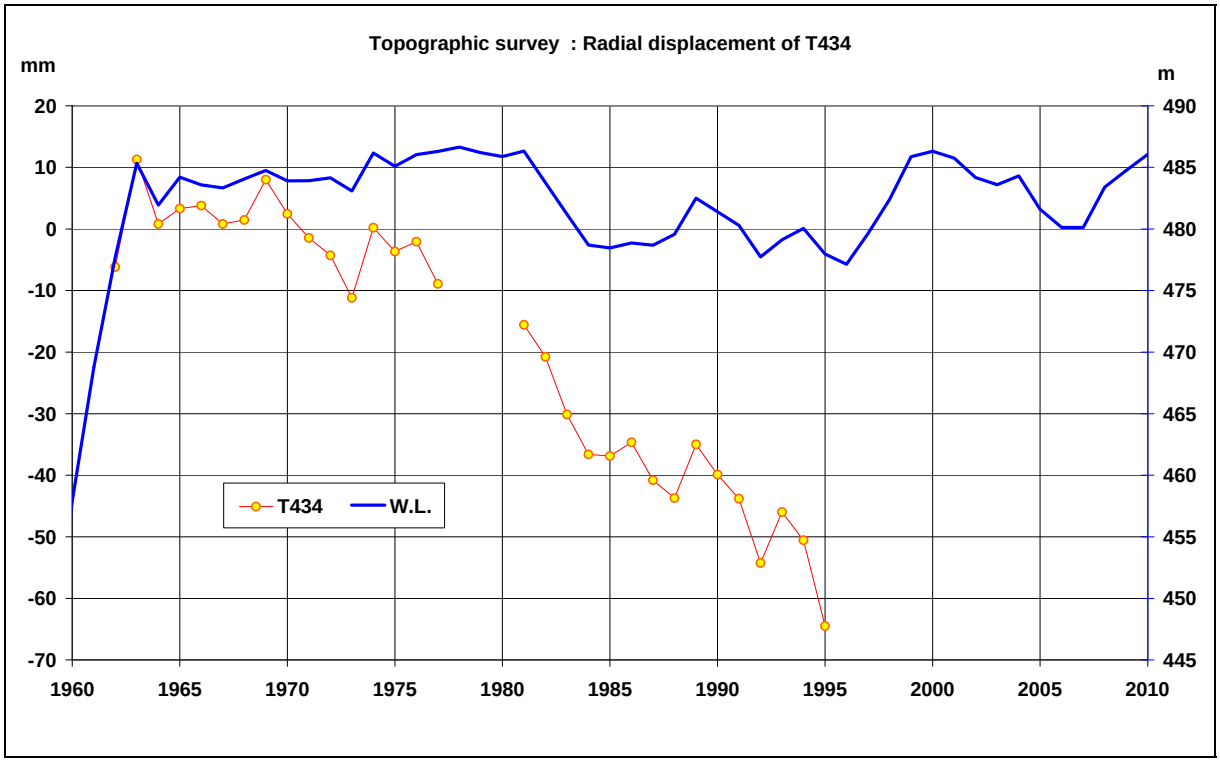

Figure 6: Radial displacements at crest of crown cantilever (target 434)

3.4.2. Dam crest leveling survey

Eight points along the dam crest have been selected. Table 2 below provides their name and their corresponding nodes of the proposed mesh, from right to left bank.

Readings of these points are given in the data file BW11A_Monitoring_data.XLS, sheet 'Data', columns G to N. Figure 7 shows their variations vs time, and Figure 8 shows their spatial distribution at several instants.

On this Figure 8, it can be noticed that the elevation rate at points n°0-2 and 3-5 is appreciably higher than their neighbors. This fact can be interpreted as being due to the presence of the spillway in the upper part of the corresponding dam blocks, through the many openings and the increased surface

of contact between concrete and water. It may therefore be wise to discard or at least put less weight on the corresponding readings, which do not represent the whole dam structure movement.

Target name	Dam block n°	Reference point	Mesh node n° Model1.mesh	Mesh node n° Model2.mesh
18-20	20	R14	1735	1822
12-14	14	R15	2135	2241
6-8	6	R16	2706	2835
0-2	0	R17	3366	3523
3-5	5	R18	4026	4211
9-11	11	R19	4686	4899
15-17	17	R20	5105	5337
21-23	23	R21	5416	5662

Table 2: Crest leveling control points and mesh nodes

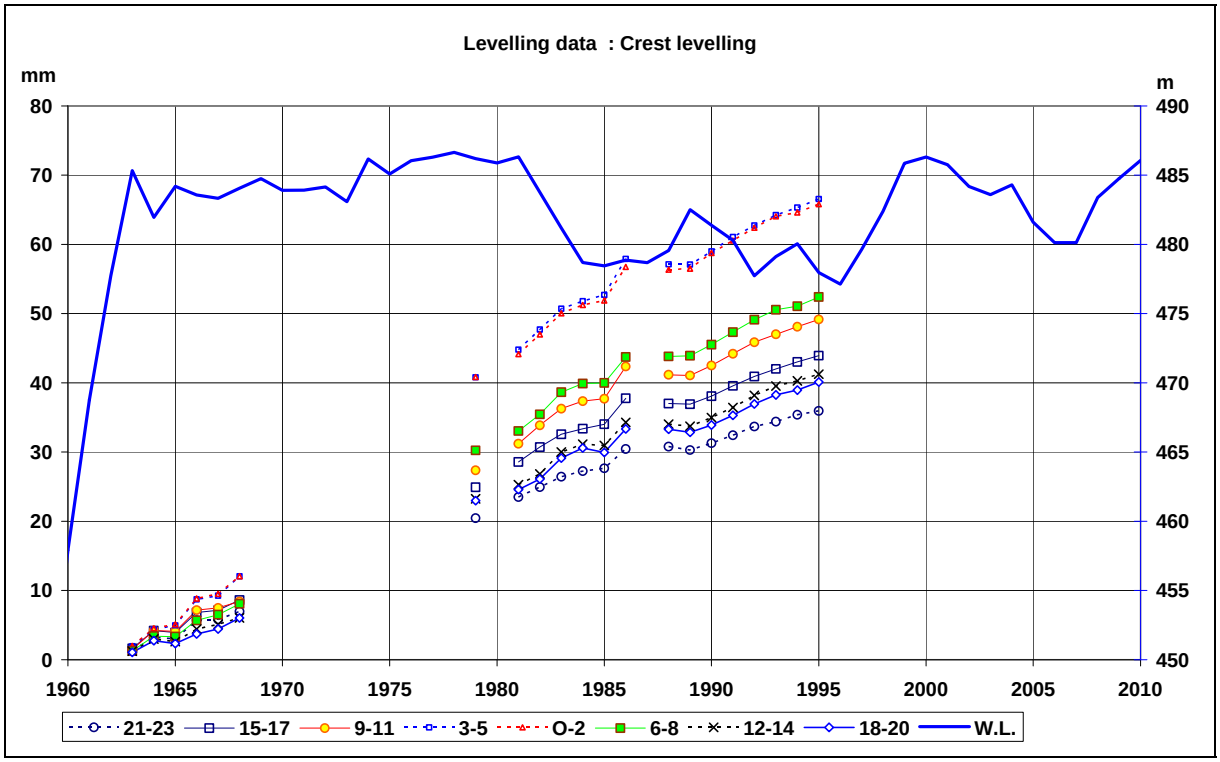

Figure 7: Vertical displacements at crest level vs time

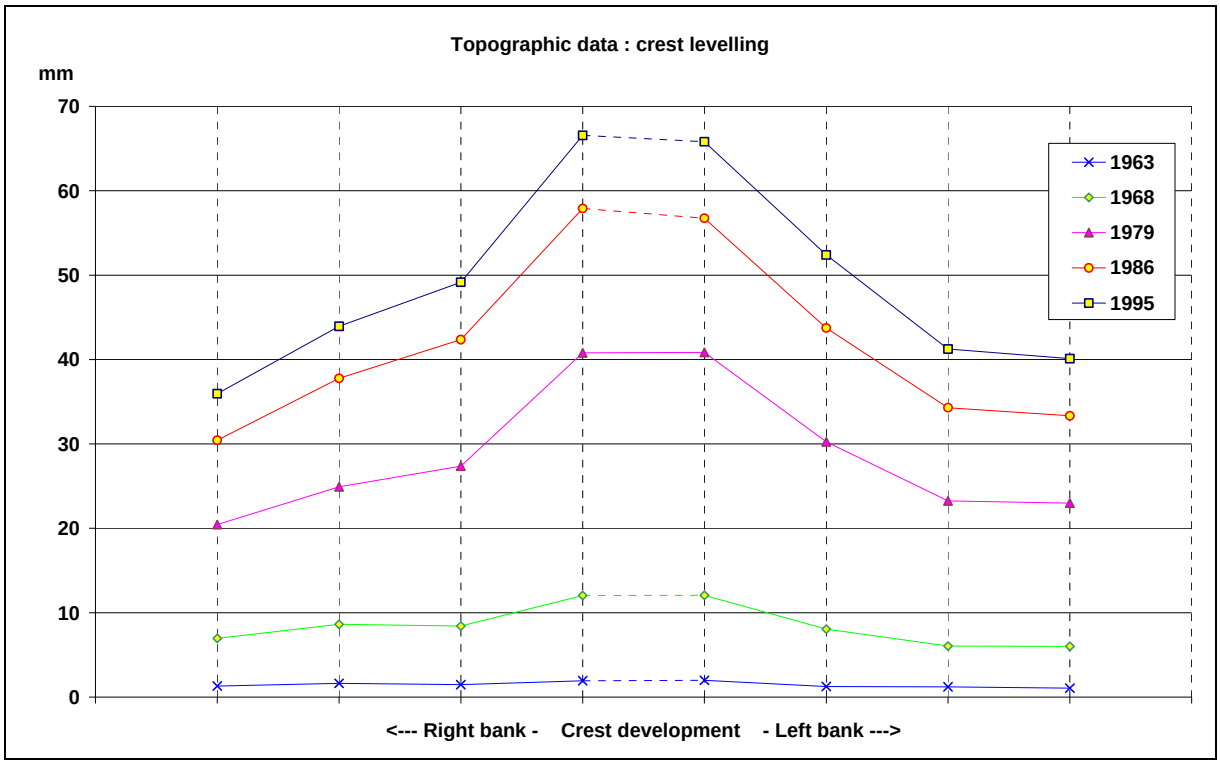

Figure 8: Distribution of vertical displacements at crest

4. Steps of the exercise

The exercise is divided into 3 successive steps.

4.1. Step 1: Reference conditions

The purpose of this initial step is to provide the response of the dam structure in normal conditions, i.e. without any swelling effect. This will be used to detect possible discrepancies between different solutions, independently from the swelling modelization. It will also provide participants with an early check of their model.

1A: Calculation of the stress field at the end of construction (displacements omitted), with the assumption of independent cantilevers and joint grouting in thermal equilibrium.

1B: Calculation of the stress and displacements fields considering a reservoir level equal to 483.80 (this is the average water level during the initial high level period 1963-1973).

1C: Calculation of the stress and displacements fields considering a reservoir level equal to 486.10 (this is the water level average during the intermediate very high level period 1974-1981).

1D: Calculation of the stress and displacements fields considering a reservoir level equal to 479.90 (this is the average water level during the last low level period 1982-94).

4.2. Step 2: Swelling during the period 1960-1994

This step is devoted to the calibration of the swelling law and parameters which allow the best identification of the drift shown by monitoring of both vertical and radial movements during the 1963-94 period.

Participants are free to use their preferred swelling model and they should adjust its parameters as required to meet the trends shown by the monitoring.

In order to keep the exercise within reasonable limits of difficulty, it is suggested to use a simplified reservoir level curve Vs time, by assuming 3 successive periods during which the water level remains constant, as shown on Figure 2.

A more drastic simplification, possible but not recommended, could be to consider that the reservoir level remains constant (at the average value of 482.70) during the whole calibration period.

4.3. Step 3: Swelling during the period 1995-2010

Using the same swelling model as in previous step, with parameters calibrated during this step, participants shall determine the stress and displacements fields predicted at the end of the prediction period, i.e. on April 30, 2010 with the water level being at El. 486.06.

5. Results required from participants

5.1. Presentation of the solution

The participant shall describe his solution in a paper which will not exceed 15 pages. The paper shall contain at least the following elements:

- Name, title, organization and coordinates of participant(s),
- Name and version of the software used,
- Characteristics of the model (conform or not to the one provided): type of elements, and any special feature added,
- Method used for the initial load inside the dam (block construction and joint grouting),
- Modelization of the hydraulic loads,
- Presentation of the concrete swelling law with details on the required parameters,
- All details needed to explain how the calibration has been carried out.

5.2. Detailed results

Each participant shall provide the results of his analyses in a single file named BW11A_Solution_XXXXXX.XLS, derived from the file included in the Theme 11A package, where XXXXXX will be replaced by the name of the participant.

Results of displacements are to be given at 22 reference points given in Table 3.

Point	Location	Elevation	Nodes model1.mesh	Nodes model2.mesh
R1	Block 20	488	1256	1322
R2	Block 20	480	1267	1333
R3	Block 20	463	1283	1349
R4	Block 20	438	1300	1366
R5	Block 20	418	1316	1382
R6	Block 0	480	2806	2940
R7	Block 0	438	2839	2973
R8	Block 0	418	2855	2989
R9	Block 19	488	5416	5662
R10	Block 19	480	5427	5673
R11	Block 19	463	5443	5689
R12	Block 19	438	5460	5706
R13	Block 19	418	5476	5722
R14	Crest Block 20	489	1735	1822
R15	Crest Block 14	489	2135	2241
R16	Crest Block 6	489	2706	2835
R17	Crest Block 0	489	3366	3523
R18	Crest Block 5	489	4026	4211
R19	Crest Block 11	489	4686	4899
R20	Crest Block 17	489	5105	5337
R21	Crest Block 23	489	5416	5662
R22	Crest Block 4	489	3127	3275

Table 3: Definition of reference points

The file for detailed results contains 3 sheets corresponding to the 3 following steps of the exercise:

5.2.1. Step 1: Reference conditions

Horizontal, vertical and major principal (compressive) stresses at all reference points:

- at the end of construction,
- at reservoir level 483,80, 486.10 and 479.90,

Vertical, radial and tangential displacements (reference zero at end of construction) at all reference points:

- at reservoir level 483.80, 486.10 and 479.90.

5.2.2. Step 2: Calibration period 1963-1995

Horizontal, vertical and major principal (compressive) stresses; vertical, radial and tangential displacements at all reference points

- at reservoir level 483,80, on 30 July 1973
- at reservoir level 486.10, on 30 May 1981
- at reservoir level 479.90, on 30 May 1994.

5.2.3. Step 3: Prediction period 1995-2010

Horizontal, vertical and major principal (compressive) stresses; vertical, radial and tangential displacements at all reference points

- at reservoir level 486.06, on 30 April 2010.

6. Evaluation and comparison of results

Detailed results will be compared and evaluated on the following bases:

- Comparison between reference results (step 1) in order to detect possible discrepancies in the fundamentals of the different models
- Swelling laws and parameters determined by participants will be compared with available laboratory tests carried out in the seventies on concrete cores extracted from the dam body
- Displacements calculated during Steps 2 and 3 will be compared to available results (readings provided plus others)

The general synthesis will be referring to a $(\sigma, \dot{\varepsilon})$ graph.

7. references

ICOLD-Durban, 1994: Q68 R86 “Kariba dam safety monitoring and resulting maintenance works

ICOLD-Firenze, 1997: Q74-9 “Reservoir level influence on concrete swelling rate: Modelization in the case of Kariba”

ICOLD-Lausanne, 1985: Q 56 R 54, Santa Clara , and

Goguel & Mpala (WPDC, June 1992)

8. Appendixes

Appendix 1: History of Kariba dam construction and operation

Appendix 2: Geometry of the dam

Appendix 3: Description of the mesh file

Appendix 1: History of Kariba dam construction and operation

- ***Construction and Impounding, 1957-1963***

The dam concrete was poured from 1957 to mid-1959. Cooling coils kept concrete temperature down to approximately 24° during construction. Concrete temperature on completion rose to 28°C with little difference between the upstream and downstream faces.

Impounding started in early 1959 when concreting was almost complete but the construction joints had only been grouted up to el. 447 m i.e. to 2/3 dam height. The upstream water level was held constant at el. 450 m in the second half of 1959, when the joint grouting was completed up to el. 460 m.

Grouting of the weathered/altered rock on the right abutment and construction of the four buttresses took place during reservoir filling, from 1960 to 1962. The buttresses therefore only provided structural support in the final stages of first impounding.

The reservoir was filled in stages.

- ***Routine dam operation, 1963-1982***

Reservoir level fluctuations remained very small (not more than 7 m) over the first twenty years of dam operation. There was little variation in concrete temperature, which remained at 28°C

The monitoring revealed one important process: A slow trend in concrete strain: The crest leveling clearly reveals an upward movement at the crest due to concrete swelling in the vertical direction (in the order of 2 mm/year). Moreover, positive strains (expansion) were measured in the lightly loaded vertical direction, and very slightly negative strains (contractions) in the direction of arch thrust.

Spilling has caused a scour hole to develop in the river channel. The “Plunge pool” is very narrow and around 70 m deep below foundation level.

- ***Low reservoir level, 1983-1997***

The reservoir has remained for a long time below el. 480 m because of a series of dry years.

In 1993-1994, drainage works along the downstream plinths (North and South) in order to recondition the existing drainage curtain across the dam foundation, in the existing adits below the south abutments and the buttresses.

- ***Normal reservoir level, 1998-2010***

The reservoir level went back over el. 480 m with some fluctuations.

Appendix 2: Geometry of the dam

The leading features of Kariba dam are:

-	Structural height above foundation (H)	128 m
-	Developed crest length (L)	617 m
-	Length/height ratio (L/H)	4,8
-	Crest thickness	13 m
-	Crest elevation	489,5 m
-	Total concrete volume, approx.	1 million m^3
-	Number of blocks	41
-	Block width	~ 14,24 m

The arch dam equations are:

- At the downstream face:

$$R(\varphi, Z) = 207{,}45 - 0{,}315Z - 1{,}2041.10^{-3} Z^2 + (-530{,}35 - 7{,}058Z - 2{,}9298.10^{-2} Z^2 - 4{,}0366.10^{-5} Z^3)\,(1 - \cos\varphi)$$

- At the upstream face:

$$R(\varphi, Z) = 185{,}44 - 1{,}289Z - 8{,}1136.10^{-3} Z^2 - 1{,}4413.10^{-5} Z^3 + (-137{,}98 - 0{,}244Z + 1{,}0171.10^{-2} Z^2 + 3{,}5823.10^{-5} Z^3)\,(1 - \cos\varphi)$$

with : Z=304,79 – Elevation

and φ : angle with the US/DS dam axis

Appendix 3: Description of the mesh and file format

I. Mesh description

Two meshes are proposed by the formulator. Both describe the dam with 3 or 4 elements in the thickness of the arch. The foundation is built with 4 layers of element around the dam.

The contact between the arch and its foundation is modelled by two ways:

- In the *BW11A_Model1.mesh* file, the arch is fully bonded to the foundation. No contact (joint) is modelled.
- In the *BW11A_Model2.mesh* file, joint elements are inserted between the dam and the foundation. Depending on the Finite Element software used, joints can modelled non linear contact behaviour like a Coulomb friction between two bodies for instance.

Both files are in text format.

II. File format

1. Line 1: COBMAIL
2. Line 2: Number of nodes, number of elements and number of elements groups
3. Line 3: Title of the study
4. Coordinate X, Y and Z of each node (1 node / line). The nodes numbers are automatically assigned from 1 to N.
5. For each group of elements:
    - Name of the group, Element type and Number of elements belongs to this group. Element types are described in section III.
    - Connectivity of each element (1 element / line)

III. Description of element types

Two element types are use in the model:

- Element type **VOLU**, which corresponds to 3D quadratic elements (). It can be a brick (20 nodes), tetrahedron (10 nodes) or prism (15 nodes).

Figure 1: Connectivity of solid elements

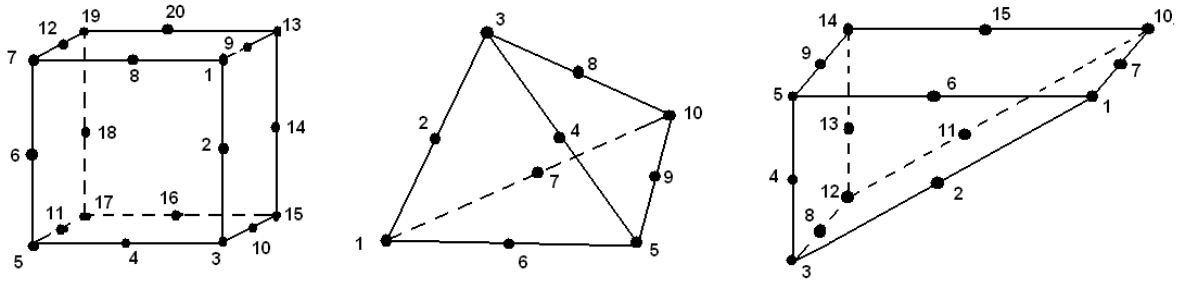

Element 1: 1 2 3 4 5 6 7 8 9 10 11 12 13 14 15 16 17 18 19 20
Element 2: 1 2 3 4 5 6 7 8 9 10 0 0 0 0 0 0 0 0 0 0
Element 3: 1 2 3 4 5 6 7 8 9 10 11 12 13 14 15 0 0 0 0 0

- Element type **JOIN**, which corresponds to a joint surface. It can be a quadrilateral (16 nodes) or a triangle (12 nodes).

Figure 2: Connectivity of joint elements

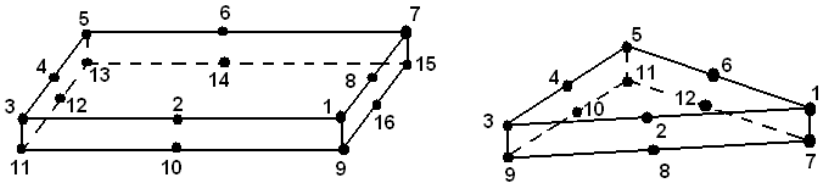

Element 4: 1 2 3 4 5 6 7 8 9 10 11 12 13 14 15 16 0 0 0 0
Element 5: 1 2 3 4 5 6 7 8 9 10 11 12 0 0 0 0 0 0 0 0

XI ICOLD BENCHMARK WORKSHOP ON NUMERICAL ANALYSIS OF DAMS

Valencia, October 20-21, 2011

THEME A

FINITE ELEMENT MODELLING OF CONCRETE SWELLING EFFECTS ON KARIBA DAM

Faggiani, Giorgia[1]

Frigerio, Antonella[1]

Masarati, Piero[1]

Meghella, Massimo[1]

CONTACT

Meghella Massimo, RSE S.p.A., Environment and Sustainable Development Department, Via R.Rubattino 54, 20134 Milan, Italy, Ph. +39 02 3992 5731, massimo.meghella@rse-web.it.

Summary

The effects of concrete swelling due to Alkali-Aggregate Reaction (AAR) on the structural behaviour of Kariba dam were evaluated by means of a concrete model accounting for stress dependent AAR induced expansion, available in the library of CANT-SD, a FEM software developed by RSE for non-linear static and dynamic analyses of dam-reservoir systems.

A model calibration step, based on the comparison with the observed behaviour of the dam from 1963 to 1994, followed by a forecasting step up to 2010, aimed at evaluating the further development of swelling effects, was carried out.

The model provided a good agreement with measured displacements, confirming the stress dependency assumption on the expansion effects.

[1] RSE S.p.A., Environment and Sustainable Development Department, Milan, Italy.

1. Introduction

Many old concrete dams are known to be affected by Alkali-Aggregate Reaction (AAR), a chemical reaction that occurs between the alkaline hydroxide ions in the cement and reactive aggregates, causing the production of an expansive gel, resulting in concrete swelling. This swelling gives rise to displacement drifts, along with an overall increase of compressive stresses in the dam body, being the structure over-constrained. Numerical analyses, with suitable constitutive laws to account for such effects, can provide realistic long term predictions of AAR induced deformation and damage.

According to the purpose of Theme A of the 11th ICOLD Benchmark Workshop on Numerical Analysis of Dams (*Noret & Molin* [1]), the effect of concrete swelling due to Alkali-Aggregate Reaction (AAR) on the structural behaviour of Kariba dam was studied. Theme A regards a large arch dam built on Zambezi river between 1956 and 1959, that showed clear signs of swelling soon after the starting of its operation. The analyses, aimed at the identification of an adequate swelling law and at its calibration in order to fulfil the observed drifts, have been carried out using the RSE in-house FEM code CANT-SD (*Masarati & Meghella* [2]), specifically designed for non-linear static and dynamic (seismic) analyses of dam-reservoir systems. This code is currently used at RSE for safety assessment of concrete dams, and in particular it was adopted to deal with some themes proposed in previous ICOLD Benchmark Workshops (*Meghella & Masarati* [3], *Meghella et al* [4], *Meghella & Mazzà* [5]*, Bon et al* [6]*, Bolognini et al* [7]). To effectively address Theme A, a macroscopic model for stress dependent AAR induced expansion and a joint model to represent the structural behaviour of discontinuity surfaces (e.g. dam-foundation interface and/or construction joints) have been used.

2. Geometrical and physical model

The FE parabolic mesh "*Model2"* provided by the formulators has been adopted unchanged (Figure 1); a monolithic behaviour of the dam body has therefore been considered, as no construction joints are modelled, while the dam-foundation joint elements have been provided with a friction no-tension, elastic-plastic model.

Dam concrete and foundation rock, assumed to behave linear-elastically, are characterized by the mechanical parameters provided by the formulators and summarized in Table 1.

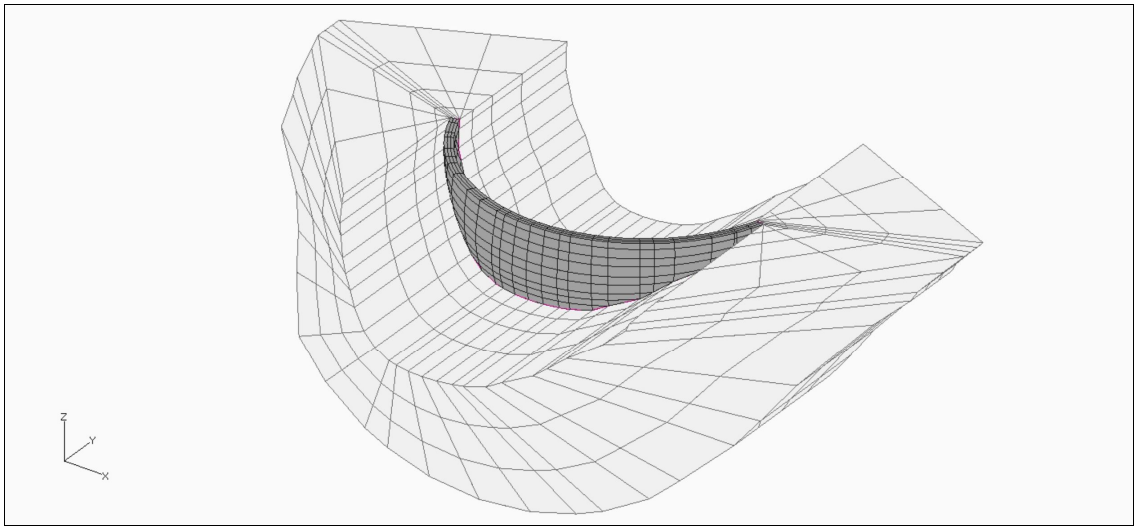

Figure 1: FEM model of Kariba dam and its foundation

Table 1: Mechanical parameters

Mechanical parameter	Foundation rock	Dam concrete
Modulus of elasticity (GPa)	10.0	22.0
Poisson's ratio (-)	0.2	0.2
Mass density (kg/m^3)	-	2350

In order to evaluate the concrete swelling affecting Kariba dam behaviour, a macroscopic stress-dependent expansion model was adopted (*Charlwood et al* [8], *Thompson et al* [9]). This model assumes that AAR effect on concrete is an anisotropic anelastic strain, whose rate is related to compressive stress according to the following set of equations:

$$\dot{\varepsilon}_i^{\,aar} = \begin{cases} \dot{\varepsilon}^{\,free} & \text{if} \quad \sigma_i \le \sigma_L \\ \dot{\varepsilon}^{\,free}\left[1 - \dfrac{\ln(\sigma_i/\sigma_L)}{\ln(\sigma_U/\sigma_L)}\right] & \text{if} \quad \sigma_L \le \sigma_i \le \sigma_U \\ 0 & \text{if} \quad \sigma_i \ge \sigma_U \end{cases} \tag{1}$$

being (Figure 2):

1. $\dot{\varepsilon}^{free}$ the free (zero stress) expansion rate
2. $\dot{\varepsilon}_i^{\,aar}$ the effective expansion rate along the i-th principal stress direction
3. σ_i the i-th principal stress (assuming positive compression stress)
4. σ_L the lower limit of compressive stress (usually assumed about 0.3 MPa)
5. σ_U the upper limit of compressive stress

Considering the principal direction i, when the compressive stress σ_i overcomes the lower limit σ_L, the effective expansion rate starts decreasing from the free expansion rate $\dot{\varepsilon}^{free}$; when the compressive stress becomes greater than the upper limit σ_U, no further increment of effective expansion occurs anymore. Nevertheless, any subsequent decrease of compressive stress below the upper limit implies the resumption of the effective expansion development.

For a given AAR-affected dam, the model parameters ($\dot{\varepsilon}^{free}$ and σ_U) have to be chosen to best fit the displacement drifts measured by the monitoring system. In the present case study the dam crest displacements have been adopted as reference data in order to identify the model parameters.

For arch dams, it is common practice to calibrate $\dot{\varepsilon}^{free}$ with reference to vertical drifts, that are much less influenced by the compressive stress state than horizontal drifts, while the latters are generally used to calibrate σ_U, being such drifts significantly influenced by the compressive stress state. In evaluating the result of the calibration process, it is important to consider that σ_U typically ranges from 5 to 10 MPa (*Thompson et al* [9], *Léger et al* [10], *Mason* [11]): values outside that range should be carefully justified on the basis of experimental tests.

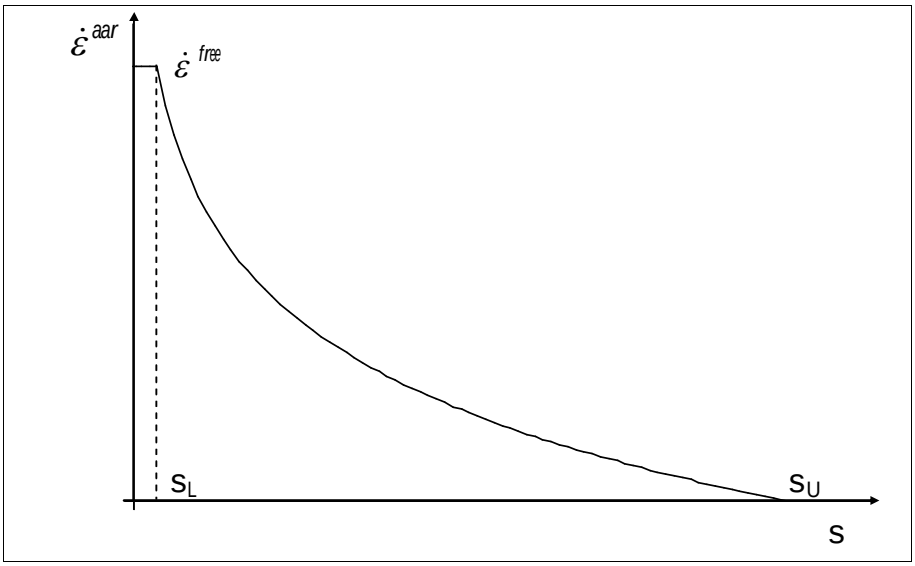

Figure 2: Expansion law related to the i-th principal stress direction

A friction no-tension elastic-plastic constitutive model has been used for the joint elements simulating the dam-foundation interface. The normal contact stress σ_n can be either compressive, in closed state, or zero, in open state (no-tension model): in closed state, the constitutive law reproduces the Coulomb friction behaviour (Figure 3). For the present case study, a friction angle α equal to 45° has been assumed.

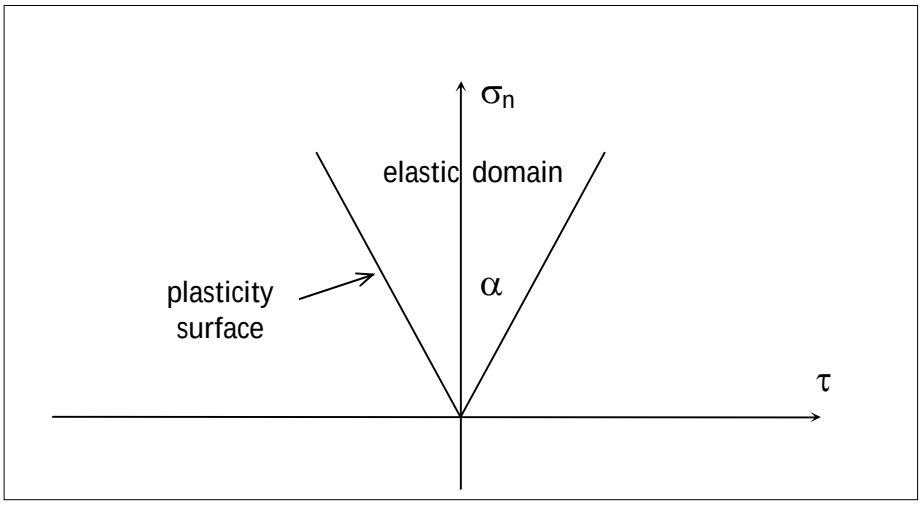

Figure 3: Joint model

3. Loadings

The numerical analyses account for the effects of the following loadings/actions:

1. dead weight (followed by joint grouting)
2. hydrostatic pressure
3. concrete swelling

The effects of loads applied during construction (e.g. dead weight) depend on the design construction scheme (including space/time sequence of concrete castings as well as of joint grouting), therefore the calculation of the actual stress-strain state at the end of construction may be a very challenging task.

Nevertheless, according to the theme requirements concrete blocks have to be considered as independent cantilevers, which fully transfer their weight to the foundation. Once vertical joints are grouted, the arch effect is activated and the dam behaves according to its monolithic design scheme. Furthermore, temperature was assumed to be uniform and constant along the whole construction process and the structural effects caused by the injection pressure of sealing grout were neglected.

To properly evaluate the stress-strain state due to the dead weight, CANT-SD provides two alternative ways: 1) through modelling of vertical joints (deactivated during the analysis step with the dead weight and activated during the following loading steps); 2) through sequentially activating/deactivating *"substructures"*, representing the concrete blocks. Based on previous experience on similar cases, the latter technique was adopted.

It is worth pointing out that the provided mesh has been considered refined enough to capture the main aspects of the structural behaviour, even if it does not allow modelling separately all the blocks of the actual dam (about forty).

In particular, the FE mesh was divided into eleven substructures: ten for the concrete blocks and one for the whole foundation rock (Figure 4). Then, the simulation sequence progressed as follows:

1. dead weight of block 1 - activation of finite elements belonging to the first concrete block and to the foundation;
2. dead weight of block i (from 2 to 10) – deactivation of elements belonging to the previously activated concrete block and activation of block i elements;
3. activation of all blocks (simulating joint grouting);
4. hydrostatic pressure – pressure applied to wet surface of the upstream dam face, according to the time-varying reservoir level (see details below);
5. swelling – application of a stress-dependent expansion law, according to the constitutive model described in § 2 (see details below).

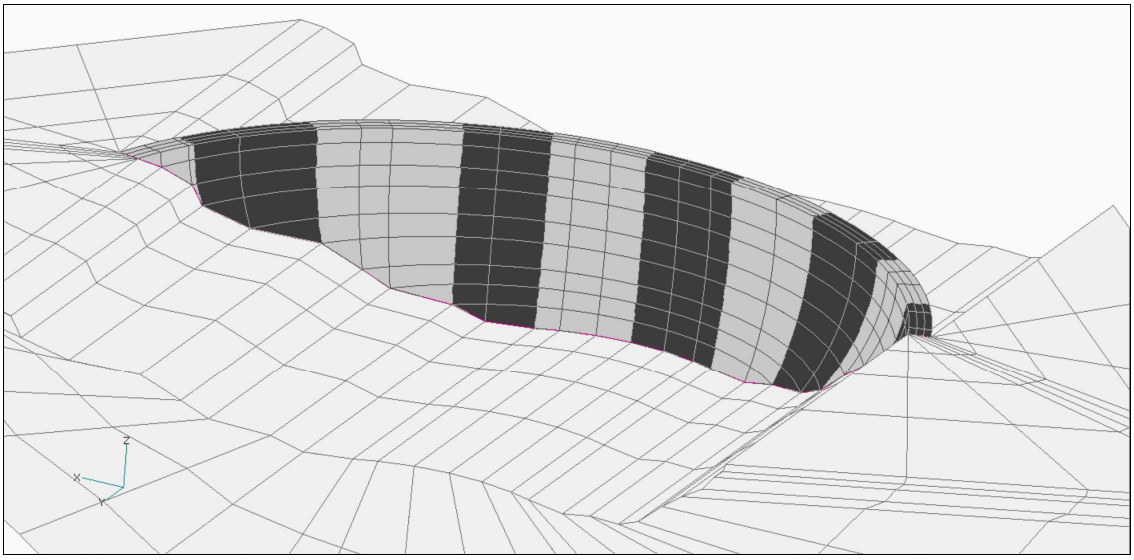

Figure 4: Model substructures

For the evaluation of hydrostatic pressure effects, according to the formulators, a piecewise constant water level from 1963 to 1994 was assumed, while from 1994 to 2010 two different approximations of the observed reservoir level curve were alternatively considered: the first one piecewise linear, the second one constant at an average water level of 483 m (Figure 5).

The radial displacement of one point on the dam crest (at the crown cantilever) and the vertical displacements of eight points along the dam crest have been provided.

Horizontal and vertical displacements of Kariba dam have shown evident signs of irreversible drifts, possibly due to concrete swelling, soon after the starting of its operation.

According to §2, the initial guess for the calibration of free expansion rate $\dot{\varepsilon}^{free}$ has been estimated from the vertical displacements, that show an upward drift of about 1.5 mm/year, resulting in a free expansion coefficient of 15 $\mu\varepsilon$/year, being the dam around 100 m high.

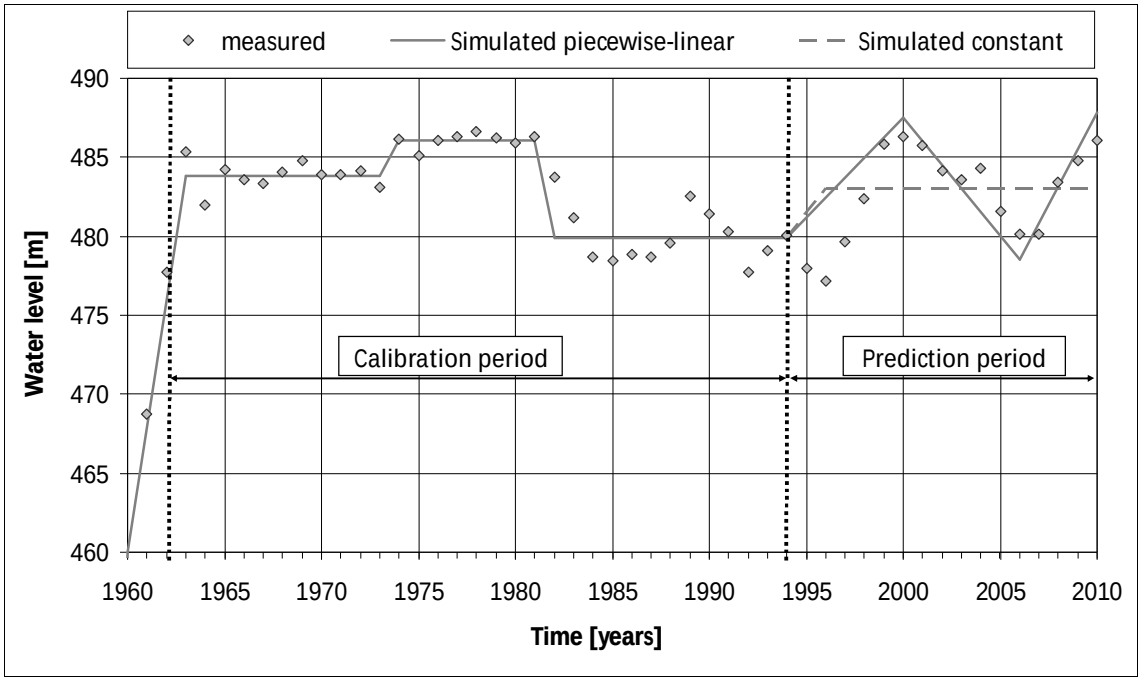

Figure 5: Measured and simulated water level of Kariba dam lake

4. Results

The stress state is represented by means of contour plots of minimum and maximum principal stresses, expressed in Pascal and positive if tensile.

The time-varying radial and vertical displacements of the dam are expressed in millimetres, positive if downstream and upward.

Vertical displacements are reported separately for measuring points in the right bank and in the left bank (Figure 6): measured data are represented with solid symbols and dashed lines. The central points (0-2, 3-5) have been discarded as suggested by the formulators.

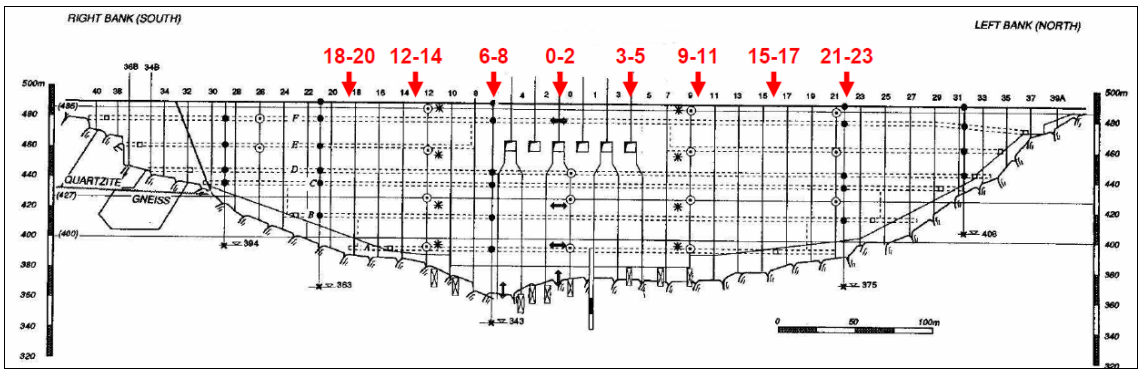

Figure 6: Location of the levelling points.

4.1. Dead weight

Compressive and tensile stress contour plots are respectively shown in Figures 7 and 8. Clear discontinuities appear between adjacent blocks, as they behave like independent cantilevers, without mutual interaction. Both compressive and tensile principal stresses are essentially vertical oriented, almost tangent to the cantilever curvature. Compression stresses act mostly on the upstream face while tensile stresses act on the downstream surface: the blocks tend to bend upstream, due to their upstream slope. Tensile stresses tend to decrease approaching the rock foundation, because of the presence of the no-tension dam-foundation interface, and, as expected, in most parts of the dam body they are negligible or nil.

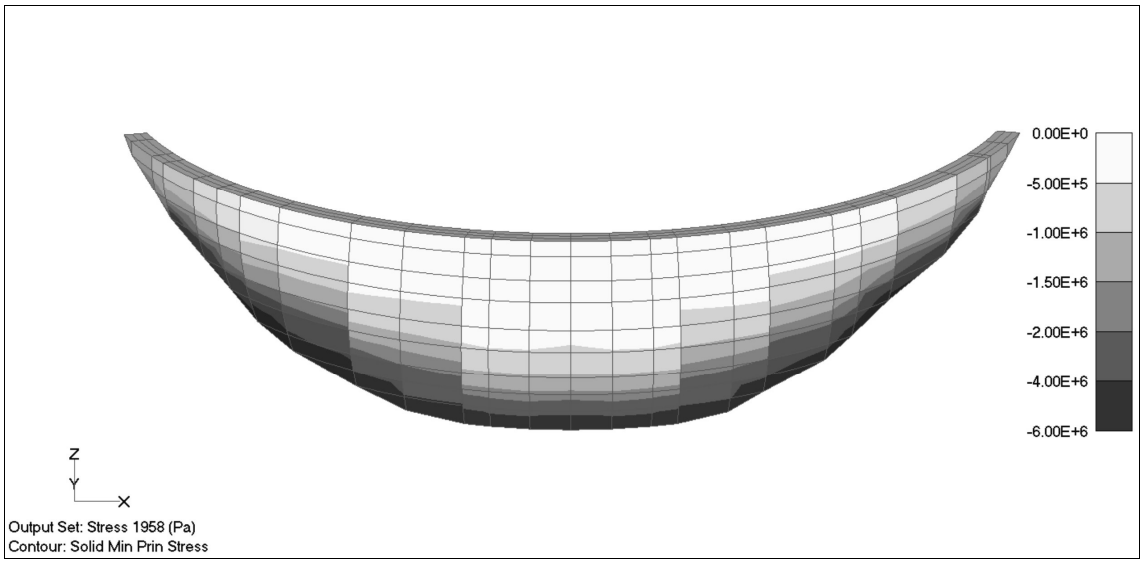

Figure 7: Dead weight, minimum principal stress, upstream view.

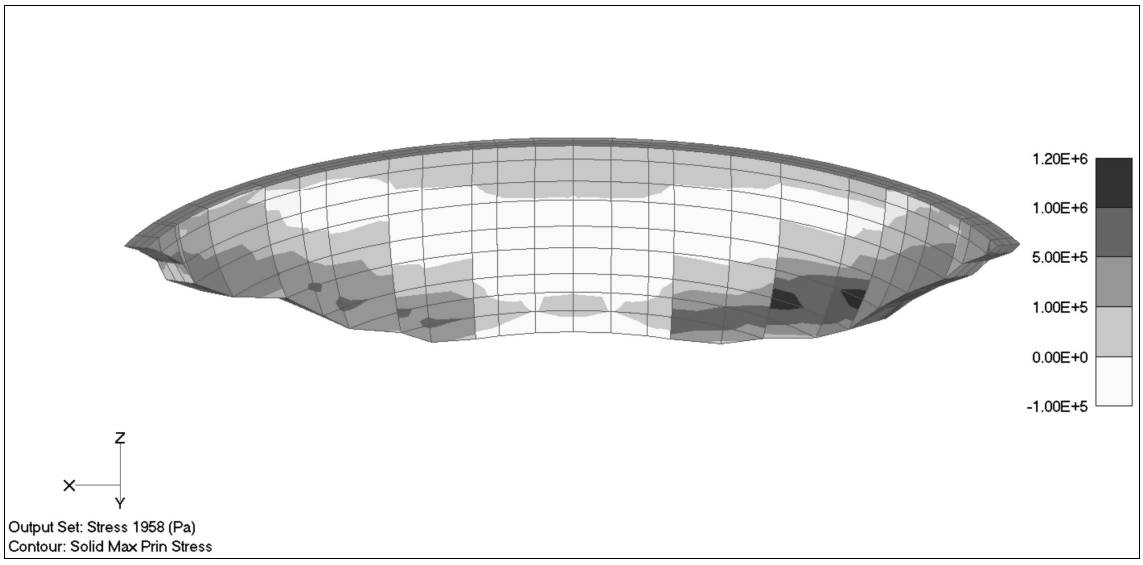

Figure 8: Dead weight, maximum principal stress, downstream view.

4.2. Hydrostatic pressure (water level 479.90 m)

The results confirm the classic stress distribution scheme of an arch dam. The principal directions for compressive stress are almost horizontal in the highest part of the dam, while they tend to become perpendicular to the abutments in proximity of the rock foundation (*arcs plongeant*). Tensile stress are essentially vertical oriented and act on downstream surface. Due to the slight asymmetry of the dam, the highest compressive stress, around 7.0 MPa, occurs in the left side of the upstream face (Figure 9) while the highest tensile stress, around 2.2 MPa, occurs in the right side of the downstream face (Figure 10).

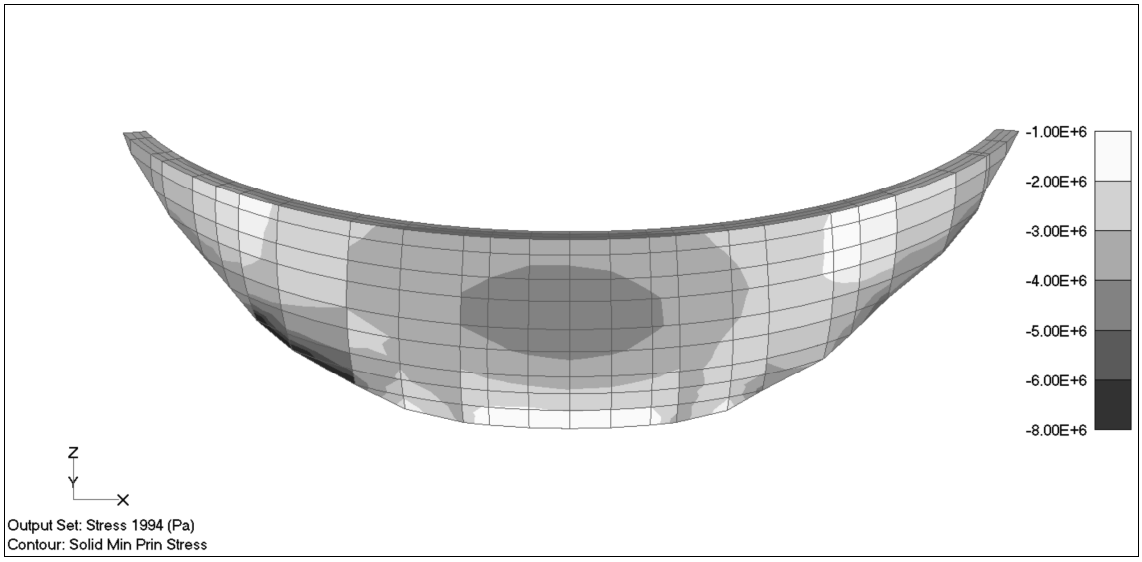

Figure 9: Hydrostatic pressure, minimum principal stress, upstream view

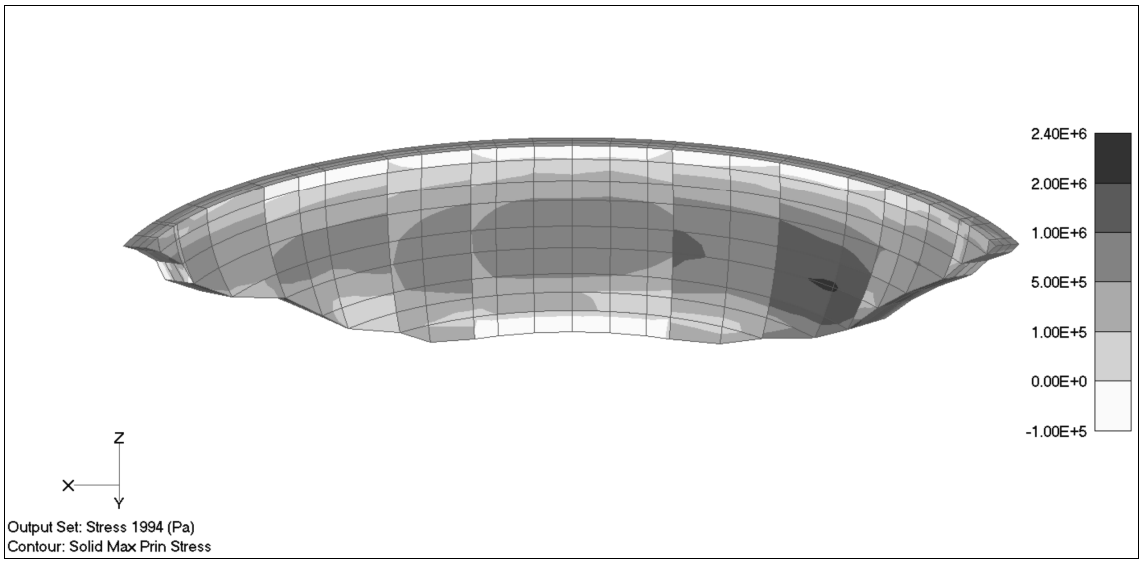

Figure 10: Hydrostatic pressure, maximum principal stress, downstream view

4.3. Concrete swelling: model calibration

A preliminary analysis, assuming a stress-independent value ($\dot{\varepsilon}^{aar} = \dot{\varepsilon}^{free}$) of 15 με/year for the effective expansion, as obtained from the vertical drifts, shows that the calculated radial displacements are much higher than the measured ones (Figure 11), while vertical displacements are quite in good agreement, confirming the assumption that horizontal drift is significantly influenced by the compressive stress state (Figures 12 and 13).

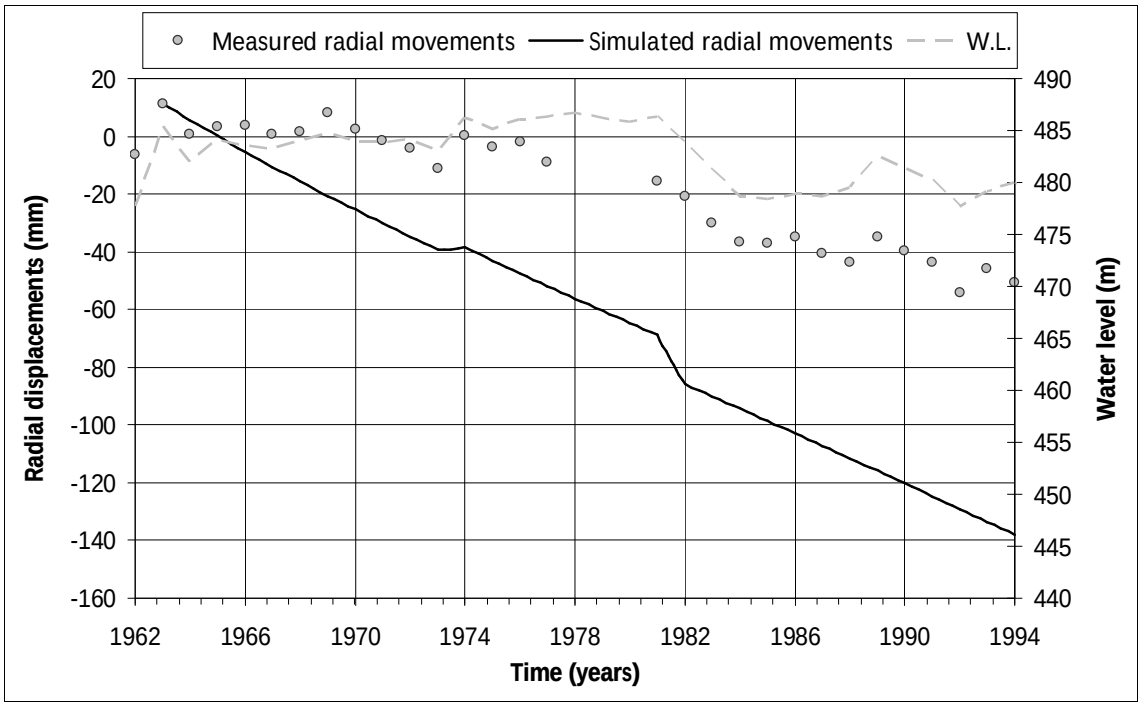

Figure 11: Model calibration - $\dot{\varepsilon}^{free}$=15 με/year, stress-independent. Radial displacements.

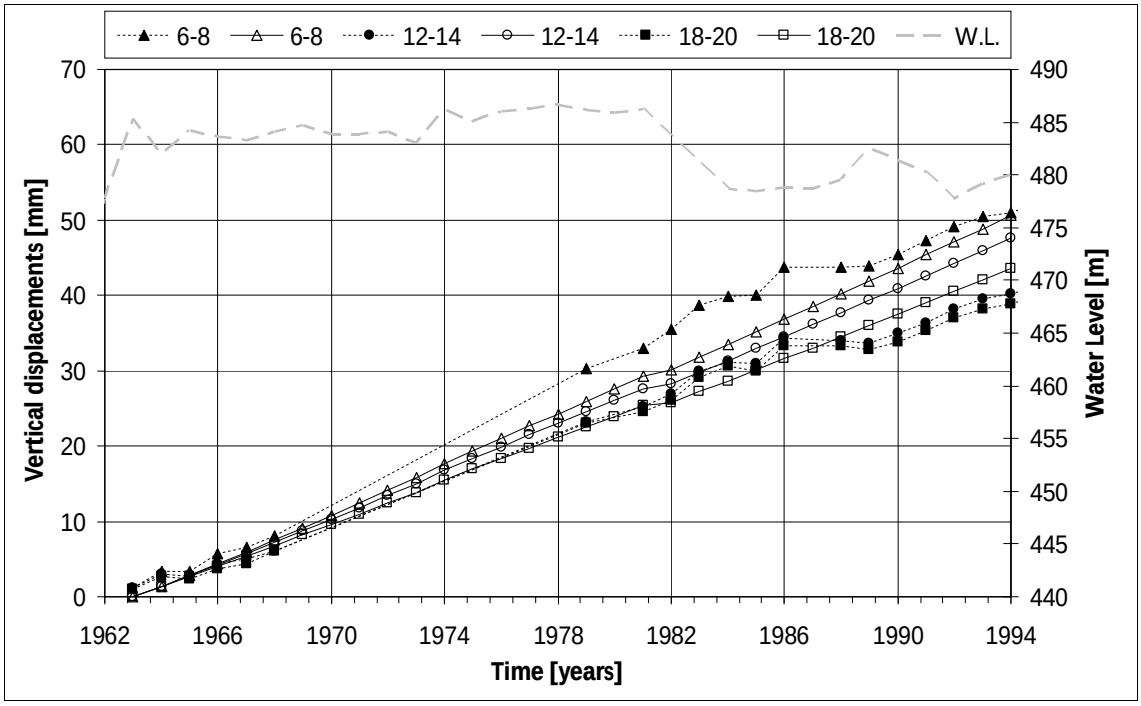

Figure 12: Model calibration - $\dot{\varepsilon}^{free}$=15 με/year, stress-independent. Vertical displacements, right abutment.

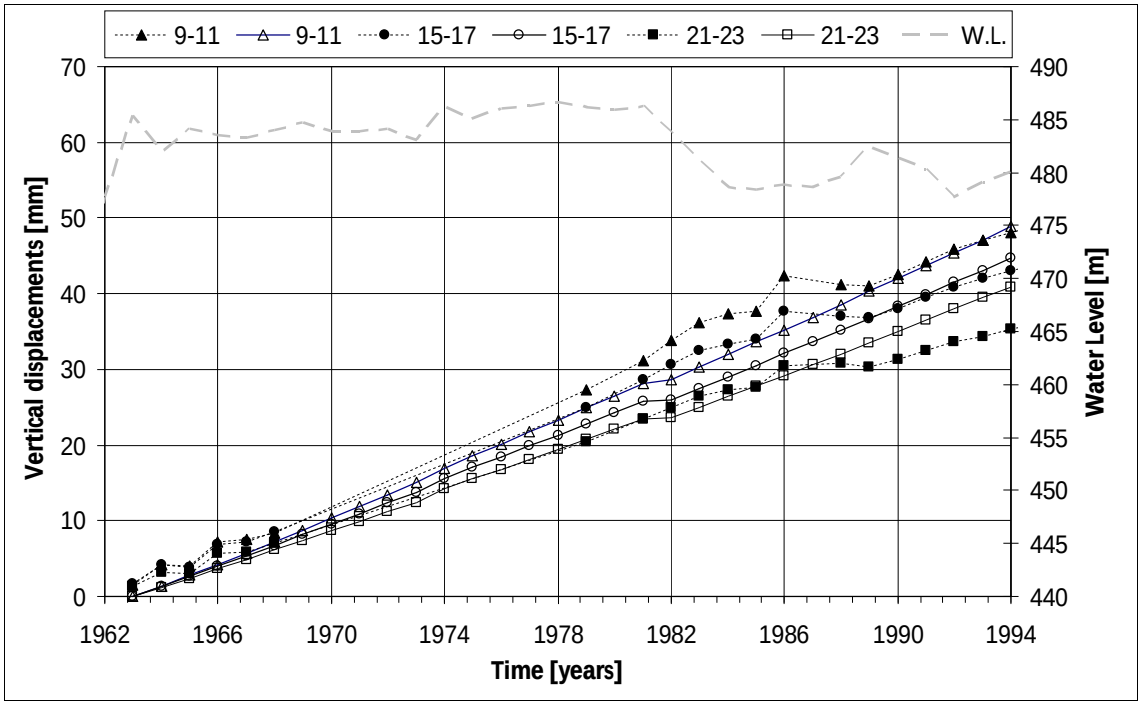

Figure 13: Model calibration - $\dot{\varepsilon}^{free}$=15 με/year, stress-independent. Vertical displacements, left abutment.

So, in order to calibrate the stress-dependent expansion model, a set of analyses has been carried out to achieve the best fit of measured displacements during the period from 1963 to 1994. The calibration process consisted in the identification of the values of $\dot{\varepsilon}^{free}$ and σ_U which minimize the difference between measured and calculated displacements (radial and vertical). The best fit of horizontal (Figure 14) and vertical displacements (Figures 15 and 16) was achieved with $\dot{\varepsilon}^{free}$ = 20 με/year and σ_U = 8.0 MPa. These values are compatible with the typical ranges provided by literature (*Thompson et al* [9], *Léger et al* [10], *Mason* [11]).

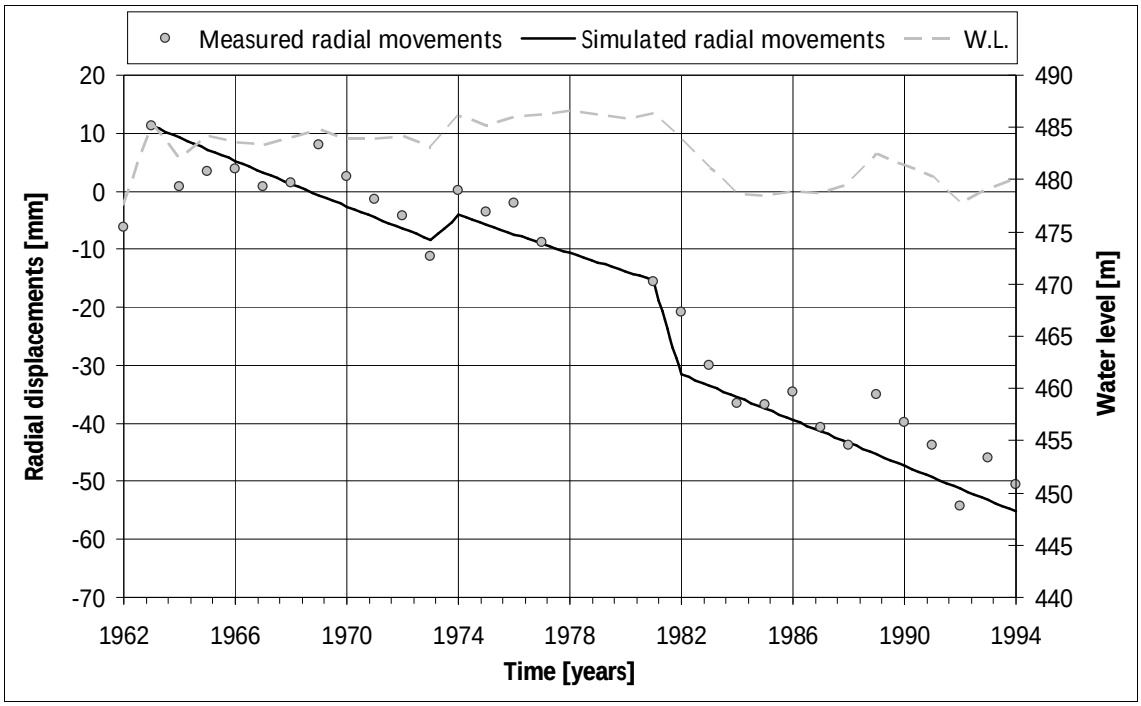

Figure 14: Model calibration - $\dot{\varepsilon}^{free}$=20 με/year, σ_u=8 MPa. Radial displacements.

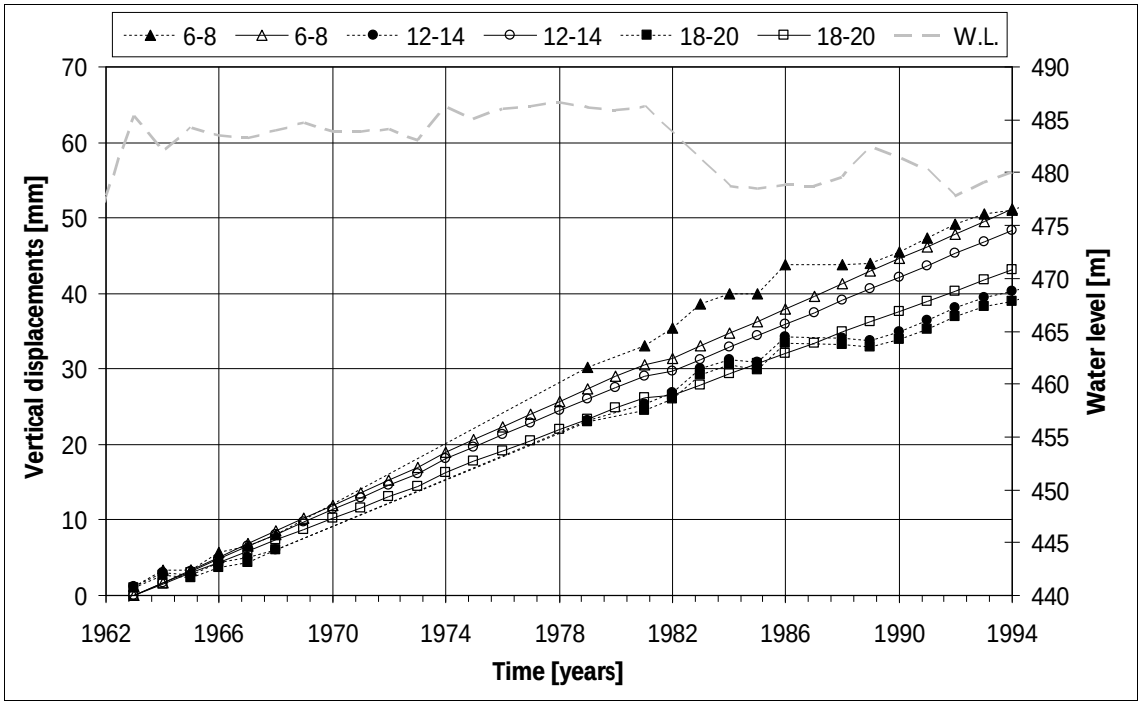

Figure 15: Model calibration - $\dot{\varepsilon}^{free}$=20 με/year, σ_u=8 MPa. Vertical displacements, right abutment.

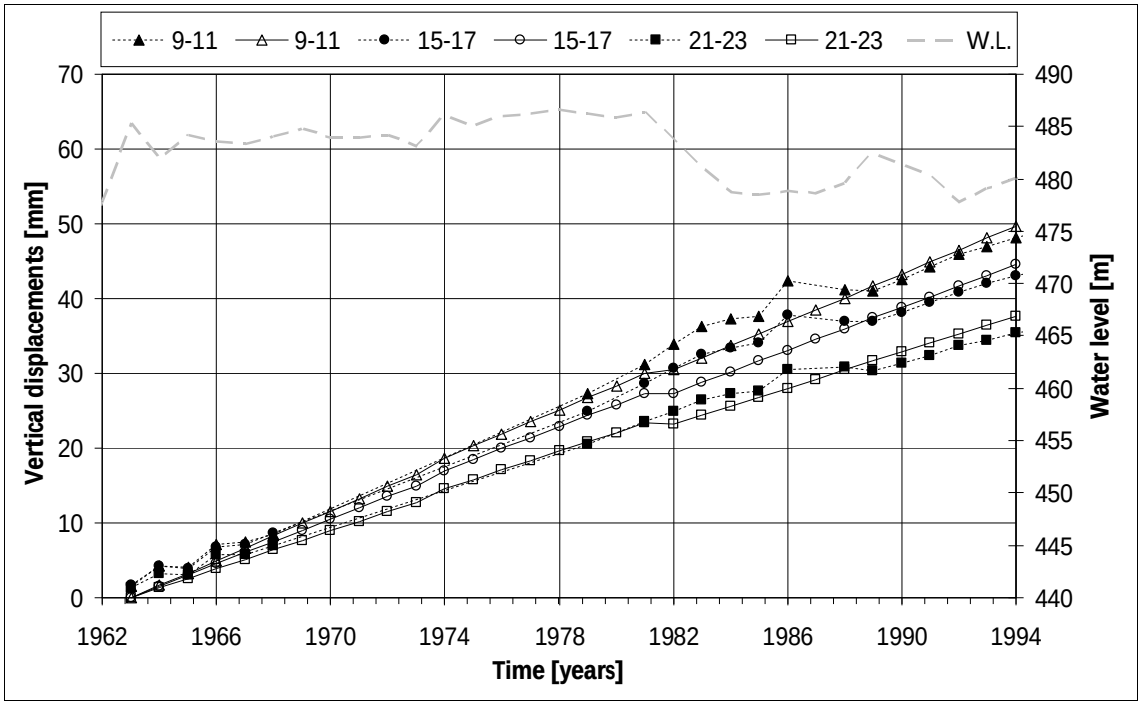

Figure 16: Model calibration - $\dot{\varepsilon}^{free}$=20 με/year, σ_u=8 MPa. Vertical displacement,s left abutment.

Compressive and tensile stresses are respectively shown in Figures 17 and 18. By comparison with the stresses without swelling (Figures 9 and 10), the following differences can be observed:

1. the typical “arcs plongeant” effect disappears. The principal directions for compressive stress tend to become horizontal in the whole dam body;
2. the highest compressive stresses in the upstream face move downward affecting most of its lower part;
3. tensile stresses tend to disappear, or drastically decrease, in the whole downstream surface, with the exception of the left and right abutments, where they slightly increase up to 2.4 MPa, remaining vertically oriented.

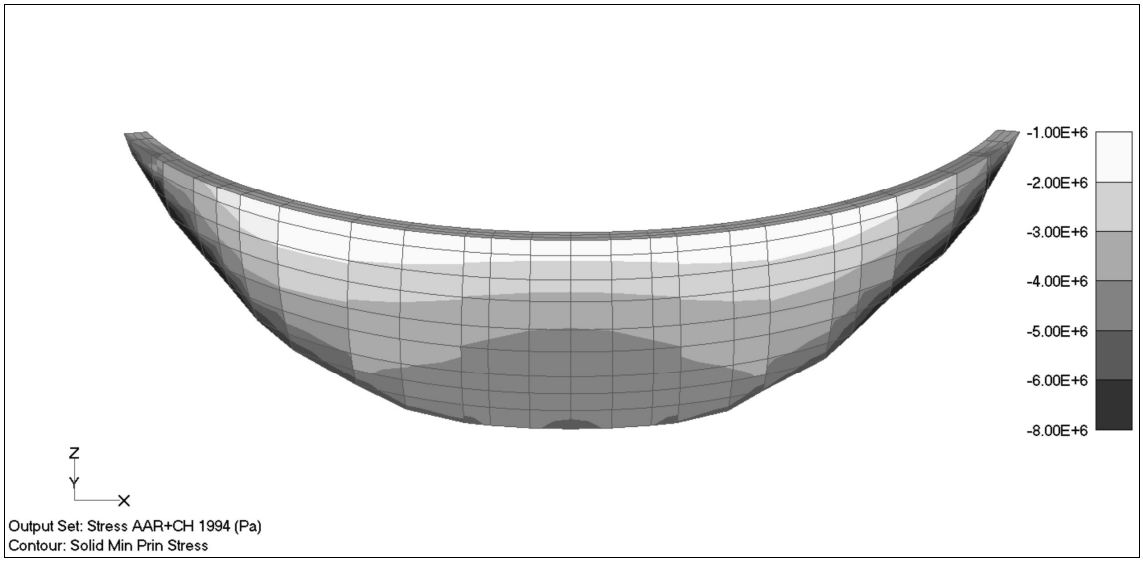

Figure 17: Concrete swelling (end of calibration period), minimum principal stress, upstream view.

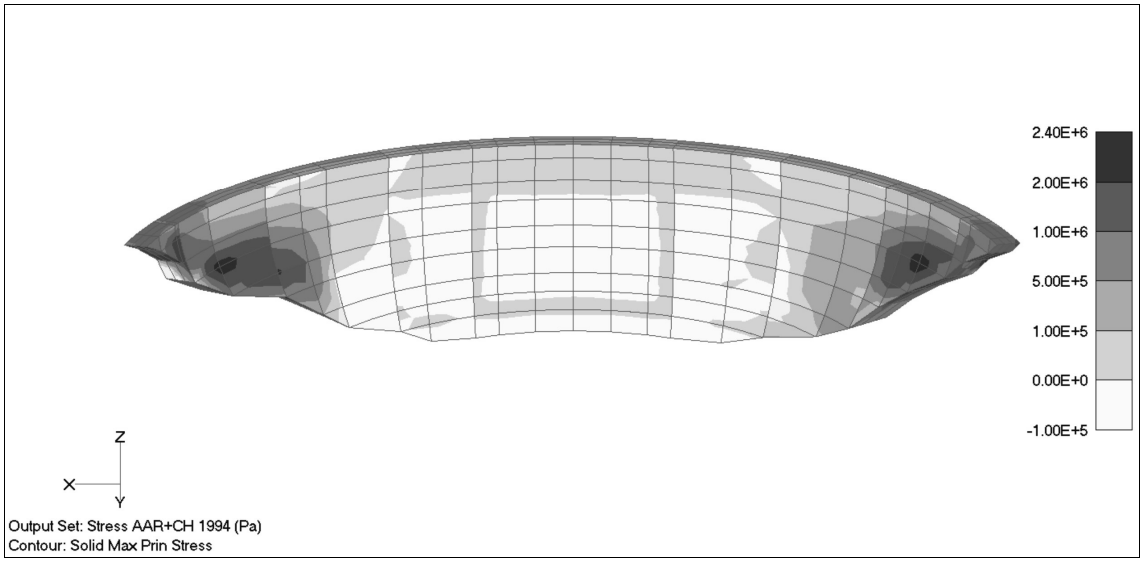

Figure 18: Concrete swelling (end of calibration period), maximum principal stress, downstream view

4.4. Concrete swelling: prediction from 1995 to 2010

Considering the identified parameters, two analyses have been carried out with two reservoir level curves (piecewise linear and constant) as defined in § 3. Figure 19 shows the development of radial displacements vs. time for the whole period 1963-2010, referred both to the case with piecewise linear and constant reservoir level.

Since radial displacements are strongly affected by the variation of the water level, the two displacement paths are quite different, but in both cases the drift clearly shows the same trend of the previous period. With the constant level the drift is clearly visible, while with the piecewise linear level the drift is not directly visible, but it can be deduced considering that, when the two level curves intestect, calculated displacements are very similar for the two simulations.

Figures 20-21 and 22-23 show the vertical displacements vs. time. Since vertical drifts are very little affected by the hydrostatic pressure, the two trends are quite similar and in good agreement with the previous period.

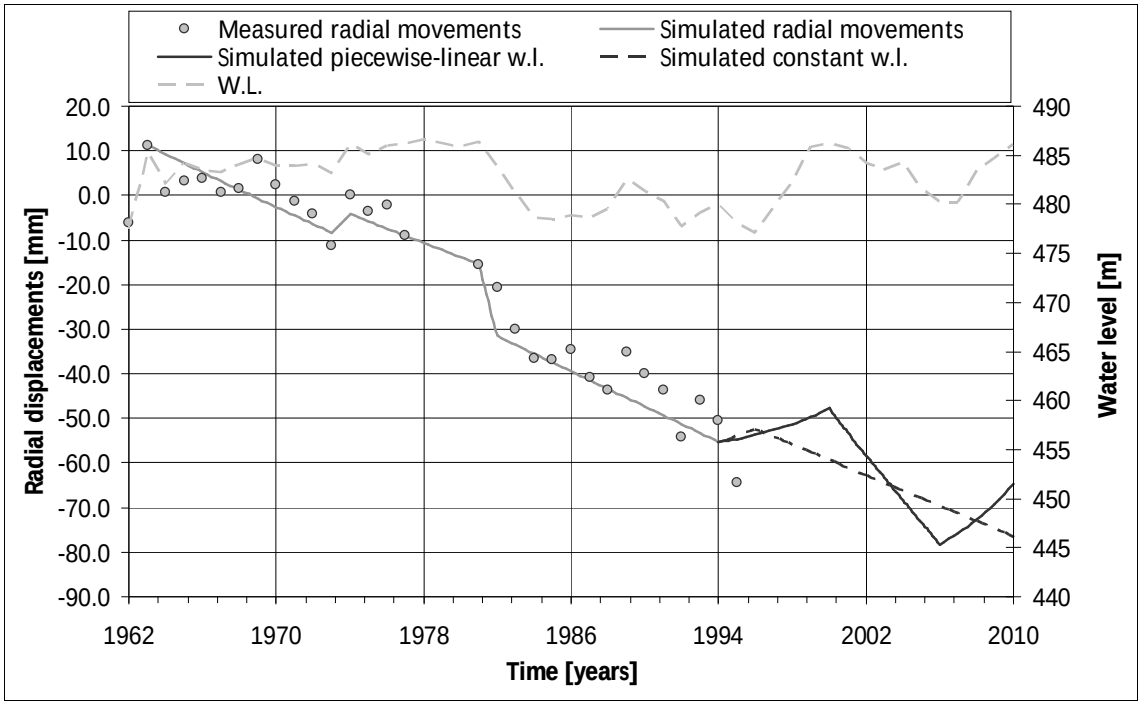

Figure 19: Prediction period. Radial displacements.

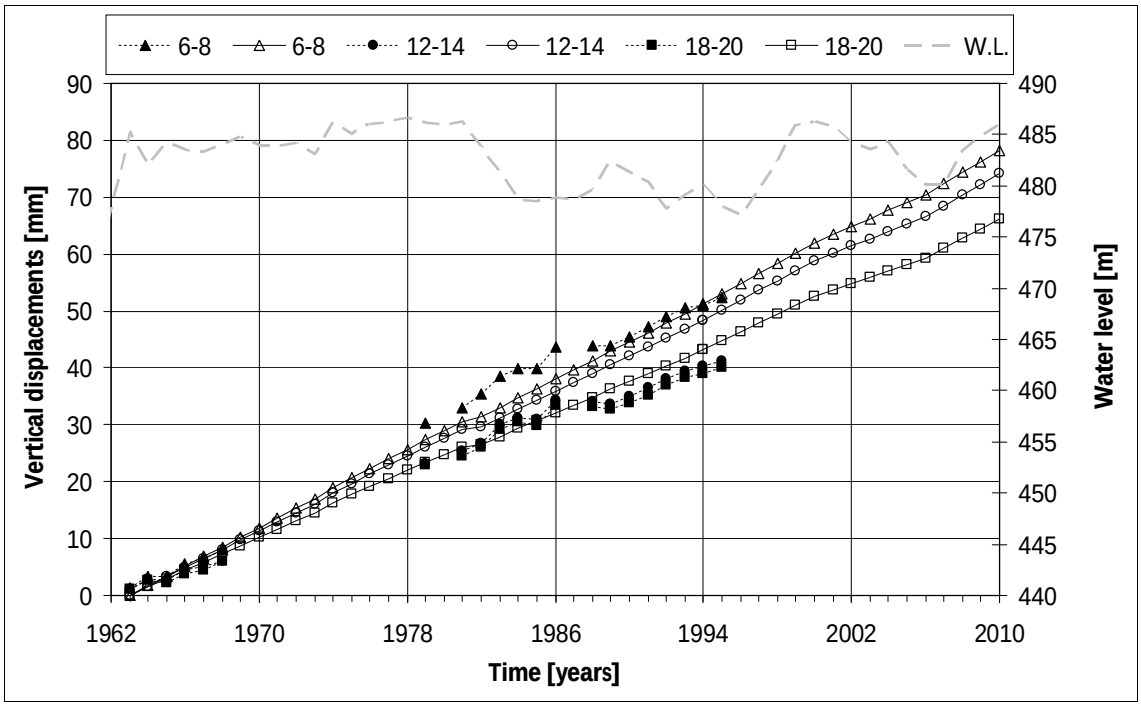

Figure 20: Prediction period (piecewise linear water level). Vertical displacements, right abutment.

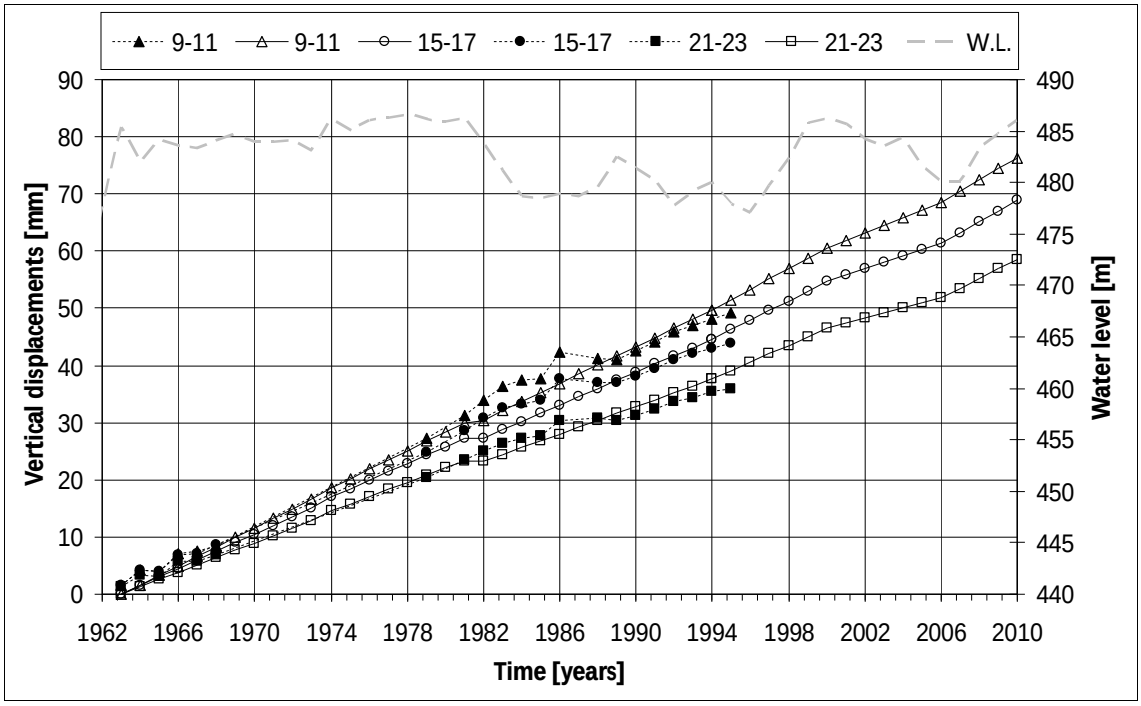

Figure 21: Prediction period (piecewise linear water level). Vertical displacements, left abutment.

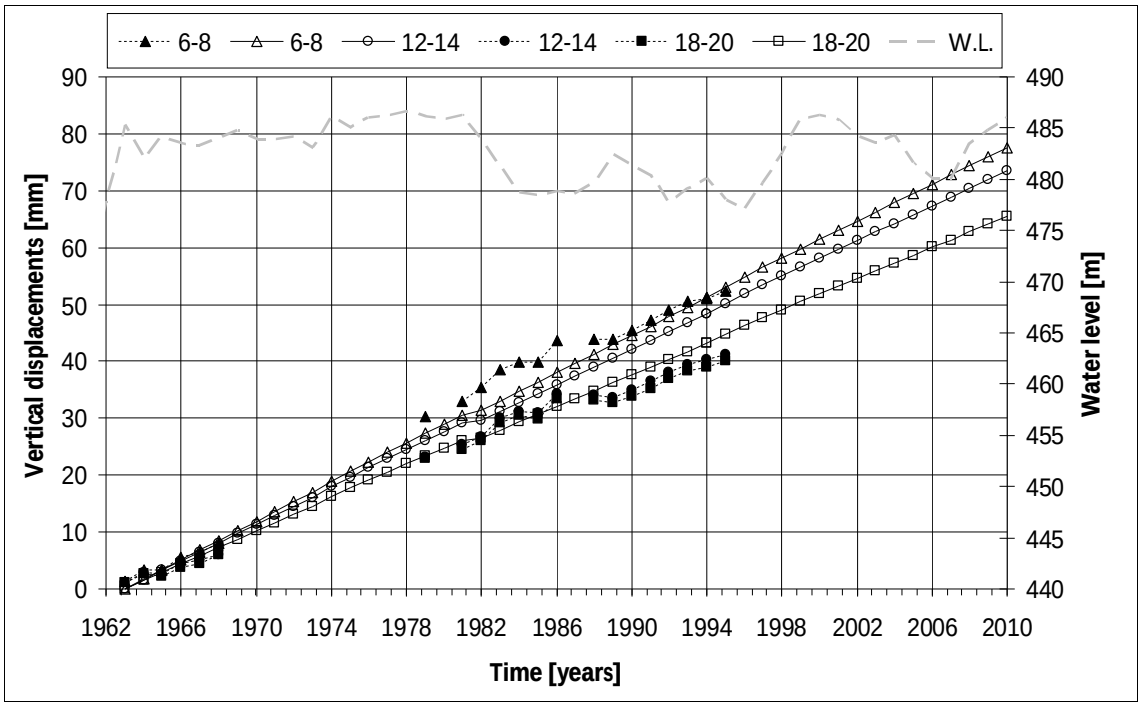

Figure 22: Prediction period (constant water level). Vertical displacements, right abutment.

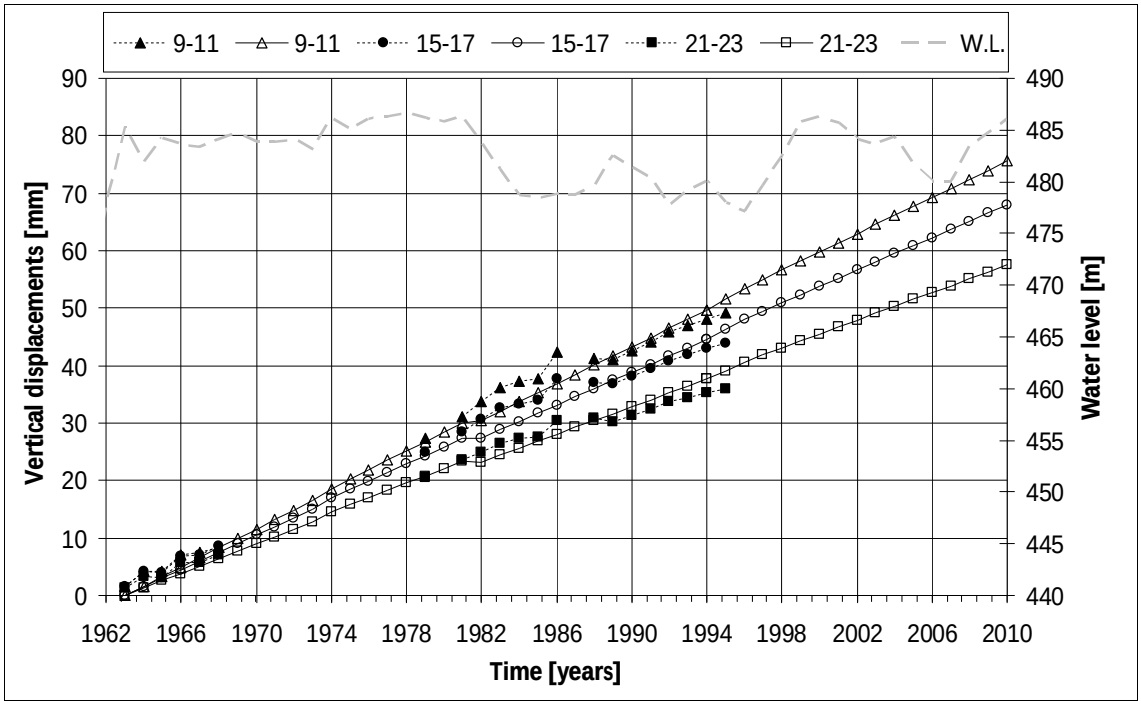

Figure 23: Prediction period (constant water level). Vertical displacements, left abutment.

With regard to the piecewise linear case, the evolution of the stress state due to the further development of the AAR expansion is shown in Figures 24 and 25, respectively for compressive and tensile stresses. By comparison with Figures 17 and 18, no significant changes of stress pattern and just a slight increase of both compressive and tensile stresses can be observed.

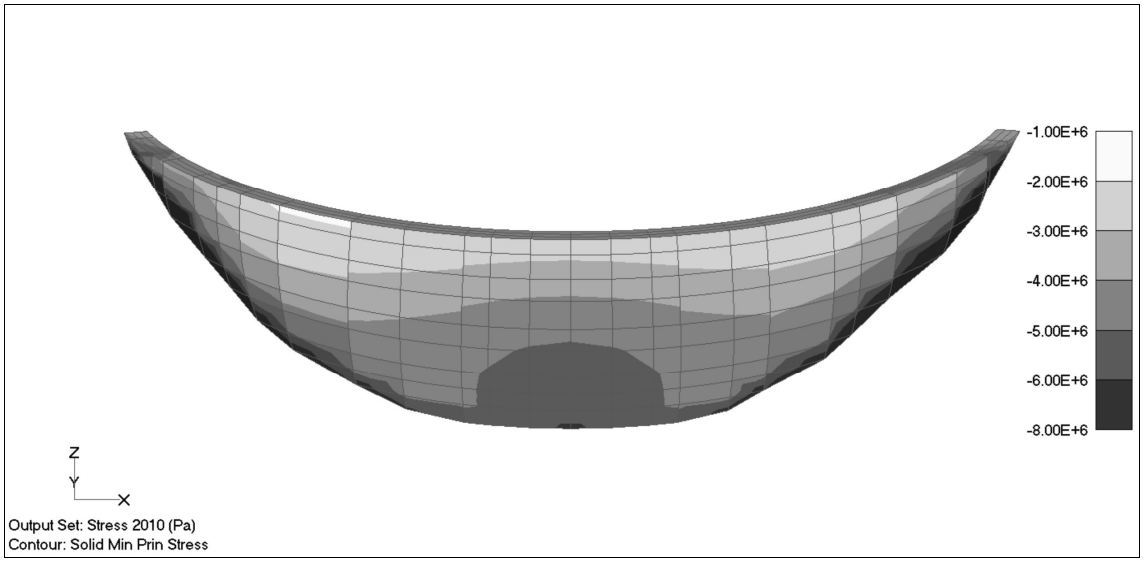

Figure 24: Concrete swelling (end of prediction period), minimum principal stress, upstream view

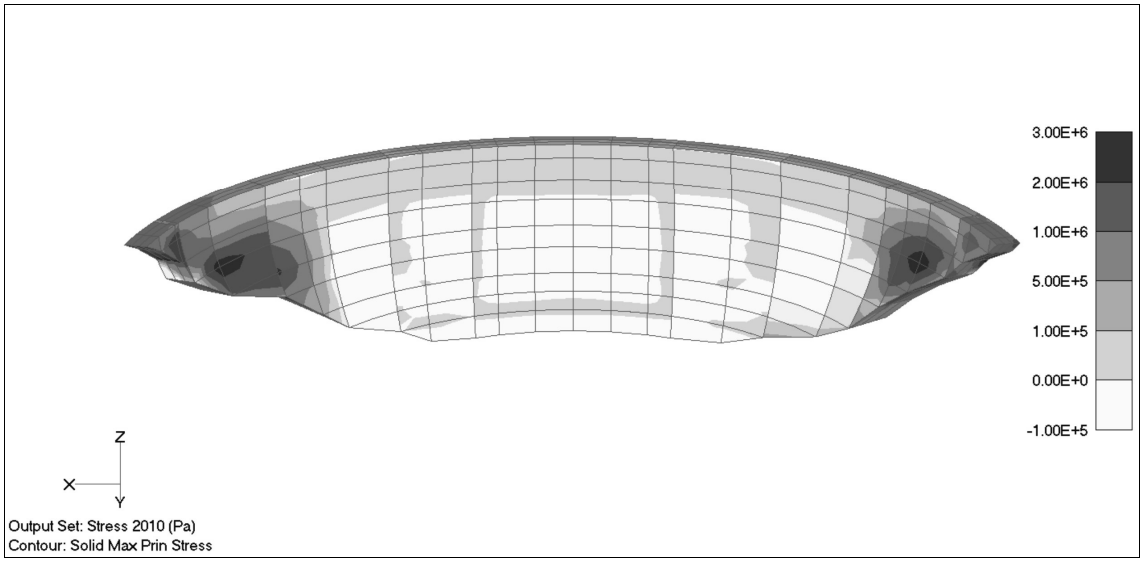

Figure 25: Concrete swelling (end of prediction period), maximum principal stress, downstream view

5. Conclusions

Theme A of the 11th ICOLD Benchmark Workshop on Numerical Analysis of Dams, dealing with the effect of concrete swelling due to Alkali-Aggregate Reaction (AAR) on the structural behaviour of Kariba dam, has been approached by using CANT-SD, a RSE in-house FEM code for non-linear static and dynamic analyses of dam-reservoir systems.

The calibrated FEM model has provided results in good agreement with the measured vertical and radial displacement drifts for the period from 1963 to 1994. The simulations to predict the structural behaviour up to 2010 have enabled to assess the further evolution of drifts and stresses, that show an overall slight increase of compressive stress, along with a slight increase of local tensile stresses.

Finally, the results of the analyses highlight in particular the importance to properly consider the anisotropy, due to the stress dependency, of the expansion effects, when modelling the structural behaviour of concrete dams affected by AAR swelling, even if a model based only on mechanical expansion is adopted.

Acknowledgements

This work has been financed by the Research Fund for the Italian Electrical System under the Contract Agreement between RSE and the Ministry of Economic Development.

References

[1] Noret, C. & Molin, X. (2011). Theme A formulation. Effect of concrete swelling on the equilibrium and displacements of an arch dam. 11th ICOLD Benchmark Workshop on Numerical Analysis of Dams, Valencia, Spain.

[2] Masarati, P. & Meghella, M. (2000). The FEM computer code CANT-SD for non-linear static and dynamic analysis of dams. Enel.Hydro rep. n. 6045, Milano, Italy.

[3] Meghella, M. & Masarati, P. (2007). FEM analyses for the interpretation of the structural behaviour of La Aceña dam. 9th ICOLD Benchmark Workshop on Numerical Analysis of Dams, St. Petersburg, Russia.

[4] Meghella, M., Frigerio, A. & Masarati, P. (2005). Evaluation of AAR on the behaviour of Poglia dam adopting two different approaches. 8th ICOLD Benchmark Workshop on Numerical Analysis of Dams, Wuhan, Hubei, P.R. China.

[5] Meghella, M. & Mazzà, G. (2003). Safety evaluation against sliding of a gravity dam with curved shape. 7th ICOLD Benchmark Workshop on Numerical Analysis of Dams, Bucharest, Romania.

[6] Bon, E., Chillè, F., Masarati, P. & Massaro, C. (2001). Analysis of the effects induced by alkali-aggregate reaction (AAR) on the structural behaviour of Pian Telessio dam. 6th ICOLD Benchmark Workshop on Numerical Analysis of Dams, Salzburg, Austria.

[7] Bolognini, L., Masarati, P., Bettinali, F. & Galimberti, C. (1994). Non-linear analysis of joint behaviour under thermal and hydrostatic loads for an arch dam. 3rd ICOLD Benchmark Workshop on Numerical Analysis of Dams, Paris, France.

[8] Charlwood, R.G., Solymar, S.V., Curtis, D.D. (1992). A review of alkali-aggregate reactions in hydroelectric plants and dams. Proceedings of the International Conference of Alkali-Aggregate Reactions in Hydroelectric Plants and Dams, CEA and CANCOLD, Fredericton, Canada, pp. 1-29.

[9] Thompson, G.A., Charlwood, R.G., Steele, R.R., Curtis, D.D. (1994). Mactaquac generating station intake and spillway remedial measures. Proceedings of 8th International Congress on Large Dams, Durban, South Africa, Vol. 1, Q. 68, R. 24.

[10] Léger, P., Côté, P., Tinawi, R. (1995). Numerical analysis of concrete dams affected by alkali-aggregate reactions. Proceedings of Research and Development in the Field of Dams, Crans-Montana, Switzerland, pp. 323-334.

[11] Mason, P.J. (1998). Recognising the effects of AAR at dams and hydro plants. Hydropower & Dams, Issue Five, pp. 90-94.

XI ICOLD BENCHMARK WORKSHOP ON NUMERICAL ANALYSIS OF DAMS

Valencia, October 20-21, 2011

THEME A

Rodríguez, Javier[1]

Lacoma, Luis[2]

Martínez, Francisco[3]

Martí, Joaquín[4]

CONTACT
Javier Rodríguez, Principia, Velázquez 94, 28006 Madrid, Spain, +34-912091482, Javier.rodriguez@principia.es

Summary
The Kariba dam is undergoing concrete expansion as a result of an alkali-aggregate reaction. The model adopted to simulate the process is explained in the paper; it is based on the model first proposed by Ulm et al, as later modified by Saouma and Perotti. It has been implemented in the commercial finite element code Abaqus and applied to solve the benchmark problem. The parameters of the model were calibrated using the data recorded up to 1995. The calibrated model was then used for predicting the evolution of the dam up to the present date. Apart from this prediction the paper offers a number of conclusions, such as the fact that the stress level appears to have a major influence on the expansion process; and it presents some suggestions to improve the formulation of the benchmark, such as providing temperature data and widening the locations and conditions of the data employed in the calibration.

[1] Principia, Madrid, Spain.
[2] Principia, Madrid, Spain.
[3] Principia, Madrid, Spain.
[4] Principia, Madrid, Spain.

1. Introduction

Concrete may undergo long term swelling as a consequence of a number of chemical reactions, including alkali-aggregate reactions (AAR). The effects of this undesired expansion are almost inevitably deleterious for the structure. The understanding and the mathematical representation of these processes are not fully satisfactory as yet, hence the relevance of the problem of chemical swelling as an active field of research.

In this context a benchmark problem was proposed to be addressed as Theme A of the 11th Benchmark Workshop organized by the International Commission on Large Dams (ICOLD). The problem is that of interpreting the movements experienced by the Kariba dam for a certain period of time and making predictions for its future evolution based on that interpretation. The present paper presents the work conducted by the authors in relation with the problem posed.

The benchmark problem was formulated by *Noret & Molin* [1]. There is little point in repeating here the information contained in that document about the Kariba dam and its evolution, but it should be clarified that the data used in the work reported here has been taken exclusively from that document.

Investigations of the AAR problem have taken place at least from the late thirties [2] and many structures are known to suffer from this problem today. In particular it affects a considerable number of concrete dams built towards the middle of the 20^{th} century in many places of the world. The pervasiveness of the problem was illustrated by *Charlwood & Solymar* [3] who listed 104 known cases of alkali–aggregate reactions (AAR) in dams worldwide.

A review of the state-of-the-art is clearly beyond the scope of the present paper. But based on the results of past investigations, it can be concluded that the factors that have a major influence in the swelling process in a general case are the following:

- Material components: reactive aggregates and alkali-rich cements are needed, additives may also influence the process.
- Time elapsed: the formation of a hydrophilic gel is not instantaneous, it has a latency time; also, once formed, its swelling via an alkali-aggregate reaction (AAR) involves a characteristic time.
- Environmental conditions: as in many chemical reactions, temperature accelerates the process and, since swelling occurs by absorbing water, moisture conditions play a significant role as well.
- Stress state: high compressive or tensile stresses may affect swelling because of their effects on water pathways, e.g.: by closing cracks or creating spaces for the expanded gel.

The significance of other factors can be considered smaller in comparison with those listed above.

2. Concrete behaviour and expansion models

Following an extensive literature review, the more promising mathematical formulation appears to be that proposed by *Ulm et al* [4], as subsequently modified and extended by *Saouma & Perotti* [5]. Both theories will be described briefly below, since they will be incorporated into a finite element code and used for analyzing the dam.

The modifications by Saouma and Perotti address the anisotropy of swelling induced by the state of stress, which is known to be an important characteristic of the swelling process in many cases, including the case of the Kariba dam. Other authors like *Baghdadi et al* [6] have made alternative proposals for describing the stress-induced anisotropy of the swelling process, but that by Saouma and Perotti appears to account reasonably well for all the relevant effects and has been adopted here.

Before going into the details of the swelling models, it is worth mentioning that the constitutive behavior assigned to the concrete was a damaged plasticity model for tensile cracking and compressive crushing. It is therefore in this mechanical framework that the expansion is assumed to take place.

2.1 Model by Ulm et al

The model by Ulm et al assumes that the reaction develops following an equation of the type:

$$1-\xi = t_c(\xi,\theta)\frac{\mathrm{d}\xi}{\mathrm{d}t} \tag{1}$$

where ξ is the extent of the reaction, t_c is the characteristic time of the reaction, θ is the absolute temperature, and t is the time elapsed. The characteristic time decreases as the reaction progresses:

$$t_c(\xi,\theta) = \tau_c(\theta)\lambda(\xi,\theta) \tag{2}$$

$$\lambda(\xi,\theta) = \frac{1+\exp\left(-\tau_L(\theta)/\tau_c(\theta)\right)}{\xi+\exp\left(-\tau_L(\theta)/\tau_c(\theta)\right)} \tag{3}$$

where τ_c is a characteristic time constant.

The latency and characteristic times are both a function of temperature, following the Arrhenius law that governs thermally activated processes. It may be noticed that the above differential equation can be solved analytically in the isothermal case. The parameters involved in the model, with the values proposed by *Larive* [7], are listed below:

- unidirectional expansion at infinite time: 0 to 0.004
- activation energy of the characteristic time: 5400 ± 500 K
- activation energy of the latency time: 9400 ±500 K

The activation energies are already divided by the Boltzmann constant, thus their K units. Figure 1a shows the physical meaning of the two time constants involved. The latency time is the time elapsed to the point of inflection of the curve that depicts the development of the reaction; it is near, but slightly differs from, the time when 50% of the reaction has taken place. The characteristic time is half of the incremental intercept produced by a tangent drawn at the inflection point. Figure 1b shows the effect of temperature in the progress of the reaction.

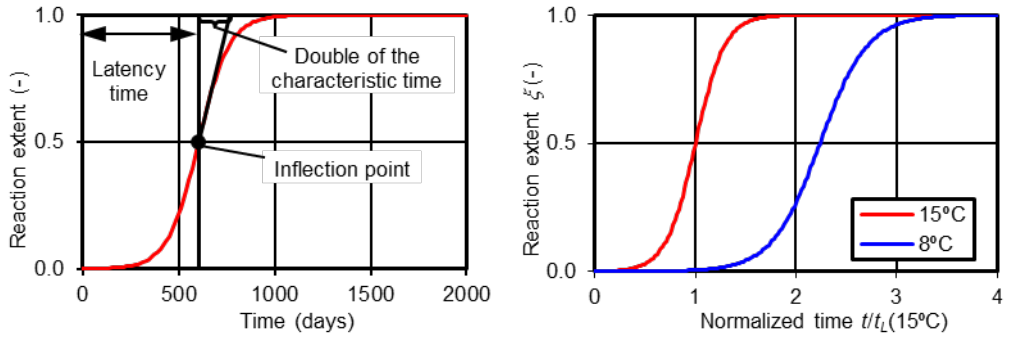

a) Reaction extent at constant temperature

b) Effect of temperature

Figure 1: Reaction extent according to Ulm et al

2.2 Model by Saouma and Perotti

The model by Saouma and Perotti was developed to represent the progress of the AAR, taking the temperature dependence from the model by Ulm et al. Saouma and Perotti propose that the effects of the volumetric reaction in one space direction will be affected by the others, that the preferred directions for expansion will be the least compressed ones, and that high normal stresses will influence the reaction through mechanisms such as providing space for gel expansion, sealing or opening pathways for water migration, etc.

The effects of the stress level are reflected through its influence on the latency time:

$$\tau_L(\theta,\bar{\sigma}) = f(\bar{\sigma})\tau_L^{\mathrm{ULM}}(\theta) \tag{4}$$

$$f(\bar{\sigma}) = \begin{cases} 1 & \text{if } \bar{\sigma} \le 0 \\ 1+\alpha\bar{\sigma} & \text{if } \bar{\sigma} > 0 \end{cases} \tag{5}$$

where $\bar{\sigma} = -(\sigma_I + \sigma_{II} + \sigma_{III})/(3f_c)$ is the normalized pressure, α is an empirical coefficient, for which Saouma and Perotti propose using 4/3 based on the tests by *Multon and Toutlemonde* [8], f_c is the compressive strength, and τ_L^{ULM} is the latency time from Ulm et al.

For the evolution of swelling the following equation is proposed:

$$\frac{\mathrm{d}\varepsilon_{\mathrm{vol}}}{\mathrm{d}t} = \Gamma_t(u_{\mathrm{ck}})\Gamma_c(\bar{\sigma})\xi(t,\theta)\varepsilon_{\mathrm{vol}}^{\infty} \tag{6}$$

where Γ_t accounts for the reduction of swelling caused by cracking with crack opening u_{ck}, Γ_c accounts for the reduction of swelling by compression with a normalized pressure $\bar{\sigma}$, and $\varepsilon_{\mathrm{vol}}^{\infty}$ is the free expansion at infinite time.

The dependence on tensile cracking is incorporated by:

$$\Gamma_t(u_{\mathrm{ck}}) = \begin{cases} 1 & \text{if } u_{\mathrm{ck}} \le \gamma_t w_c \\ \Gamma_r + (1-\Gamma_r)\dfrac{\gamma_t w_c}{u_{\mathrm{ck}}} & \text{if } u_{\mathrm{ck}} > \gamma_t w_c \end{cases} \tag{7}$$

where γ_t governs the reduction of expansion in tension, Γ_r is the coefficient of residual expansion in tension, w_c is the maximum crack opening in the tensile softening curve. The effect of compression is introduced as:

$$\Gamma_c(\bar{\sigma}) = \begin{cases} 1 & \text{if } \bar{\sigma} \le 0 \\ 1 - \dfrac{e^{\beta}\bar{\sigma}}{1+(e^{\beta}-1)\bar{\sigma}} & \text{if } \bar{\sigma} > 0 \end{cases} \tag{8}$$

where β is an dimensionless parameter.

Apart from determining the volumetric expansion, the model must also distribute it among the three space directions. For example, in uniaxial tension, the amount of chemical swelling would be identical in all directions; but in uniaxial compression, with the stress above a certain threshold σ_u, the chemical expansion would only occur in the two transverse directions. Figure 2 shows how the model distributes the expansion in the various stress states.

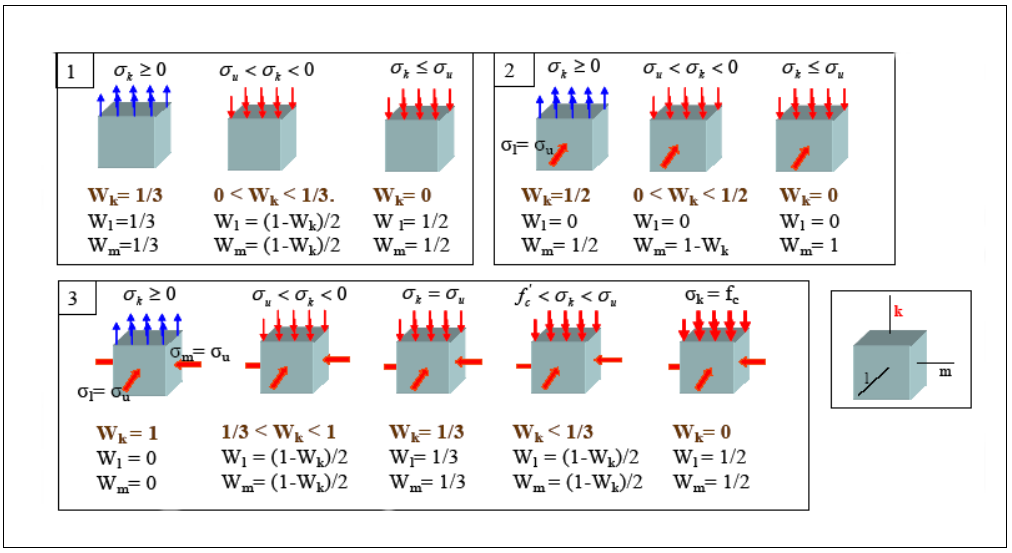

Figure 2: Distribution of expansion after Saouma and Perotti

3. Numerical implementation

The model by Saouma and Perotti described in the previous section was implemented in Abaqus/Standard [9]. For this purpose a user subroutine was created to determine incrementally the imposed deformations caused by both the expansive chemical reaction and thermal dilation. Such increments are a function of temperature, progress of the reaction, pressure, and crack opening.

The calculation requires information about the principal stresses and directions and must be combined with the plasticity and the continuous damage model of the concrete. State and field variables are updated in another user subroutine and moisture is introduced as an independent field variable. The rest of the variables are updated at the beginning of each time step, thus in an explicit scheme, but are extrapolated to mid-step from their most recent values. The size of the time step may therefore play an important role and the sensitivity to this parameter should be studied for each specific application. For cases such as discussed in the present paper, experience indicates that generally 2 weeks is an adequate time step. Other subroutines were also written to impose yearly periodic boundary conditions for thermal analyses and to vary the hydrostatic pressure.

4. Application to the Kariba dam

4.1 Approach adopted

When modeling swelling problems, a rigid connection between concrete and rock would give rise to unrealistic stress concentrations at the interface. This led to adopting the finite element mesh Model2.mesh, excluding the JOIN elements because in Abaqus contact surfaces are defined as element faces. The friction coefficient assumed is 1.4. The mesh, shown in Figure 3, is composed of 1278 second-order brick elements with reduced integration, 238 second-order wedge elements, and 2 second-order tetrahedrons. The total number of variables is 23427.

The stress field at the end of construction is obtained using a reduced elastic modulus in the hoop direction (1% of the real value), thus forcing the dam to behave as a series of independent cantilevers. During this initial phase the dam is tied to the rock because no debonding is expected. The stress field determined is then imported as the initial state for subsequent analyses during operation.

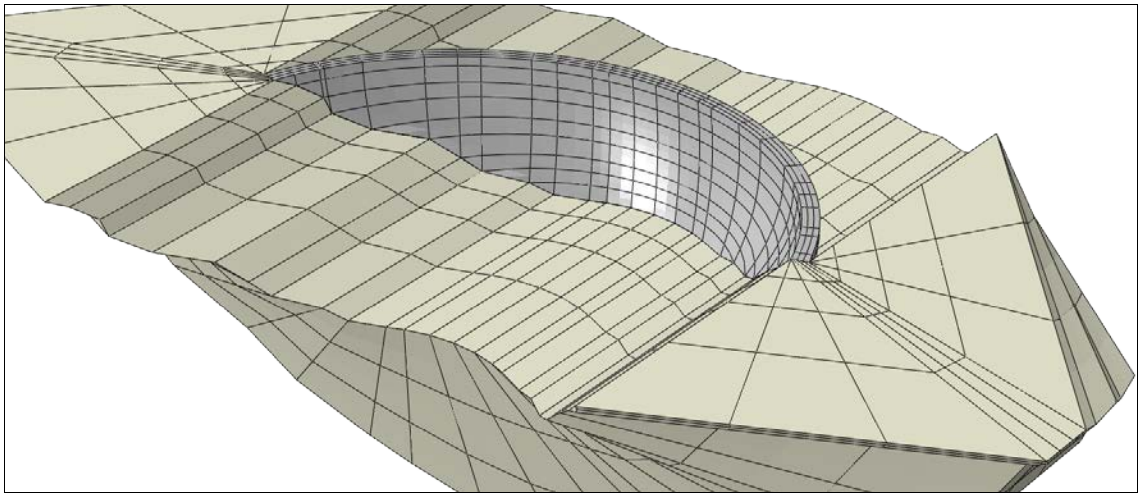

Figure 3: Finite element mesh

The histories of recorded movements provided do not really allow an accurate calibration of any logistic curves, as would be required to estimate the time constants. Because of this difficulty the rate of unidirectional free expansion has been assumed to remain constant over the period of interest. In practice this is equivalent to simplifying the model proposed by Saouma and Perotti to:

$$\frac{\mathrm{d}\varepsilon_{\mathrm{vol}}}{\mathrm{d}t} = \frac{3\Gamma_c(\bar{\sigma})\dot{\varepsilon}_0}{f(\bar{\sigma})} \tag{9}$$

where $\dot{\varepsilon}_0$ is the rate of unidirectional free expansion.

Since most of the concrete would be expected to remain in compression, there is essentially no need to consider the effects of tensile stresses in the expansion. Once the increment of volumetric expansion is determined, it is distributed among the three instantaneous principal directions as in the original model. The compressive and tensile strengths of concrete have been taken as 25 MPa and 2 MPa, respectively.

The values proposed by Saouma and Perotti for the expansion parameters have been adopted, namely α = 4/3 and σ_u = -10 MPa. However, two of the parameters were calibrated based on the data: $\dot{\varepsilon}_0$ and β, the parameter that governs the reduction of expansion with compression. The calibration was based on the data produced during the period 1982-1995 for the radial displacement of target T434 and in the crest leveling survey. The specific time period was selected because at earlier times the evolution may be affected by other phenomena, such as transient temperatures and creep; also, it directly precedes the prediction period and, furthermore, the water levels in the reservoir can be taken to be constant, equal to 479.9 m.

For predicting the evolution during the period 1995-2010, the actual water levels in the reservoir were introduced to the analyses via a user subroutine without any time averaging.

One final consideration is in order. The formulators of the benchmark problem appear to believe that, because ambient temperatures are reasonably constant in the area, any thermal effects on the swelling process can be disregarded. With all due respect to their long experience in analysing the Kariba dam, this hypothesis is unlikely to be a good representation of reality. The process is so sensitive to temperature that minor temperature changes would have noticeable consequences; for example, differences in insolation, which are certain to occur in a double-arch dam, or in the

upstream and downstream conditions, would suffice to generate such effects. Good temperature data in the concrete would most probably allow improving the quality of the numerical simulation.

4.2 Results produced

The first results presented are those generated by construction and by imposing the pressure field corresponding to a water level 483.8 m, which represents the average during the initial high level period. The resulting distributions of stresses and displacements are presented in Figures 4 and 5, respectively.

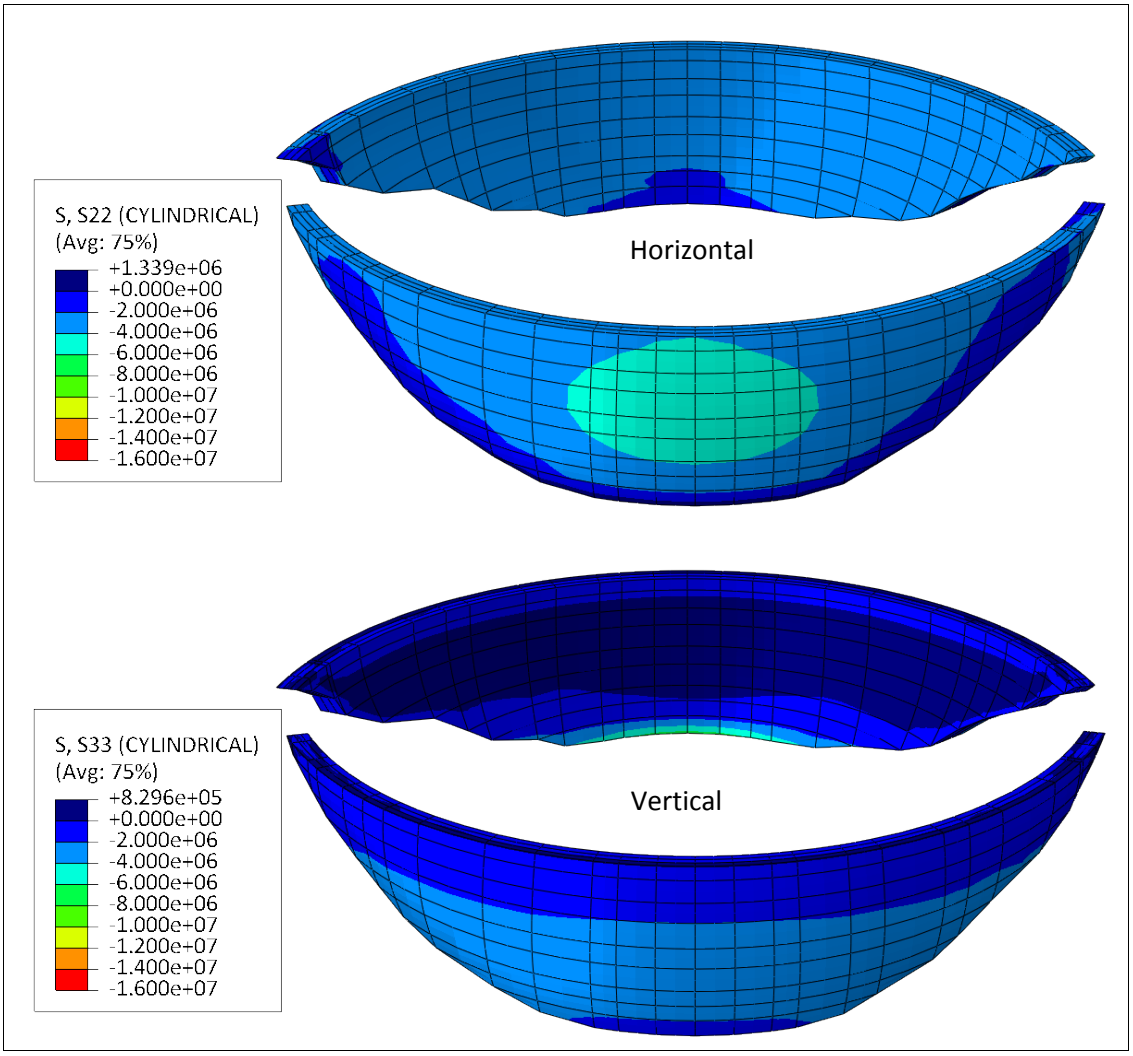

Figure 4: Stresses in 1963 with water level at 483.8 m (Pa)

The parameters of the expansion law are then calibrated using the data from the surveys, assuming the averaged water levels shown in Figure 6. The formulators of the benchmark state that the zero values of the series cannot be considered reliable, thus the curves obtained by simulation can be translated vertically to match the experimental data. In other words, the calibration of the parameters is only based on the slopes of the series, without relying on the zero values.

Using the above strategy, the parameter values that result from the calibration are $\beta = 4$ and $\dot{\varepsilon}_0 = 39$ με/year. When those values are used, the calculated and experimental slopes for all the data series are very close over the calibration period, as can be seen in Figures 7 and 8.

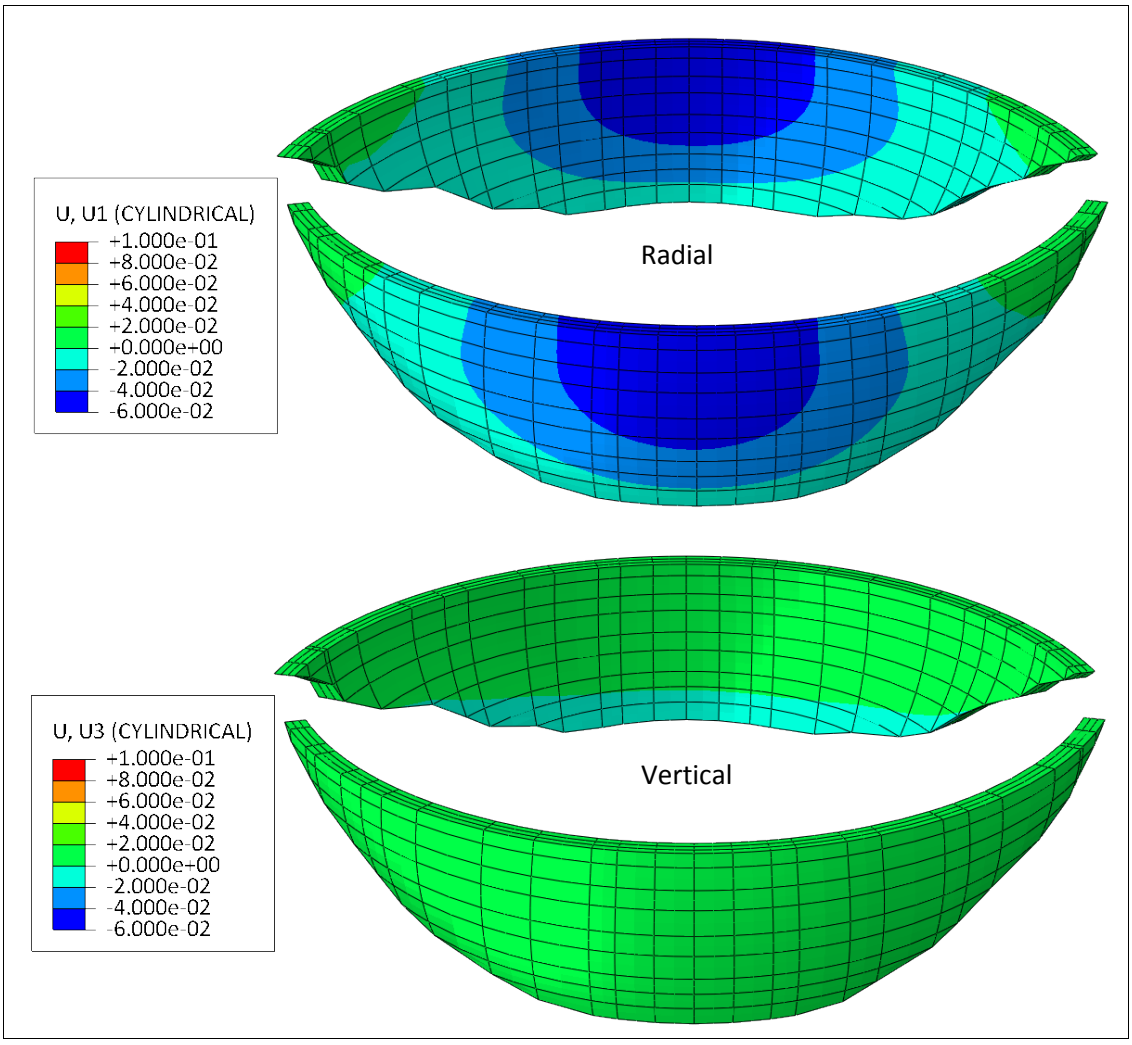

Figure 5: Displacements in 1963 with water level at 483.8 m (m)

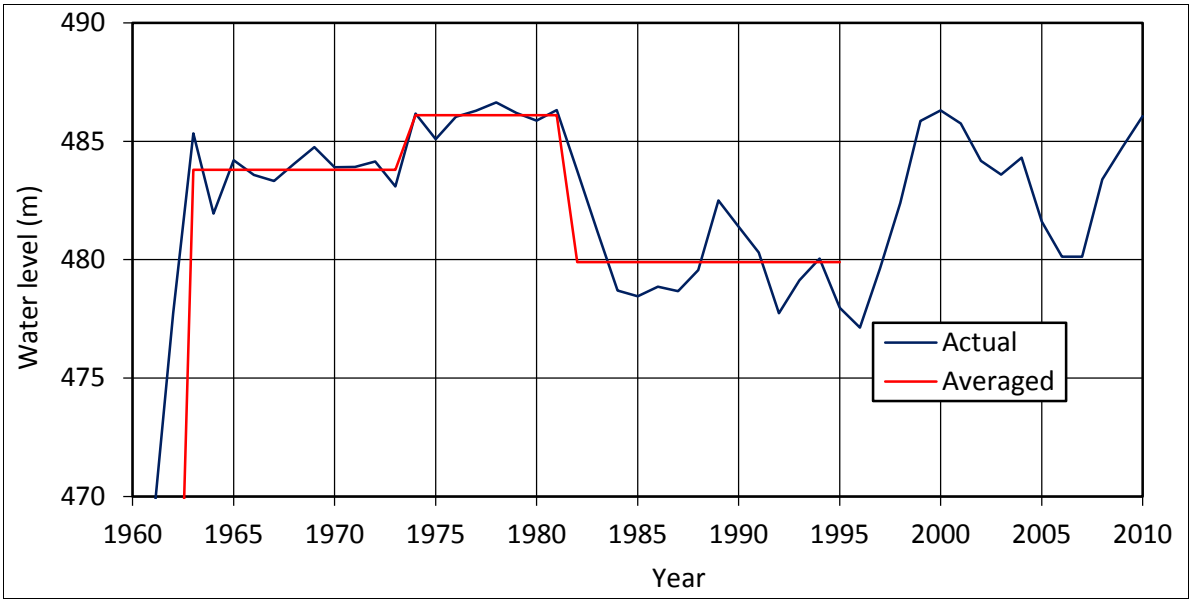

Figure 6: Water level

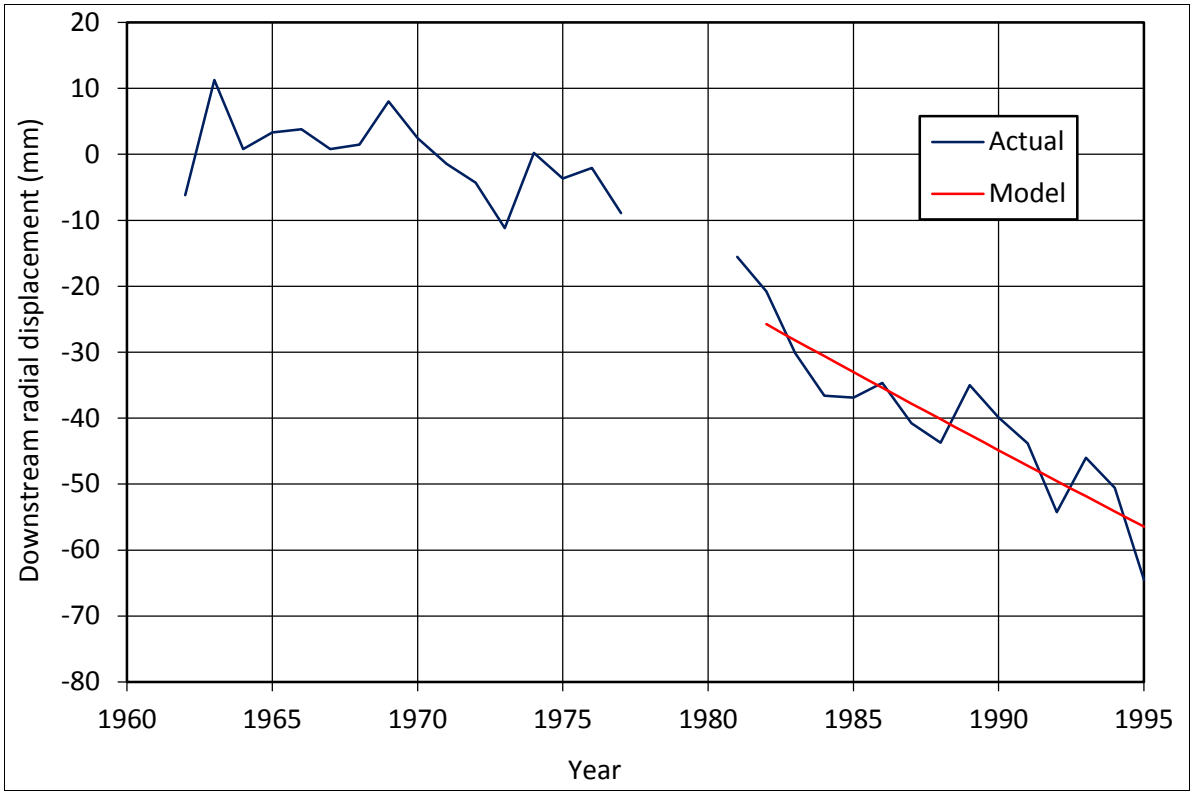

Figure 7: Radial displacements during the calibration period

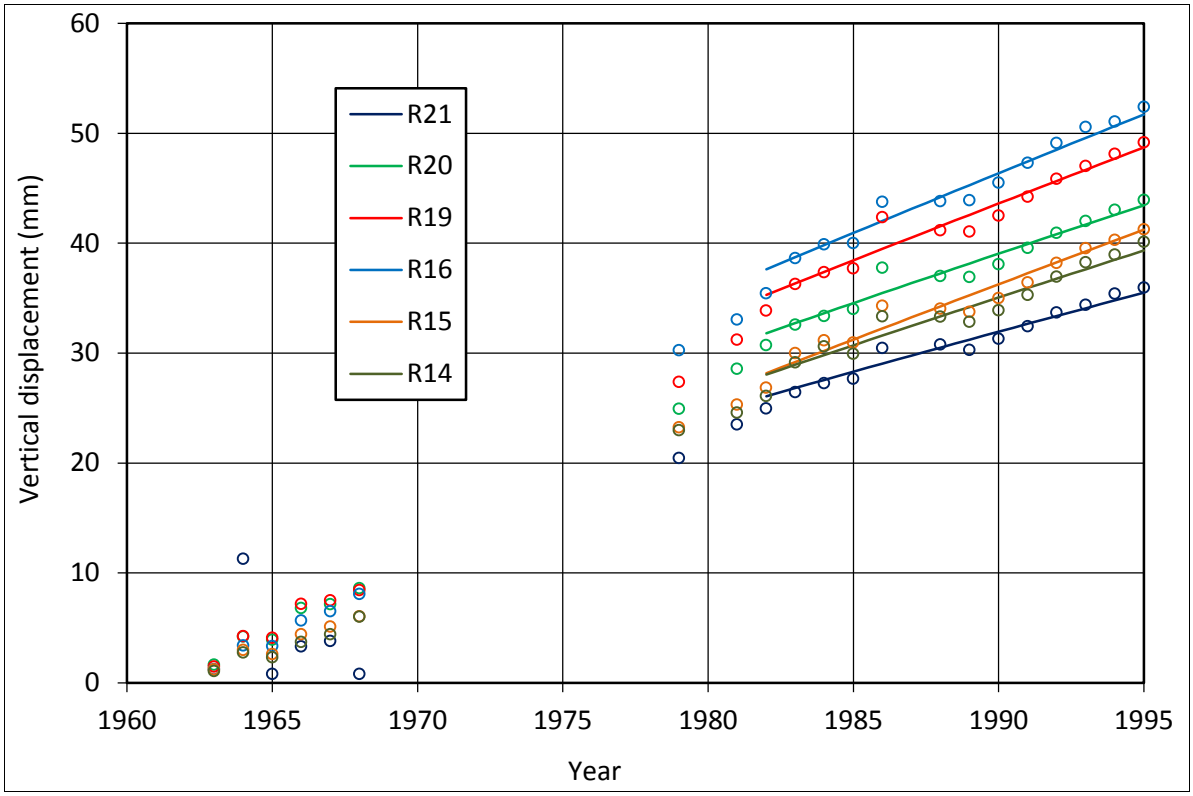

Figure 8: Vertical displacements during the calibration period

It is also of interest to determine, using the calibrated values of the parameters, the rate of unidirectional expansion that would result for concrete cores subjected to different levels of uniaxial compression. The expansion rates calculated are plotted in Figure 9 as a function of the stress level.

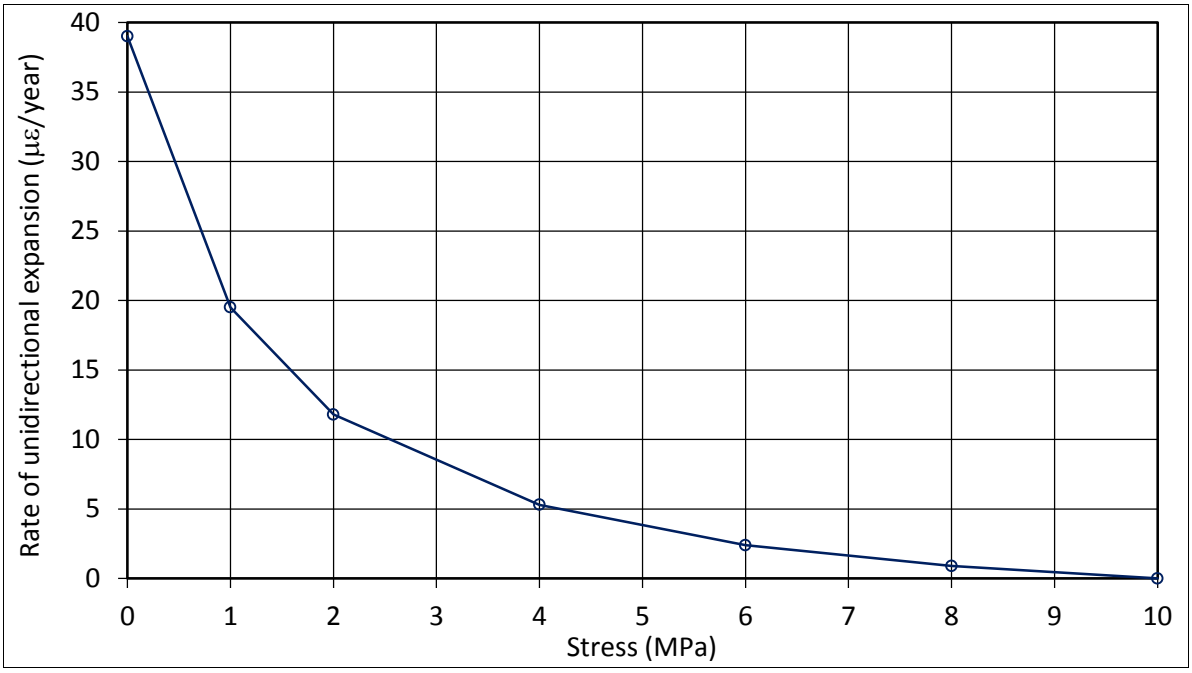

Figure 9: Rate of expansion under compression

Using those values of the calibrated parameters, predictions have also been made as to the likely conditions in 2010. The distributions of stresses and displacements at that time are respectively shown in Figures 10 and 11.

The calculated expansions along the three space directions, again for the year 2010, are provided in Figure 12. As could be expected, those expansions are greater in the radial and vertical directions than in the hoop direction; this is a consequence of the greater levels of compressive stresses that develop in the hoop direction.

The predicted evolution of the radial displacements for the period 1995-2010 is presented in Figure 13. Similarly, the evolution of the various vertical displacements appears in Figure 14 for that same time period.

As a final comment, the amount of information given for conducting the benchmark is considered to be somewhat scarce. The unreliability of the zero values, the lack of temperature data, and the number of locations where data are provided illustrate that scarcity. The end result is that the range of conditions covered by the calibration is relatively narrow, giving the possibility that other models, even some conceptually quite different, might provide a similar match.

5. Conclusions

Having introduced in Abaqus/Standard the simplified expansion model originally described by Ulm et al, including the modifications and expansions later proposed by Saouma and Perotti, its parameters were calibrated to fit the movements detected in the Kariba dam up to 1995. The resulting model was then used to predict the future evolution of the dam.

As a consequence of the work conducted, the following conclusions can be offered:

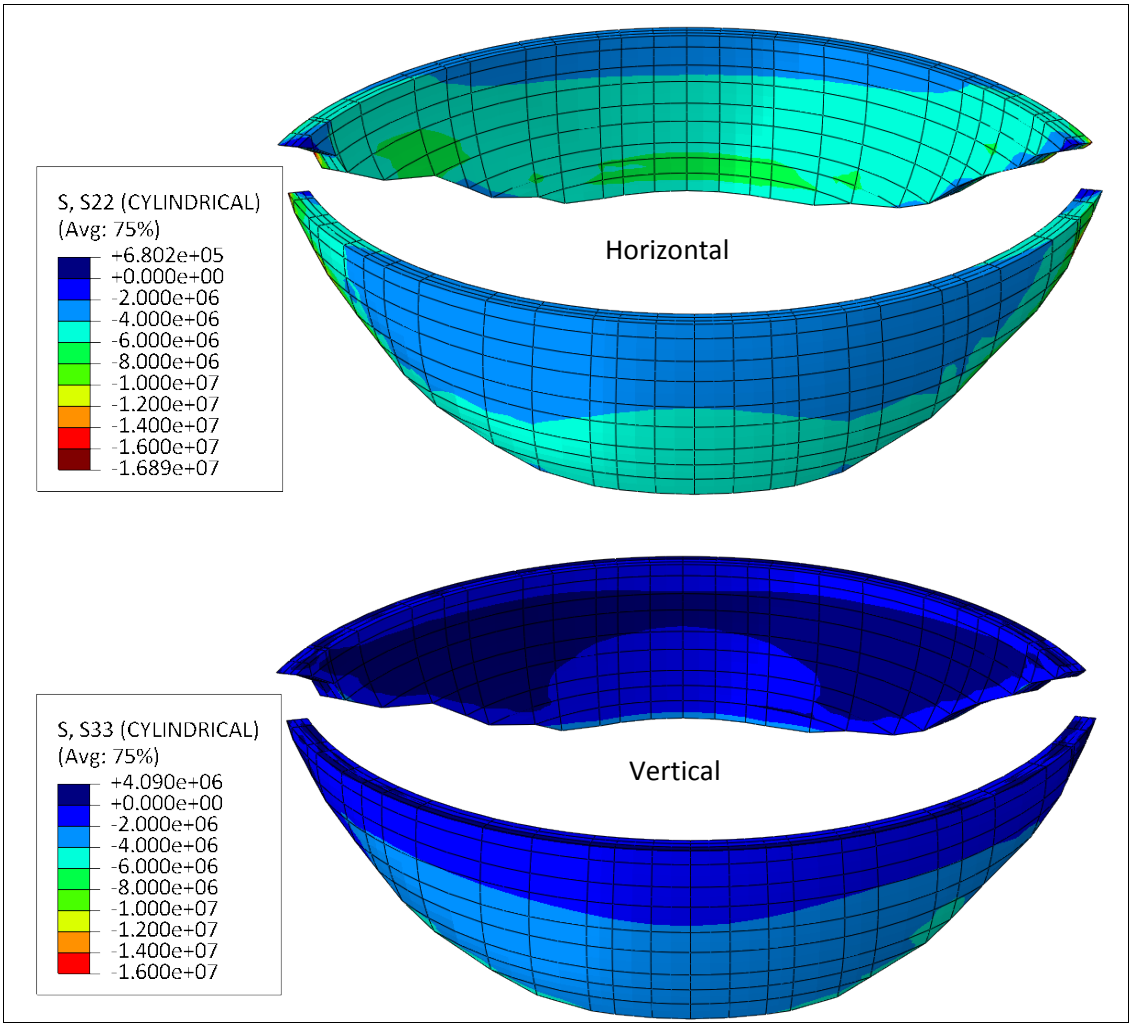

Figure 10: Stresses in 2010 with water level at 482.7 m (Pa)

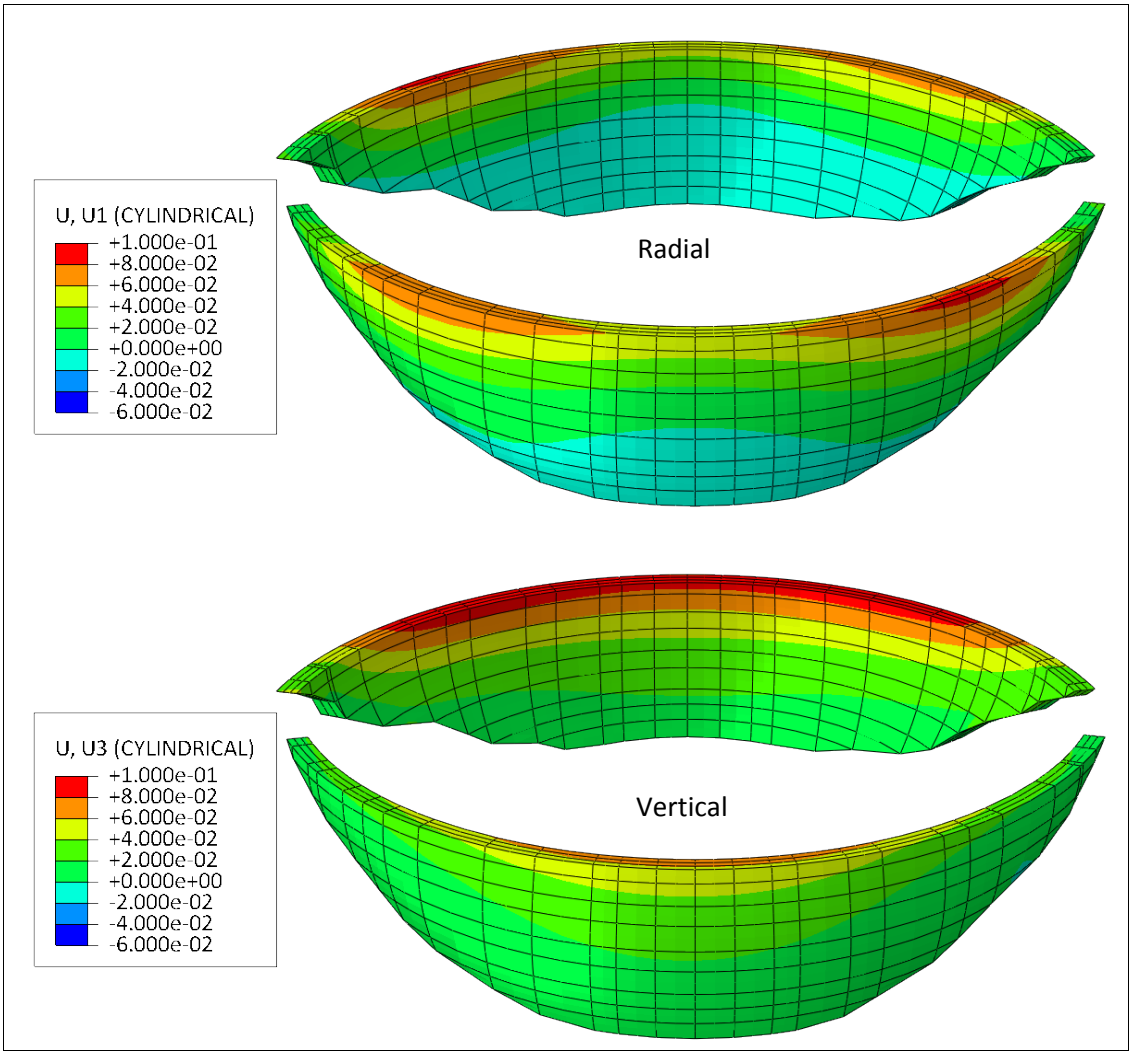

Figure 11: Displacements in 2010 with water level at 482.7 m (m)

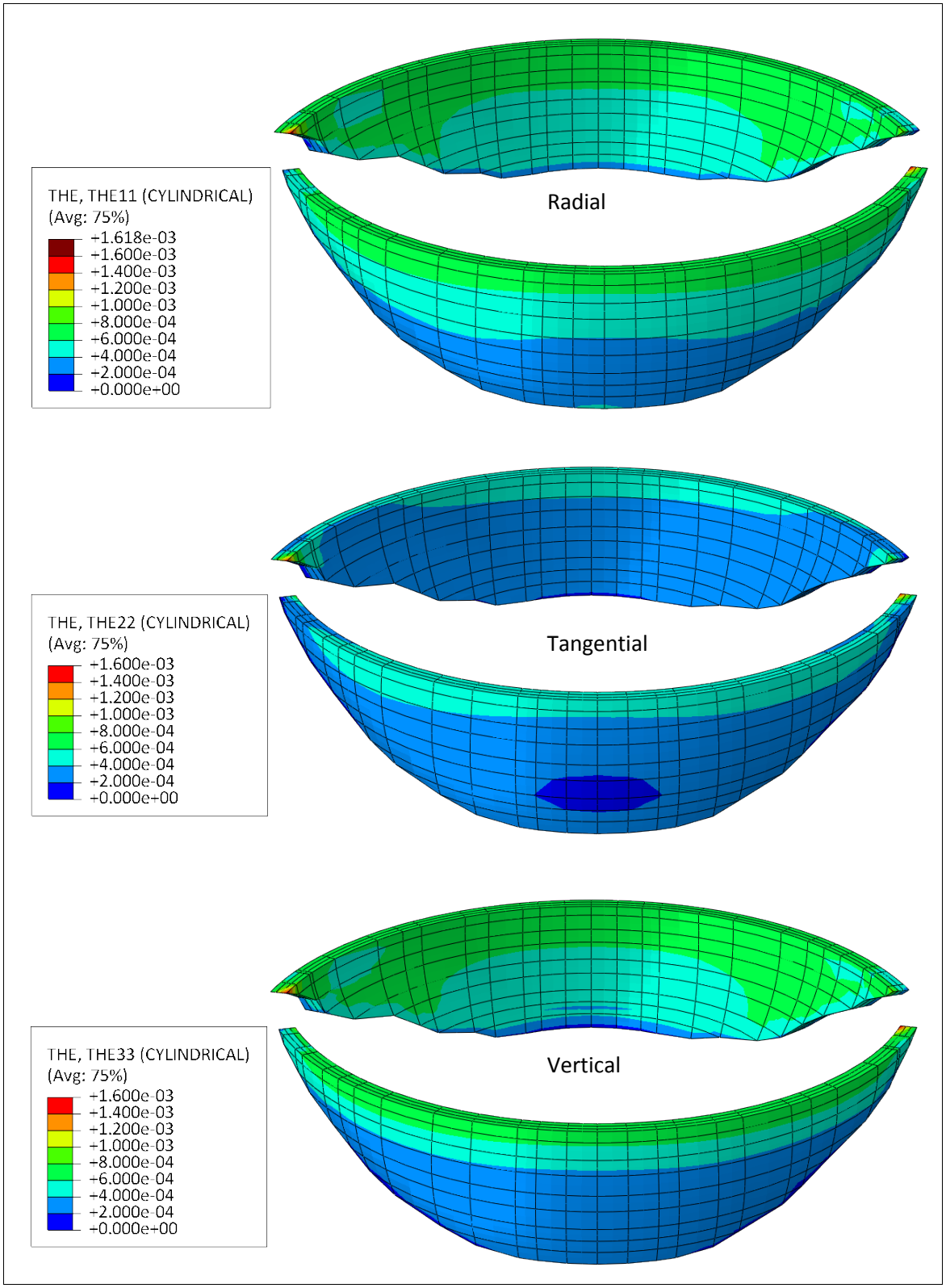

Figure 12: Expansion along each direction in 2010 (-)

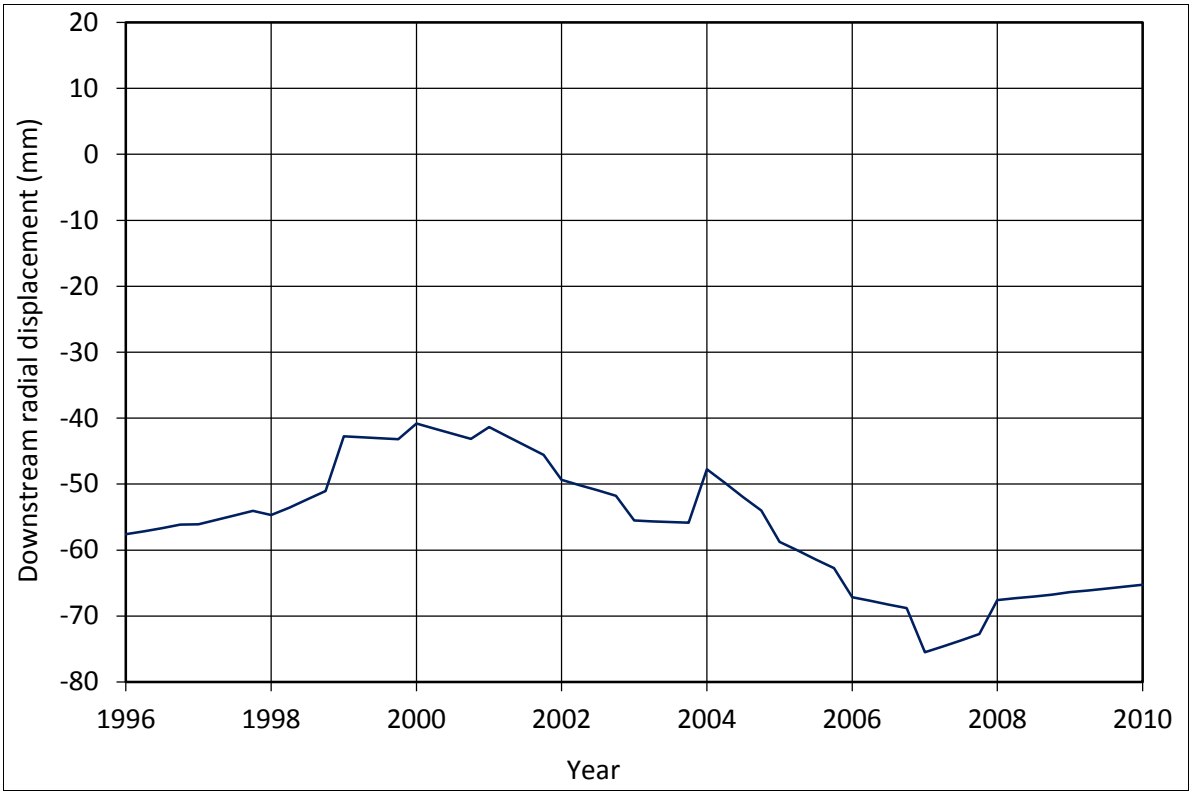

Figure 13: Radial displacements during the prediction period

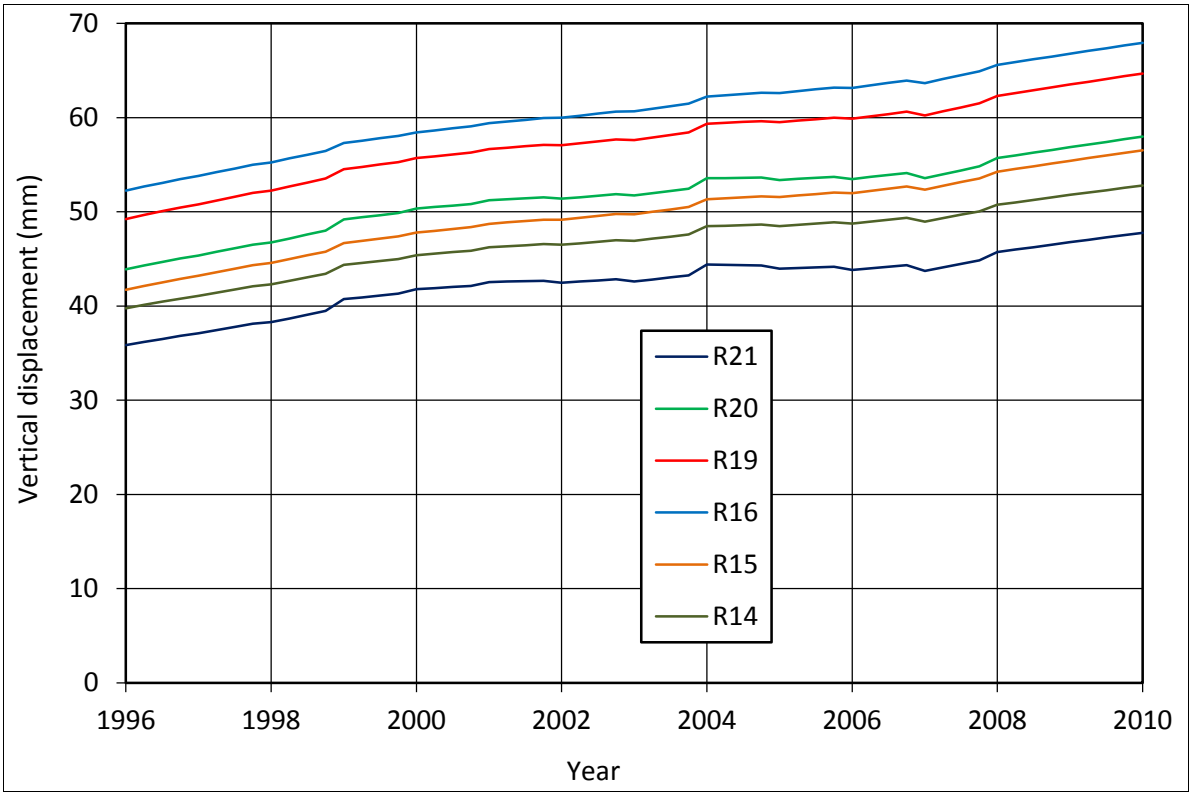

Figure 14: Vertical displacements during the prediction period

- The unidirectional rate of expansion for uncompressed concrete is around 39 με/year during the periods studied.
- The rate of expansion is very sensitive to the existing level of compression. By way of example the unidirectional rate of expansion decreases to only 5 με/year under compressive stresses of 4 MPa.
- As a result, the concrete expansion undergone is considerably greater in the radial and vertical directions than in the hoop direction, where expansion leads to a greater levels of compression.

Finally, in spite of the relatively small variation of the local temperatures during the year, it is suspected that these may play a non negligible role. The process is so sensitive that minor temperature changes would have noticeable consequences; for example, differences in insolation, which are certain to occur in a double-arch dam, or in the upstream and downstream conditions, would suffice to generate such effects. Good temperature data in the concrete would most probably allow improving the quality of the numerical simulation. The calibration would also improve if the data supplied covered a wider range of conditions.

References

[1] Noret, C. and Molin, X. (undated). "Theme A. Effect of concrete swelling on the equilibrium and displacements of an arch dam. October 17-18, 2011, Valencia, Spain".

[2] Stanton, T.E. (1940). "Expansion of concrete through reaction between cement and aggregate". In: Proc. of the American Society of Civil Engineers, Vol. 66, pp. 1781-1811.

[3] Charlwood, R. G. and Solymar, Z. V. (1995). "Long-Term Management of AAR-Affected Structures - An International Perspective", In: Proc. of the 2nd International Conference on Alkali–Aggregate Reactions in Hydroelectric Plants and Dams, US Committee on Large Dams, Chattanooga, Tenn., October 22-27, pp. 19-55.

[4] Ulm, F.-J., Coussi, O., Keifei, L, and Larive, C. (2000). "Thermo-chemo-mechanics of ASR expansion in concrete structures, ASCE Journal of Engineering Mechanics, Vol. 126, no.3, pp. 233-242.

[5] Saouma, V. and Perotti, L. (2006). "Constitutive model for alkali-aggregate reactions", ACI Materials Journal, Vol. 103, no. 3, pp. 194-202.

[6] Baghdadi, N., Toutlemonde, F., and Seignol, J.F. (2007). "Modélisation de l'Effet des Contraintes sur l'Anisotropie de l'Expansion dans les Bétons Atteints de Réactions de Gonflement Interne", XXVèmes Rencontres Universitaires de Génie Civil, Association Universitaire du Génie Civil, Bordeaux, France, 23-25 May.

[7] Larive, C. (1998). "Apports combinés de l'experimentation et de la modelélisation à la compréhension de l'alcali réaction et ses effets mécaniques", Études et Recherches des LPC OA 28. Laboratoire Central des Ponts et Chaussées, Paris, France.

[8] Multon, S. and Toutlemonde, F. (2006). "Effect of applied stresses on alkali-silica reaction-induced expansions", Cement and Concrete Research, Vol. 36, pp. 912-920.

[9] SIMULIA (2010). *"Abaqus Users' Manual",* Version 6.10, Providence, RI.

XI ICOLD BENCHMARK WORKSHOP ON NUMERICAL ANALYSIS OF DAMS

Valencia, October 20-21, 2011

THEME A

Grimal, Etienne[1]

Moles-Dimartino, Jaime[2]

CONTACT

Etienne GRIMAL, Eléctricité de France, Centre d'Ingénierie Hydraulique, EDF-CIH Technolac 73373, le Bourget du Lac Cedex, France, etienne.grimal@edf.fr, +33(0)479606174

Summary

Modeling the behavior of alkali aggregate reaction (AAR) damaged concrete is made complex by the large number of elementary physical phenomena to be taken into account (concrete reactivity, thermal activation, moisture dependence, concrete rheology, and damage interaction). This paper presents the elementary physical principles that lead to the formulation of a visco-elasto-plastic orthotropic damage model including chemical pressure induced by AAR. Particular attention is also paid to the modeling of moisture effects on AAR development and on the influence of creep on the behavior of affected structures. The constitutive modeling proposed is developed into the framework of an anisotropic damage theory to realistically model the strong cracking anisotropy and swelling observed on affected structures.

The ICOLD propose trough the Benchmark Workshop an exercise of real swelling, Kariba Dam, to be modeled. After a calibration phase, on only one observed structural displacement rate at a given period, the model is used to predict the dam behavior and is validated through the comparison between the displacement of instrumented points predicted by the calculations (not used for fitting) and the variations measured on the dam. The main results concern the capability of the model to reproduce simultaneously strong anisotropic swelling, damage observed, and structural displacements. Finally, calculations were performed to predict the future displacements, stresses evolutions and damage fields of the dam.

Keywords: Benchmark workshop, ICOLD, Kariba's dam, Alkali Aggregate Reaction, swelling, numerical model, finite elements, creep.

[1,2] EDF, Hydro Engineering Centre, civil engineering department, 73373 Le Bourget du Lac, France

1. Introduction

The main objective of the Benchmark Workshop is to compare the different existing theories and models which allow us to represent and to predict the real swelling process which takes place in dams all over the world. At the present time, no international mutual agreement has been found to model this well known pathology. Therefore, a subject has been proposed to solve a real swelling case.

The Alkali Aggregate Reaction (AAR) causes considerable damage in concrete structures and is responsible for irreversible expansion and cracking which can affect their functional capacity. In consequence, AAR poses maintenance problems for firms in charge of the dams. In this way, the study of this reaction seems important to reassess the durability and the security of these constructions, or to predict the evolution of the reaction in the following years. Unconventional concrete structures lead us to consider the finite element numerical analysis as a possible alternative to model the AAR.

Following this purpose, the civil engineering and structures department of EDF-CIH, in collaboration with LMDC Toulouse, has developed a numerical model [1],[2] which allows to predict the swelling process due to AAR, in concrete structures, and to improve the structures maintenance of EDF is responsible for. The model considers both physical and chemical effects which are evolving in the cement paste.

The constitutive model is based on a global rheological scheme which considers the porous pressures, by drying or other intra-porous phenomena (such as AAR), the external loading, and the concrete matrix as a representative elementary volume where the coupling between the swelling, creep and anisotropic damage takes place.

The model has been compared to experiments, in order to check its robustness [1],[2]. After calibration of model's parameters, results provide a satisfactory prediction of AAR evolution and of the structure's performance on a long term.

The 11^{th} Benchmark Workshop, which takes place in Valencia, proposes in Theme A, a real swelling exercise caused by the AAR (Alkali Aggregate Reaction) in the Kariba dam (Zimbabwe). The data provided by the organization helped us to calibrate the numerical model proposed by EDF and to predict the posterior performance of the dam until 2010.

2. Model description

The main developments brought by this model concern interactions between AAR pressure and long term strain (creep) on the one hand, and the swelling anisotropy induced by oriented cracking on the other hand. Particular attention is also paid to model moisture effects on both AAR and long term strains (shrinkage). The AAR swelling dependence on the stress state is then a consequence of all these elementary phenomena [1], [2]. Hence, the mechanical effects of AAR are the consequences of a long-term internal loading due to chemical pressure (P_g in Fig. 1). In addition to external loading, Pg loads concrete, which is considered as a visco-elasto-plastic-damaged medium (module VEP+VD^t in Fig. 1). Several authors [4] have suggested that the basic creep of concrete is mainly due to the C-S-H behavior (CSH sliding and consolidation).

Therefore, we have developed a Visco-Elasto-Plastic (VEP) orthotropic damage model including chemical AAR pressure. To model CSH sliding and consolidation the model is separated into

two levels: a first rheological level (VEP) based on a division of the strain and stress state in a spherical part (module VEPs) and a deviatoric part (module VEPd). The response of the CSH structure under hydrostatic stress (consolidation) is modeled by the spherical part, while the deviatoric part takes into account CSH sliding (without volumetric change) under shear stress.

A second plastic level (VD^t), linked to an orthotropic AAR traction damage model, allows us to model large strains encountered into AAR problem. P_w is the capillarity pressure present in the porosity of the concrete. The plastic level (VD^t) allows relaxation of self equilibrated tensile stresses induced by the gel pressure around reactive aggregates in order to regulate the tensile damage. The rheological module (VEP^s and VEP^d) also contributes to the tensile damage mitigation and allows a realistic modeling of triaxial compressive creep.

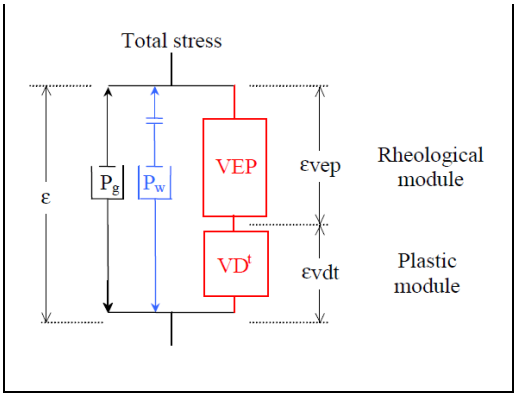

Figure 1: Rheological model principle

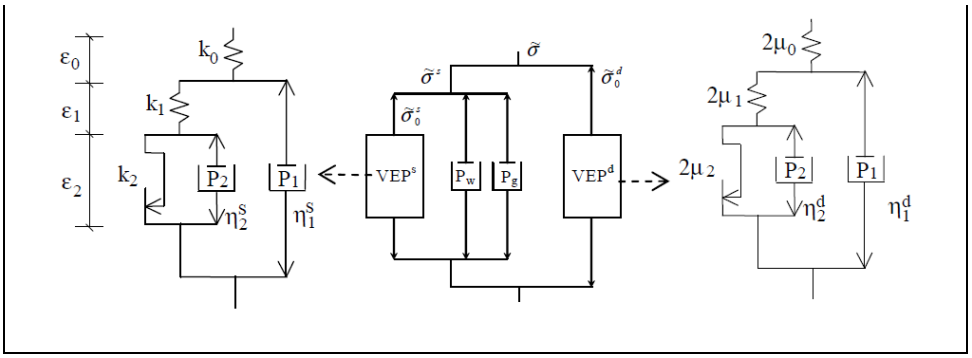

Figure 2: Visco elasto plastic module (VEP) with his Spherical part CSH consolidation and his deviatoric part CSH sliding.

2.1. Rheological module

The detailed spherical and deviatoric rheological schemes are represented in Fig 2. It takes into account the multiscale porous structure of the cement paste: '1' refers to the micro capillary porosity while '2' to the CSH inter layer porosity. The constitutive relations used for each module are basically the same, differences remaining in the fitted coefficients used.

2.2. AAR Plastic module

This VD^t module takes into account an increase of plastic strain when the concrete is submitted to tensile stresses induced by AAR. The AAR plastic strain rate is given by equation 1 [5] :

$$\varepsilon_{vdt_i} = \varepsilon_0 \frac{d_i^{AAR}}{1 - d_i^{AAR}} \tag{1}$$

In this phenomenological equation, ε_0 is a parameter obtained by experimental results; d^{AAR} is the AAR damage. According to the previous work [3] the damage eigen values are estimated with effective tensile stresses evaluated in the rheological model, following Eq. 2:

$$D_{AAR} = 1 - \exp\left[-\frac{1}{m} \left(\frac{\min(\tilde{\sigma}, b_g.P_g)}{\tilde{\sigma}_u} \right)^m \right] \tag{2}$$

Where σ is a principal effective tensile stress governed by the Rankin orthotropic criterion, $b_g.P_g$ is the gel pressure effect on the concrete skeleton (Pg is the gel pressure defined below and b_g is a constant parameter playing the same role of the Biot coefficient in the porous mechanic theory). m and σ_u are damage evolution law parameters. The constitutive law linking the different states variables of the model is defined by:

$$\sigma = (1-D) : \left(\underbrace{C^0 : (\varepsilon - \varepsilon_{vep} - \varepsilon_{vp} - \varepsilon_{th})}_{\tilde{\sigma}} - (b_g P_g + b_w P_w) I \right) \text{ with } D = \max(D_{AAR}, D_{mech})$$
$$\text{and } D_{mech} = 1 - \exp\left[-\frac{1}{m} \left(\frac{\tilde{\sigma}}{\tilde{\sigma}_u} \right)^m \right] \tag{3}$$

The Eq. 3 links all the state variables which compose the model, in this law, σ is the apparent stress, C_0 the stiffness matrix of sound material, ε the total strain, ε_{vep} the total creep and shrinkage strains, ε_{th} the thermal strains, b_wP_w the water pressure effect and b_gP_g the AAR gel pressure effect.

2.3. Modeling of alkali aggregate reaction

The gel pressure modeling is based on the assumption of uncoupling between stress and AAR gel formation. Eq. 4 gives the swelling pressure induced by AAR "P_g" [1,2]:

$$P_g = M_g \left[A V_g - \left(A_0 V_g + b_g tr\varepsilon \right)^+ \right]^+ \tag{4}$$

Where M_g is an elastic modulus, b_g is an effective strain coefficient, V_g is the maximum gel volume fraction that can be created by the AAR and $(\,)^+$ is the positive part of equation. A is the chemical advancement of the reaction (increasing from 0 to 1); A_0V_g is the gel volume necessary to fill the porosity connected to the reactive aggregates. Eq. 5 determine the chemical advancement thank to a law inspired from Poyet's works [6]:

$$\dot{A}(Sr,t) = \alpha_0 . \exp\left[\frac{Ea}{R}\left(\frac{1}{T_{ref}} - \frac{1}{T_{corr}}\right)\right] . \frac{\left(Sr - Sr^0\right)^+}{1 - Sr^0} . [Sr - A(Sr,t)] \quad (4)$$

Where α_0 is a relevant parameter for the kinetics, E_a is the activation energy of the AAR, R the gas constant, T_{ref} is the absolute temperature of the test where α_0 is evaluated and T_{corr} is the temperature where the test is carried out. S_r and S_{r0} are, respectively the current saturation degree, and the smallest saturation degree necessary to allow the chemical reaction.

3. Kariba's dam modeling

In order to study the swelling phenomena, the model previously described will be applied on Kariba's dam.

Several important hypotheses have been assessed and, even though they let us simplify the problem to keep it within reasonable limits of difficulty, the results obtained cannot be taken, obviously, as exact to reality.

The AAR induces important displacements in the dam, but others phenomenon as basic creep, shrinkage have to be evaluated to consider long term deformations in the structure.

All deformation causes are integrated in a single model to obtain the total displacement considering their interaction and allows computing of damage and stresses evolutions. Nevertheless, we do not have all the necessary data for modeling these phenomena (creep and shrinkage tests).

The purpose will be to understand the reaction and understand the possible divergences.

3.1. Hypothesis and data

Before using the model, exercise sets data to follow :

First of all, dam's structure is composed by 26 independent concrete cantilevers (41 in reality), which are modeled in the proposed mesh,

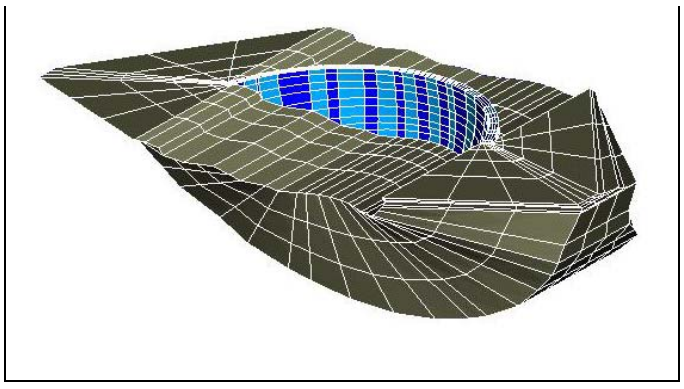

Figure 3: Mesh view in Salome

To continue, dam's temperature remains uniform and constant during all the computation. The picked temperature is the average dam temperature since its building that is 27°C,

The real water level is considered in the model (Fig. 4),

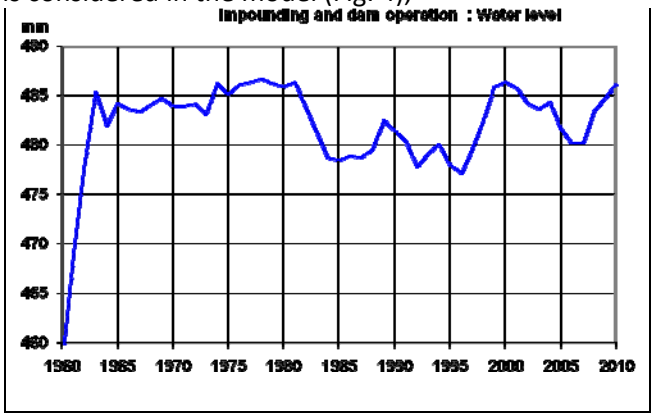

Figure 4: Water level

To model the behavior of the structure, some assumptions are necessary:

1. The first measures started in 1963, so the experimental data doesn't consider the displacements caused by the first impoundment of Kariba's dam. The first point of monitoring will be reset on the displacement curve obtained by the model,
2. The points 3-5 and 0-2 of monitoring are not representative of the whole dam structure movement,
3. In spite of a better procedure to calibrate the damage by breaking samples of concrete from the Kariba dam in the laboratory, we are going to consider usual damage parameters for the concrete,
4. The model integrates different displacement effects apart from the AAR, such as creep and shrinkage. However, some data are missing to correctly calibrate creep and shrinkage effects in safe concrete. Therefore, two hypothesis emerge :
    - The maximal displacements due to shrinkage occur a few days after the setting of concrete. After four years (the dam was finished in 1959 and the time period of measurement began in 1963) the effects of shrinkage will be minimal. Therefore, the shrinkage effects are ignored, considering they have no repercussion in the model,
    - However, the creep can't be avoided in a long term modeling. We must investigate it for a true representation of the phenomena developing in healthy Kariba Dam. However, we do not have the necessary data to indentify creep parameters and therefore, we will assume that they are equal to those obtained in Temple-sur-Lot dam which is under the supervision of EDF.

3.2 Mechanical properties of materials

For the exercise, the mechanical properties of concrete are summarized in table 1 :

Table 1: mechanical properties of the dam

E (modulus of elasticity)	22 (GPa)
NU (Poisson's ratio)	0.2
RHO (unit weight)	2350 (KN/m)

Table 2 gives the mechanical properties of rock foundation.

Table 2: mechanical properties of the rock

E (modulus of elasticity)	10 (GPa)
NU (Poisson's ratio)	0.2
RHO (unit weight)	Not considered

In spite of creep parameters calibration (cf. assumption), the table 3 exposes the creep properties of concrete.

Table 3: creep parameters

K_RS (long term modulus of reversible compressibility)	7245 MPa
K_IS (long term modulus of reversible compressibility)	12455 MPa
ETA_RS (viscosity associated to K_RS)	353990 MPa·mois
ETA_IS (viscosity associated to K_IS)	10843893 MPa·mois
K_RD (long term modulus of irreversible shear)	10868 MPa
K_ID (long term modulus of irreversible shear)	18683 MPa
ETA_RD (viscosity associated to K_RD)	2123903 MPa·mois
ETA_ID (viscosity associated to K_ID)	12846617 MPa·mois
EPS_0 (characteristic viscoplastic deformation of strain)	0.0035
TAU_0 (characteristic time associated to EPS_0)	20 days

In spite of damage's parameters calibration (cf. assumption), the Table 4 presents damage parameters chosen.

Table 4: damage parameters

F_C (compressive strength)	30 (MPa)
F_T (tensile strength)	3 (MPa)
EPS_COMP (strain on compressive strength)	2e-3
EPS_TRAC (strain on traction strength)	2e-4

For the swelling properties, the parameters to calibrate are the volume of gel, the kinetic parameter and the porosity connected to the reaction site. Others parameters (mechanical parameters) are supposed to fall within the normal limits and to be equal to those obtained on similar structures.

3.2. Prediction of elasticity behavior of the dam for different water levels

3.2.A : After building, near water

In situ, the dam is composed of 41 cantilevers, the mesh, imposed by the exercise, is only composed of 26.

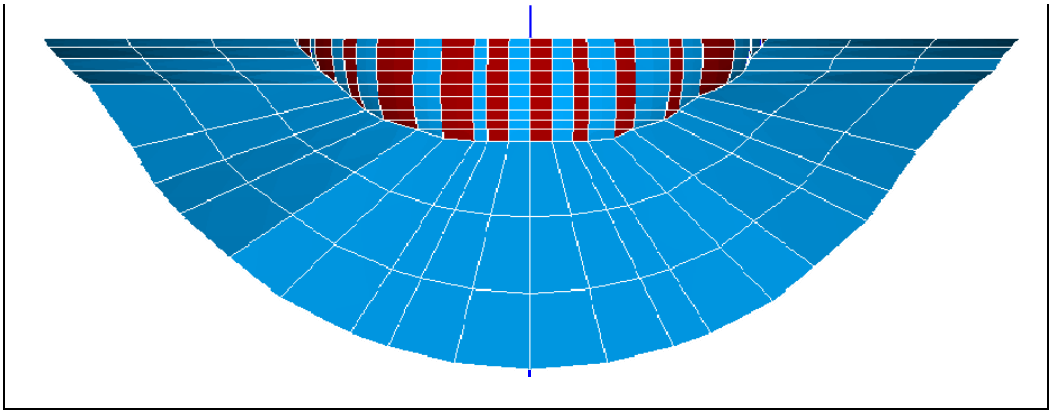

Figure 5: Division of the dam in even and odd cantilevers, upstream view

To model the construction, two mesh groups are defined alternatively, even cantilevers and odd cantilevers (Fig. 5). They are affected by the mechanical properties of the concrete dam, without swelling parameters. Before the launching, a first calculation will be run to obtain respectively the stress and the intern variables fields in these two groups. Finally, the complete model (we will consider the mesh completed, without any division in even and odd cantilevers), considering these fields as initial conditions will be computed.

The results have been added to the Excel file given by the ICOLD organization.

We can observe that the displacements field is not void after the launching of the model. These phenomena can be explained.

This non linear model calculates the stress and variable fields from the displacement field. Therefore, if we introduce a stress or internal variable as initial conditions, the model will calculate the respectively associated displacement. That's why the displacement field is not null after the launching. This displacement is considered and has to be deducing from the model as has been requested in the Benchmark.

The table 6 shows the stresses, at the end of construction, for the required points defined in the workshop :

Solution 1A : End of construction

Point	Location	Elevation	STRESSES (MPa)		
			Horizontal	Vertical	Mayor Principal
R1	Block 20	488	3.18E-01	-1.02E-03	-3.59E-03
R2	Block 20	480	2.17E-01	-2.14E-01	-2.25E-01
R3	Block 20	463	1.27E-01	-6.54E-01	-6.67E-01
R4	Block 20	438	-2.03E-02	-9.75E-01	-9.72E-01
R5	Block 20	418	4.57E-02	-6.96E-01	-6.40E-01
R6	Block 0	480	1.54E-01	-2.05E-01	-2.08E-01
R7	Block 0	438	2.50E-01	-1.12E+00	-1.12E+00
R8	Block 0	418	1.59E-01	-1.48E+00	-1.49E+00
R9	Block 19	488	2.11E-01	1.47E-04	-1.69E-02
R10	Block 19	480	1.58E-01	-2.14E-01	-2.17E-01
R11	Block 19	463	1.22E-01	-6.45E-01	-6.48E-01
R12	Block 19	438	2.28E-02	-9.80E-01	-9.94E-01
R13	Block 19	418	-5.72E-04	-9.93E-01	-9.92E-01
R14	Crest Block 20	489	2.63E-01	4.69E-04	-3.41E-02
R15	Crest Block 14	489	1.90E-01	2.63E-04	-6.36E-02
R16	Crest Block 6	489	1.33E-01	-2.27E-04	-4.50E-02
R17	Crest Block 0	489	1.36E-01	-2.71E-04	-1.21E-03
R18	Crest Block 5	489	2.04E-01	-1.34E-05	-2.09E-02
R19	Crest Block 11	489	2.99E-01	2.80E-04	-5.45E-02
R20	Crest Block 17	489	3.44E-01	7.29E-04	-4.24E-02
R21	Crest Block 23	489	2.11E-01	1.47E-04	-1.69E-02
R22	Crest Block 4	489	2.76E-01	4.86E-03	4.78E-03

3.2.B : reservoir level water equal to 483.80

Using the results obtained in the last sub step, the reservoir level water equal to 483.80 (this is the average water level during the initial high level period 1963-1973) can be introduced in the model. To check the displacements and stresses fields without considering the swelling AAR phenomena, but taking into account the effects of creep. The objective is to compare the results with other proposed models to determine the differences between models without swelling.

3.2.C : reservoir level water equal to 486.70

In this step, the same procedure will be followed. Using the results obtained in the sub step 1A, the reservoir level water equal to 486.70 (this is the average water level during the intermediate very high level period 1974-1981) can be introduce in the model and check displacements and stresses fields.

3.2.D : reservoir level water equal to 486.70

Using the results obtained in the sub 3.2.A, the reservoir level water equal to 479.90 (this is the average water level during the last low level period 1982-1994) can be introduced in the model and check the displacement and stress fields.

Stresses and displacement's values, for the required points, obtained for the different steps (3.2.A, B, C, D), have been introduced in the Excel table given by the ICOLD workshop.

In the following sections, the kinetic constant and the gel volume adjustment are presented.

3.3. Determination of kinetic constants and gel volume

To predict the behavior of the dam in the next years, it's necessary to calibrate the swelling model. To get the best representation of the reality, some parameters need to be adjusted.

As previously explained in the hypothesis section, the volume of gel, the kinetic parameter and the lineal progress of the AAR are the parameters to calibrate.

To calibrate the model, the provided displacements by data will be compared to those obtained with the model. For that, we have developed a fitting program. This program is based on an equivalent strain to simulate a free swelling test, regardless of the effect of stresses. This allows us to find an initial value for the parameters. However, the model is influenced by other variables as creep, stress or the effect of the water pressure, that's why several iterations are necessary to find the best combination.

As a result, it seems necessary to know how these parameters are going to act in the curve displacement-time.

Fig. 6 suggests the volume of gel acts in the height of the final point but not in the shape of the curve.

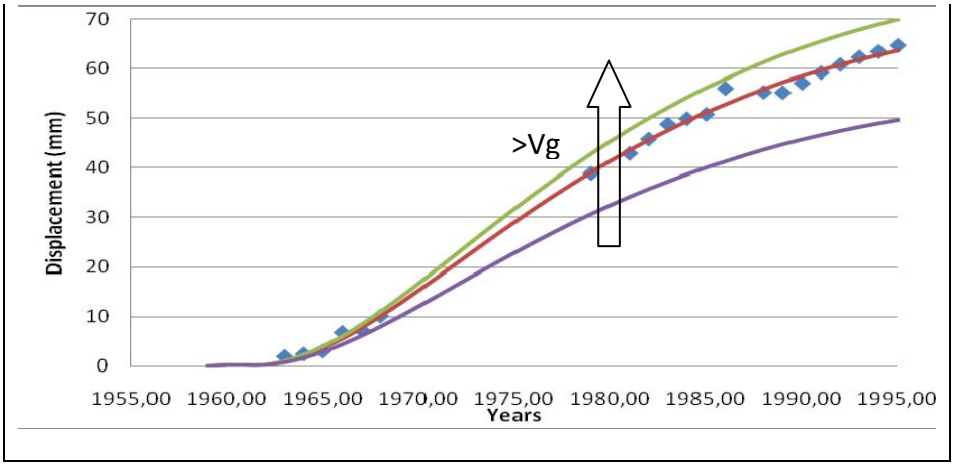

Figure 6: Volume de gel influence

The kinetic parameter modifies in the shape of the curve. So, with a high α value, the reaction occurs.

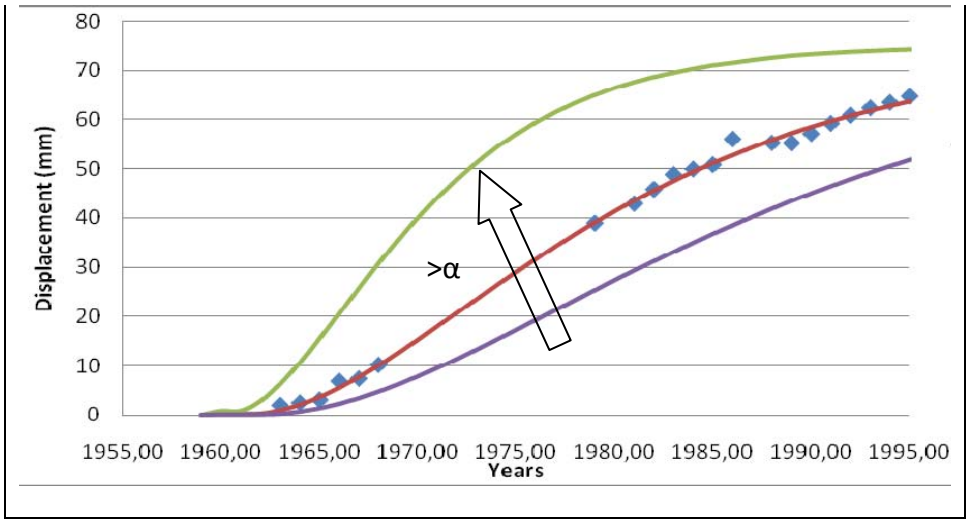

Figure 7: Kinetic parameter influence

Finally, the progress of the AAR (A) has similar action as the volume of gel but in a reverse sense. A must always be over zero.

After several iterations, the swelling's parameters were retained:

Table 6: Swelling parameters calibrated

Volume gel	10.20e-4
Kinetic parameter	0.052 années^{-1}
AAR progress	0.1217

For example, the comparison between the experimental displacements and the model displacements for the point R16 (6-8) is shown in Fig. 8:

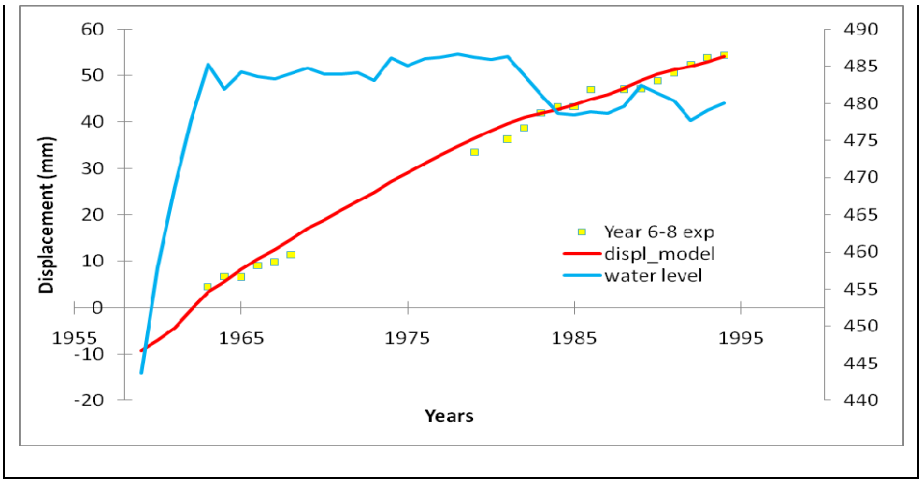

Figure 8: R16 experimental and model vertical displacement of 1963-1994 period

As we can see on fig. 8, the model makes a good representation of the real swelling in this calibration period. Nevertheless, around 1985, we can observe that the observed displacement is higher than the calculated done. This period corresponds to a great decrease of the reservoir level and so, a reduction of the displacements is expected. Therefore, the result obtained is logical. The origin supposed of the dysfunctionality can be the assumptions done in neglecting temperature or humidity effects. The problem occurs in a sudden change of the water level and a bigger part of the dam is exposed to the sun. This exposed concrete has a different temperature than the submerged concrete. This situation can induce displacement, not considered in the model. According to O. Ozanam [7] the dam of Kariba is stress-dependent. Therefore, the swelling is evidently slowered down, or even reversed by compresses stresses. We can suppose too, that a reduction of the compressive stresses can promote the swelling of the dam that is, an unexpected increase of displacements which is our case.

After this calibration phase, the model prediction capability was validated through the comparison between the displacement of instrumented points predicted by the calculations and the variations measured on the dam.

The radial displacement at crest of crown cantilever is represented in fig. 9.

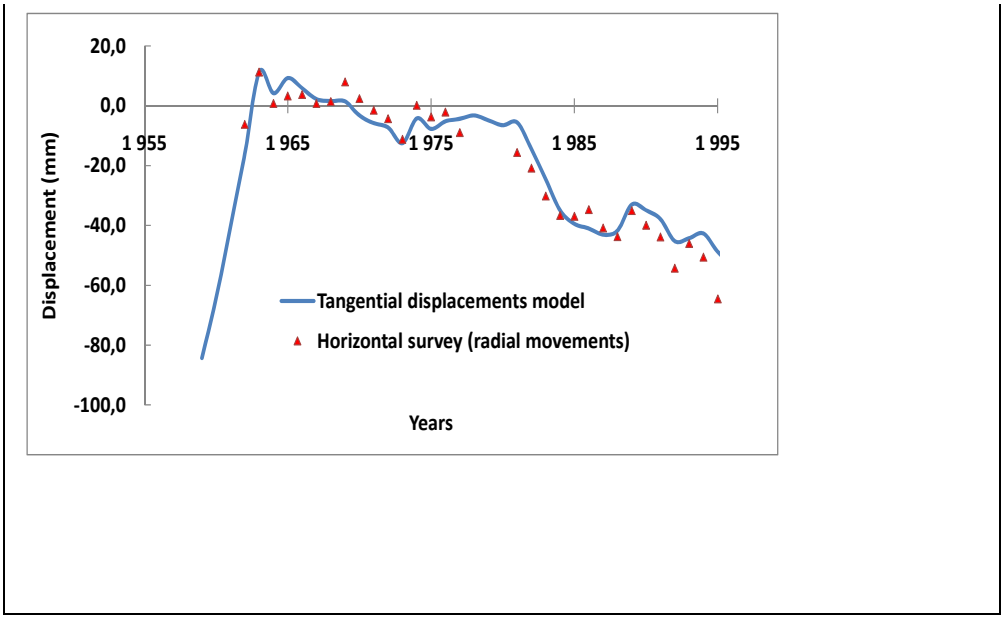

Figure 9: R16 experimental and model radial displacement at crest of crown cantilever (T434)

The radial displacement obtained by the model is in accordance with monitoring results. Nevertheless, in the reality, the dam goes more upstream. That is explained as a major real swelling or a different creep behavior. The non consideration of joints to simplify the problem, can explain these differences. An identification of swelling parameters on the cantilever 3-5 can explain the radial displacement by a greater swelling of the dam central part (blue curve in fig 9).

As in 3.2, stresses and displacement's value, for the required points have been introduced in the Excel table.

3.4. Prediction of Kariba's dam behavior

In this section, we should predict the behavior of the dam in the 1994-2010 period. For this, we will use the parameters which have been calibrated in the step 2 and launch the model, pending that the results will predict the behavior of the dam affected by the AAR.

The fig. 10 shows us the displacement for the point R18 :

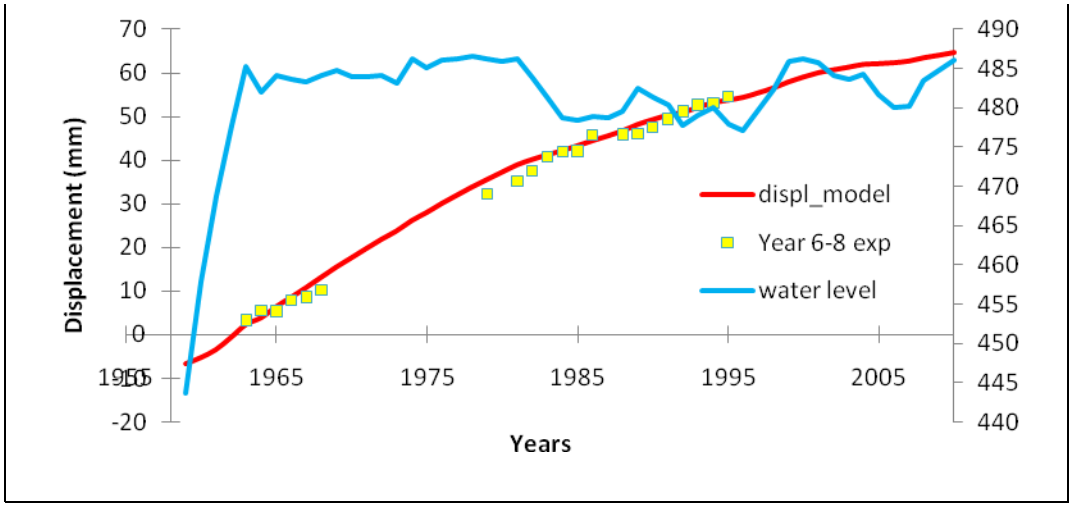

Figure 10: R16 experimental and model vertical displacement between 1963 and 2010.

Fig. 10 shows the predicted displacement versus the trend of the measured displacements on the end of 1994.

The displacements calculated for all the points are represented in fig. 11. If the model is well calibrated, the displacements obtained by the model will represent the real comportment of the dam.

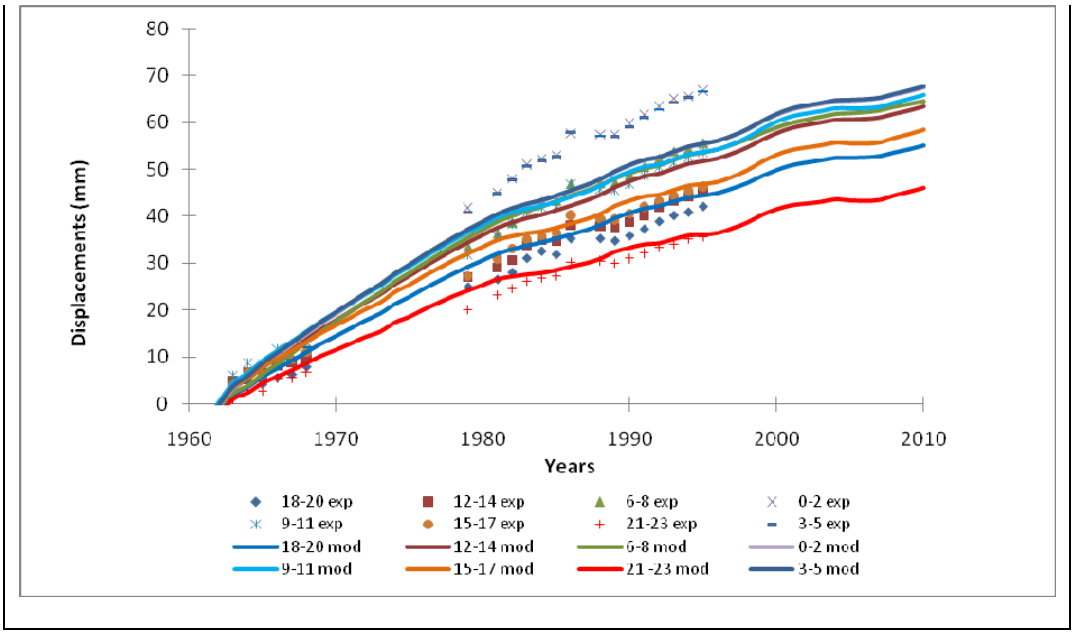

Figure 11: Vertical displacements between 1963 and 2010

As we can observe, the points 0-2 and 3-5 have a lower displacement than measured. This result is in accordance with the assumptions. For the rest of the points, the model represents correctly the displacements measured by monitoring and therefore, we suppose the prediction is well calculated. Figs 12, 13 and 14 allow us to study the displacements of the cantilevers more accurately.

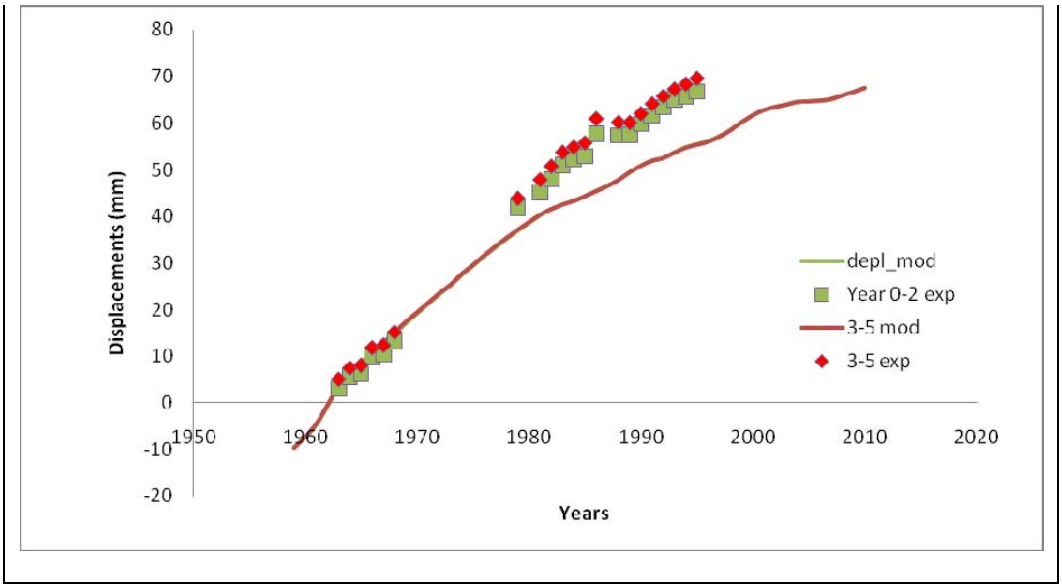

Figure 12: Vertical displacement for the cantilevers 0-2 and 3-5.

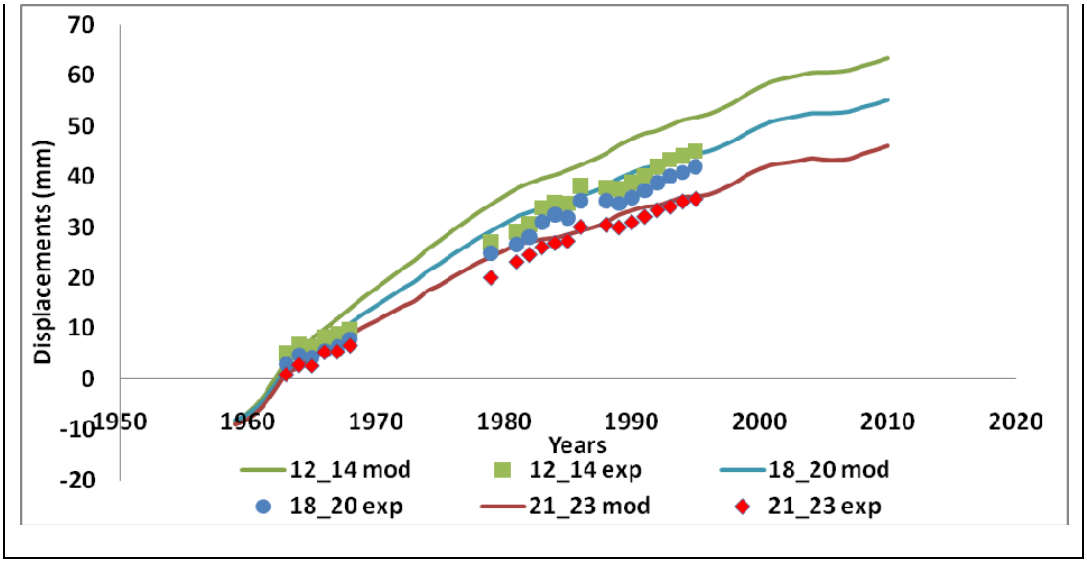

Figure 13: Vertical displacement for the cantilevers 12-14, 18-20 and 21-23.

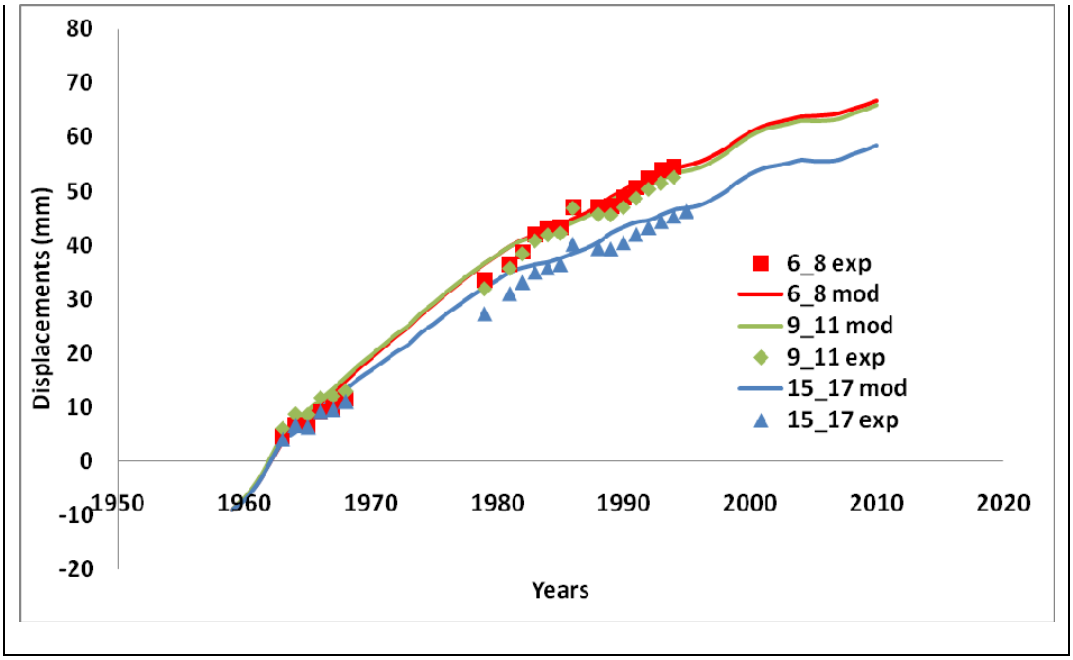

Figure 14: Vertical displacement for the cantilevers 6-8, 9-11 and 15-17.

Fig. 15 shows the radial displacement prediction at crest of crown cantilever.

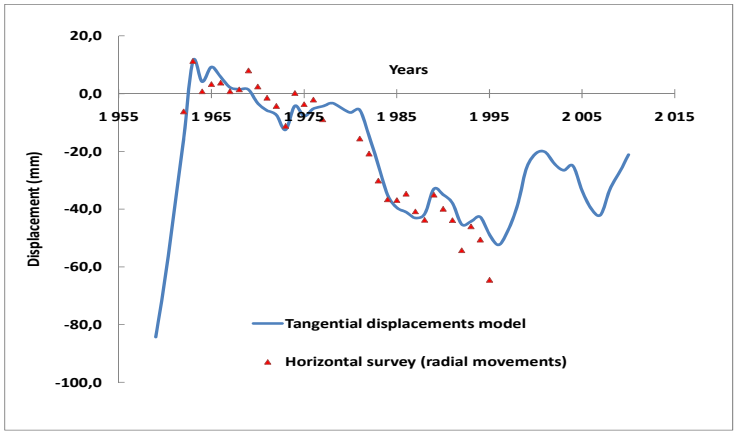

Figure 15: R16 experimental and model radial displacement at crest of crown cantilever (T434)

Around the year 2000, the rise of the water level in the reservoir causes the downstream displacement of the dam attenuated by the swelling process which moves the crest to upstream.

The predictions of the stresses and the displacement's values have been introduced in the Excel table.

To study the behavior of the dam since its impoundment in 1963 until 2011 the developed model allows us to extract several interesting results. The objective is to study the evolution of the behavior of the dam affected by the AAR and to determinate the usage status of the dam.

In this way, the extraction of the equivalent stresses and the eigenvector of the main stresses show the evolution in time of the stress field because the AAR swelling. Figs 16 and 17 show the main compressive stresses on upstream and downstream faces of the dam in 1963 (after impoundment) and nowadays. The eigenvector field is showed by the fig 18 and 19.

1963

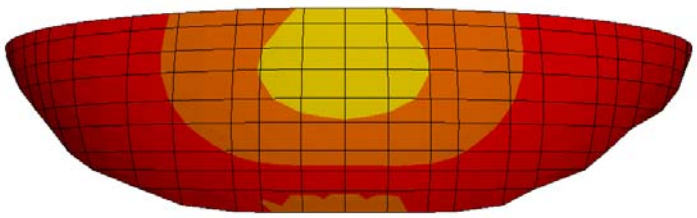

2011

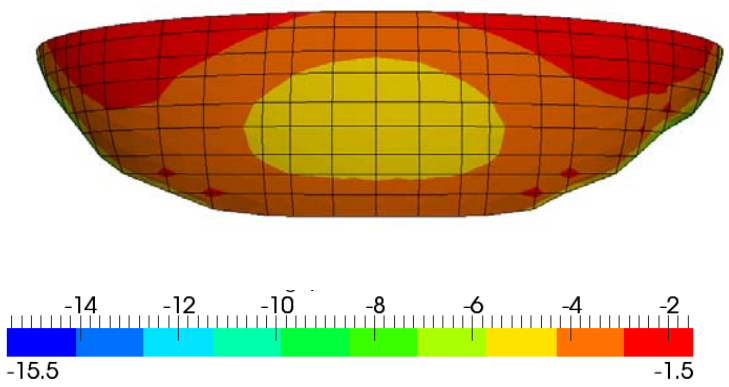

Figure 16: Main stresses field on upstream face [MPa]

1963

2011

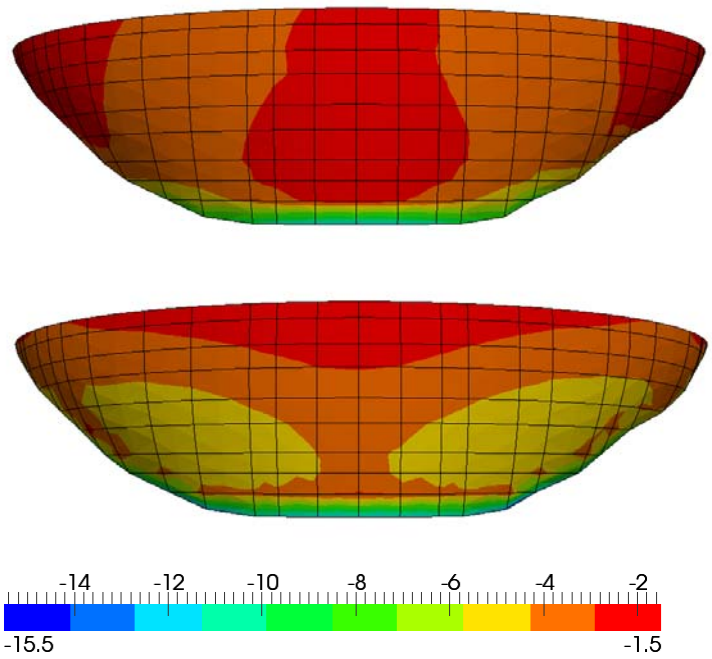

Figure 17: Main stresses field on downstream face [MPa]

1963

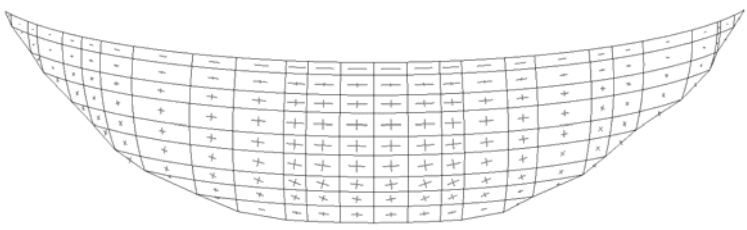

2011

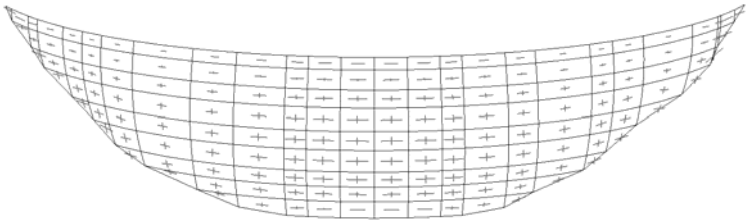

Figure 18: Eigenvector stresses on upstream face.

1963

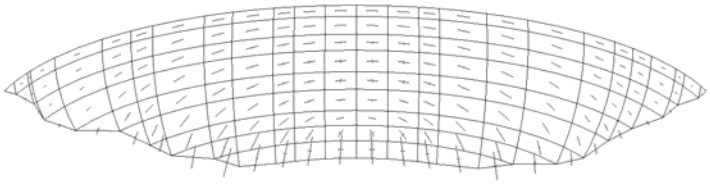

2011

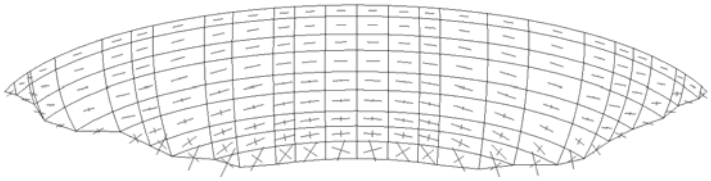

Figure 19: Eigenvector stresses on downstream face.

We can appreciate an evolution of the stresses which have been increased since 1963, especially in the contacts with the rock of the foundation. A rotation of the direction of the principal stresses is observed too: vertical in 1963 because a major importance of the weight and horizontal in 2011 because of swelling effect.

We are interesting to know the situation of the dam nowadays. The contact dam-rock and the damage of the concrete have been studied.

Figs 20 and 21 show the normal and tangential stress in the contact dam-rock in 2011. When tangential stress increases, cohesion has been necessary. The value of cohesion has given in fig 22.

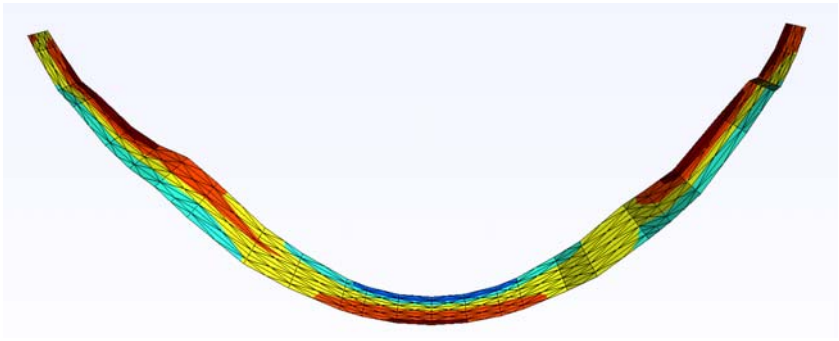

Figure 20: Normal stresses on the contact dam-rock (2011) [MPa]

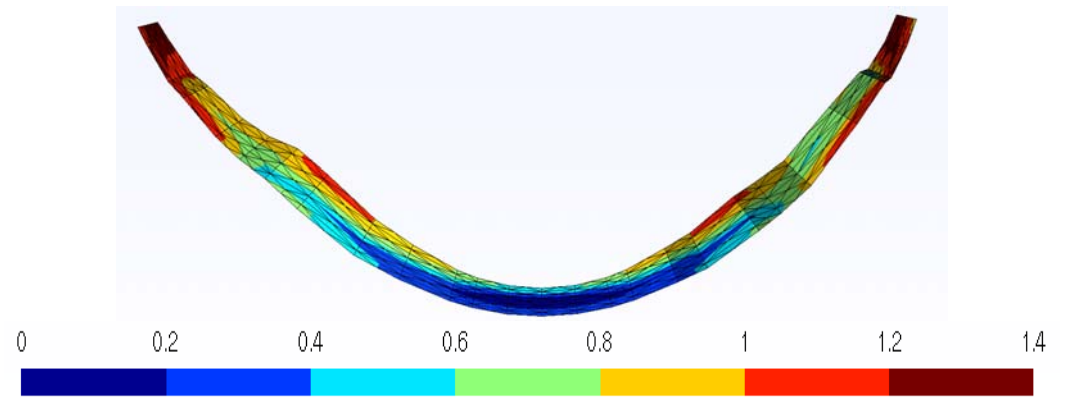

Figure 21: Tangential stresses on the contact dam-rock (2011) [MPa]

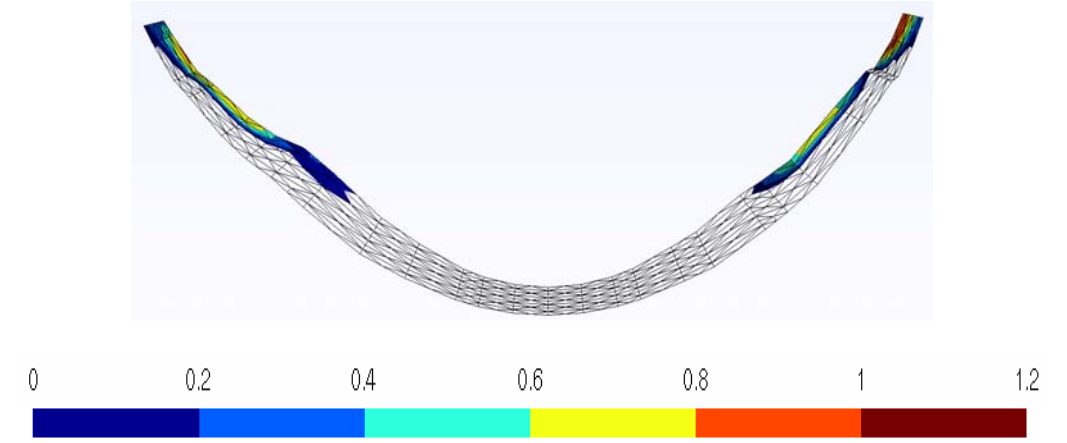

Figure 22: Potential cohesion on the contact dam-rock (2011) [MPa]

The model allows us to get the damage field of the dam and know where the cracking could be important and need to be repaired. Fig 23 shows the damage field of the dam in 2011.

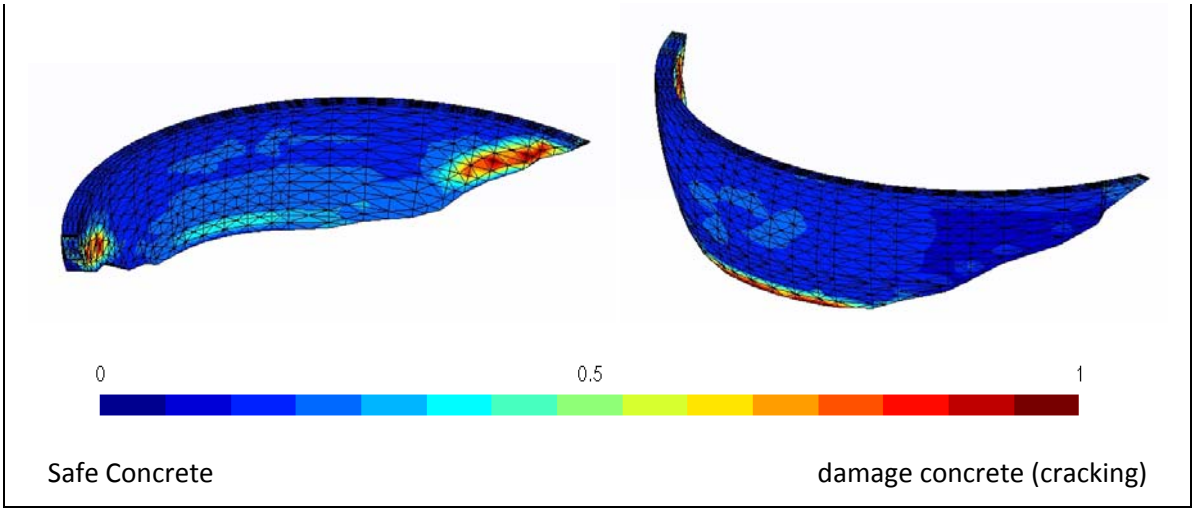

Figure 23: Damage field on the dam (2011).

The damages calculated are important in areas around the foundation at the base and on the sides of the dam. It seems possible that a horizontal cracking can be developed in the damaged areas.

4. Conclusions

The physical phenomena involved in the structural effects induced by AAR have been presented and a model proposed for each of them, leading to a global phenomenological modeling. In this modeling, a rheological model is used to control the long-term behavior of concrete including creep and shrinkage phenomena. An orthotropic damage model based on the effective stress concept allows swelling transfer between strain-constrained directions and free-swelling directions to be taken into account. After the calibration phases, the model was used to reproduce the behavior of Kariba's dam. A comparison with experiments showed the model's capability to reproduce displacements with acceptable accuracy.

The calibration process used, allows us, to find model parameters to represent the movement of the cantilever 6-8. The behavior obtained for the other points are similar to those measured by monitoring. Nevertheless, the thermal effects can influence the production of differential displacements in the contact between the concrete immersed and exposed to the sun. Thus, while the radial displacement follows the same behavior as the reality, the difference may be explained by the inclusion or not of thermal effects and by a greater swelling in the central part.

The AAR development produces efforts in the dam. Stresses will increase at the dam-foundation contact and the direction of the main compressive stress will turn from vertical to horizontal, involving a decrease of arc effect. The model represents this evolution. The model also allows us to locate damaged areas of the dam will need a greater consideration. Contact with bedrock, hard and stable, resulting in the accumulation of effort and damaged concrete can crack and endanger the building that must be controlled. We conclude that the model proposed by EDF allows us to model satisfactorily the dam behavior affected by AAR. Nevertheless, in spite of the well representation of the monitoring by the model, we can improve the Kariba's dam behavior knowledge, considering another assumption as environmental condition, different cement dosage, or improving identification of creep and the AAR chemical kinetic by laboratory tests.

References

[1] Grimal E., Caractérisation des effets du gonflement provoqué par la réaction alcali-silice sur le comportement mécanique d'une structure en béton, PhD thesis, Université Paul Sabatier Toulouse, France, 2007. (in French)

[2] Grimal E, SELLIER A., LE PAPE Y., BOURDAROT E., Creep shrinckage and anisotropic damage in AAR swelling mechanism, part I and part II, ACI Materials Journal/May-June 2008, 105-m26 and 105-m27.

[3] Sellier A., Bary B., Coupled damage tensors and weakest link theory for describing crack induced orthotropy in concrete, Engineering Fracture Mechanics n°1629, (may 2002).

[4] Acker, P., Sur les Origines du Retrait et du Fluage du Béton, Revue Française de Génie Civil, V. 7, No. 6, 2003, pp.761-776. (in French)

[5] Institution of Structural Engineers, Structural Effect of Alkali Reaction, Technical Guidance on the Appraisal of Existing Structures, published for the Institution of Structural Engineers, London, 1992.

[6] Poyet S., Etude de la Dégradation des Ouvrages en Béton Atteints par la Réaction Alcali-Silice: Approche Expérimentale et Modélisation Numérique Multi-échelles des Dégradations dans un Environnement Hydro-chemo-mécanique Variable, PhD thesis, Université de Marne La Vallée, France, 2003. (in French)

[7] Ozanam O., Reservoir level influence on concrete swelling rate : Modelisation in the case of Kariba, ICOLD, Florence, 1997

XI ICOLD BENCHMARK WORKSHOP ON NUMERICAL ANALYSIS OF DAMS

Valencia, October 20-21, 2011

THEME A

A MODEL OF CONCRETE SWELLING FOR DESCRIBING THE KARIBA DAM

Menouillard, Thomas[1]

Seignol, Jean-François[2]

Boldea, Liviu-Ioan[3]

Roure, Patricia[4]

Tzenkov, Anton[5]

Gunn, Russell Michael[6]

CONTACT

Liviu-Ioan Boldea and Thomas Menouillard
Stucky SA, Rue du Lac 33, 1020 Renens VD, Switzerland, Phone +41 21 637 1518
Email: liboldea@stucky.ch ; tmenouillard@stucky.ch

Summary

The Kariba Dam is a hydroelectric dam in the Kariba Gorge of the Zambezi river basin between Zambia and Zimbabwe. This double curvature concrete arch dam was built between 1955 and 1959. The observation of data from monitoring systems shows a strong anisotropic (vertical and horizontal) swelling of the dam concrete. The upcoming question is now to predict the behavior (such as displacement field, stress, strain and swelling) of the dam. A model is developed to take into account the concrete swelling effect in the behavior, and integrated into a Finite Element Code. It is based on the Larive's law whose parameters depend on the temperature and moisture determined in a previous computation. This Finite Element Method (FEM) code is the numerical tool which will allow the behavior of the dam concrete in the past and future years to be simulated. Firstly, the concrete swelling model is calibrated in terms of model parameters to obtain a good correlation between the data from the monitoring system and the numerical results. Secondly, the behavior of the dam related to the swelling phenomenon is predicted for the future years. The present model and methodology are not restricted to the Kariba dam, but can also be successfully applied to similar civil engineering structures.

[1] Stucky SA, Rue du Lac 33, 1020 Renens VD, Switzerland.
[2] IFSTTAR, Boulevard Newton, 77447 Marne la Vallée Cedex 2, France.
[3] Stucky SA, Rue du Lac 33, 1020 Renens VD, Switzerland.
[4] ITECH, Tour Orion, 12-16, rue de Vincennes, 93100 Montreuil/Bois, France
[5] Stucky SA, Rue du Lac 33, 1020 Renens VD, Switzerland.
[6] Stucky SA, Rue du Lac 33, 1020 Renens VD, Switzerland.

1 Introduction

This paper describes the method used to simulate concrete swelling on an existing dam, i.e. Kariba dam, where the alkali-aggregate reaction was actually noticed many years ago. This challenging work aims at testing the proposed constitutive model for this study both qualitatively and quantitatively.

Firstly, observational data (displacements), which are available during the period 1960-1996, are used to calibrate the numerical model. Secondly, as a major goal, the objective is to predict the behavior of the dam in terms of displacements and stresses up to 2010.

The paper is organized as follows: Section 2 presents the mechanical model of the Kariba dam and the foundation; Section 3 describes the model for concrete swelling which will be used in the numerical simulations; Section 0 presents the calibration of the model and the results for predicting the future behavior of the dam and finally, Section 5 concludes with remarks.

2 Mechanical model of the Kariba dam

2.1 Geometry and mesh

The geometry and mesh as supplied by the benchmark formulators has been adapted for the software used as shown in **Figure 1** without any modifications (finite element type, etc.).

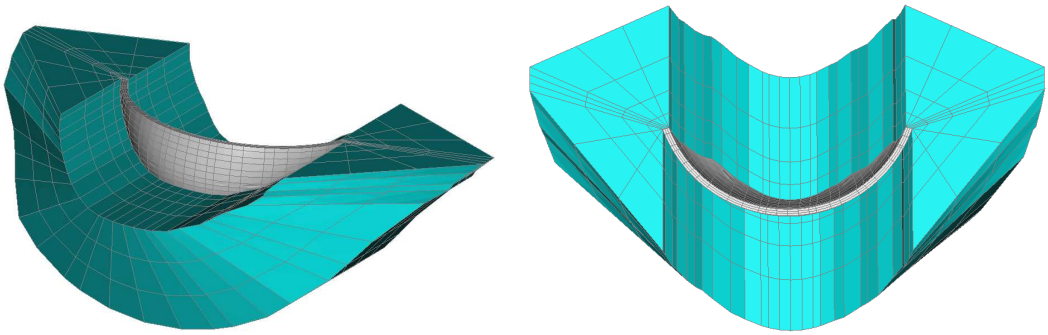

Figure 1 : Overview of the geometry and mesh of the Kariba dam and foundation

2.2 Loads definition

2.2.1 Self-weight

The self-weight is applied in one step in the whole dam at the first step of simulation. The density of the concrete is 2,350 kN/m^3, and the density is not considered for the foundation. It is recognized that the initial stress state, as would normally be determined by a phased analysis for such a structure (for example, consideration of independent cantilevers and then the build-up by construction stages to the monolith structure), could play an important role in the calibration/behavior of the numerical model.

2.2.2 Hydrostatic pressure

This load depends on the water level varying during the period 1959-2010. The pressure increases linearly with the depth under the water level, and is applied on the upstream surface of the dam.

Figure **2** presents the water level history, and Figure **3** the deformed shape of the dam due to hydrostatic pressure.

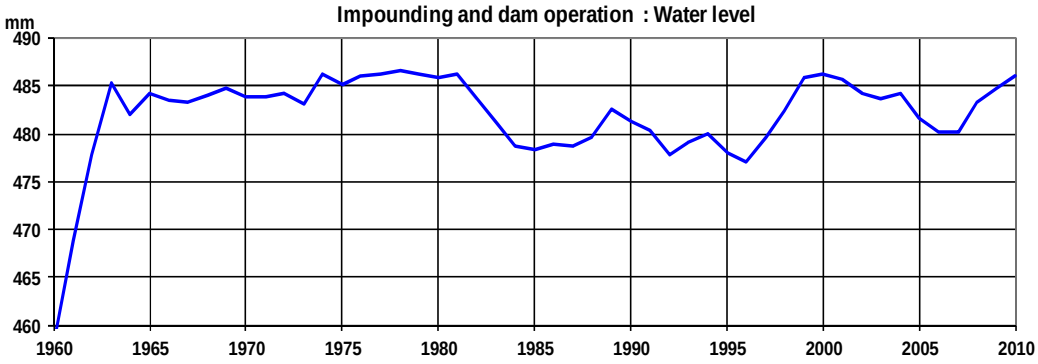

Figure 2 : Water level as a function of time.

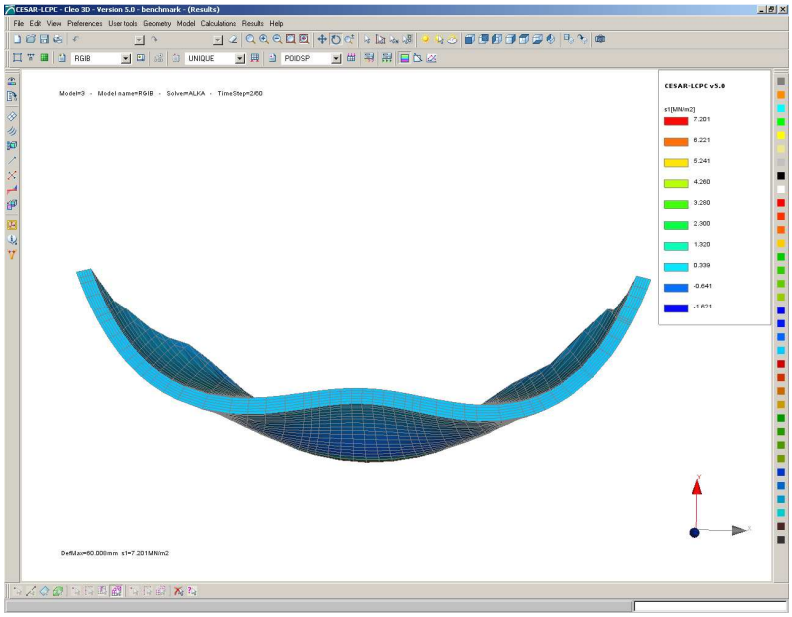

Figure 3 : Deformed mesh (hydrostatic pressure on upstream face).

3 Presentation of the concrete swelling law with details on the required parameters

3.1 Constitutive model

The constitutive model used to simulate AAR (Alkali-Aggregate-Reaction) of concrete structures was developed at LCPC by *Coussy, Larive and Li* [1]. The model represents AAR development as the prescribed expansion of a gel in the concrete porous network, considered as linear elastic. Gel swelling is assumed to be linearly proportional to the extent of AAR chemical content, $\xi(t)$ (scalar function of time *t*) which induces a pressure $k \cdot \xi(t)$ on the solid skeleton. With some simple assumptions, the constitutive equation for the AAR-affected concrete can be written as follows for the strain components:

$$\underline{\underline{\varepsilon}} = \underline{\underline{\varepsilon}}_e + \underline{\underline{\varepsilon}}_\chi(\underline{\underline{\sigma}}) \qquad \textbf{(1)}$$

Where: ε_e represents the elastic part of the strain (based on Hooke's law) and ε_χ, the AAR-induced strain.

3.1.1 Orientation of the stress tensor

When a stress tensor $\underline{\underline{\sigma}}$ is applied, the chemical expansion is restrained in the more compressed direction(s), and it is transferred to the least compressed one(s). This experimental fact is taken into account by the model developed by *Multon and Toutlemonde* [2] with the following expression:

$$\underline{\underline{\varepsilon}}_{\chi}(\underline{\underline{\sigma}}) = 3\underline{\underline{b}}(\underline{\underline{\sigma}}) \cdot \underline{\underline{\varepsilon}}_{\chi}(\underline{\underline{0}}) \quad \textbf{(2)}$$

The anisotropy tensor $\underline{\underline{b}}$ (in the frame of stress tensor eigen directions) is given by

$$\underline{\underline{b}}(\underline{\underline{\sigma}}) = \begin{pmatrix} \cos^2\alpha\cos^2\beta \\ \cos^2\alpha\sin^2\beta \\ \sin^2\alpha \end{pmatrix} \quad \textbf{(3)}$$

where α and β are defined by

$$\begin{cases} 2\tan^2\alpha = \dfrac{f_{ct}^2\cdot(1-\nu)}{\left(s_3 - f_{ct}\right)^2} + \nu \\ 2\tan^2\beta = \dfrac{1+\dfrac{f_{ct}^2\cdot(1-\nu)}{(2+\nu)\cdot\left(s_2 - f_{ct}\right)^2}}{1+\dfrac{f_{ct}^2\cdot(1-\nu)}{(2+\nu)\cdot\left(s_1 - f_{ct}\right)^2}} \end{cases} \quad \textbf{(4)}$$

Where $s_{i=1,2,3}$ are the eigenvalues of stress-tensor, f_{ct} is concrete tensile strength and ν its Poisson's ratio.

3.1.2 Kinetic of the reaction

In the case of stress-free expansion under laboratory conditions (which means at a constant reference temperature T_0 = 38° and $h_0 = 100\%$ relative-moisture), the chemical strain tensor is written as

$$\underline{\underline{\varepsilon}}_{\chi}(\underline{\underline{0}}) = \varepsilon_{\infty}\,\xi(t)\,\underline{\underline{I}}_{d} \quad \textbf{(5)}$$

Where: ε_{∞} is the maximum strain observed during the free-expansion tests at 100% moisture, and $\underline{\underline{I}}$ is the unit-tensor (the double-underlining denotes tensors). The zero tensor denotes the stress state zero. The evolution of ξ versus time *t* is given by Larive's model:

$$\xi(t) = \frac{1-\exp\left(-t/\tau_c\right)}{1+\exp\left(-t/\tau_c+\tau_l/\tau_c\right)} \quad \textbf{(6)}$$

which depends on two parameters τ_l (latency time) and τ_c (characteristic time). The S-shaped curve of ξ versus *t* is given in Figure 4.

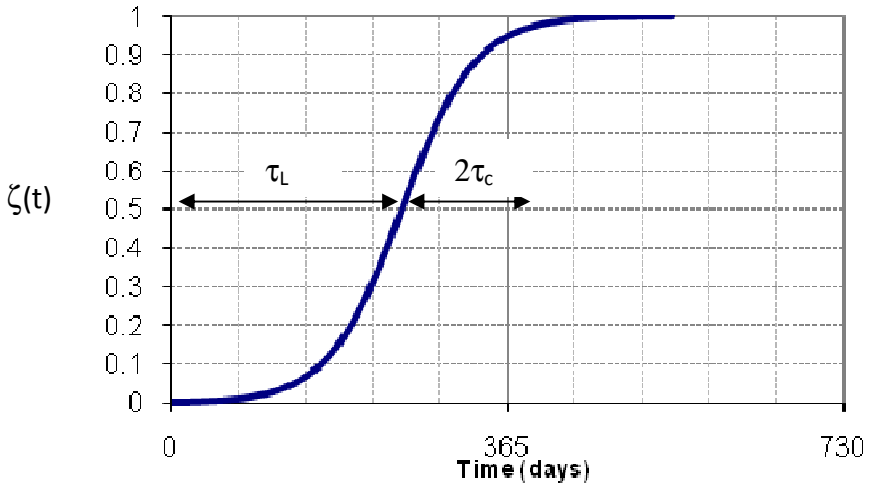

Figure 4: Representation of Larive's law.

However, the kinetics of the AAR depends on the temperature and the moisture. Therefore, the parameters of the Larive's law take into account these dependences. The influence of the temperature *T* and moisture *h* on AAR is taken into account by having these parameters varied as follows:

$$\tau_c(T,h) = \tau_c(T_0,h_0)\, f_c(h) \exp\left(U_c\left(\frac{1}{T_0}-\frac{1}{T}\right)\right) \quad \textbf{(7)}$$

$$\tau_l(T,h) = \tau_l(T_0,h_0)\, f_l(h) \exp\left(U_l\left(\frac{1}{T_0}-\frac{1}{T}\right)\right) \quad \textbf{(8)}$$

$$f_c(h) = 0.326\exp(9.5085 - 8.3755h) \quad \textbf{(9)}$$

$$f_l(h) = 0.139\exp(10.761 - 8.8066h) \quad \textbf{(10)}$$

$$\varepsilon_\infty(h) = \exp\left(8.15604(h-1)\right)\varepsilon_\infty(100\%) \quad \textbf{(11)}$$

Figure **5** presents the dependence of the Larive's law with the temperature and moisture through the parameters of the law. It shows the link between the Larive's law at 38° (experimental laboratory setup) and 27° (current temperature assumed in the dam). In addition, the moisture play an important role in the kinetic too, as it is shown in Figure **5**. Figure **6** presents the functions f_c and f_l of Equations 6 and 7; it shows the dependence with the moisture. Figure **7** presents the evolution of the normalized expansion with the moisture too. Note ε_∞ is not influenced by the temperature *T*. The link between AAR kinetics and the temperature, based on Arrhenius' law, is given by energy U_c = 5500 K and U_l = 9500 K.

To conclude, the complete kinetics of the AAR only depends on the temperature and the moisture. These two parameters actually drive the Larive's law which lead to the advance of the reaction. Without humidity, there is no AAR: the latency and characteristic times are very high (see Equations 4 to 7), which characterizes a very slow reaction, and the expansion is very low (see Equation 8).

To conclude, the kinetic of the Alkali Aggregate Reaction is driven by the temperature and moisture, and strain tensor is oriented by the stress state.

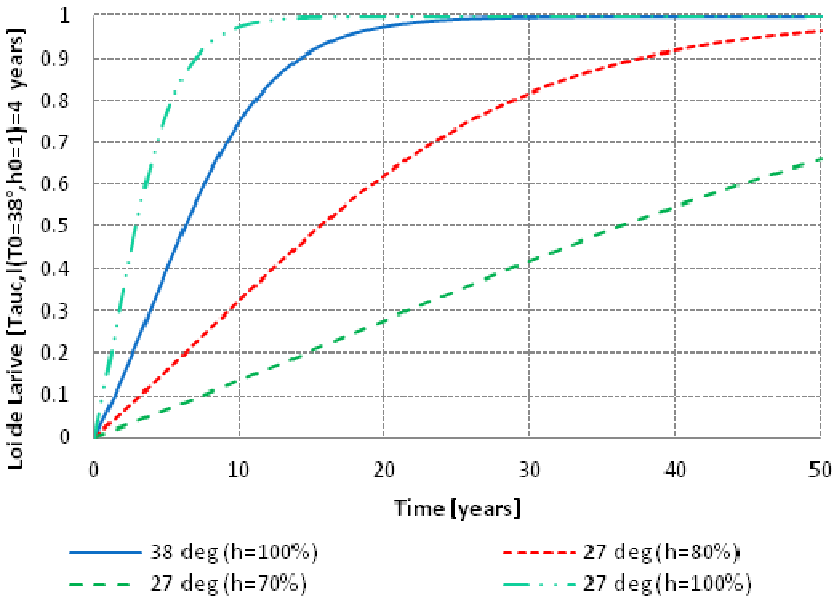

Figure 5 :Larive's law depending on the temperature and humidity.

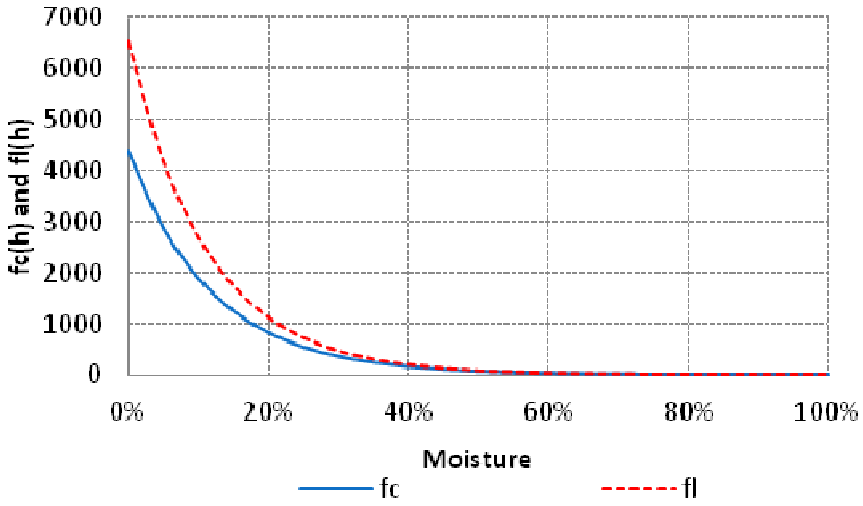

Figure 6 : Functions f_c and f_l depending on the moisture.

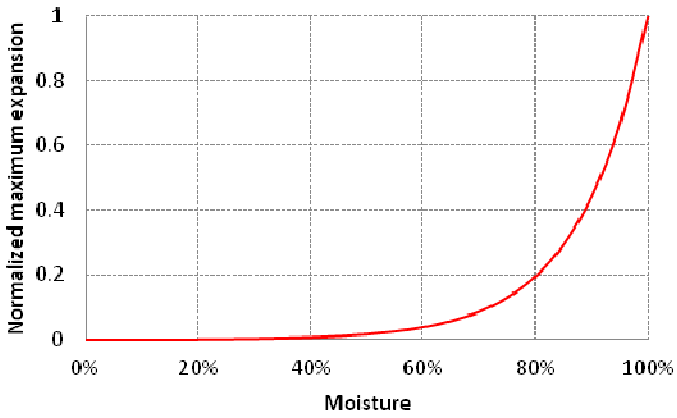

Figure 7 : Normalized maximum expansion as a function of the moisture (Equation 8).

3.2 Strategy

The AAR model needs thermal and hydric inputs for the computation of the concrete swelling in order to determine the temperature and moisture in the structure.

Therefore a first thermal simulation has to be run in order to evaluate the temperature in the concrete during the considered period. For the particular case of Kariba dam, the temperature is assumed to be constant at about 27°C. This assumption is verified by the climatic conditions for nearby South Africa.

A second simulation is required in order to evaluate the moisture of the concrete during the considered period. These are quasi-static simulations in time, computed along the period 1960-2010. To deal with these simulations, the software CESAR from Itech-soft was used.

Third, the AAR simulation can be run using as input the temperature and moisture determined in the two previous computations.

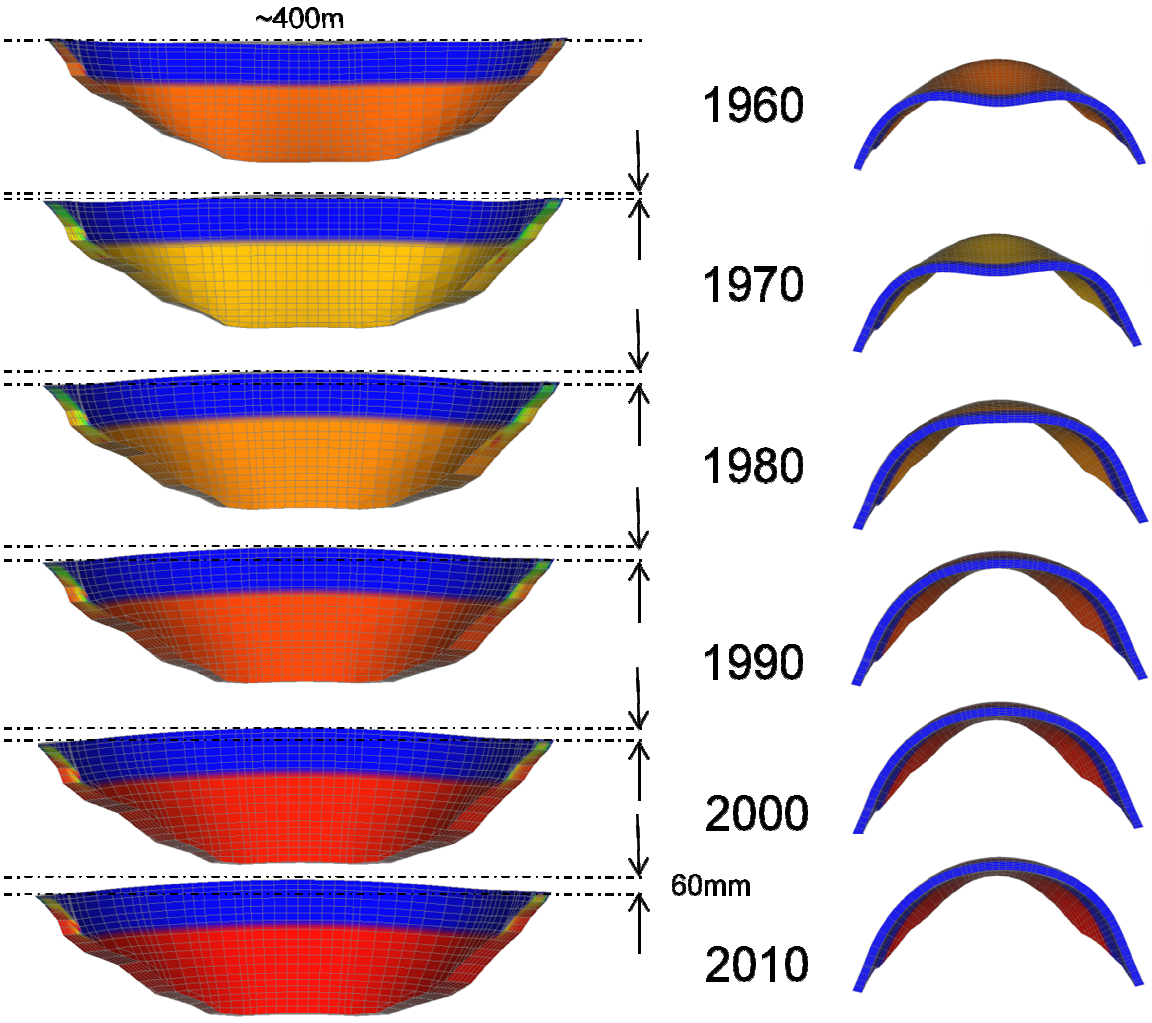

Figure 8 : Amplified deformed mesh of the Kariba dam due to AAR (the color describes the moisture: blue for 0% and red for 100%).

4 Numerical results

4.1 Calibration of the model: Determination of the parameters of the AAR law

To calibrate the model, crest leveling observations of the dam are taken as the reference values (vertical displacements). Figure **9** presents the position of the monitored points for crest leveling. Figure 10 presents the crest leveling data of different points on the dam shown in Figure **9**.

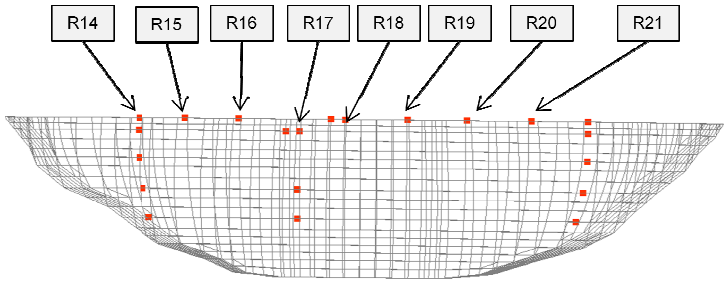

Figure 9 : Position of the monitored point for crest leveling.

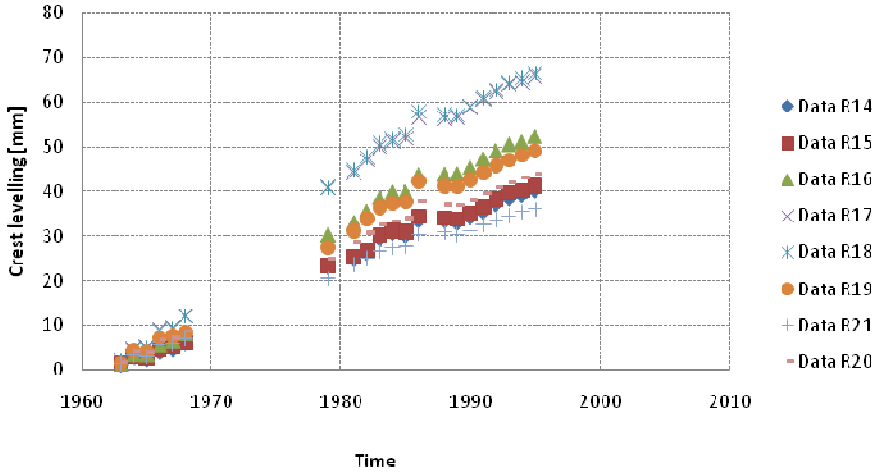

Figure 10 : Crest leveling observations.

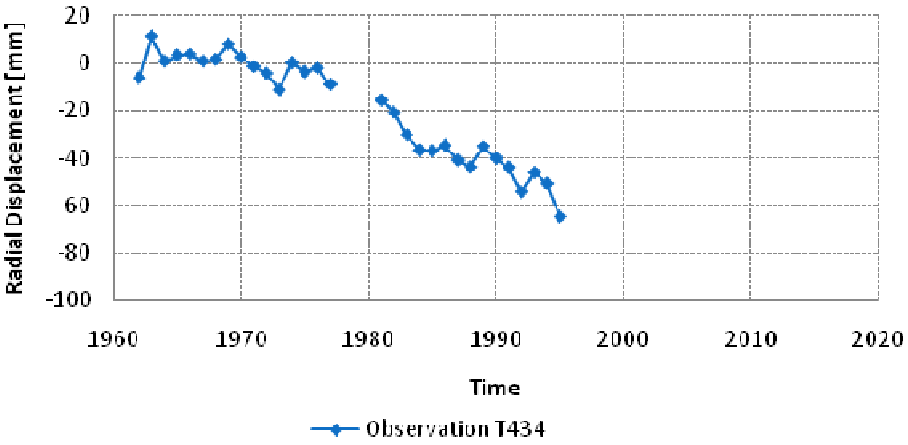

Figure 11 : Observed radial displacement of point T434 (center of the crest).

The parameters involved in the calibration are the following:

- $\tau_l(T_0,h_0)$ the latency time (shown in Equation 5),

- τ_c (T_0,h_0) the characteristic time (shown in Equation 4),
- And ε_∞ (h_0=100%) the maximal strain observed during free-expansion tests.

Where the temperature T_0 is 38° and h_0 100% moisture. These are the three parameters of the isotropic concrete swelling law. Figure 12 to Figure 17 present some results of calibration for different parameters. One can notice the influence of each of the three parameters.

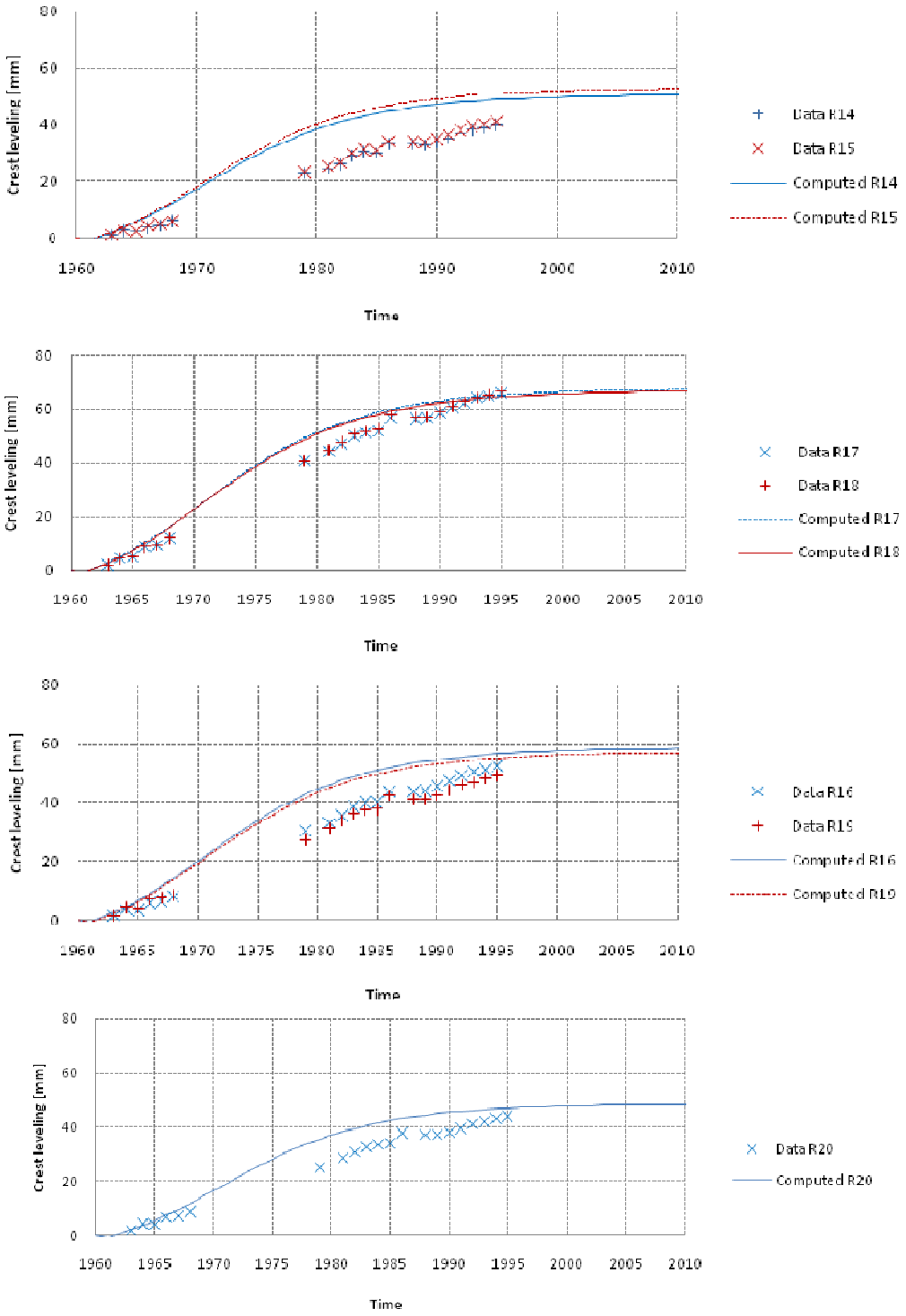

Figure 12 : Calibration results for the following parameters of the AAR law: τ_c=2 years, τ_L=3 years and ε_∞=0.0017%.

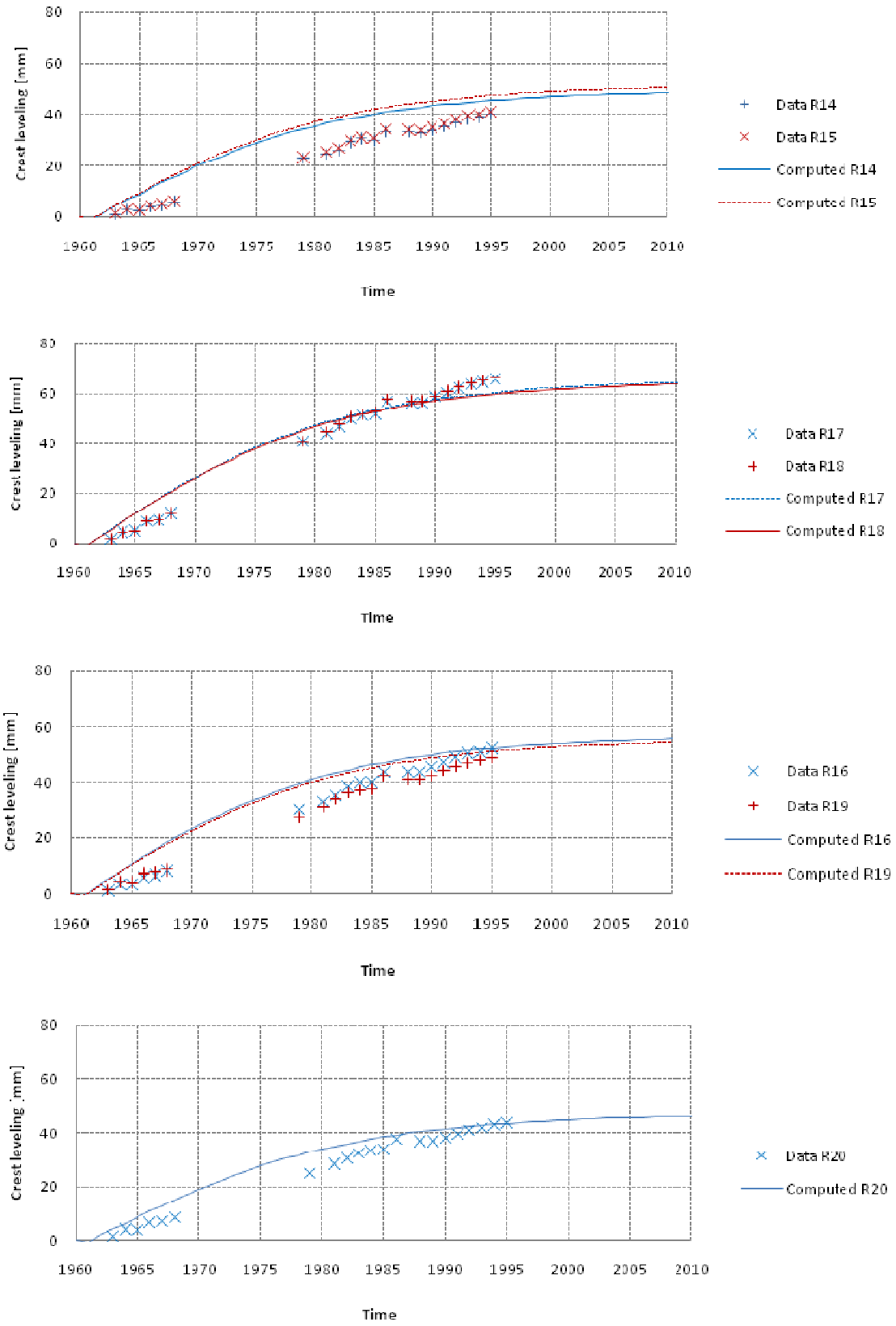

Figure 13: Calibration results for the following parameters of the AAR law: τ_c=4 years, τ_L=2 years and ε_∞=0.0017%.

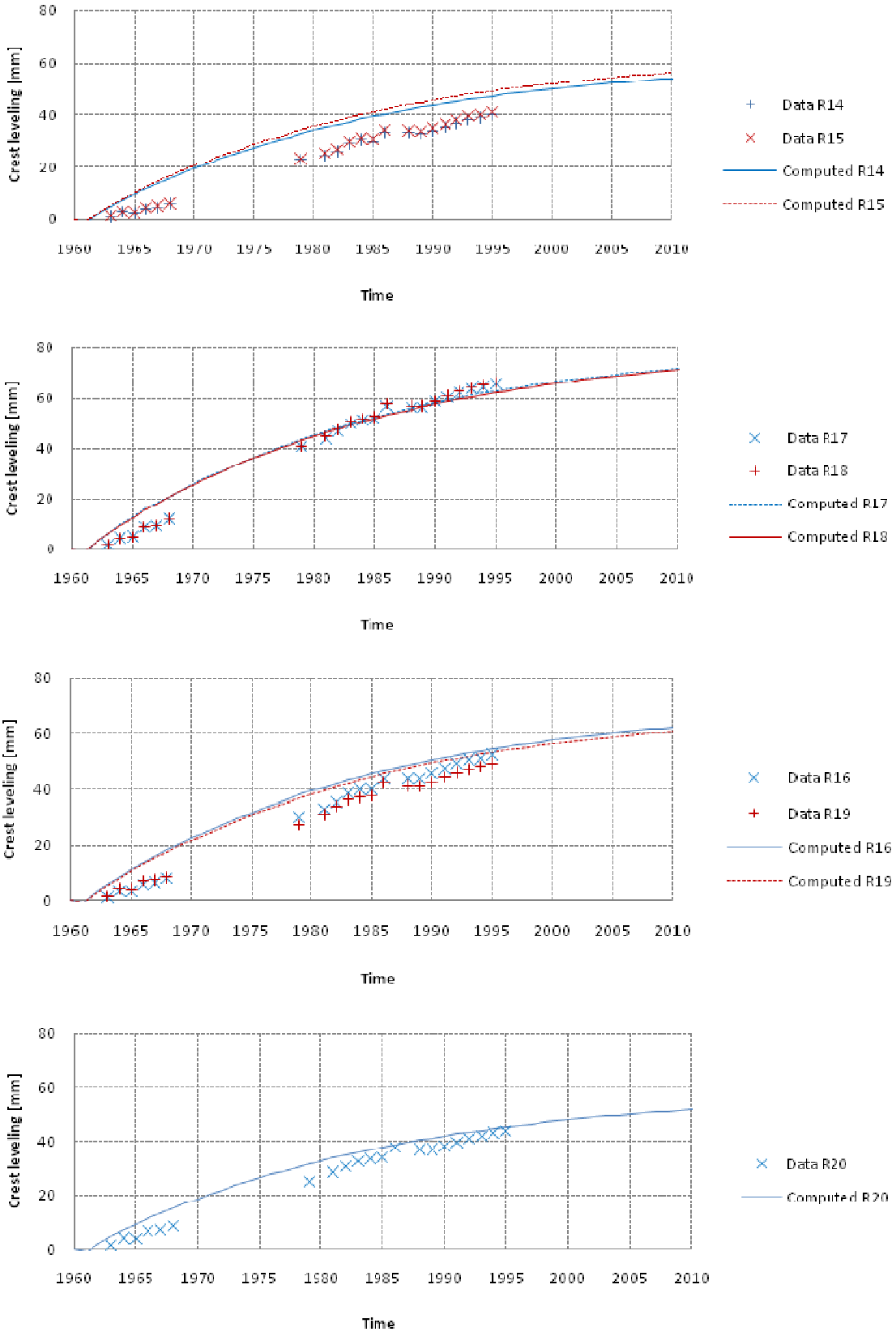

Figure 14: Calibration results for the following parameters of the AAR law: τ_c=5 years, τ_L=1 years and ε_∞=0.0021%.

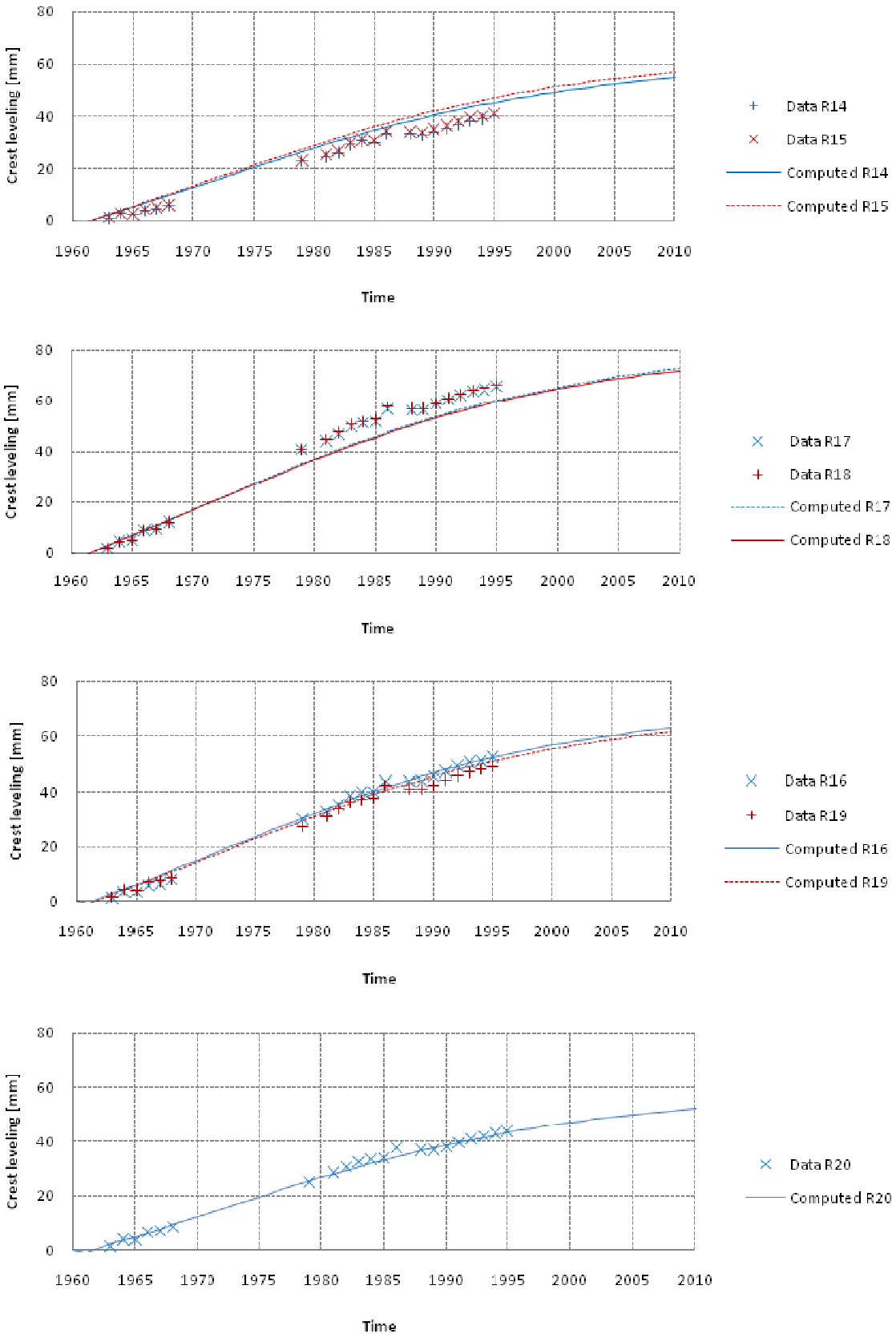

Figure 15: Calibration results for the following parameters of the AAR law: τ_c=2 years, τ_L=2 years and ε_∞=0.0021%.

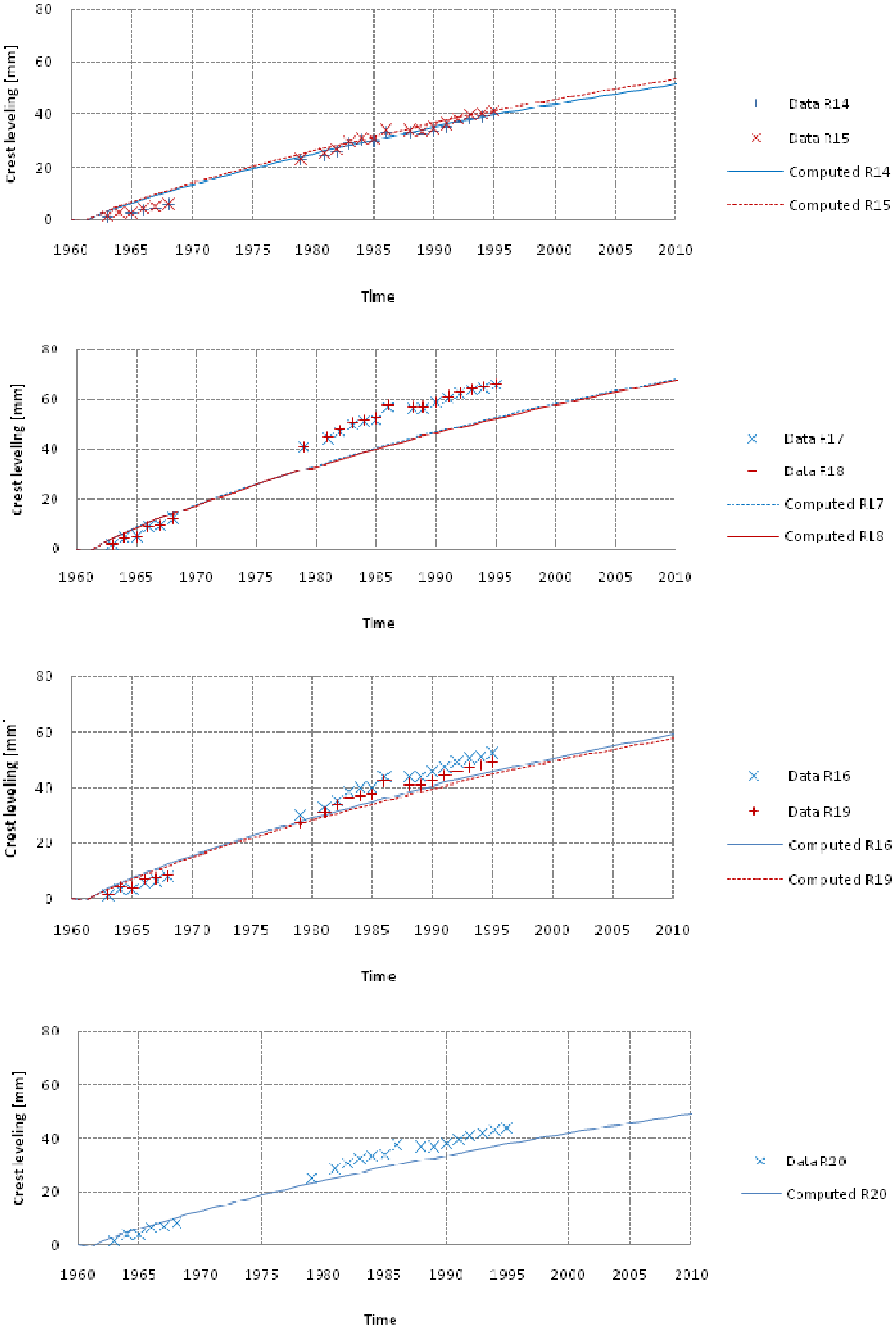

Figure 16: Calibration results for the following parameters of the AAR law: τ_c=10 years, τ_L=2 years and ε_∞=0.0021%.

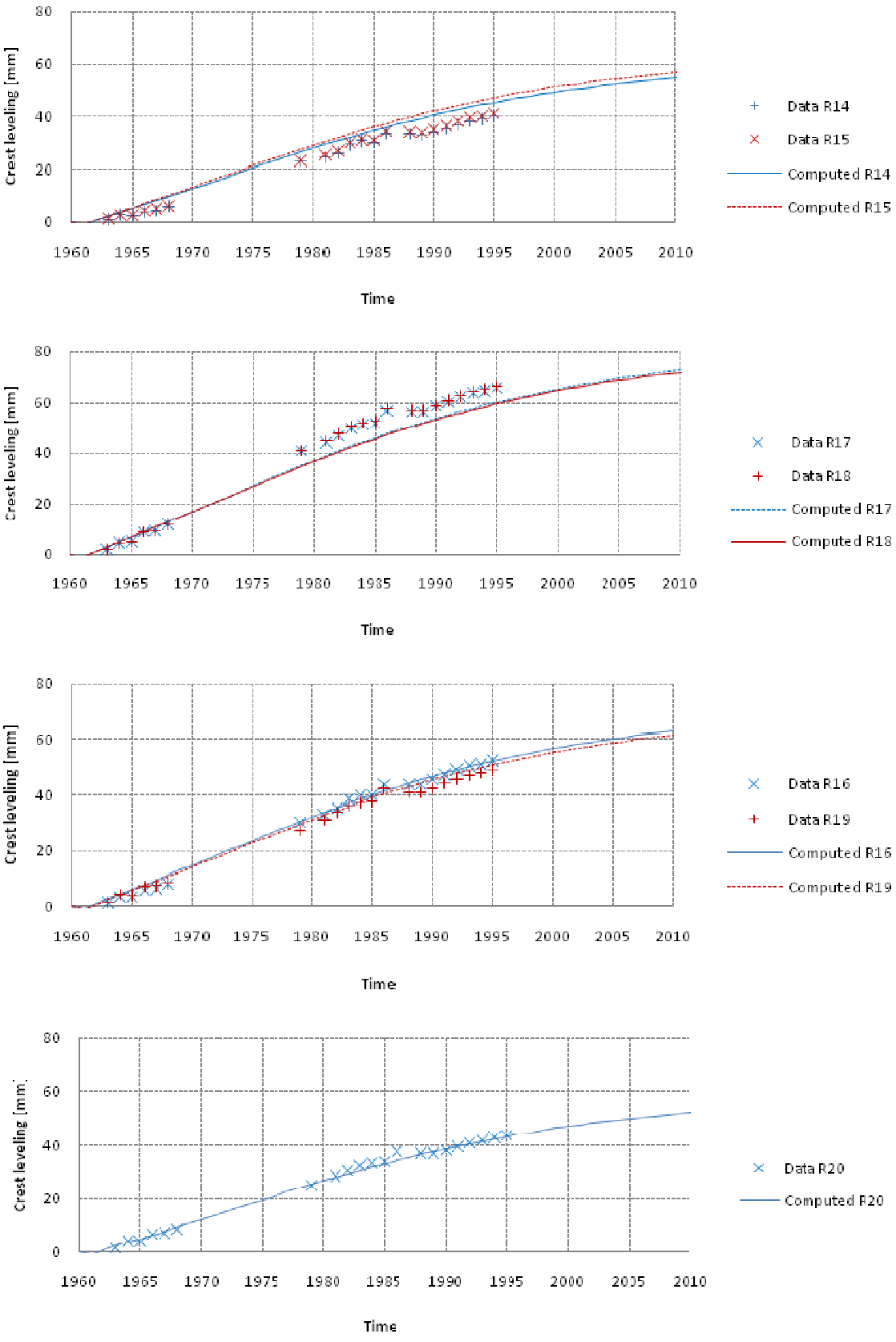

Figure 17 : Calibration results for the following parameters of the AAR law: τ_c=4 years, τ_L=4 years and ε_∞=0.0021%.

For some set of parameters, the behavior seems to be linear, i.e. when the characteristic time is much longer.

The conclusion is that the best match is quite obtained with the following parameters (see Figure 17): $\tau_l(T_0,h_0)$ the latency time of 4 years, $\tau_c(T_0,h_0)$ the characteristic time of 4 years, and $\varepsilon_\infty(h_0)$ the maximum strain expansion of 0.021%. Note that these characteristics are given at T_0=38° and h_0=100%. Figure 18 presents the comparison between numerical results and observation of the radial displacement of point T434.

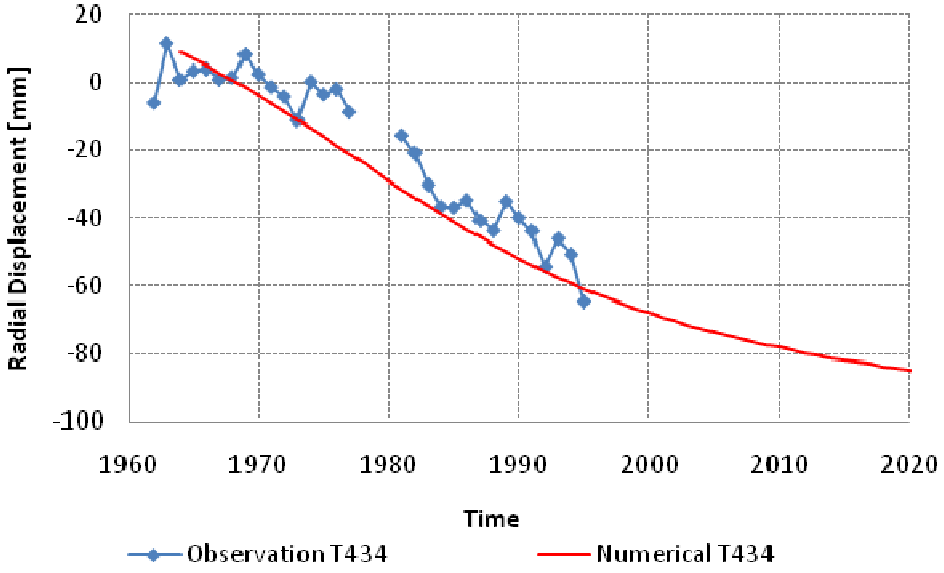

Figure 18 : Radial displacement of point T434 : comparison between numerical results and observation.

The corresponding results for this set of parameters are shown in Figure 17. It presents the results in detail for a selected number of points. One can notice that the computed results agree well with the observations.

In addition, the computed results show that the crest leveling increases less and less with time. The law is not linear, and a slight curvature is shown in the simulated behavior.

These numerical results show a good agreement with the available observational data which therefore concludes the calibration of the AAR model used in the simulation.

4.2 Numerical results for prediction of Kariba dam behavior

Figure 19 presents the leveling along the crest at three different dates: 1979, 1985 and 1995. This shows a quite good agreement between the numerical results and the observation. However, there is still a difference near the center of the crest. Figure 20 presents the evolution of the major principal stress at some points near the crest (where the reaction advanced) which can quantify the risk of cracking.

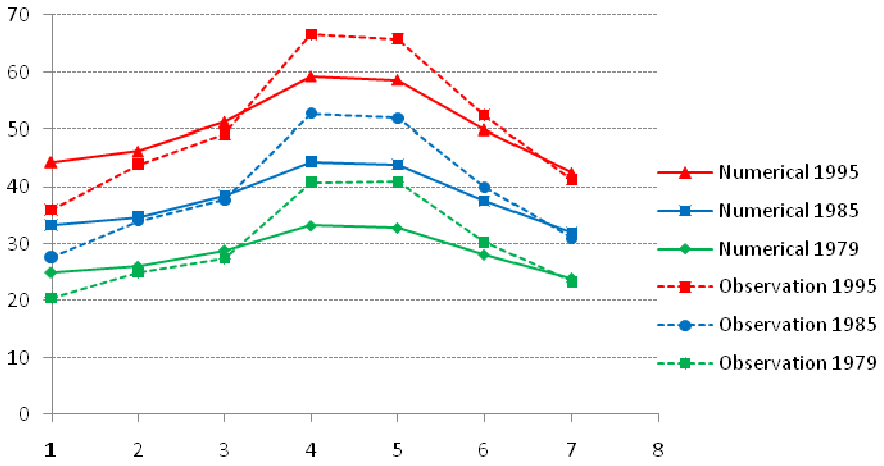

Figure 19 : Leveling along the dam crest at different time: comparison between numerical results and observation.

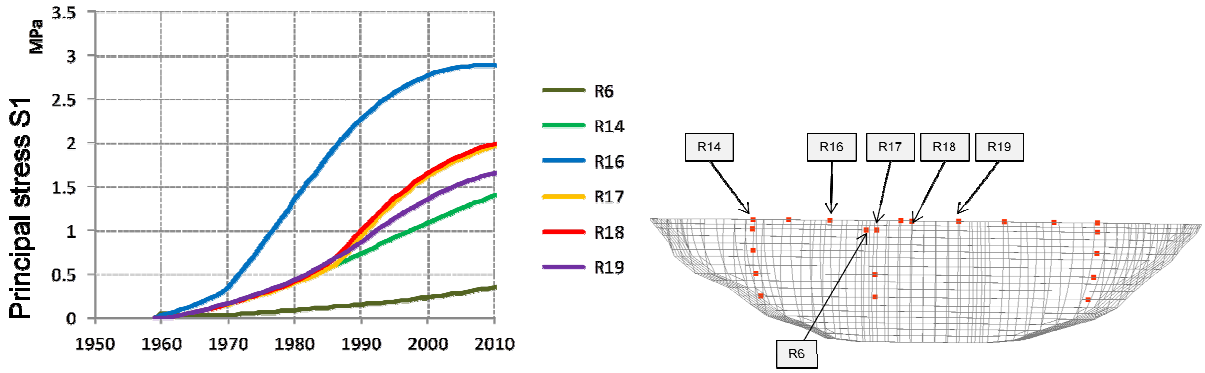

Figure 20 : Principal stress evolution ear the crest : tension appearing with the AAR.

5 Conclusions

In conclusion, a model for describing alkali aggregate reaction has been presented and used in order to simulate the behavior of the Kariba dam. The model has first been calibrated according to the observational data available during the period 1960-2010 (calibration results are shown in Figure 17). Once the calibration is reached, the displacement and stress states of the dam can be predicted.

References

[1] Li, K., Ulm, F.-J., Coussy, O., Larive, C., and Fan, L. (2000). Chemo-elastic modeling of alkali-silica reaction in concrete. In *11th Int. Conf. on Alkali-Aggregate Reaction in Concrete*, Quebec, pp. 989-998.

[2] Multon, S. and Toutlemonde, F. (2006). Effect of applied stress on alkali-silica reaction-induced expansion. *Cement and Concrete Research* 36, 912-920.

[3] Multon, S. , Seignol, J.F. and Toutlemonde, F. (2006). Chemo-mechanical Assessment of Beams Damaged by Alkali-Silica Reaction, journal of Materials in Civil Engineering 18, 500-509.

[4] Charlwood, R. and Sans, J. B. (Eds.) (2007). Chemical Expansion of Concrete in Dams & Hydro-Electric Projects, Granada, Spain. ICOLD Committee on Concrete Dams, Spanish Committee on Concrete for Dams, International Journal on Hydropower and Dams. http.//dam-research.org/Granada-2007.

XI ICOLD BENCHMARK WORKSHOP ON NUMERICAL ANALYSIS OF DAMS
Valencia, October 20-21, 2011

THEMA A

NUMERICAL SIMULATION OF CONCRETE STRUCTURE AFFECTED BY AAR: THE CASE STUDY OF KARIBA DAM

Esposito, Rita[1]

Handriks, Max A.N.[2]

Lilliu, Giovanna[3]

Schreppers, Gerd-Jan M.A.[4]

CONTACT

MSc Rita Esposito, Delft University of Technology, Department of Structural Mechanics, Stevinweg 1 (2628 CN, Delft, The Netherlands), +31 (0)15 27 82537 r.esposito@tudelft.nl.

Summary

Durability of concrete structures and infrastructures is a relevant topic for civil engineers. Long term effects that include chemical reactions producing concrete swelling are one of the aspects related to durability of concrete structures.

The Kariba dam is a representative case study for investigating swelling in concrete structures due to Alkali-Aggregate Reaction (AAR). In this paper the dam is analyzed with a modified version of the DIANA Finite Element program [1].

AAR damage is evaluated with a thermo-chemo-mechanical model based on an approach by Ulm et al [2]. The Larive's law [3] is adopted to define the AAR expansion evolution as function of time. The influence of imposed stresses on orthotropic chemical strains is also taken in account, as suggested by Saouma and Perotti [4]. The results are compared with results obtained from a simplified solution in which the stress dependency is considered constant in time and space.

[1] Delft University of Technology, Department of Structural Mechanics, Delft, The Netherlands.
[2] Delft University of Technology, Department of Structural Mechanics, Delft, The Netherlands.
[3] TNO DIANA BV, Delft, The Netherlands.
[4] TNO DIANA BV, Delft, The Netherlands.

1. Introduction

The Kariba dam is an example of concrete structure affected by AAR. This dam has already been object of several studies [5], [6] and it is now proposed for the 11th Benchmark Workshop on Numerical Analysis of Dams [7].

The Kariba dam is a double curvature arch dam built across the Zambezi River between 1956 and 1959. The dam has shown evident signs of swelling soon after starting of its operation; for this reason the dam has been instrumented over the years for monitoring its behavior.

In this paper the dam is analyzed with a modified version of the DIANA program [1]. A 3D mesh is defined and interface elements are placed between dam and foundation. An elastic behavior is considered for concrete and soil. A thermo-chemo-mechanical model, on the basis of Ulm's model [2], is implemented in a modified version of the DIANA code [1]. The model takes into account the effect of stress state on the orthotropic swelling, according to Saouma and Perotti [4]. Parameters in the Larive's law [3] are calibrated in order to match the measurements. The results of this advanced solution are compared with a simplified approach in which the AAR stress dependency is considered constant in time and space.

2. Adopted model

2.1. Finite Element Model

Quadratic brick elements with 3x3x3 integration schema are adopted to model the dam and the foundation (Figure 1). Contact between dam and foundation is modeled with quadratic interface elements with a Newton-Cotes integration scheme, with 3x3 integration points. The mesh is based on the second mesh proposed in the Benchmark Guidelines [7].

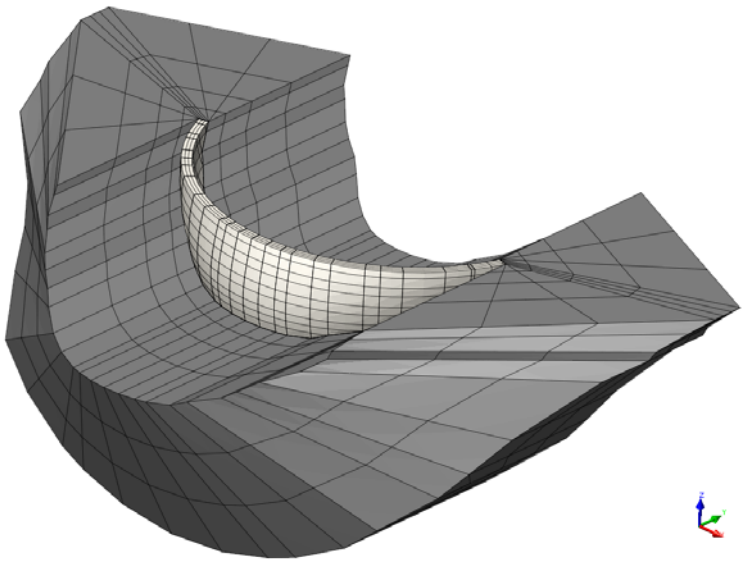

Figure 1: Finite elements mesh [7].

A phased analysis is performed in order to simulate the behavior of the dam during the construction and operation phase. In the first phase, the cantilevers are physically and topologically isolated and the dead weight is applied. The stress determined in the first phase are included as initial stresses in the second phase of the analysis, omitting the displacements. During the operation period (1962-2010), rigid links (tyings) are used for connecting the cantilevers.

Due to the location of the dam, a small temperature variation around 27 °C is observed during the year; for this reason thermal effects are not included in the analysis.

As proposed in the Benchmark Guidelines [7], the water pressure is considered constant through four subsequent periods. The four main levels are given in Table 1.

Table 1: Applied water level.

Period	Water level
1962-1973	483.80 m
1974-1981	486.10 m
1982-1995	479.90 m
1995-2010	483.00 m

A step size of one year is used.

2.2. Material model

Concrete and soil are modeled as linearly elastic; their mechanical characteristics are given in Table 2, according to the Benchmark Guidelines [7].

Table 2: Mechanical properties of concrete and soil [7].

Property	Unit	Foundation rock	Dam concrete
Elastic modulus	N/m^2	$1.0\ 10^7$	$2.2\ 10^7$
Poisson's ratio	-	0.2	0.2
Unit weight	N/m^3	Not considered	$2.35\ 10^3$

Nonlinear interface elements are placed between dam and foundation. In the normal direction the elastic stiffness is set to 10^{11} N/m^3 in compression and 10^3 N/m^3 in tension. This means that the interface is stiff in compression and nearly stress free in tension. In the shear direction the stiffness is constant and equal to 10^{10} N/m^3

The chemical aspect of AAR is included in the model through the Larive's formulation [3].

$$\varepsilon^{vol} = \varepsilon_{\infty} \frac{1-\exp(-t/t_c)}{1+\exp\left(\frac{t_l - t}{t_c}\right)} \tag{1}$$

where ε_∞ is the asymptotic volumetric expansion, t_l and t_c are the latency and characteristic time, respectively.

In Figure 2 and Table 3 the adopted kinetic law and the selected parameters, for the reference temperature of 27 °C, are given. It is assumed that expansion starts immediately after impounding.

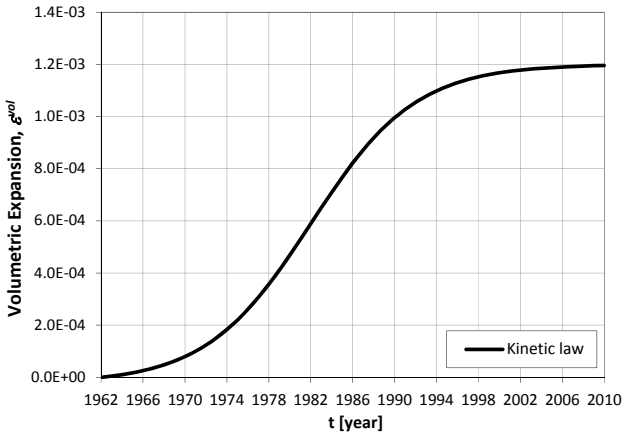

Figure 2: Adopted kinetic law.

Table 3: Parameters of the kinetic law.

Parameter	Value
Ref. temperature T_{ref}	27 °C
Asymptotic expansion ε_∞	0.12 %
Latency time t_l	20 years
Characteristic time t_c	5 years

The kinetic law is calibrated including the "*expansion transfer*" concept. As shown by Multon and Toutlemonde [8], the volumetric strain due to AAR swelling can be redistributed on basis of the principal stresses. In order to take into account this effect, weight coefficients are adopted to define the linear expansion due to AAR, as proposed by Saouma and Perotti [4]. The linear expansion, ε^i_{AAR}, along the *i-th* principal stress direction is defined as:

$$\varepsilon^i_{AAR} = w_i \; \varepsilon^{vol} \qquad i = 1,2,3 \tag{2}$$

where ε^{vol} is the volumetric expansion defined in accordance with the kinetic law, and w_i is the weight for the *i-th* principal stress direction.

The three weights for a generic stress situation are defined as linear interpolation from four specified "nodal" values:

$$w_i = \sum_{j=1}^{4} N_j(\sigma_I, \sigma_{II}) \cdot W_j\left(\sigma_{III}\right) \tag{3}$$

where σ_I, σ_{II} are the principal stresses in the plane perpendicular to *i-th* direction and σ_{III} is the principal stress along *i-th* direction (see Figure 3 (a)). W_j are fixed weights defined for sixteen specific situations (see Figure 3 (b)), and N_j is the bilinear shape function used in finite element formulations.

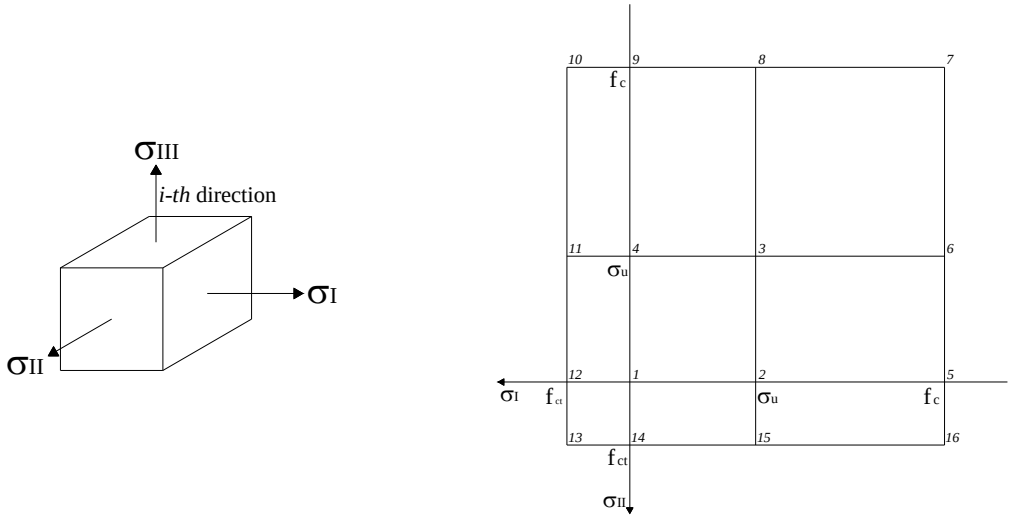

(a) (b)

Figure 3: (a) Principal stresses nomenclature for *i-th* direction. (b) Weight region [4].

The weight coefficients are defined for a stress range between the tensile strength, f_{ct}, and the compressive strength, f_c, (see Figure 3 (b)). On basis of experimental tests of Struble and Diamond [9], the threshold value σ_u, above which no expansion occurs, is taken equal to -1.0 10^7 N/m^2. Outside the range definition, which is possible in a linear analysis, the weights are considered constant and equal to the values of the nodes on the border line.
The weight coefficients along the global axes can be derived as:

$$w_k^{XYZ} = \frac{\varepsilon_{AAR}^k}{\varepsilon^{vol}} \qquad k = X, Y, Z \tag{4}$$

where ε_{AAR}^k is the AAR strain along the *k-th* global axis, obtained from the principal AAR strain through the transformation matrix between principal and global directions.
The values adopted for the compressive and tensile strength are -12 10^6 N/m^2 and 1.1 10^6 N/m^2 , respectively.

3. Numerical results

In this section the numerical results are reported and commented. First, the advanced solution obtained with the model described in the previous section is shown; then, a simplified approach in which the AAR stress dependency is considered constant in time and space is presented.

3.1. Advanced solution

The numerical results are compared with measurements from nine instruments (Figure 4) through the calibration period (1962-1994).

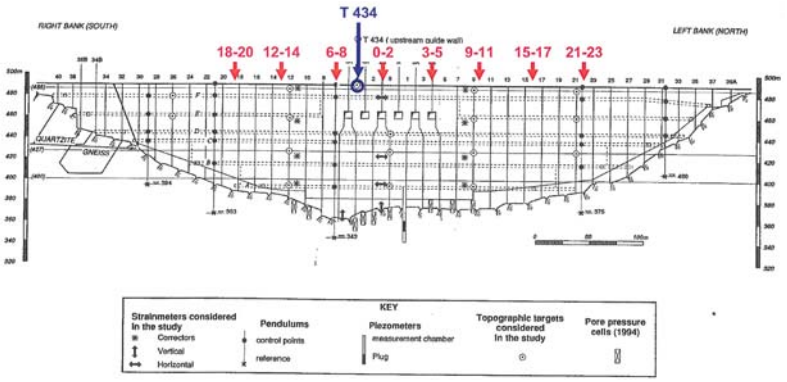

Figure 4: Location of the main instruments [7].

Figure 5 shows the comparison between measured and numerical results. The displacements in radial direction are calculated in a cylindrical reference system with the axis in Z-direction and the origin at the point X=0 m, Y=230 m, Z=0 m in the rectangular coordinate system. The initial displacement due to impounding is subtracted both from the vertical and the radial displacements.

These results derive from a calibration of the kinetic law. The value of the latency time is chosen in agreement with the delay shown in the radial displacement (1962-1975). The value of the characteristic time and the asymptotic expansion are defined in agreement with the vertical displacement at the end of the calibration period (1994).

Figure 6 shows the variations in time of stresses and weights for three selected elements along the height of the dam. Along the X-axis the highest compressive stress (Figure 6 (b)) is observed and the weight coefficient varies between 0.32 to 0.36 (Figure 6 (e)). The weights along Y and Z-axis vary between 0.1 to 0.35 (Figure 6 (f)) and between 0.3 and 0.52 (Figure 6 (g)), respectively. This confirms the anisotropic behavior observed during measurements.

Comparing Figure 6 (e), (f) and (g), it is possible to observe that the deeper is the position of the element, the higher is the variation of the weights in time. This trend could be explained with the fact that the elements near the bottom part of the dam are constrained more by the foundation.

An observation should be made on the origin of the weights: in each step the weights are calculated with an explicit formulation which take into account the stress state of the previous time step.

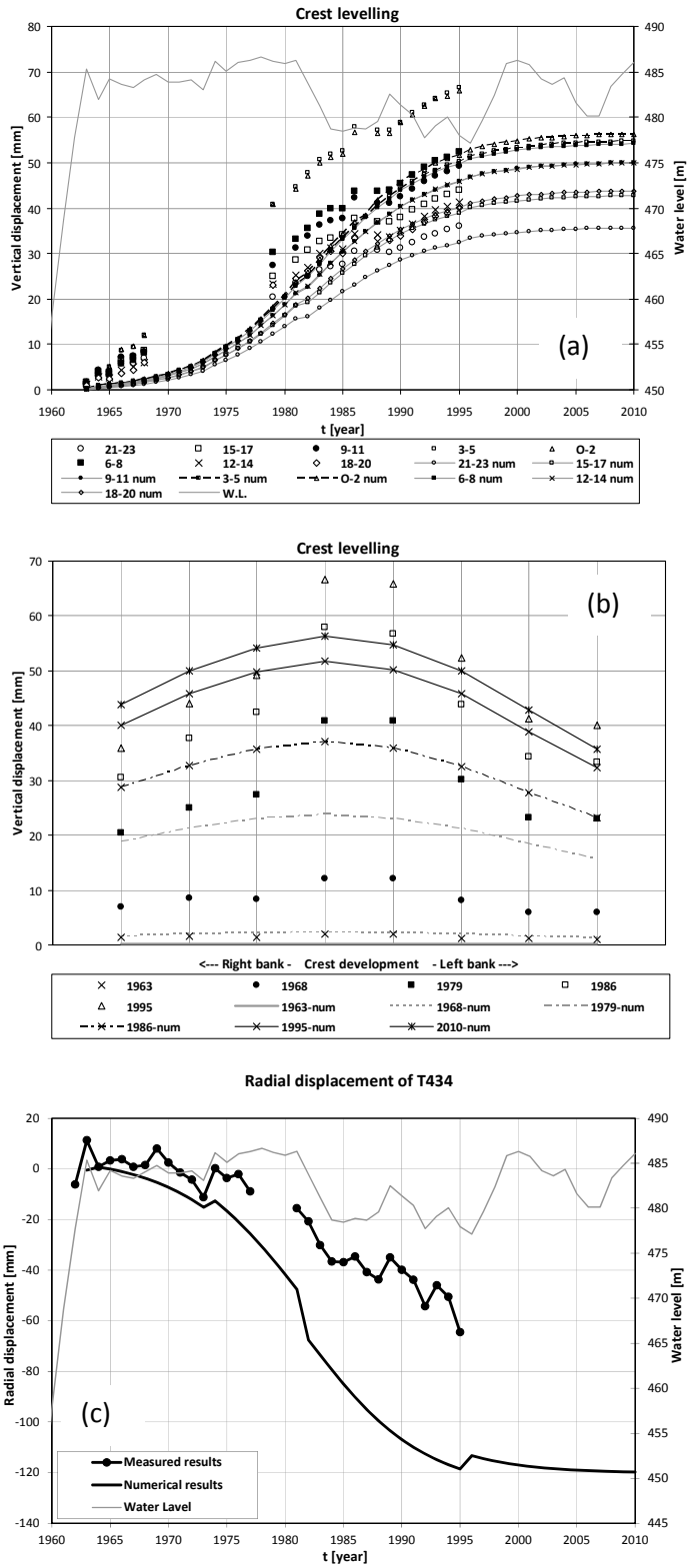

Figure 5: Comparison between numerical results (advanced solution) and measurements.

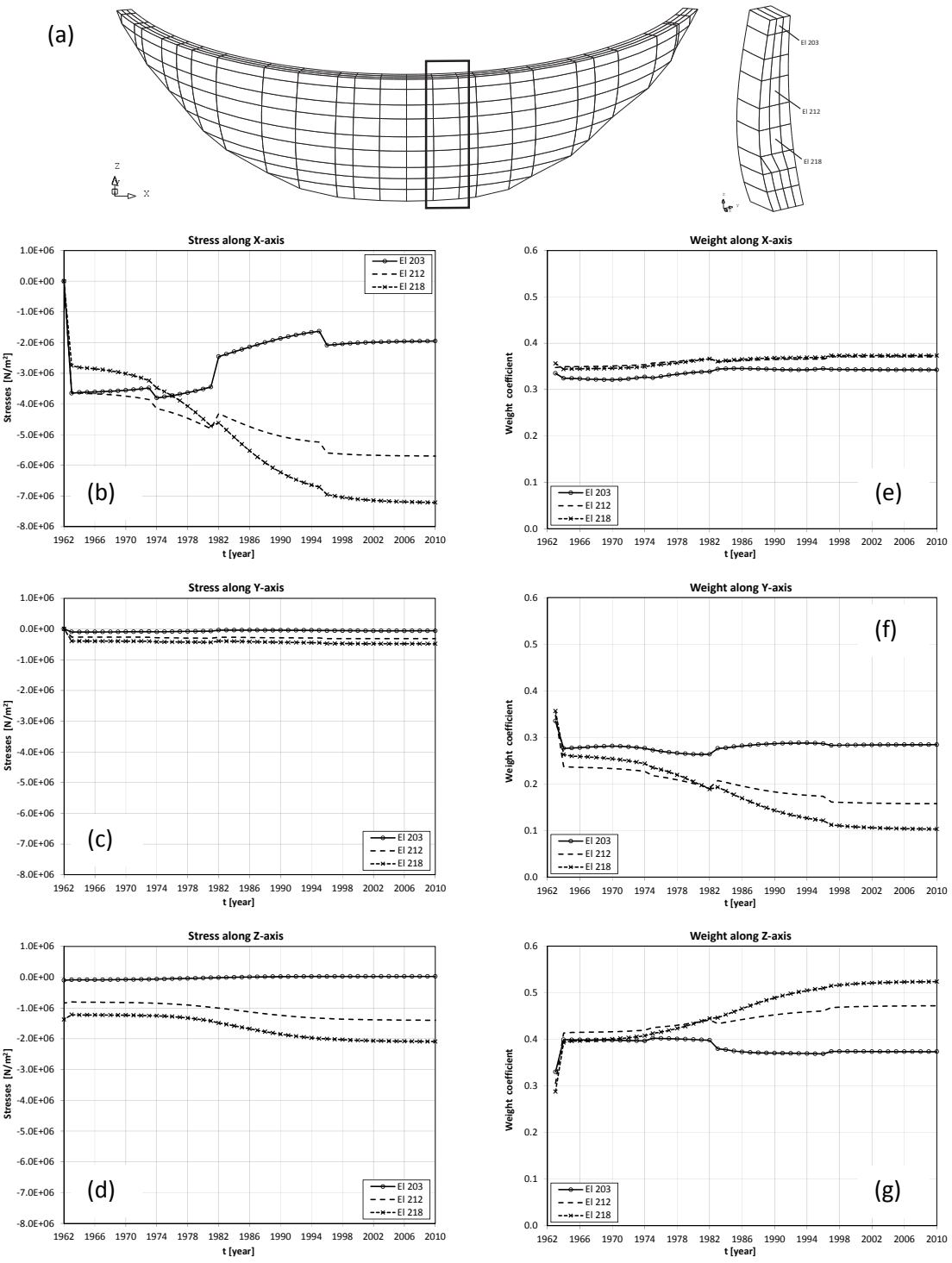

Figure 6: (a) Selected elements; (b)-(d) variation of stresses and (e)-(g) variation of weight coefficients w^{XYZ} along X,Y and Z-axis.

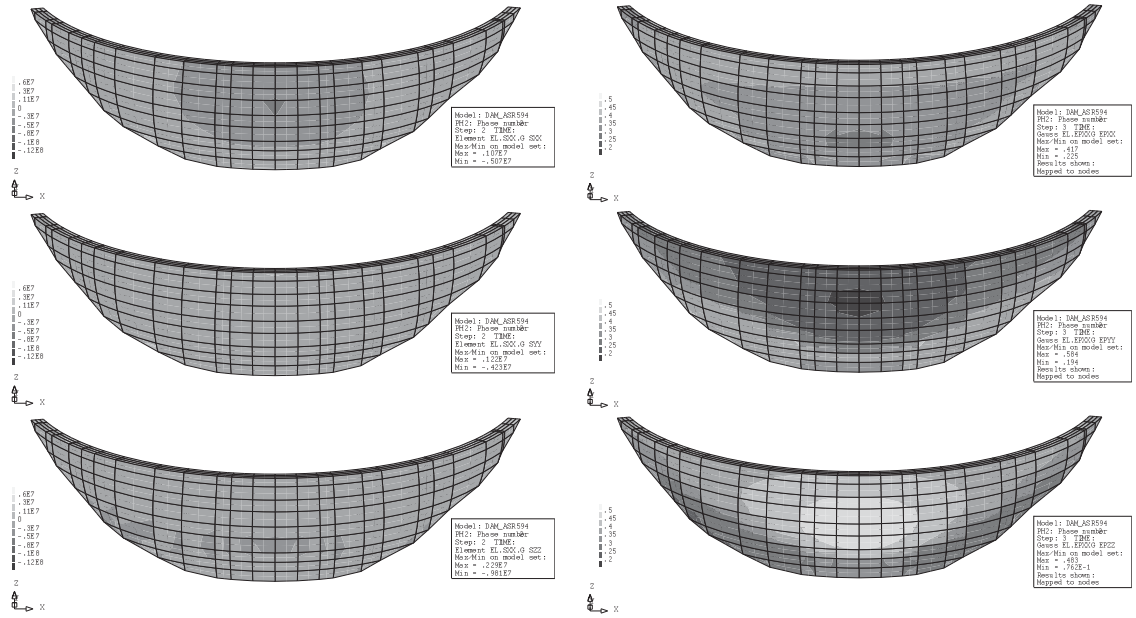

(a) (b)

Figure 7: Numerical results after impounding: (a) stresses and (b) weight coefficient w^{XYZ}.

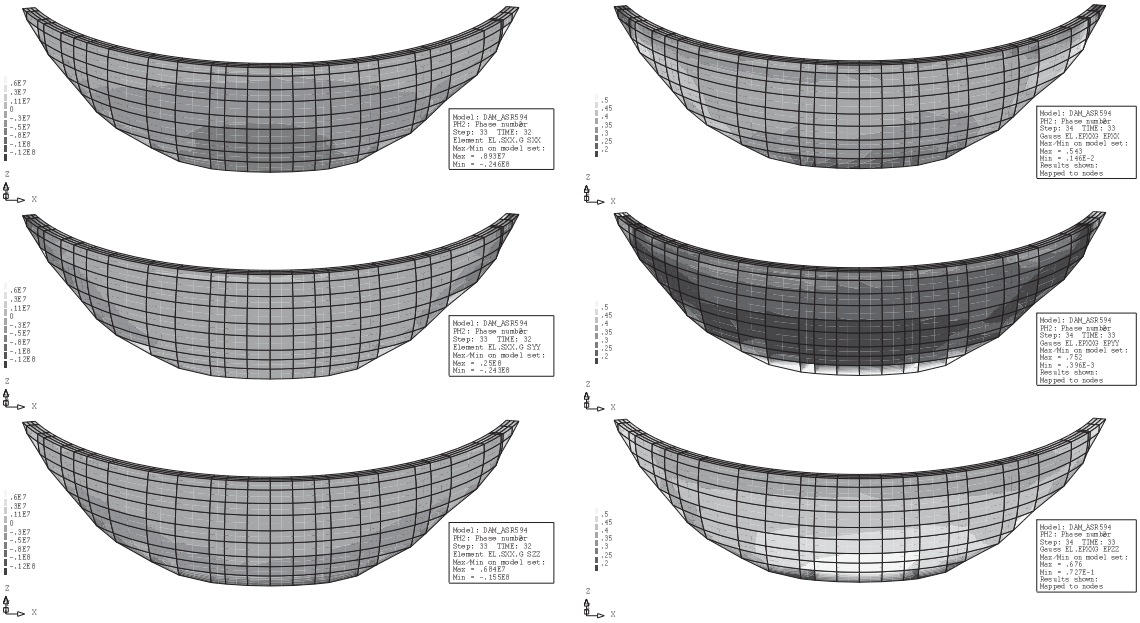

(a) (b)

Figure 8: Numerical results at the end of the calibration period: (a) stresses and (b) weight coefficient w^{XYZ}.

Figure 7 and Figure 8 show contour plots of stresses and weight coefficients in the global axis after impounding (1963) and at the end of the calibration period (1994). In line with the explicit formulation, the numerical results for the weights are presented for the respective subsequent steps: 1964 in Figure 7 (b) and 1995 in Figure 8 (b).

It is possible to observe a non-homogeneous distribution of the weights in the dam, especially after the impounding Figure 7 (b).

In order to understand the relevance of the weights' variation a simplified analysis with an homogeneous distribution of the weights, which are also kept constant in time, is carried out and shown in the following section.

Figure 9 shows the mean stresses along X, Y and Z-axis in element 218 for the advanced solution and for an analysis without AAR. Due to the arch shape of the dam, a big difference is observed for the stresses along the X-axis. Indeed along Y-axis, the expansion is free and no generation of stress due to AAR swelling is observed.

Furthermore the stresses for the analysis which does not take into account the AAR effect, are nearly constant in time, due to the small fluctuation of the water level during the time.

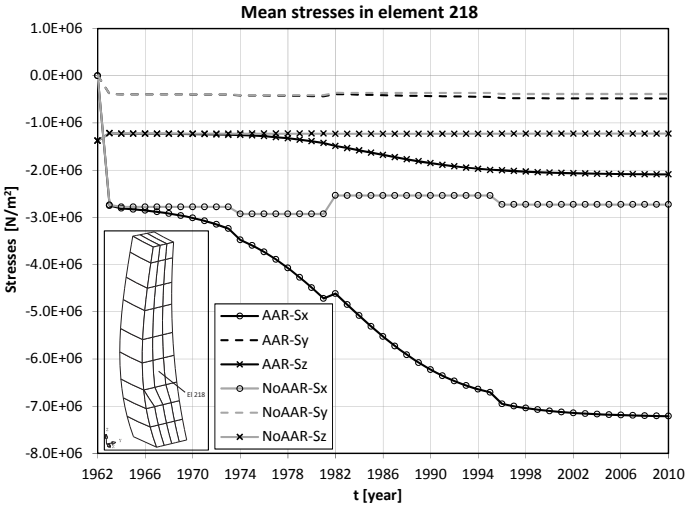

Figure 9: Stresses in element 218 obtained with the advanced solution and an analysis without AAR.

Figure 10 and Table 4 give the prediction of the dam behavior in 2010.

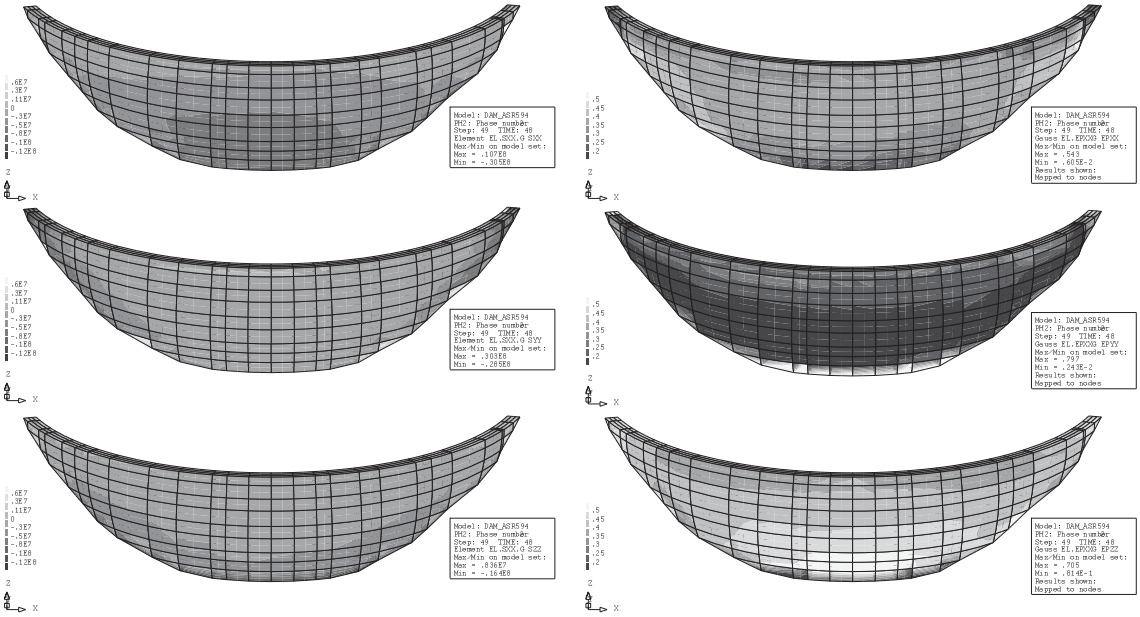

(a) (b)

Figure 10: Numerical results at the end of the prediction period: (a) stresses and (b) weight coefficient w^{XYZ}.

Table 4: Prediction of vertical and radial displacement of reference points in 2010.

Reference point	Vertical displacement [mm]	Radial displacement [mm]
18-20	43.82	-42.64
12-14	49.97	-80.58
6-8	54.21	-108.28
O-2	56.32	-123.12
3-5	54.73	-115.92
9-11	50.01	-89.06
15-17	42.74	-46.58
21-23	35.63	-7.24
T434	59.12	-119.77

3.2. Simplified solution

In this section the results of a simplified solution in which the weights are fixed and based on the stress situation after impounding are presented. The weights are calculated as the average of the values in the three elements shown in Figure 6 (a). A homogeneous distribution in space is considered.

Table 5: Parameters of kinetic law and weights for the two simplified solutions.

Parameter	Advanced solution	Simplified solution
Asymptotic expansion ε_∞	0.12 %	0.12 %
Latency time t_l	20 year	20 year
Characteristic time t_c	5 year	5 year
w_X^{XYZ}	Stress dependent	0.34
w_Y^{XYZ}	Stress dependent	0.26
w_Z^{XYZ}	Stress dependent	0.40

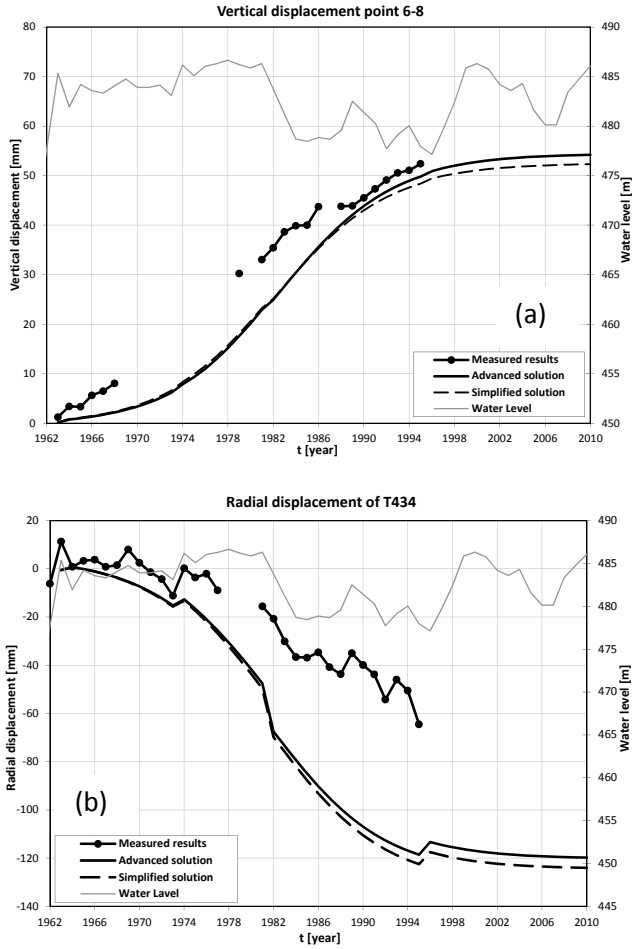

Figure 11: Comparison between the advanced and the simplified solution.

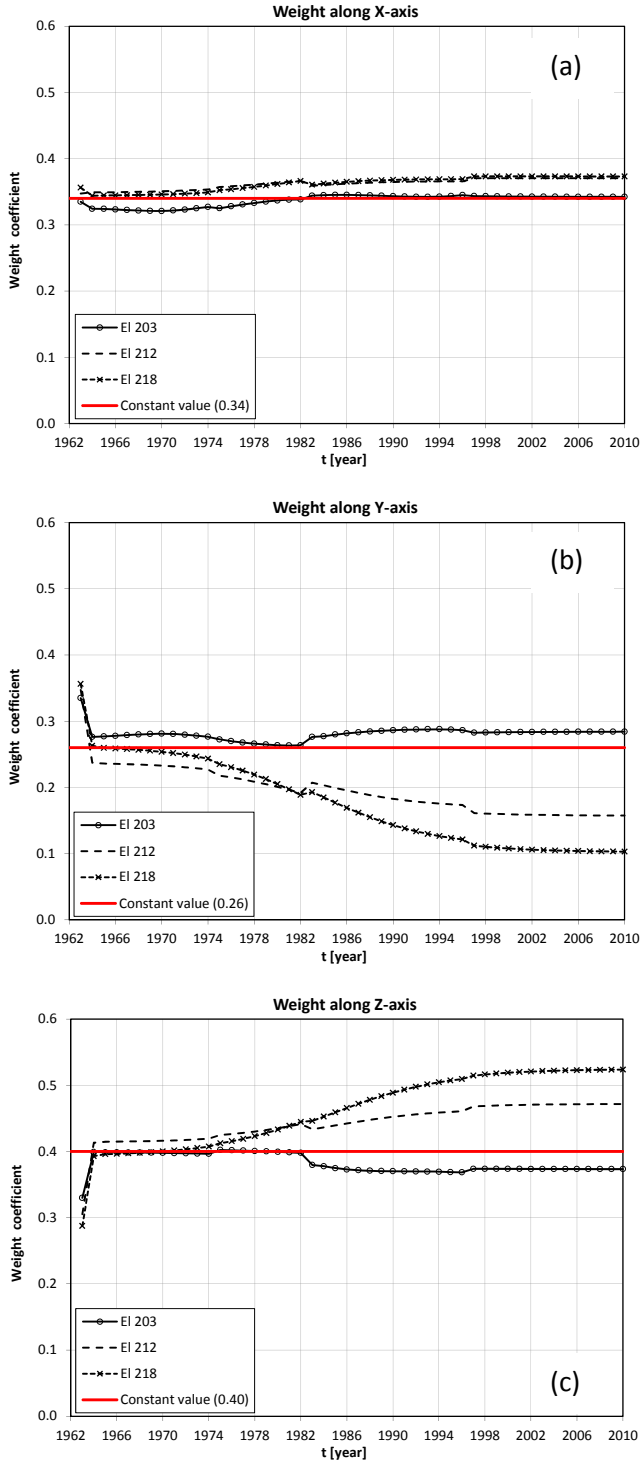

Figure 12: Comparison between weights adopted in the advanced solution (see Figure 6) and in the simplified solution (constant values).

In Figure 11 numerical results obtained with the advanced solution and the simplified solution are compared.
Both the radial and the vertical displacement obtained through the simplified solution are close to the results of the advanced one in the period from 1962 to 1982. This could be explained by the small difference observed between the constant weights adopted in the simplified solution and the stress dependent weights adopted in the advanced one (Figure 12 (b) and (c)).
In period 1982-2010 the difference in displacement between the two analyses is larger, as is the difference between the weights (Figure 12).
The small difference between the advanced and simplified solution leads to the conclusion that the stress redistribution of the AAR swelling can be predicted on the basis of the initial stress in the dam and considered constant in time and space. Note that for the structure presented here, the stress state due to external load is nearly constant in time. Extra stress variation due to varying external loads would make a simplified solution less adequate.

4. Conclusion

The Kariba dam is adopted in this paper as a case study for analyzing effects of swelling due to AAR. In order to predict the behavior of the dam in 2010, a 3D finite element analysis is carried out with a modified version of DIANA.
A linear chemo-elastic behavior is adopted for the dam and its foundation. Interface elements with nonlinear behavior are introduced between dam and foundation. Rigid links are introduced between adjacent cantilevers to simulate grouting of the vertical joints after construction.
Due to the small variation of temperature in the dam's site, the thermal effects are neglected.
Evolution in time of swelling due to AAR is defined according to the Larive's kinetic law [3]. Calibration of the parameters in this kinetic law (asymptotic expansion, latency and characteristic time) takes into account *"expansion transfer"* concept according to Saouma and Perotti formulation [4].
The results of this advanced solution are compared with a simplified approach in which the AAR stress dependency is considered constant in time and space. In the simplified solution the weight coefficients, which defined the redistribution of the volumetric expansion along the global axis, are calculated on the basis of the stress state achieved after impounding.
The comparison between the advanced and simplified solution leads to a similar behavior in terms of radial and vertical displacements of the dam's crest.
The simplified solution could be a good approach to take in account the *"expansion transfer" concept* in structures in which the stress state due to external loads is constant in time.

Acknowledgements

The authors wish to express their thanks to the Dutch Technology Foundation STW for its financial support.

References

[1] DIANA program www.tnodiana.com
[2] Ulm, FJ, Coussy, O, Kefei, L, Larive, C (2000). Thermo-chemo-mechanics of ASR expansion in concrete structures. ASCE Journal of Engineering Mechanics Vol. 126, 3, pp. 233-242.
[3] Larive, C (1998). Apports combinés de l'expérimentation et de la modélisation à la comprehension de l'alcali-reaction et de ses effets mécaniques. Monograph LPC, Laboratoires des Ponts et Chaussées, Paris.
[4] Saouma, V, Perotti, L (2006). Constitutive model for alkali-aggregate reaction. ACI Material Journal, Vol. 103, 3, pp. 194–202.
[5] ICOLD-Durban (1994) Q68 R86 Kariba dam safety monitoring and resulting maintenance works
[6] ICOLD-Firenze (1997) Q74-9 Reservoir level influence on concrete swelling rate: Modelization in the case of Kariba.
[7] Noret, C., Molin, X. (2011). Eleventh Internationa Benchmark Workshop on Numerical Analysis of Dams, THEME A, Effect of Concrete swelling on the equilibrium and displacements of an arch dam, October 20-21, Valencia, Spain.
[8] Multon, S, Toutlemonde, F (2006): Effect of applied stresses on alkali-silica reaction-induced expansions. Cement and Concrete Research, (36): 912–920.
[9] Struble, L., Diamond, S. (1981), Swelling Properties of Synthetic Alkali Silica Gels. Jurnal of the American ceramic Society, Vol. 64, 11, pp. 652-655.

XI ICOLD BENCHMARK WORKSHOP ON NUMERICAL ANALYSIS OF DAMS
Valencia, October 20-21, 2011

THEME A

PREDICTION OF SWELLING DUE TO AAR IN KARIBA DAM

Schreppers, Gerd-Jan
Lilliu, Giovanna

CONTACT
Dr. Gerd-Jan Schreppers, TNO DIANA BV, Delftechpark 19a (2628 XJ, Delft, The Netherlands), +31-883426200, info@tnodiana.com (http://tnodiana.com).

Summary
Swelling due to alkali aggregate reaction (AAR) is predicted using the finite element program DIANA [1]. The dam body and the rock foundation are modelled in 3D, with interface elements placed between the dam and the rock, which allow only transmission of compressive stresses. The same type of nonlinear interfaces is also used to model the vertical joints during construction and grouting of the joints is modelled by changing the stiffness of the interface elements. Both concrete and rock are modelled as linear elastic materials.
It is assumed that swelling of concrete is homogeneous and that anisotropic volumetric strains develop in time according to the model of Larive [3]. Anisotropic expansion is assumed with a larger expansion in vertical direction. The parameters of Larive' model and of the anisotropic expansion are chosen such that the best possible fitting between measurements and analysis results is achieved. In this manner, the radial and vertical displacements of the reference points at crest level recorded in the period 1963-1995, can be reproduced with the finite element model within accuracy of circa 5 mm.
Extrapolation of this prediction to 2010 brings to the conclusion that the maximum radial and vertical displacement at crest level, with reference to the situation immediately after impounding (1963), is 56 mm.

1. Introduction
The Kariba dam is a large arch dam built on the Zambesi river, which has shown signs of swelling due to AAR soon after start of operation. This dam is subject of the 11th Benchmark Workshop on Numerical Analysis of Dams [1]. Formulators of this theme, Theme A, have provided mesh and linear elastic material properties both of the dam and of the rock foundation, together with the water level in the reservoir immediately after impounding until 1995. As the dam is located in an area with minimal temperature variations during the year, formulators have suggested neglecting the effect of temperature on swelling. Stresses and displacements at target points have also been provided through the period 1962-1995.
This paper describes the contribution of TNO DIANA to Theme A. The analyses have been performed with DIANA, release 9.4.4., using the standard functionalities in the program and without developing any specific AAR model. Swelling due to AAR is modelled as a homogeneous, time dependent volumetric expansion. Different time functions are considered (linear and according to the model of Larive) and both the cases of isotropic and

anisotropic expansion are studied. The different numerical results are discussed and compared with the measurements provided by the formulators of the benchmark.

2. Finite Element Model

2.1 Mesh

The same mesh of the dam body is used, as it has been provided by the formulators. The mesh of the foundation has been modified as shown in Figure 1 in order to make definition of boundary conditions more straightforward. In order to facilitate comparison of the numerical results with the measurements, numbering of nodes and elements in the dam body is the same as in the model that is provided.

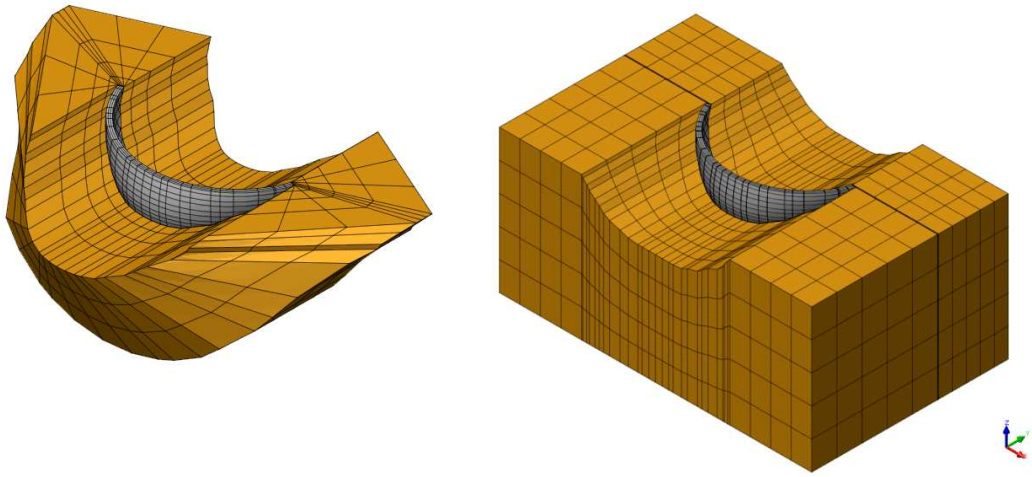

Figure 1: Mesh provided by the formulators (left) and adapted in this contribution (right).

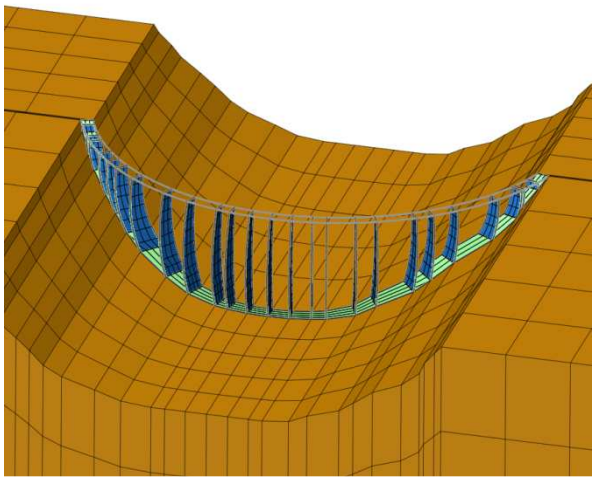

Figure 2: Interface elements between dam and foundation, and at the vertical joints.

Interface elements are introduced between the dam and its foundation, and between two adjacent pendula. As the mesh is not fully consistent with the location of the vertical joints, the interfaces are placed between adjacent columns of elements. All these interfaces are tension stress free. Furthermore, reduced shear stiffness is assumed in the vertical interfaces

during the construction phase. After construction phase, for simulating grouting of the joints, stiffness in normal and shear direction in vertical joints is increased as if nodes of the interface would be tied.
The nodes at the outer boundaries of the foundation are supported in the direction normal to these surfaces only.

2.2 Material properties

Both the rock foundation and concrete of the dam body are considered linear elastic, with properties as specified in Table 1.
The elastic stiffness of the interface between dam and foundation is set at 1.E+12 Pa/m in tangential direction. The same stiffness is assumed in normal direction for compression, while is 1.E+0 Pa/m in tension.
The same properties in the normal direction are assumed also for the vertical interfaces during construction of the dam, but the shear stiffness is reduced to 1.E+10 Pa/m. After construction, grouting of the vertical joints is simulated by increasing the stiffness in tension and in shear to 1.E+12 Pa/m.

Table 1: Material parameters

	Rock	**Concrete**
Young's modulus	10.0 GPa	22.0 GPa
Poisson ratio	0.20	0.20
Density	0	2350 kg/m3

2.3 Loads

Loads acting on the structure are the weight of the dam and the hydrostatic pressure of the water in the reservoir. As requested by the formulators, in a preliminary analysis stresses and displacements are calculated ignoring the effects of swelling and considering four different water levels in the reservoir, as specified in Table 2.

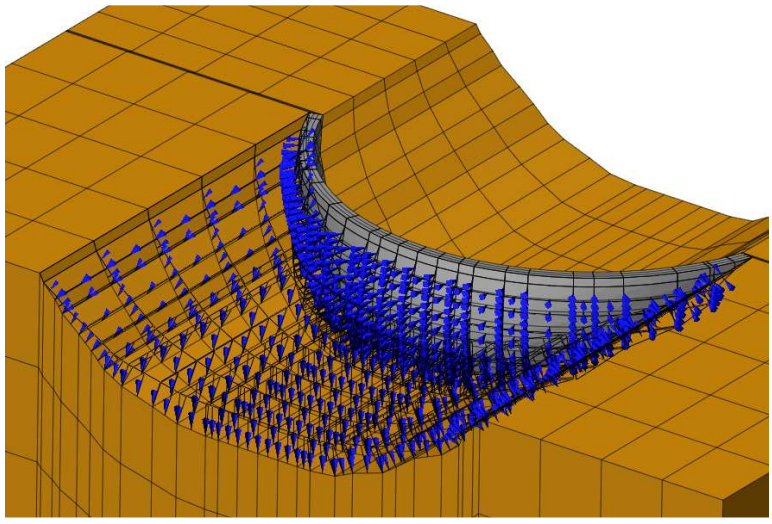

Figure 3: Hydrostatic pressure.

Table 2: Load cases

Load-case	Type	Value	Period
1	Weight	9.81 kg/m2	always
2	Hydrostatic	483.8 m	1962-1972
3	Hydrostatic	486.1 m	1972-1981
4	Hydrostatic	479.9 m	1981-1995
5	Hydrostatic	483.0 m	1995-2010

2.4 Element types

The finite elements in the foundation and in the dam are quadratic brick elements of hexahedral, pentahedral and tetrahedral shape. The interface elements at the base of the dam and at the vertical joints are quadratic interfaces. The shape of the interfaces is quadrilateral or triangular (see Figure 4). The integration scheme adopted in the interfaces is a Newton-Cotes integration scheme with 3x3 integration points in the quadrilateral interfaces and with 3 integration points in the triangular interfaces.

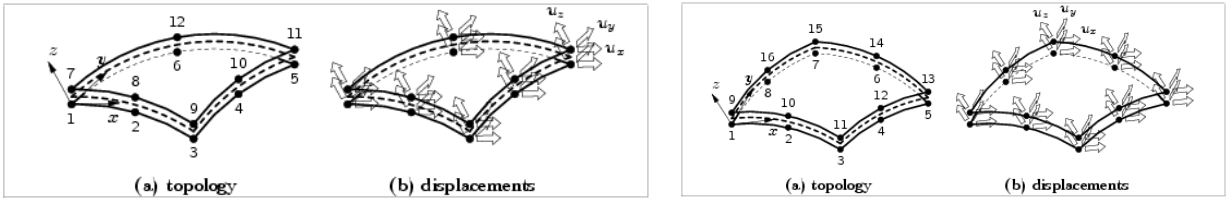

Figure 4: Triangular (left) and quadrilateral (right) interfaces.

2.5 Analysis procedure

A phased analysis is used to simulate construction and operation of the dam. In the first phase, the weight is applied considering the concrete blocks separately. In the second stage the dam is considered as a monolith by grouting the vertical joints, and the hydrostatic pressure of the water is applied. Displacements and strains are reset to zero after end of construction.

3. Results without swelling

Figure 5 shows the normal traction in the interfaces at end of construction. The colour scale is in the range 0 (red) to -3 MPa (blue). The vertical joints are overall stress free, except near the base of the dam, where small normal stresses arise. In the interface between dam and foundation compressive stresses are concentrated at the upstream side.

Figure 6 shows relative displacements in the normal direction of the interfaces at end of construction. The colour scale varies from 0 (blue) to 7 mm (red). The maximum opening takes place in the upper part of the vertical joints.

In Figure 7 the principal stresses in developed view of down-stream and upstream dam-faces at the end of construction are displayed as vectors. The maximum principal stress is near the base of the dam, at the upstream side, and is in the order of 3 MPa.

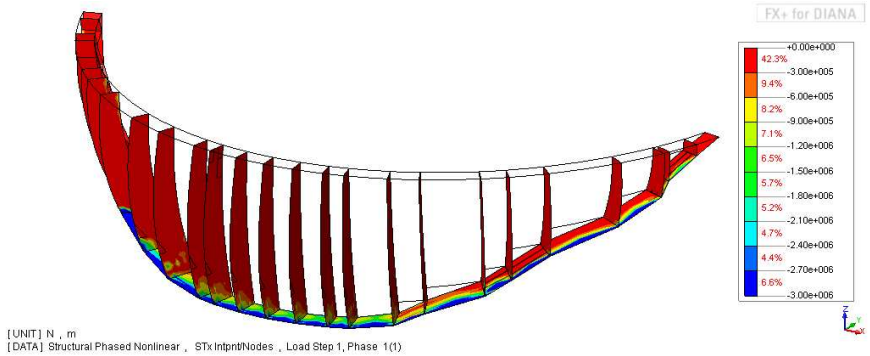

Figure 5: Tractions in the interfaces at the end of construction.

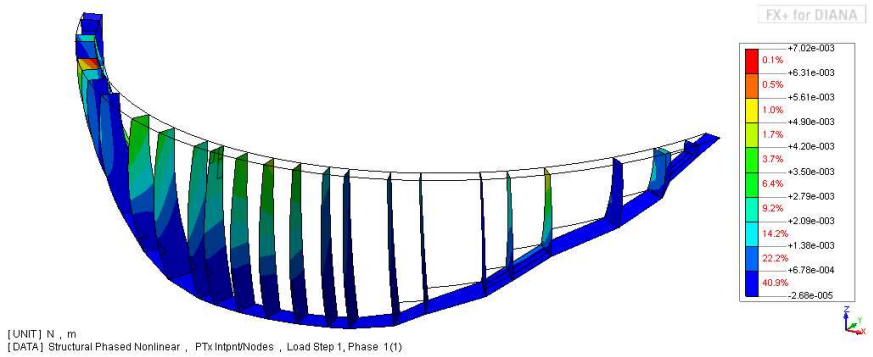

Figure 6: Relative displacements in the interfaces at the end of construction.

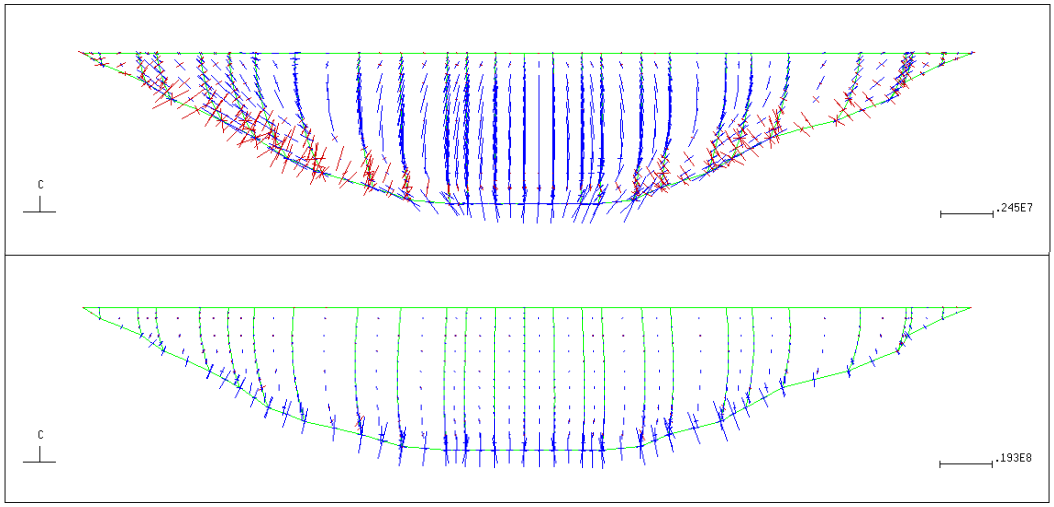

Figure 7: Developed view of downstream face (top) and upstream face (bottom) with principal stresses (blue in compression and red in tension) at end of construction.

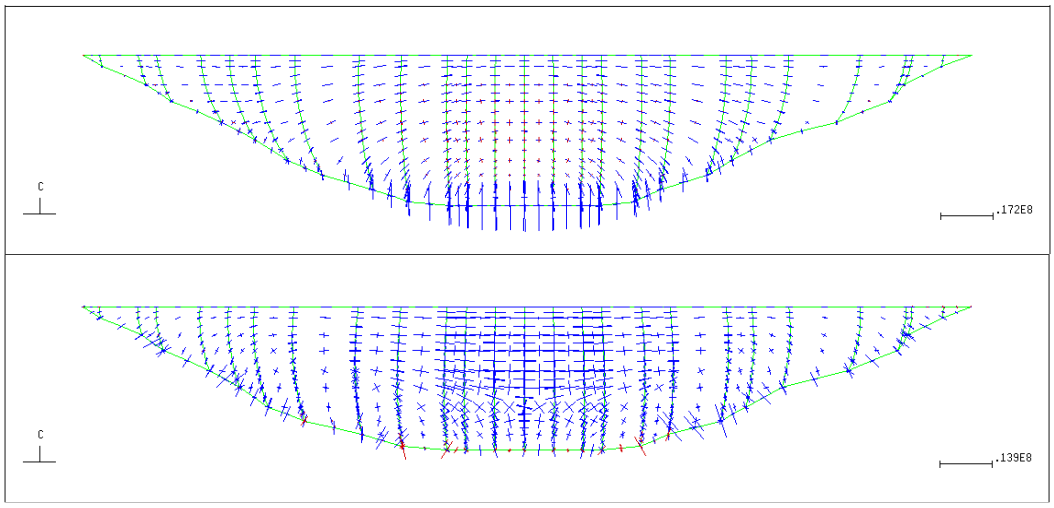

Figure 8: Developed view of downstream face (top) and upstream face (bottom)
with principal stresses (blue in compression and red in tension) after initial impounding.

Figure 8 shows the stresses in the dam after impounding (1963). The dominant vertical stresses at the end of construction are now replaced by an arch pattern at the downstream face of the dam and by circumferential stresses at the upstream face of the dam. In this model, which does not consider swelling, the circumferential stress is dominant in the central part of the dam. As the largest deformation for swelling is in the direction perpendicular to the maximum compressive stress, the direction of maximum expansion is the vertical direction.

4. Results with linear development in time of swelling and anisotropic expansion

Swelling is introduced in the model first as a linear function of time, see Figure 9. An anisotropic expansion is assumed, with prevailing expansion in the vertical direction, where it is as large as 2.5x the expansion in the other two directions. The slope of the curve and the factor of anisotropy are tuned in order to achieve the best possible matching of numerical results and measurements. The expansion strain loading is applied in DIANA as an equivalent concentration load, applied to all the elements in the dam.

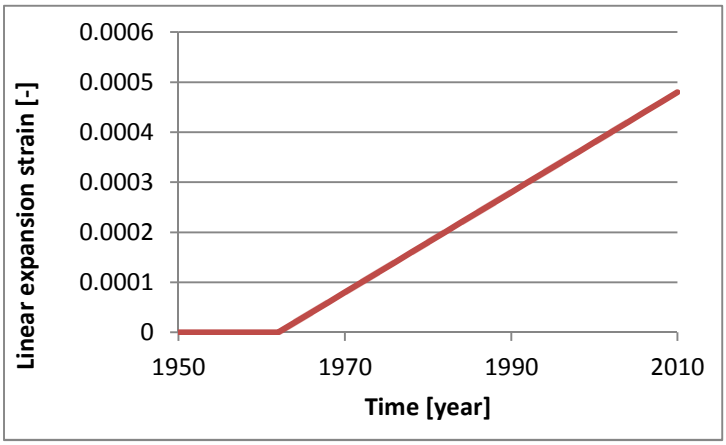

Figure 9: Linear expansion strain due to AAR versus time.

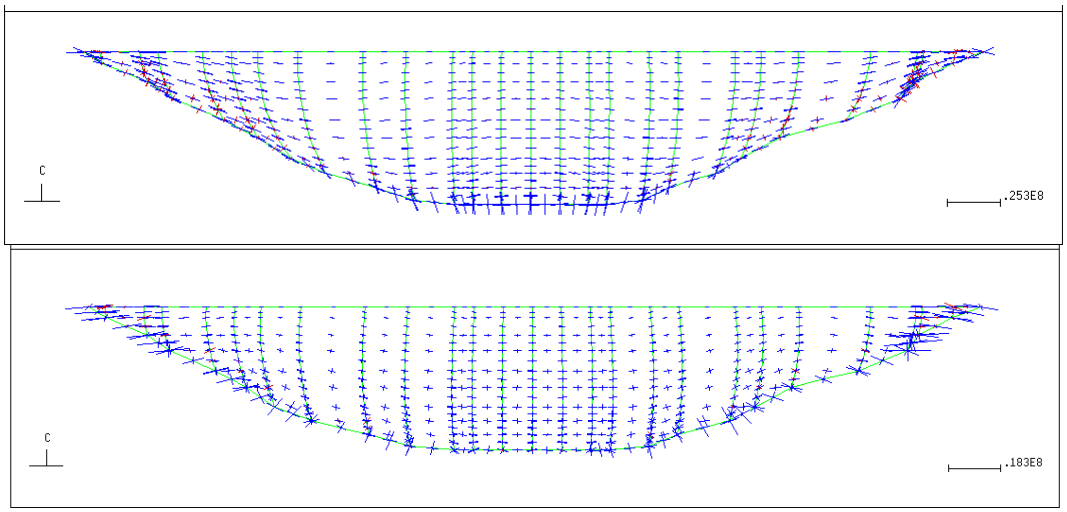

Figure 10: Developed view of downstream face (top) and upstream face (bottom) with principal stresses (blue in compression and red in tension) in 1995.

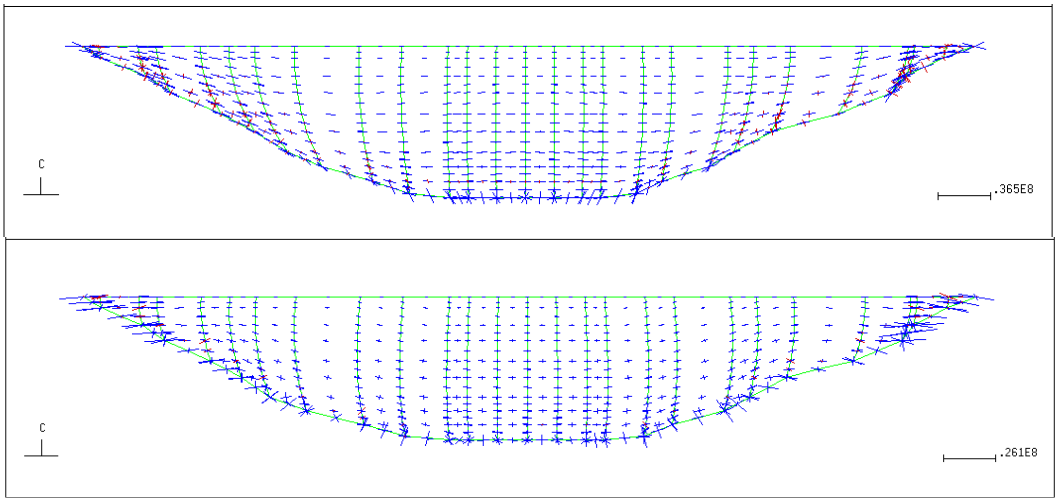

Figure 11: Developed view of downstream face (top) and upstream face (bottom) with principal stresses (blue in compression and red in tension) in 2010.

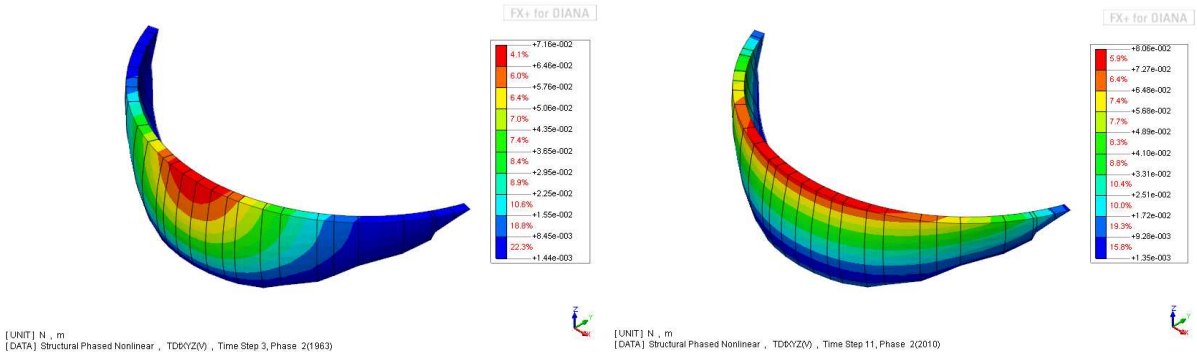

Figure 12: Vertical displacements at end of impoundment (left) and in 2010 (right).

Figure 10 shows the stresses in 1995, which is the last time for which measurement data have been provided. Both at the downstream and upstream face the stresses are mainly in

circumferential direction. Figure 11 shows the same results for 2011. The stress pattern is similar as in 1995 but stress-levels are higher.
For this model the calculated maximum total displacements reach 9 cm in the center of the crest of the dam. In Figure 13, the measured and calculated radial displacements of the crest are displayed as function of time, where the end of impounding (1963) is chosen as reference (=0 result). A radial displacement of 74 mm is predicted at the crest of the dam in 2010.

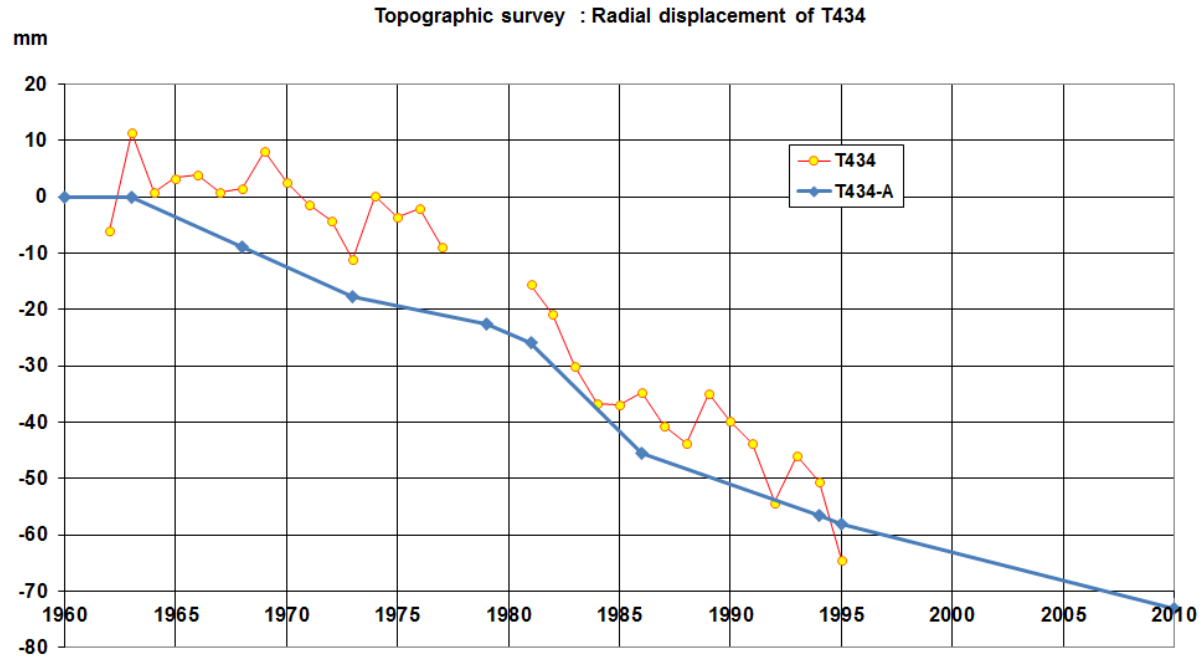

Figure 13: Measured (T434) and calculated (T434-A) radial displacement at the crest of the crown cantilever.

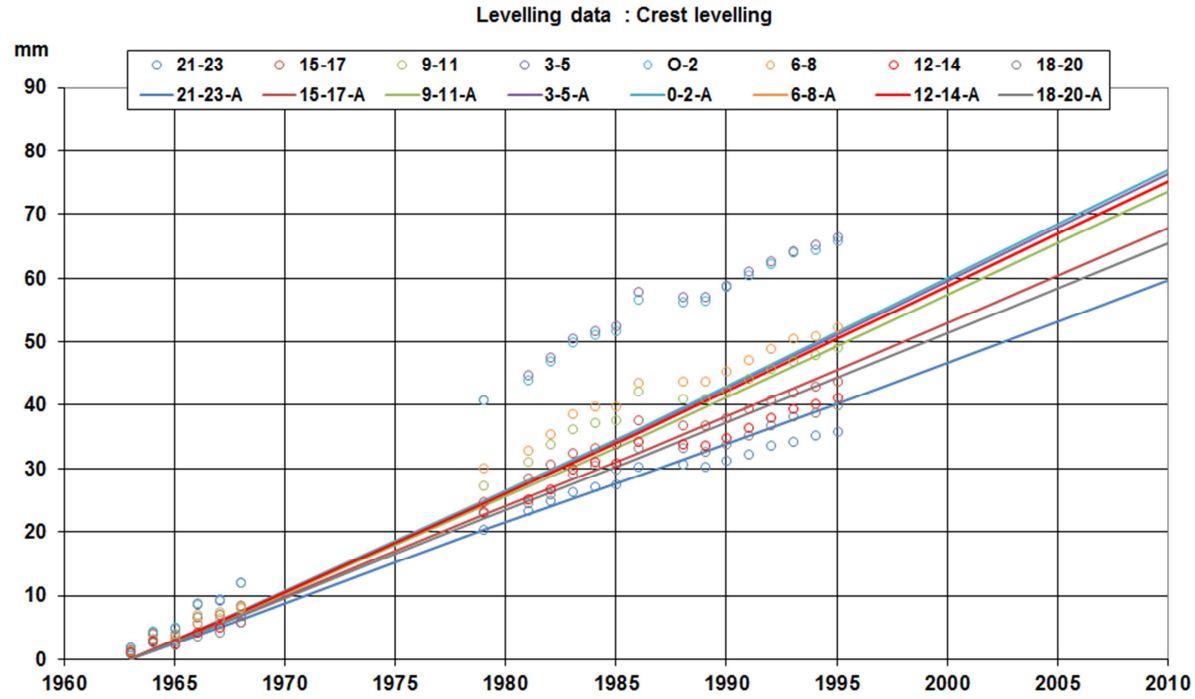

Figure 14: Measured (symbols) and calculated (lines) vertical displacement at crest level.

Figure 14 and Figure 15 show the measured and calculated displacements at eight different locations at the crest of the dam, where the calculated displacements were reset to zero in 1963, just after initial impounding. Numerical results match reasonably well with measurements except than at locations 0-2 and 3-5, 15-17 and 21-23. At these locations the calculated displacements are smaller and larger, respectively, than the measured displacements. As it has been suggested by the formulators, higher elevation rate at points 0-2 and 3-5 is appreciably higher than their neighbors due to the presence of the spillway in the upper part of the corresponding dam blocks, through the many openings and the increase surface of contact between concrete and water. For this reason, it has been suggested to discard these measurements. Comparing results of linear-time-function analysis with measurements, it seems that levelling in the measurements starts a little later, speeds up in the period 1975-1985 and lays behind the analysis results after 1990.

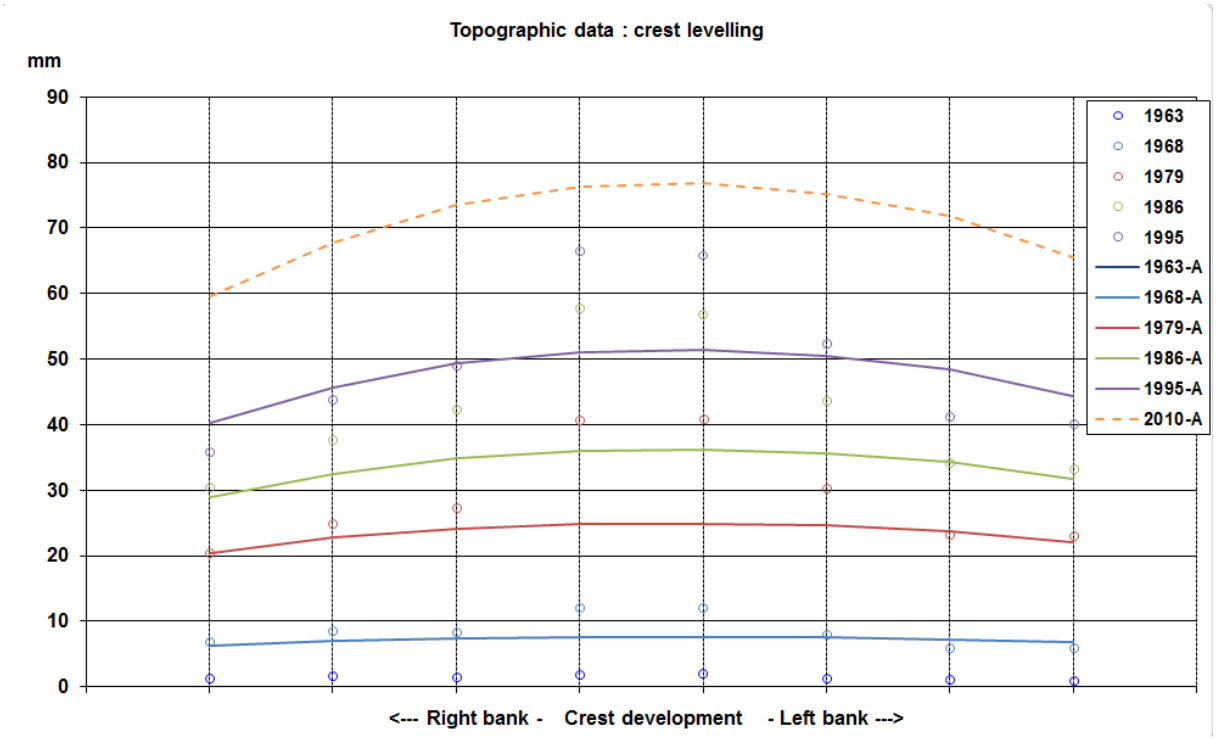

Figure 15: Measured (symbols) and calculated (lines) vertical displacement at crest.

5. Results with the model of Larive and anisotropic expansion

As an improvement to the model with swelling developing linearly in time, the model of Larive [3] is considered. Also in this case, the expansion in vertical direction is assumed 2.5 times as larger than in the horizontal direction. The equations describing the model of Larive are:

$$\varepsilon(t) = \varepsilon(inf)\xi(t) \tag{1}$$

$$\xi(t) = \frac{1 - \exp(-\frac{t - \tau_0}{\tau_c})}{1 + \exp(-(t - \tau_0) + \frac{\tau_L}{\tau_c})}$$

(2)

Table 3: Parameters in the model of Larive

Parameter	Value
ε(inf)	0.00035
τ_c	9 years
τ_L	9 years
τ_0	1965 years

The parameters adopted in the model are listed in Table 3. These parameters are chosen for obtaining the best possible fitting of the numerical results with the measurements. Figure 16 shows the comparison between the expansion strain varying linearly in time and according to the model of Larive.

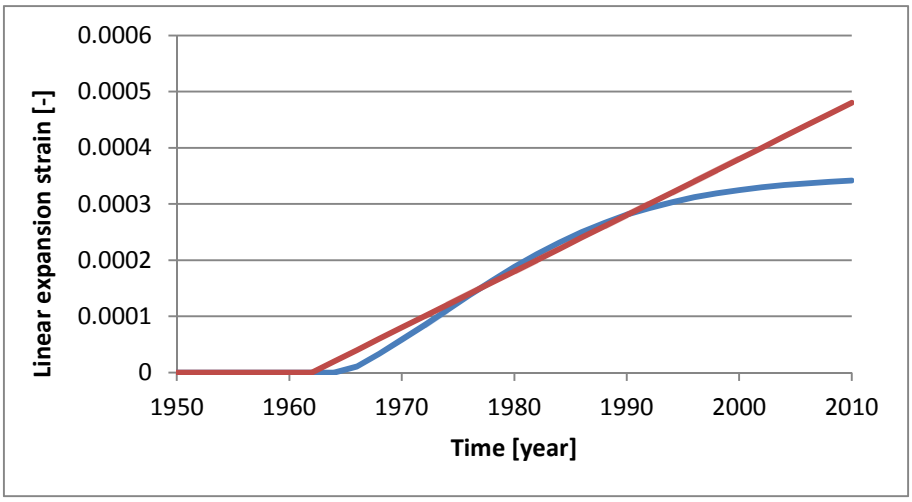

Figure 16: Expansion strain versus time: comparison between the simplified and the model of Larive.

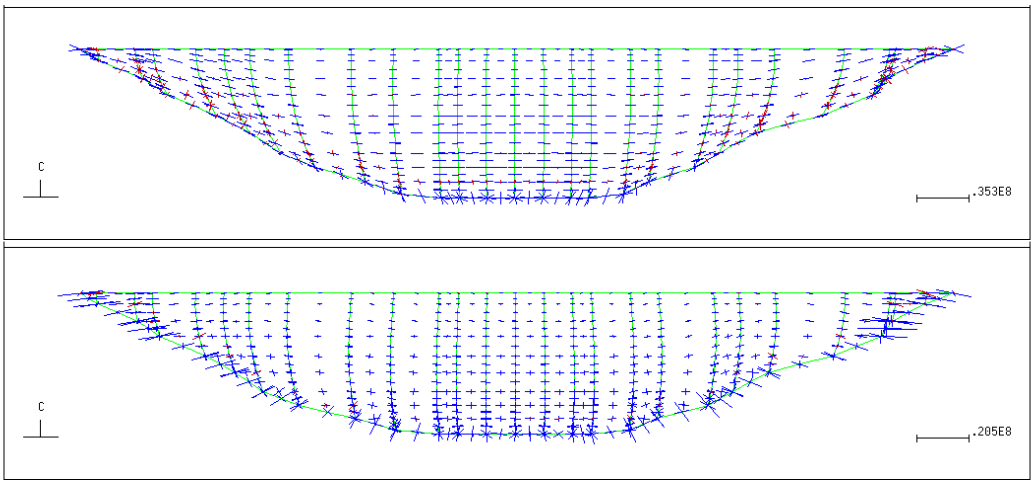

Figure 17: Developed view of downstream face (top) and upstream face (bottom) with principal stresses (blue in compression and red in tension) in 1995.

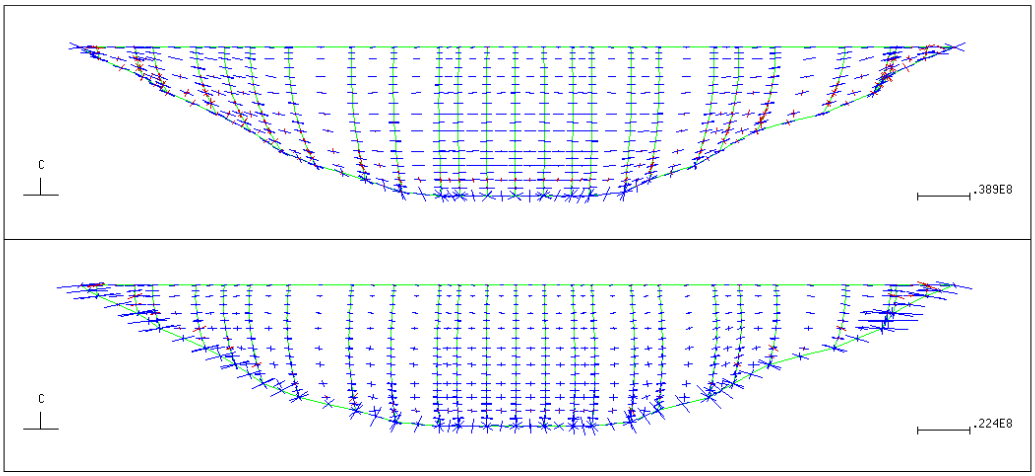

Figure 18: Developed view of downstream face of dam (top) and upstream face of dam (bottom) with principal stresses (blue in compression and red in tension) in 2010.

Figure 17 shows the stresses in 1995 and Figure 18 shows the stresses as they are predicted by the model in 2010. The stress pattern is similar to the stress pattern in the model with linear swelling, but horizontal stress levels are lower. Figure 19 shows the vertical displacements. The maximum vertical displacement at the crest of the dam is 5.5 cm.

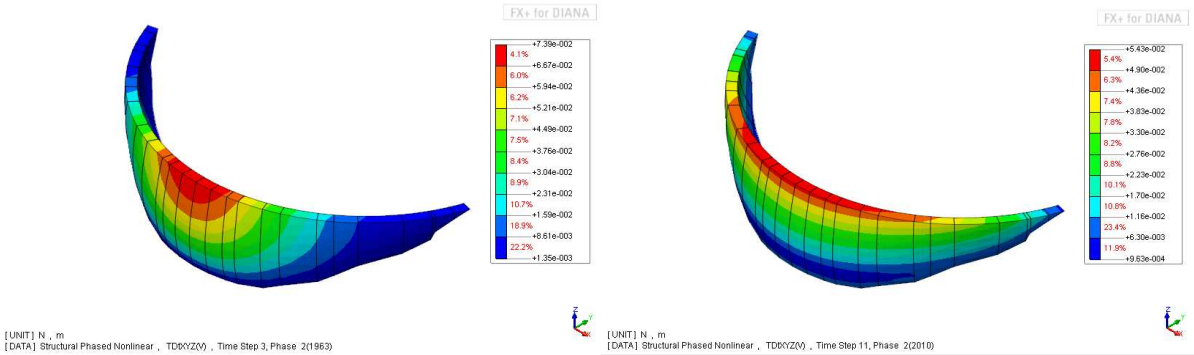

Figure 19: Vertical displacements at end of impoundment (left) and in 2010 (right).

In Figure 20, the measured and calculated radial displacements of the crest are displayed as function of time. Also in this graph the displacements are relative to the end of impounding (1963). A maximum radial displacement of 55 mm is predicted at the crest of the dam in 2010.

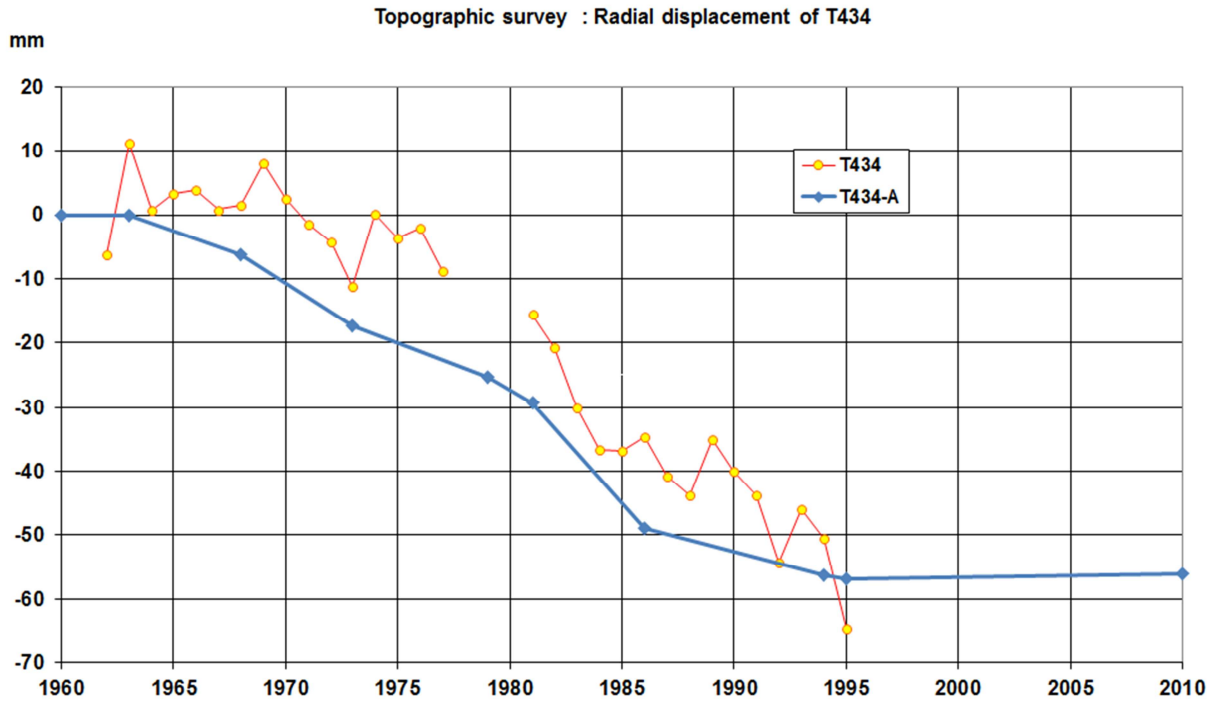

Figure 20: Measured (T434) and calculated (T434-A) radial displacement at the crest of the crown cantilever.

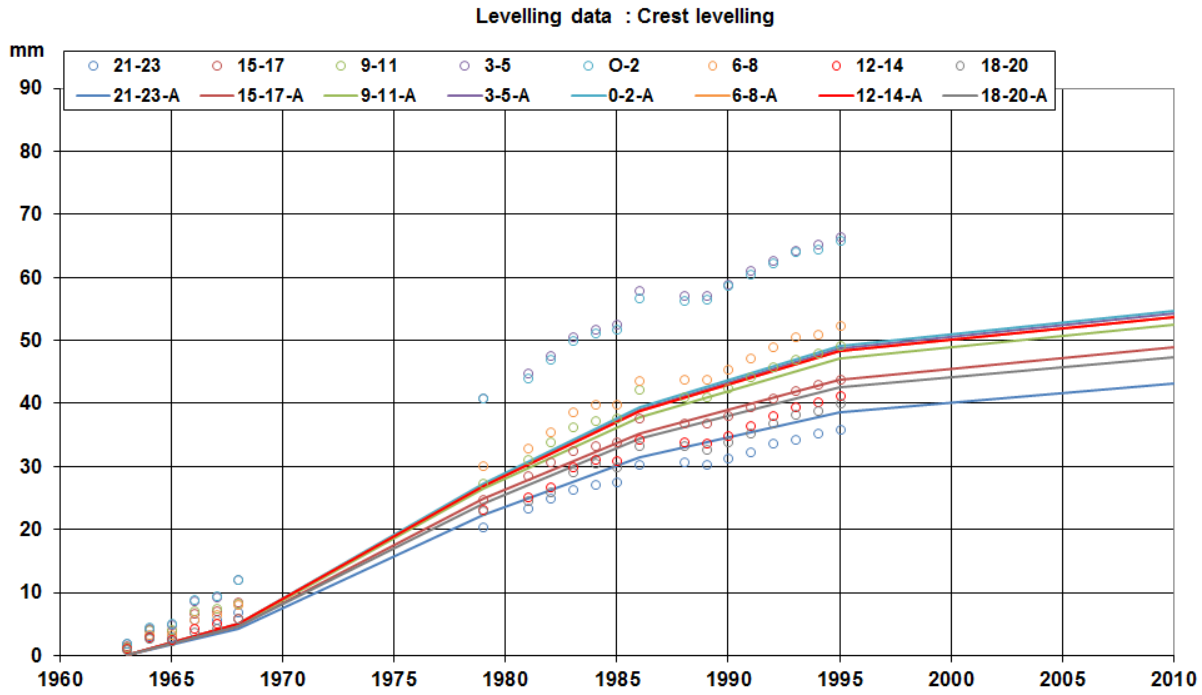

Figure 21: Measured (symbols) and calculated (lines) vertical displacement at crest level.

Figures 21 and Figure 22 display the elevations at different location of the crest as function of time. It can be observed that the numerical results are in this case in better agreement with the measurements than in the case of linear swelling function.

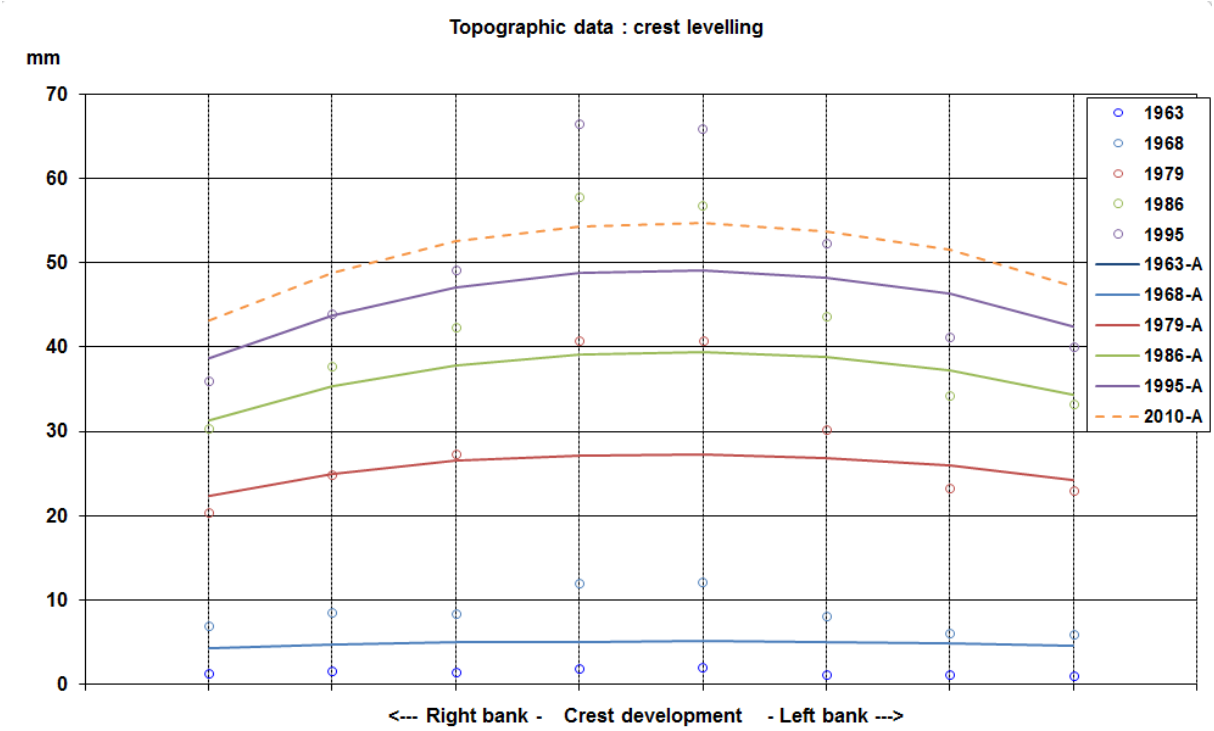

Figure 22: Measured (symbols) and calculated (lines) vertical displacement at crest.

6. Results with the model of Larive and isotropic expansion

Finally, the model with swelling developing according to the function of Larive and isotropic expansion is considered. Results are shown in Figures 23-27.

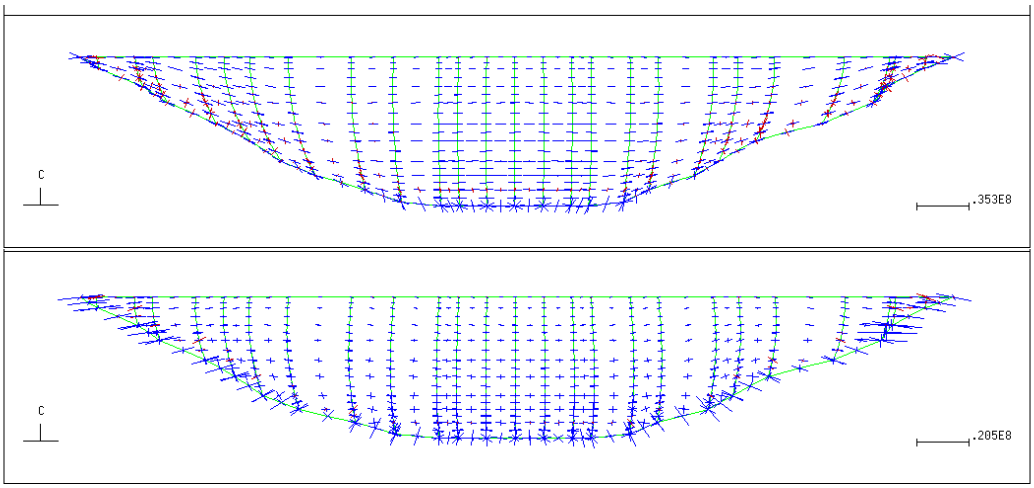

Figure 23: Developed view of downstream face (top) and upstream face (bottom) with principal stresses (blue in compression and red in tension) in 1995.

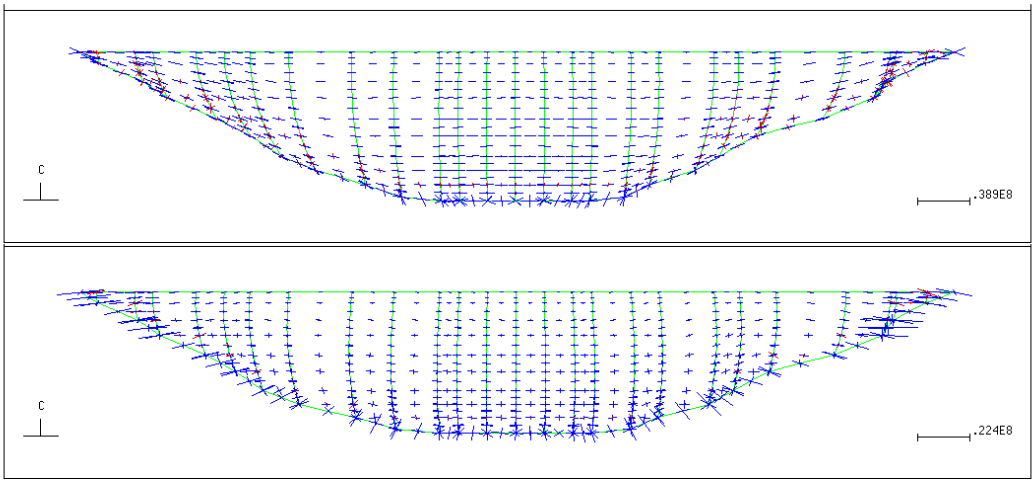

Figure 24: Developed view of downstream face (top) and upstream face (bottom) with principal stresses (blue in compression and red in tension) in 2010.

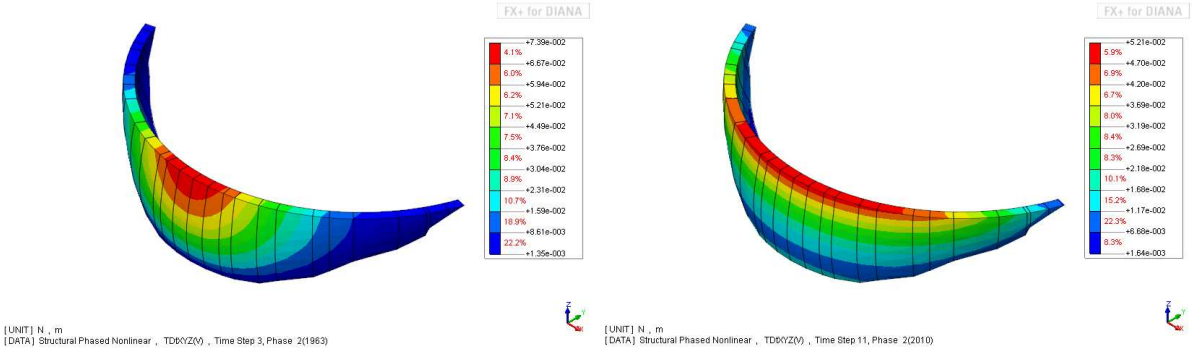

Figure 25: Vertical displacements at end of impoundment (left) and in 2010 (right).

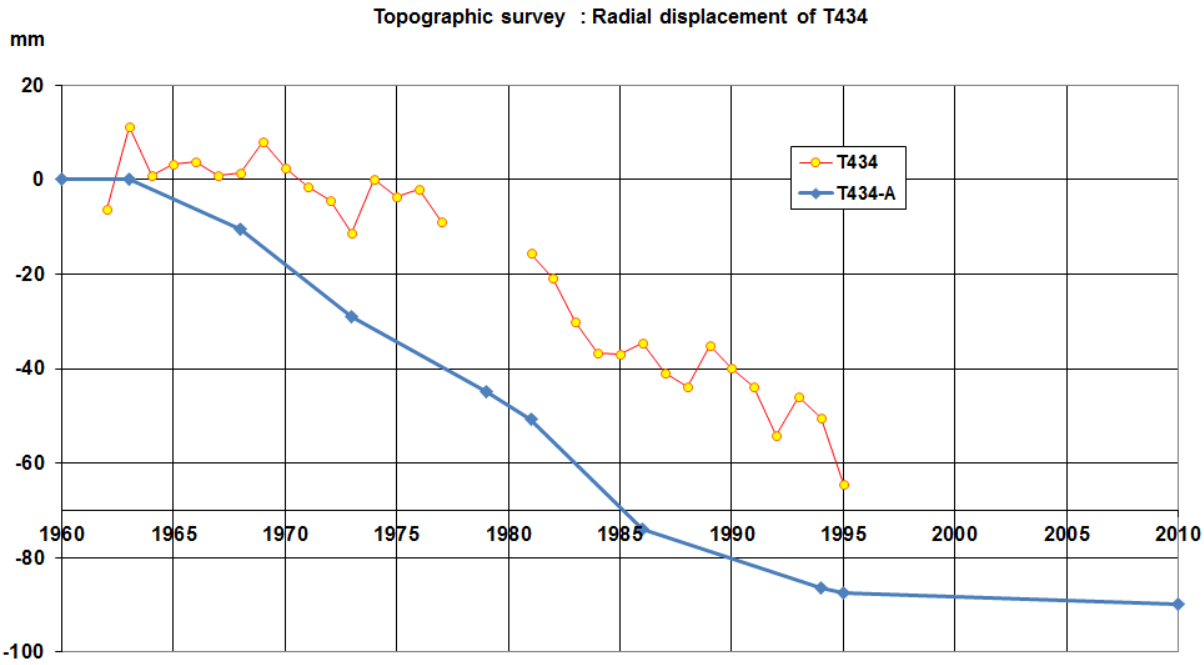

Figure 26: Measured (T434) and calculated (T434-A) radial displacement at the crest of the crown cantilever.

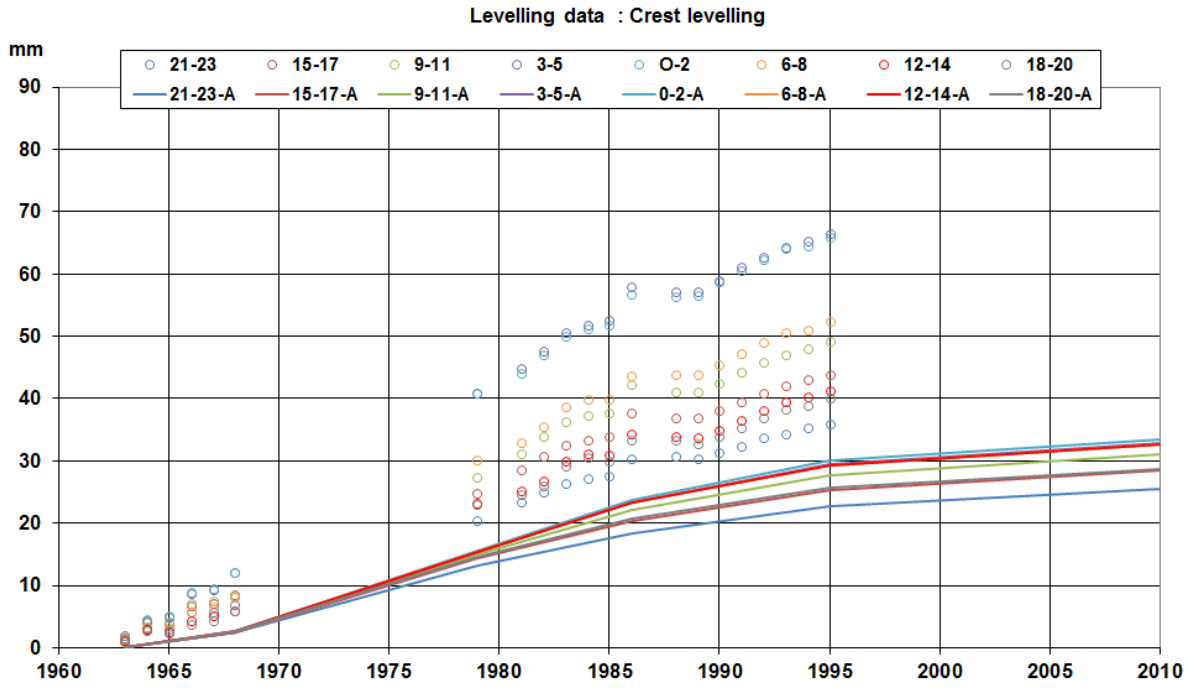

Figure 27: Measured (symbols) and calculated (lines) vertical displacement at crest level.

The radial displacements at the crest are in this case considerable larger than the values obtained with the model with anisotropic expansion model, up to 90 mm.
Figure 27 and Figure 28 show that the model with isotropic expansion underestimates the elevations significantly. From this model variation we can conclude that the anisotropy of swelling must be considered in order to get acceptable predictions for both radial and vertical displacements of the crest.

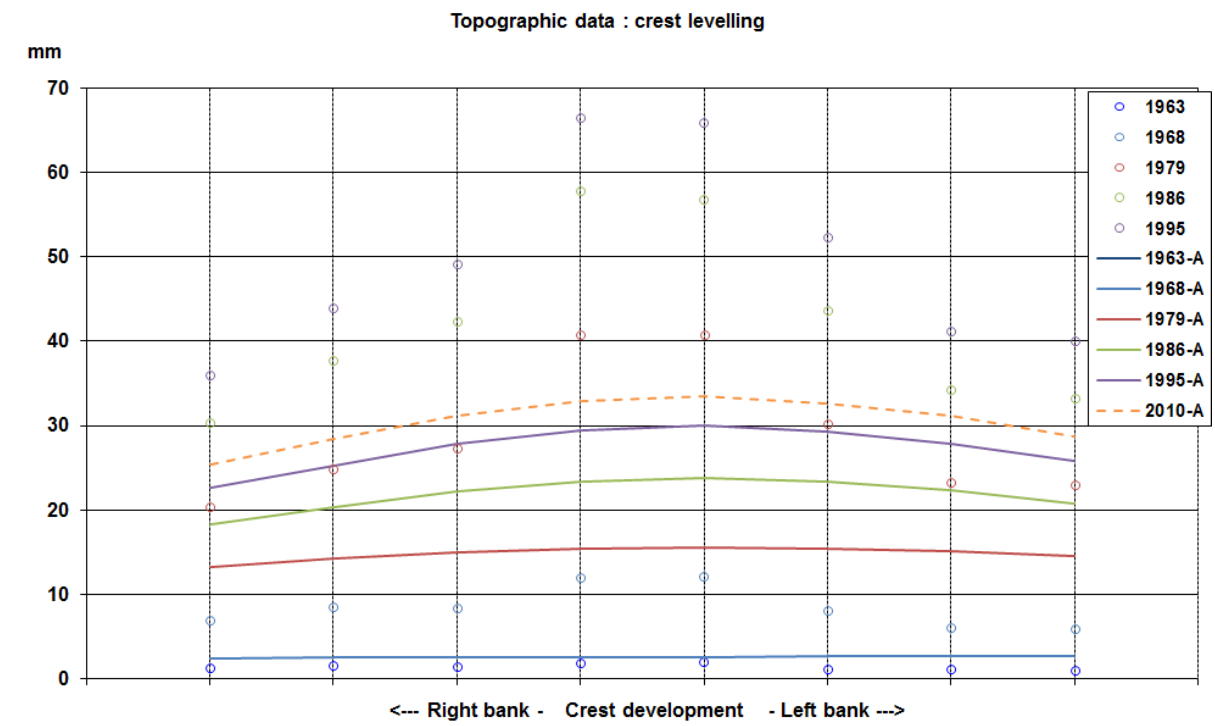

Figure 28: Measured (symbols) and calculated (lines) vertical displacement at crest.

7. Conclusions

A 3D finite element model with linear elastic materials for the dam and the foundation, and nonlinear elastic interfaces between the dam and its foundation, and between the concrete blocks, is used in this paper for predicting stresses and displacements induced by AAR in the Kariba dam on the Zambesi river. Swelling is defined as a volumetric strain function of time. Both the case of isotropic and anisotropic expansion is considered. Swelling is assumed homogeneous in the dam.

Displacements at the crest of the dam in radial and vertical direction in the period 1963-1995 can be reproduced considering a volumetric expansion developing in time according to the function of Larive and introducing an anisotropy factor. The best fit between measurements and numerical results is achieved for the set of parameters: $\varepsilon(inf)=0.00035$, τ_c = 9 years and τ_L = 9 years, and an expansion in vertical direction that is 2.5 as large than in the horizontal directions. The prediction of the maximum radial and vertical displacement at the crest in 2010 is 55 mm.

References

[1] DIANA 9.4.4 www.tnodiana.com

[2] Noret, C. & Molin, X. (2011). Eleventh International Benchmark Workshop on Numerical Analysis of Dams, THEME A, Effect on concrete swelling on equilibrium and displacement on an arch dam, October 17-18, 2011, Valencia, Spain.

[3] Ulm, F.-J., Coussy, O., Kefei, L. & Larive, C. (2000). Thermo-Chemo-Mechanics of ASR Expansion in Concrete Structures, Journal of Engineering Mechanics, March 2000, pp. 233-242.

XI ICOLD BENCHMARK WORKSHOP ON NUMERICAL ANALYSIS OF DAMS

Valencia, October 20-21, 2011

THEME A

Kostylev, Vladimir

CONTACT
Vladimir Kostylev, The B. E. Vedeneev VNIIG, Inc.
21, Gzhatskaya St., Saint Petersburg, 195220, Russia.
+7(812) 493-93-77, KostylevVS@vniig.ru

Summary

The stress strain state of the Kariba arch dam is analysed. Anisotropic swelling law was used to model the concrete expansion due to AAR. Results are compared with available instrument data and fifteen years dam state predictions are made.

1. Introduction

In the following paper the Kariba arch dam is analysed, see Noret and Molin [1]. The finite element mesh provided has been exported into Ansys 11 finite element software without any modifications. Serendipity finite elements with midside were utilized. To simplify the analysis no joint elements have been used, the arch was considered to be fully bonded to its foundation.

2. Stress field at the end of construction

According to the simplification suggested for the benchmark solutions in the Noret and Molin [1] them A formulation paper, it was suggested that "the dam concrete blocks have been erected first, then the contraction joints have been grouted, then the impounding of the reservoir started". This doesn't completely coincide with the real construction sequence but seems to be close to it and simplifies the solution technique. Also, in the present paper no construction sequence of each separate cantilever has been taken into account. All after all for the initial stress field computation the following algorithm has been utilized.

At first, the finite element model had been cut into 25 separate cantilevers each but one of those was 1 element in width along the crest direction (one narrow element layer had been added to neighboring cantilever). Then, the self weight with g=9.8 m/c^2 had been applied to dam elements and the first calculation had been held. The mesh deformed accordingly to the solution obtained is shown in figure 1. Next, the joint grouting process was simulated by coupling the coincident finite element nodes on cantilever interfaces while adding the fixed gap between each degree of freedom of coincident nodes based on the difference of the solution in those nodes. I.e. after obtaining the initial solution u^0 the following constraint equations were applied for each degree of freedom in each interface node pair

$$u_i - u_j = u_i^0 - u_j^0, \forall (i,j): x_i = x_j, y_i = y_j, z_i = z_j \tag{1}$$

This way in further calculations the initial construction sequence is considered automatically as soon as one apples full load including self weight to the model.

Another approach to consider the construction sequence (suitable for linear problems only) which we are actually used to is based on summing up the solutions from different load cases. But it seems that it would be less convenient for the present work as it complicates the automatic principal stress field calculations.

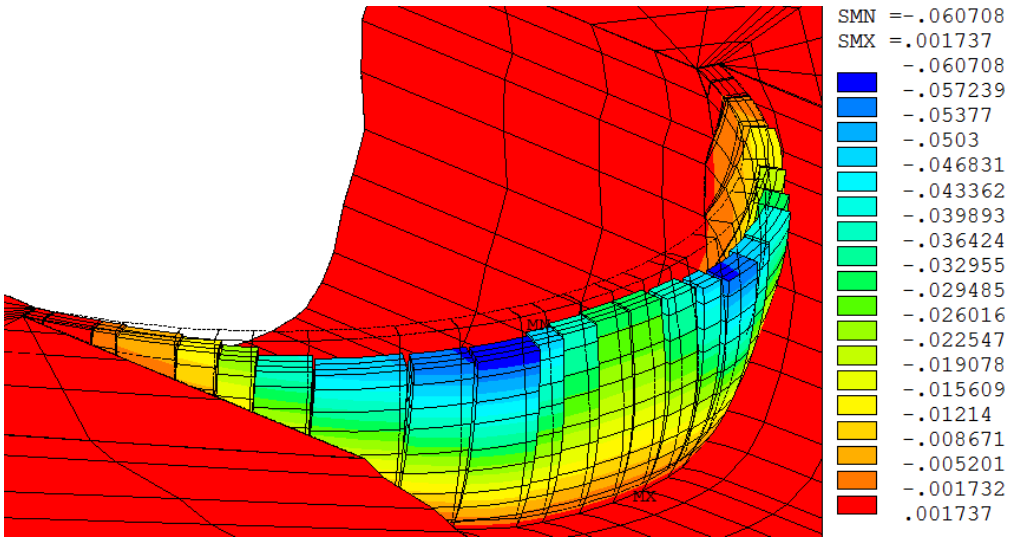

Figure 1: Self weight load. Immediately constructed independent cantilevers. Radial displacements, m

No specific boundary conditions have been set for the model. The arch dam foundation boundary was constrained along all directions in all calculations.

2. Hydraulic loads modelization and field data analysis

Hydraulic forces acting on the foundation-dam structure have been taken as follow. Triangular diagram for the uplift pressure have been considered. Reservoir pressure acting on the upstream part of the foundation has not been taken into account neither by surface neither by volumetric forces. Hydrostatic pressure on dam upstream face has been ordinary applied.

As soon as problem modelization used in the present study is linear, a number of additional calculations were held in order to normalize the results obtained with different water levels. Some fixed water level had been chosen (e.g. 485.33 m), the difference between actual water level and the reference one was calculated for each year and applied as the only load to the dam-foundation system. The results of the subsequent calculations were subtracted from the monitoring data. The results obtained are shown in figures 2, 3. All results are plotted in increments over the values obtained for year 1963.

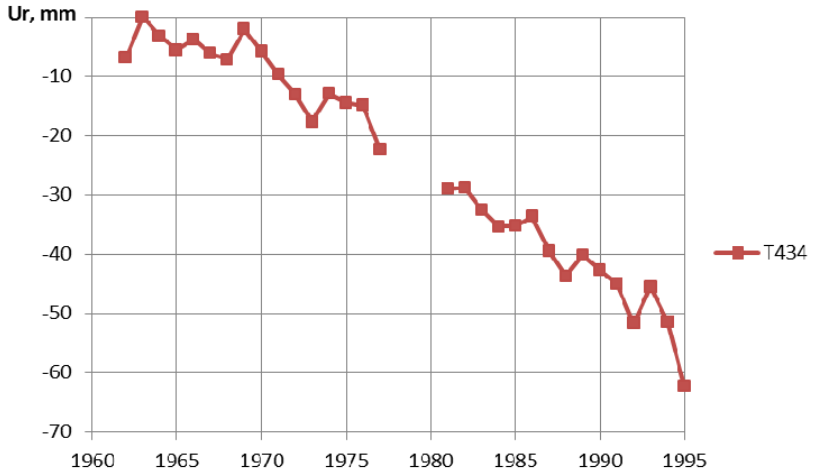

Figure 2: Radial displacements of target T343 recalculated to uniform water level, mm

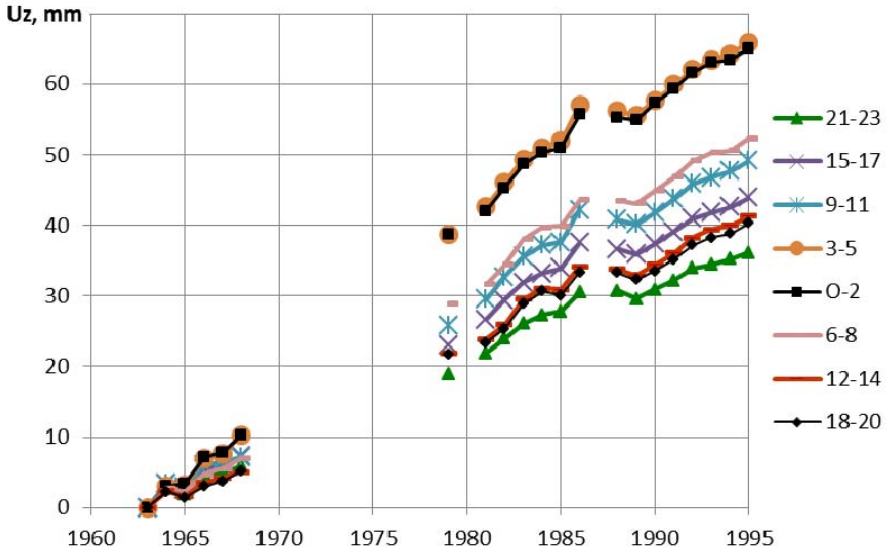

Figure 3: Crest rise at control points recalculated to uniform water level, mm

It can be seen that normalized data shown in fig. 2, 3 is still not smooth. The variations can be explained by temperature effects or some other factors not considered in the present study.

Next, the uniform swelling law was applied to the model. For this purpose the unit temperature load was applied to all elements. Linear thermal expansion coefficient have been chosen to be 1×10^{-5}. Results of the corresponding calculations are listed in table 1 (no other loads but unit temperature applied). Then the swelling rate needed to fulfil the monitoring data of each instrument separately was calculated, see fig. 4. One can see that if we try to fulfil the crest radial displacements rate, then we will highly underestimate the crest rise. And vice versa, if we choose uniform swelling rate that gives the correct values for the crest rise, then radial movement will be strongly overestimated. This fact is actually nothing new for Kariba dam analysis, the anisotropic expansion effect is mentioned in the current benchmark exercise formulation paper for example. So the anisotropic swelling model presented in the following section was applied to address this feature.

Table 1: Uniform expansion with 1×10^{-5} amount. Control point displacements, mm

Ur_T434	Uz_21-23	Uz_15-17	Uz_9-11	Uz_3-5	Uz_0-2	Uz_6-8	Uz_12-14	Uz_18-20
-3.26	0.92	1.03	1.10	1.15	1.12	1.04	0.92	0.80

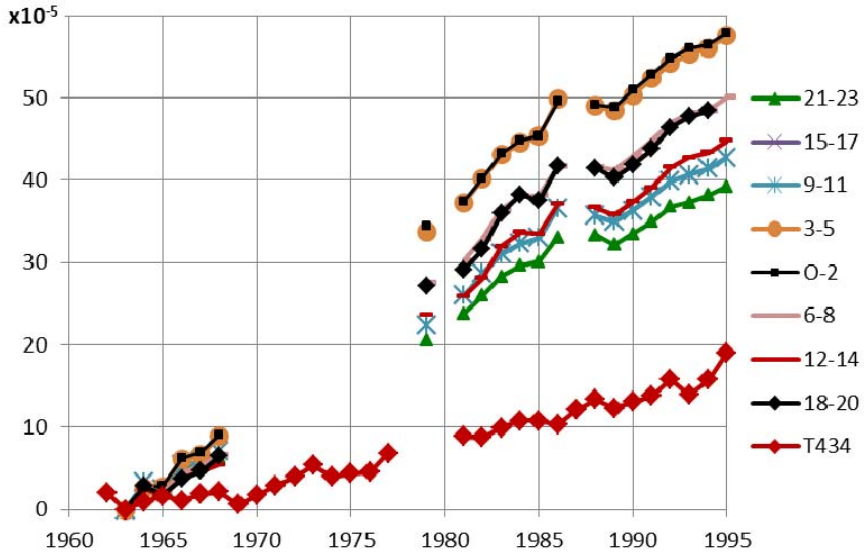

Figure 4: Uniform swelling amounts needed to fulfil separate readings of different instruments

3. Concrete swelling modeling

The major numerical investigation of AAR affected structures started not so many years ago and has not still got a mature form. Probably the most comprehensive numerical model for AAR expansion up to now is presented in Saouma & Perotti [2], [3]. See references therein for previous study overview. For us it was a quite new field of study and we tried to keep the expansion model as simple as possible. However as it is shown above, if one tries to calculate the Kariba arch dam displacements using the uniform swelling approach, he will totally fail. So the following anisotropic swelling model was used. For the kinetics of the reaction we took the model developed by C. Larive in 1998 which is utilized in Saouma & Perotti [2], [3] as well. Based on data presented in fig. 2, 3 the latency and characteristic times τ_L and τ_C (in general stress and temperature dependent) were chosen to be 18 and 10 days respectively and the following formulae for the swelling rate coefficient was employed

$$\xi(t) = C_{sw} \cdot \frac{1}{1+e^{-(t-\tau_L)/\tau_C}} e^{-t/\tau_C}, \qquad (2)$$

where the constant term C_{sw} was identified later by minimizing the distance between the monitoring data and actual solution results.

For the mechanics of AAR expansion our first choice was to assign different weights to expansion rate in 3 principal stress directions. I.e. if for the current solution stage the principal stress tensor and principal directions in the given point are calculated, then the swelling strain tensor in stress principal directions coordinate system will be

$$\varepsilon_{sw}^{\infty} = \begin{pmatrix} \alpha_1 & 0 & 0 \\ 0 & \alpha_2 & 0 \\ 0 & 0 & \alpha_3 \end{pmatrix}, \qquad (3)$$

where $\alpha_1, \alpha_2, \alpha_3$ are some stress dependent coefficients. The state of the art and experimentally approved way of choosing values for these coefficients is particularly described in Saouma & Perotti [3]. However in order to simplify the calculations for this particular dam we started from some stress independent values of swelling coefficients and took them to be $(\alpha_1, \alpha_2, \alpha_3) = (1.5, 1.0, 0.5)$. The solution obtained in such a way showed much better match with monitoring data than the uniform swelling law. After that we tried to implement some simple stress dependent model for these coefficients based mainly on the assumption that the swelling rate will increase in the tensioned directions. But this didn't bring us much luck in harmonization the numerical results with monitoring data provided. So after all we ended with stress independent coefficients written above. There exist experimental reportings that AAR expansion is inhibited under high compressive stresses. We also carried out numerical tests in which we stopped the expansion in given direction if compressive stress in this direction is below -10 MPa, but it didn't noticeably affect the solution for the Kariba dam problem.

The final results for radial displacements of target T434 and the crest rise are shown in figures 5, 6. Again, all shown values are in increments to the corresponding values for year 1963. As partially stated above, the parameters in formulae (2), (3) are taken as follow: τ_L= 18 days, τ_c= 10 days, C_{sw} = $50 \cdot 10^{-5}$, $(\alpha_1, \alpha_2, \alpha_3) = (1.5, 1.0, 0.5)$. The concrete expansion was supposed to start in 1960, which was taken as a start time (*t=0*) in formula (2).

Figure 7 shows the increase of radial displacements from year 1963 (water level 485.33) to year 2010 (water level 492.96). It shows that maximum radial displacement calculated takes place somewhere near the midside of the dam crest and is 9.1 mm greater than those of T434 target (-70.25 mm maximum vs. -61.15 mm at T434 location). Figure 8 similarly shows the corresponding increase of vertical displacements.

As for numerical implementation of the described model, the separate program for calculating the swelling forces has been written. The calculation process driven by a simple macros written on the Ansys script language is organized as follow. A certain number of substeps is taken for each year in order to minimize increments of concrete expansion between steps. Actually we took just 3 steps, but test showed that it doesn't significantly affect the solution. For a given year at a subsequent substep all the loads including hydrostatic pressure, self weight and swelling loads from previous step are applied. Then the solution obtained by Ansys software is saved to the text file and the external program to calculate swelling forces is called. This program calculates appropriate nodal forces depending on the principal stress field and saves them to the Ansys input file. Also a separate command file used to subtract free swelling strain tensor from the result strain tensor is saved and utilised by Ansys for stress output (actually for convenience we just write the command file with stress subtraction commands, not the components of the strain tensor itself). Program also stores the another same file with free strain tensor components in all dam nodes which is updated each step and allows to correct the stress field imported from Ansys. This subtraction of free strain is

completely similar to what one should do if he manually applies the temperature load by corresponding nodal loads. After the stress field correction, the principal stresses and directions can be calculated. One should remember that principal stresses are not summable and need to be recalculated for stress output. It is worthwhile to note one serious drawback occurred. When we properly calculate the stress field and swelling strain in each integration point (we used $3 \times 3 \times 3$ point Gaussian quadrature on each element) in order to get nodal forces, the final results obtained are totally meaningless. Up to now we can't say if this is due to the defective swelling model or there are any other reasons. In order to overcome this drawback we moved to calculating the principal stress dependent swelling strain in the finite element centroids only. Principal stresses are calculated just in element centres as well and they are much smoother in this case.

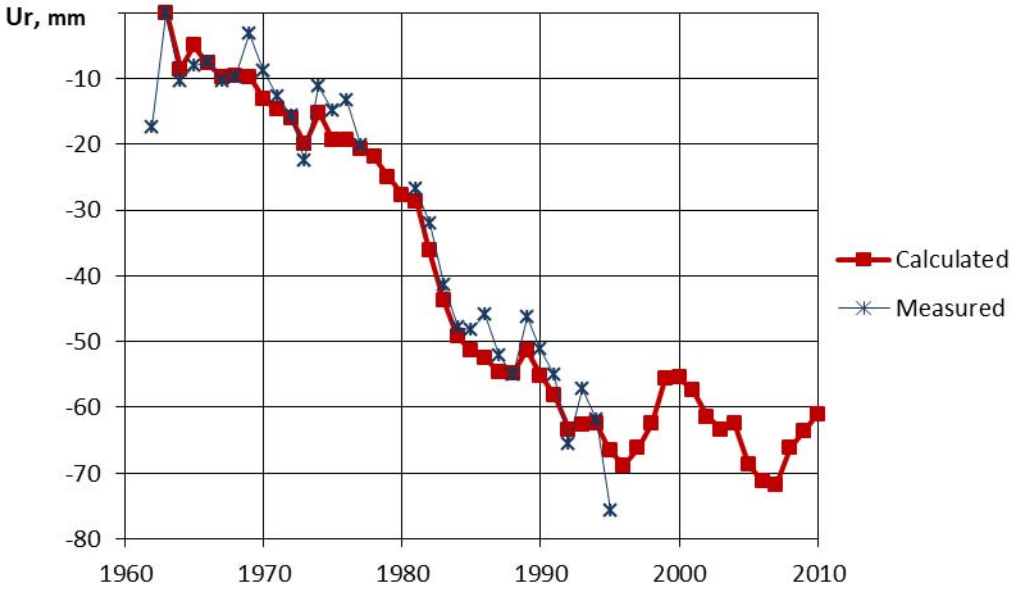

Figure 5: Radial displacements of target T434, mm

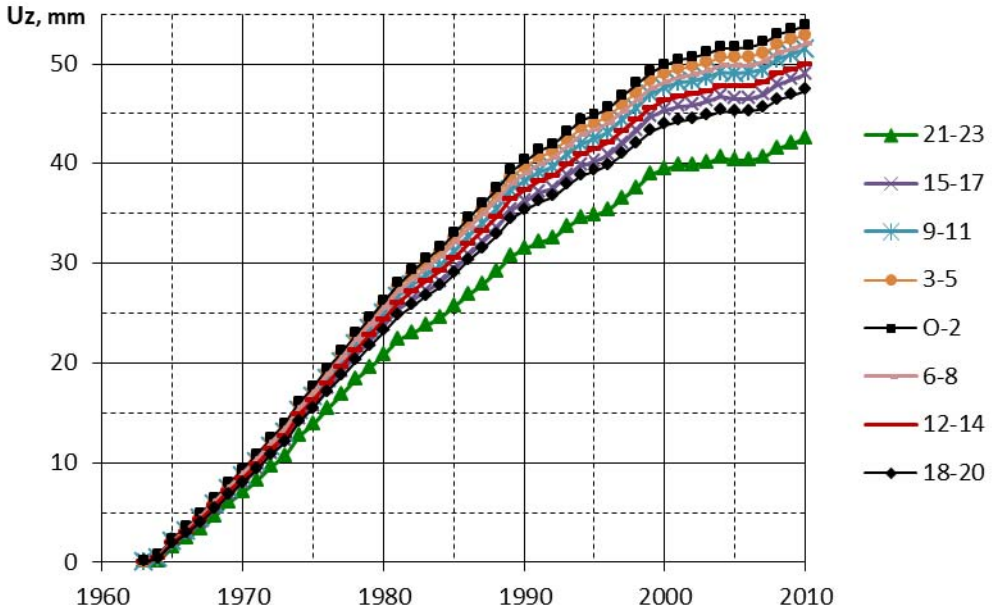

Figure 6: Calculated crest rise, mm

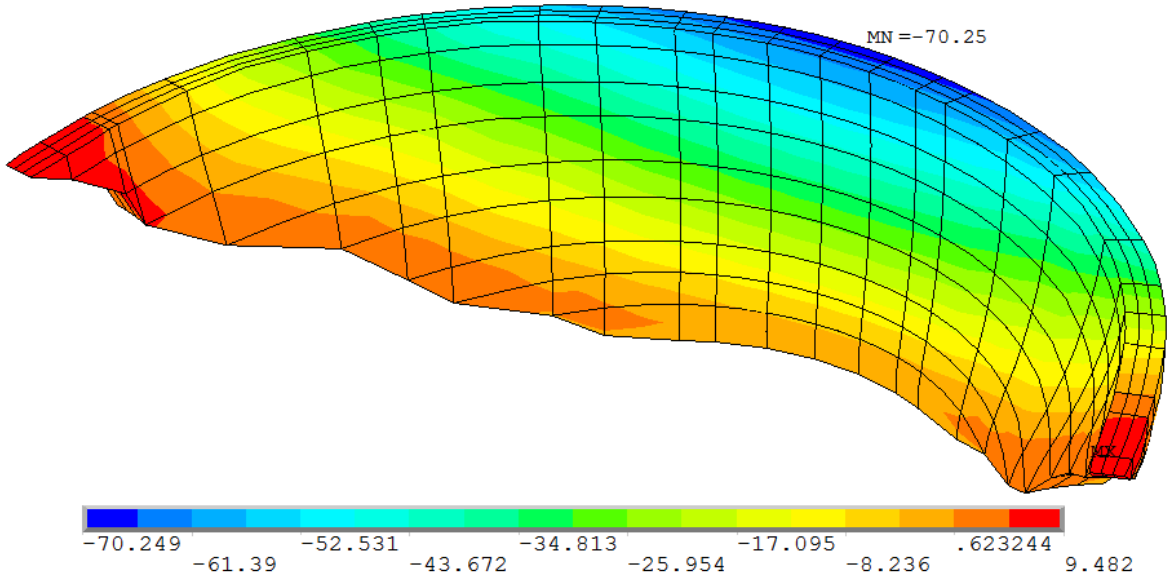

Figure 7: Increase of radial displacements from 1963 to 2010, mm. Deformed mesh

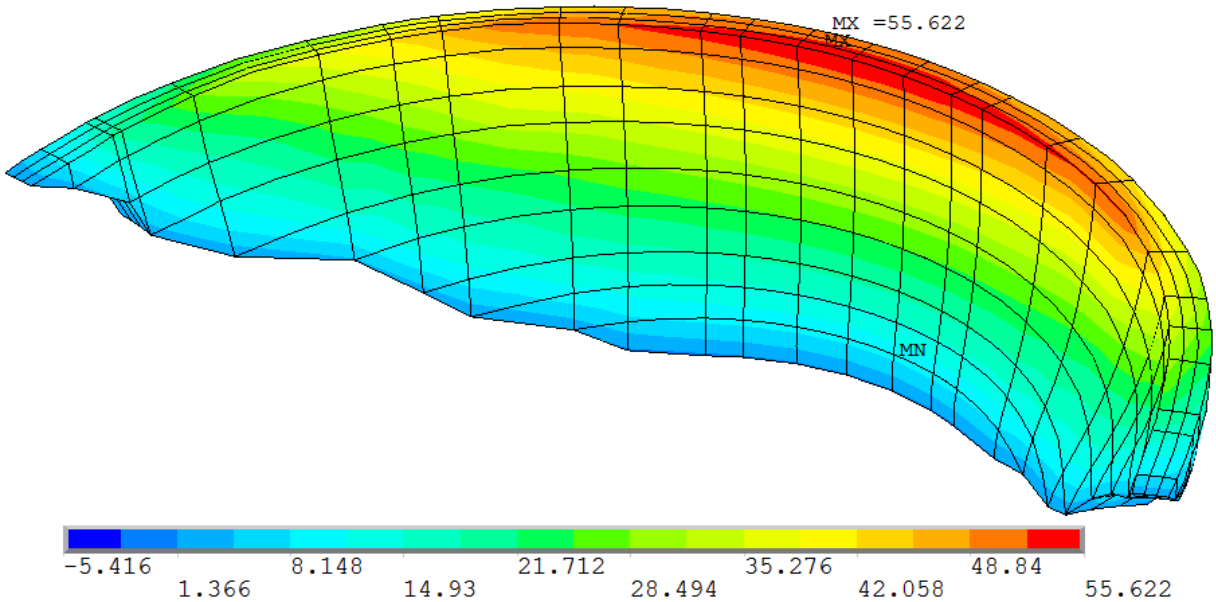

Figure 8: Increase of vertical displacements from 1963 to 2010, mm. Deformed mesh

4. Conclusions

The stress dependent swelling law has been applied to the Kariba arch dam. Results show that even with the simple expansion model one can obtain results that coincides with the field measurements significantly better than those based on uniform swelling law. However in order to obtain correct stress field inside the dam one should surely also consider more comprehensive swelling laws available. As soon as it comes to long term prediction of the dam state the appropriate kinetic law for the reaction intensity should be applied.

References

[1] Noret, Chr. & Molin, X. (2011). Theme A. Effect of concrete swelling on the equilibrium and displacements of an arch dam. 11th International Benchmark Workshop on Numerical Analysis of Dams theme A formulation paper.

[2] Saouma, V. Perotti, L. (2005). Alkali aggregate reactions in dams; Stress analysis and long term predictions, ASDSO Dam Safety Conference, New Orleans, Sept. 2005.

[3] Saouma, V. Perotti, L., (2006). Constitutive Model for Alkali Aggregate Reactions, American Concrete Institute, Materials Journal, Vol. 103, No. 3, pp. 194-202, May-June, 2006.

XI ICOLD BENCHMARK WORKSHOP ON NUMERICAL ANALYSIS OF DAMS

Valencia, October 20-21, 2011

THEME A

ANALYSIS OF AAR LOADING ON KARIBA DAM USING GROW3D ROUTINES

Curtis, D, D.

Feng, L.

Lafreniere, M

CONTACT

Curtis, D, D., Hatch Ltd., Civil/Structural, L2E 7J7, Niagara Falls, Canada, 905-357-6998, DCurtis@hatch.ca.

Feng, L., Hatch Ltd., Civil/Structural, L2E 7J7, Niagara Falls, Canada, 905-374-0701 x5296, lfeng@hatch.ca.

Lafreniere, M., Hatch Ltd., Civil/Structural, L2E 7J7, Niagara Falls, Canada, 905-374-0701 x5365, mlafreniere@hatch.ca.

Summary

A finite element stress analysis was undertaken using the GROW3D subroutines driven by the ANSYS finite element program. The analysis was undertaken using the guidelines provided by Theme A Benchmark Workshop Committee. The analysis includes the stress dependent nature of concrete expansion due to alkali aggregate reaction (AAR) as well as the enhanced creep behavior of AAR-affected concrete. The results of the analysis are presented in the form of contour plots of displacements and stresses. In additions stress changes caused solely by AAR are also presented.

1. Introduction

The GROW3D finite element program was originally developed in the early 1990s to analyze the effects of concrete expansion due to AAR at Mactaquac Generating Station in New Brunswick, Canada [1]. The GROW3D was calibrated to field measurements of both displacements and stresses. It was found that concrete expansion due to AAR at Mactaquac is quite sensitive to stresses and good model calibrations were achieved when stress dependency and enhanced creep behavior were modeled. The Mactaquac project is unique in that the rates of measured concrete expansion are the highest observed anywhere in the world at 80 to 160 micro-strain per year.

GROW3D was also used to analyze Seminoe arch in Wyoming which also suffers from continued concrete expansion due to AAR [2]. The finite element model was calibrated to field measurements and the results were presented to the United States Bureau of Reclamation (USBR) who own and operate the dam. Subsequently, USBR measured stresses in the dam using the overcoring technique. An excellent agreement was found between measured and computed stresses.

Hatch linked the GROW3D routines to user subroutines available in the general purpose finite element program ANSYS. The new GROW3D program was then used to analyze dams owned by the Tennessee Valley Authority (TVA). These dams included Fontana, Hiwassee and Chickamauga. The results on an analysis of one of the TVA dams are given in [3].

A discussion of AAR effects in arch dams is given in [4]. This reference also presents the results of a GROW3D stress analysis of Kouga arch dam which is located in South Africa.

Using GROW3D in ANSYS has proved to be very beneficial in that the ANSYS solvers are quite powerful; therefore very large models have been developed. In addition, the non-linear contact surfaces in ANSYS allow modeling of sliding, joint opening and closing, slot behavior, etc.

2. GROW3D Program Description

It is very important to note that the stress-dependent model was developed using field data. It is known that the stress-dependent nature of accelerated laboratory tests could be substantially different than prototype behavior.

The stresses caused by concrete growth increase with time; therefore, the concrete growth analysis increments through time in a step-by-step fashion. The rate of concrete growth at each time step is updated in accordance with the magnitude and direction of principal stresses. As such, concrete growth initial strain load inputs vary in magnitude and direction throughout the structure.

The stress dependent concrete growth from our GROW3D program is input to ANSYS using the user programmable features within ANSYS.

The concrete is assumed to be linear elastic material, although cracks can be introduced in the model if deemed significant. The effect of creep due to sustained loads is accounted for by using creep coefficients and effective modulus approach. The effective modulus of concrete is defined as

$$E_{eff} = \frac{E_{ci}}{\left(1 + \emptyset(t)\right)} \tag{1}$$

where

E_{ci} = instantaneous elastic modulus of concrete

$\phi(t)$ = effective modulus factor to account for creep over time. This factor varies with time, 2.5 is used for long-term AAR loading.

The stress dependent growth law characterizing AAR-induced growth of concrete is given as follows:

$$\dot{\epsilon}_{gi}(t) = \dot{\epsilon}_{go}(t), for\ \bar{\sigma}_i < \sigma_o \tag{2}$$

$$\dot{\epsilon}_{gi}(t) = \dot{\epsilon}_{go}(t) - K\left[log\left(\frac{\bar{\sigma}_i}{\sigma_o}\right)\right], for\ \sigma_o < \bar{\sigma}_i < \sigma_{lim}$$

$$\dot{\epsilon}_{gi}(t) = 0, for\ \bar{\sigma}_i > \sigma_{lim}$$

where

$\dot{\epsilon}_{gi}(t)$ = Concrete growth strains in principal directions at time (t)

$\dot{\epsilon}_{go}(t)$ = Unrestrained concrete growth rate at low stress at time (t)

K = Slope of the line defining the concrete growth rate versus the log of stress

$\bar{\sigma}_i$ = The three principal stresses (I = 1 to 3)

σ_o = A low compressive stress cut-off, whereby at lower compressive stresses or any tensile stress, the concrete growth rate is set at the unrestrained growth rate, and, at larger compressive stresses, the concrete growth rate is reduced according to the above logarithmic growth law.

σ_{lim} = Cut-off stress level beyond which no growth is assumed to occur.

In the concrete growth law (Equation 2), compressive stress is positive (compression is negative in ANSYS). At each time interval, the concrete growth strains are computed based on the prevailing stress state. The concrete growth strain increments are resolved in the direction of the principal stresses. These strain increments are resolved in the direction of the principal stresses. These strain increments are the initial strain loads (internal loads) used in the finite element analysis of a given time step. The rate of concrete growth depends on the temperature of concrete. For example, in the dam, a gradient of concrete growth occurs from upstream to downstream because the downstream portion of dam piers is warmer and hence the concrete growth rate is higher in this area. Temperature effects were not considered here.

The concrete growth strain rates are computed at each of the eight integration points within each solid element. Therefore, there can be considerable variation in concrete growth rates even within an element. These strain rates are the initial strain loads used in the finite element analysis of a given time step. The analysis may step through time using 1-yr time increments or smaller increments are used if thermal stresses are included. The initial conditions consist of initial stresses due to self-weight, equipment and hydrostatic loads. The model is stepped through time and results are output at selected dates in the past (for calibration) and future (for assessment).

3. Analysis Approach

The benchmark analyses can be somewhat time consuming, therefore some simplifications were made in the analysis of Kariba Dam. Two finite element models were provided by the benchmark committee. Model 1 had the dam fully bonded to the foundation rock. Model 2 used joint elements between the dam and foundation rock contact surface. We initially

considered using Model 2 modified to also include the vertical contraction joints between each concrete monolith. However, it was decided that the level of additional effort for such non-project work was beyond our intended scope. Therefore, Model 1 was used for analysis presented herein.

The dead load was applied with a simple gravity turn-on approach. The dead load calculation is approximate, however the AAR-loading will cause a significant change in stresses in the dam, hence this approximation will not have a significant effect on the overall results.

The hydrostatic load was applied as recommended by the Workshop Committee. The reservoir was assumed to be at the following levels:

- Reservoir level at 483.8 m from 1963 to July 30 1973
- Reservoir level at 486.1 m from August 1973 to May 30 1981
- Reservoir level at 479.9 m from June 1981 to May 30 1994
- Reservoir level at 486.06 m from June 1994 to April 20 2010

The concrete modulus is 22 GPa and the rock modulus is 10 GPa. Both materials have a Poisson's ratio of 0.2. The concrete density is 2350 kg/m^3. The unrestrained concrete growth rates at low stresses varied from 16 to 26 micro-strain per year. The typical rate of concrete expansion was 25 micro-strain per year. The concrete growth law assumed that low stress limit for concrete expansion was 0.1 MPa i.e., with tensile stresses or compressive stresses less than 0.1 MPa the concrete would expand at the unrestrained rate. The limiting compressive stress at which the concrete would stop expanding was assumed to be 7.0 MPa. A high limiting stress was selected in order to estimate the maximum build-up of stress in the dam. From our experience on other dams, the limiting stress is typically about 4 to 5 MPa. It is noted that laboratory testing will generally predict a lower limiting stress.

The GROW3D subroutines also have "coupling" relationships whereby a high compressive stress in one direction can reduce the rate of concrete growth in the two orthogonal directions. However, these coupling relationships were not used herein.

The effect of enhanced creep is included in the analysis using an effective modulus approach. The enhanced creep behavior affects the response to the AAR loads. Creep is only applied to dead and AAR loads in this paper.

The analysis reported herein was undertaken using ANSYS Version 12.0.1 with the Hatch GROW3D subroutines complied and linked using the User Programmable features in ANSYS.

4. Results

It is very important that the dates given above for water level changes are used when comparing results to other solutions. The importance of this is shown in Figure 1 where the reservoir levels were changed as described above. It is noted that the displacements are "relative" assuming zero displacement in 1963. The AAR-induced displacements cause the dam to deflect upstream as observed from the slope of lines given in Figure 1. From Figure 1, the computed displacements show a sudden jump in 1994 when the reservoir level was changed from el 479.9 m in May 1994 to 486.06 m in June 1994. The reservoir water levels plotted in Figure 1 show the reservoir did not actually reach el 486 m until 1998. From Figure 1, the

associated change in radial displacements due to the reservoir level change from 479.9 to 486.06 m is about 20 mm.

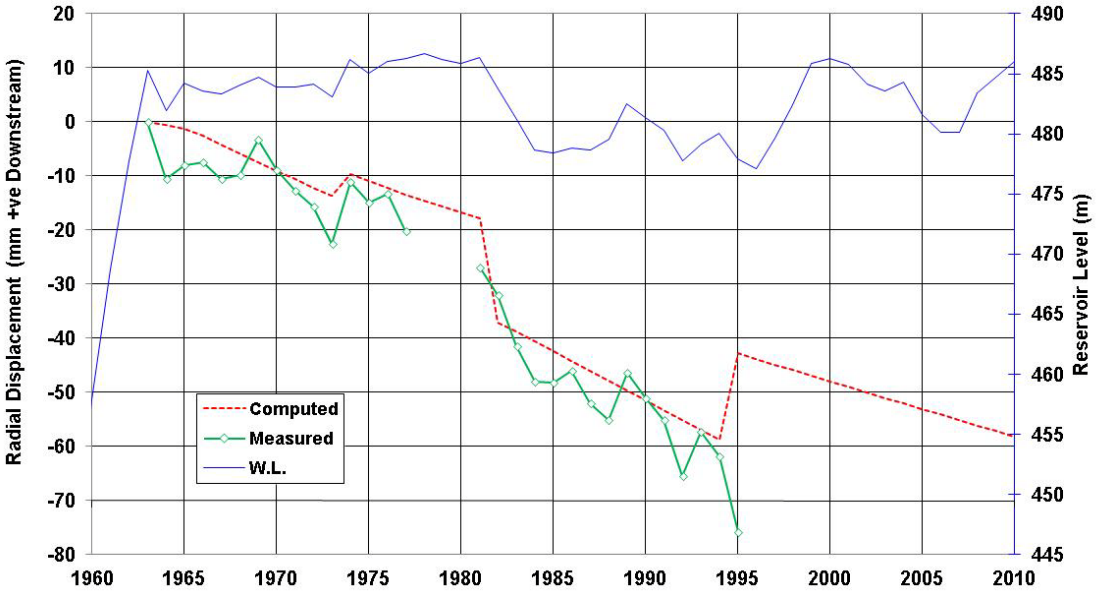

Figure 1 Measured and Computed Radial Displacements at T434

A comparison of measured and computed vertical displacements using 1994 measurements is given in Figure 2. From Figure 2, the finite element model under predicts the vertical rise in the central portion of the dam. The reason for the under prediction in this area is attributed to the fact that the vertical contraction joints in the dam were not modeled with surface contact which would allow relative vertical slip between monoliths. In the central portion of the dam, the concrete monoliths are higher than monoliths near the abutments hence we would expect some vertical relative slip between blocks in the central portion of the dam.

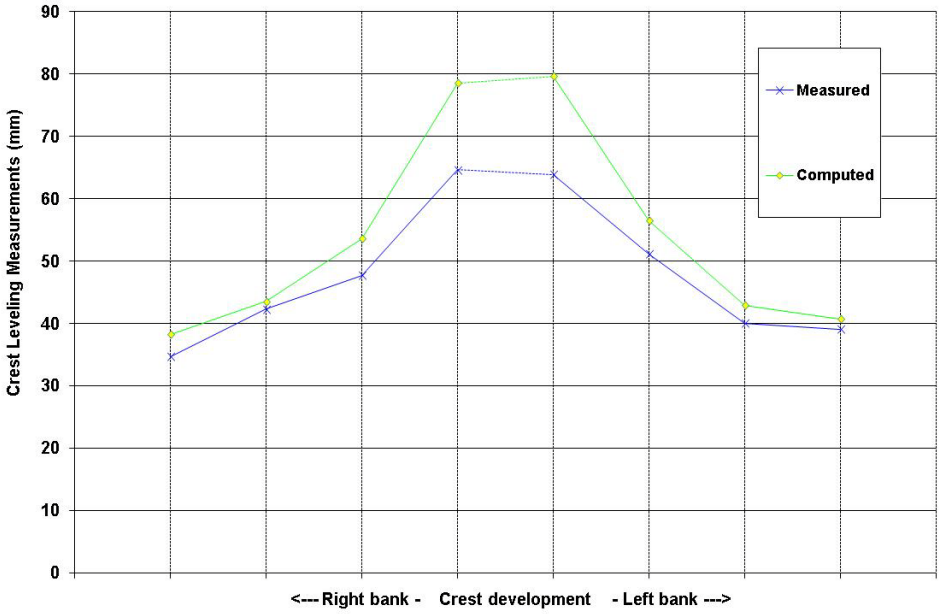

Figure 2 Comparison of Measured and Computed Vertical Movements in 1994

4.1 Results of Analysis in the Year 2010

Figures 3 to 6 present contours of arch and cantilever stresses on the upstream and downstream faces of the dam in the year 2010. From Figure 3, the maximum arch stress on the upstream face is about -6 MPa (compressive stresses are negative). The maximum arch stress occur in the upper portion of dam near the abutments. In the central portion of the dam the maximum arch stress on the upstream face is about 5 MPa. The arch stresses on the downstream face are presented in Figure 4 where in general the magnitude of stress is arch stress is lower compared to the upstream face. Figure 5 shows the contours of cantilever stresses on the upstream face of the dam. From Figure 5, maximum computed tensile stress is about 1.0 MPa and it occurs at the base of the central cantilever. It is noted that the foundation rock elements immediately upstream of the dam were assigned a reduced elastic modulus as a means of eliminating the fictitious tensile stresses that would develop in these elements. Figure 6 presents contours of cantilever stresses on the downstream face of the dam. From Figure 6, the maximum stress at the base of the dam is -8.9 MPa.

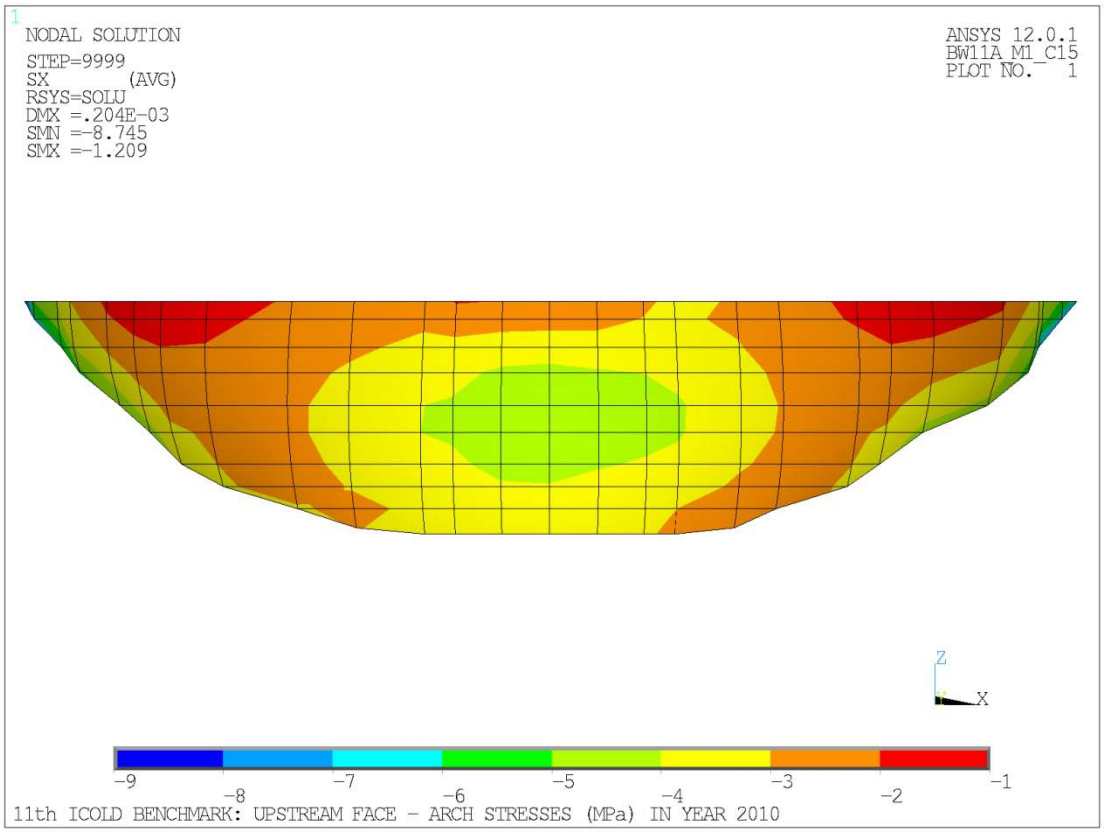

Figure 3 Upstream Face Arch Stresses (MPa) in Year 2010

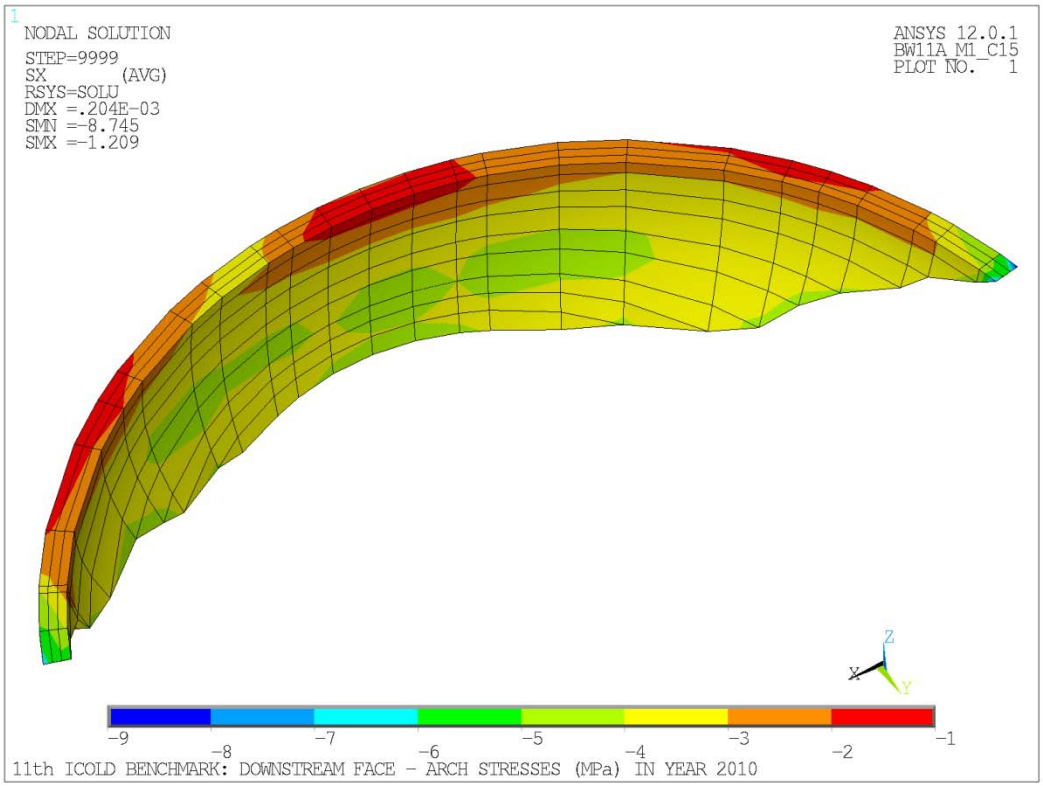

Figure 4 Downstream Face Arch Stresses (MPa) in Year 2010

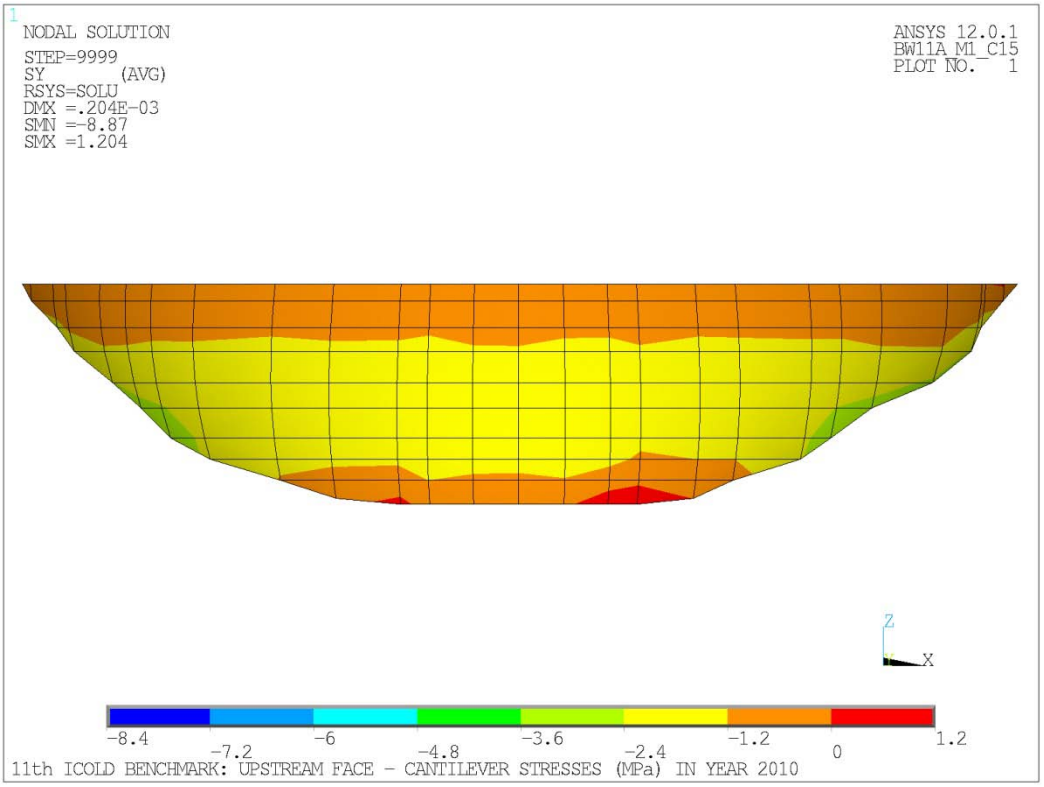

Figure 5 Upstream Face Cantilever Stresses (MPa) in Year 2010

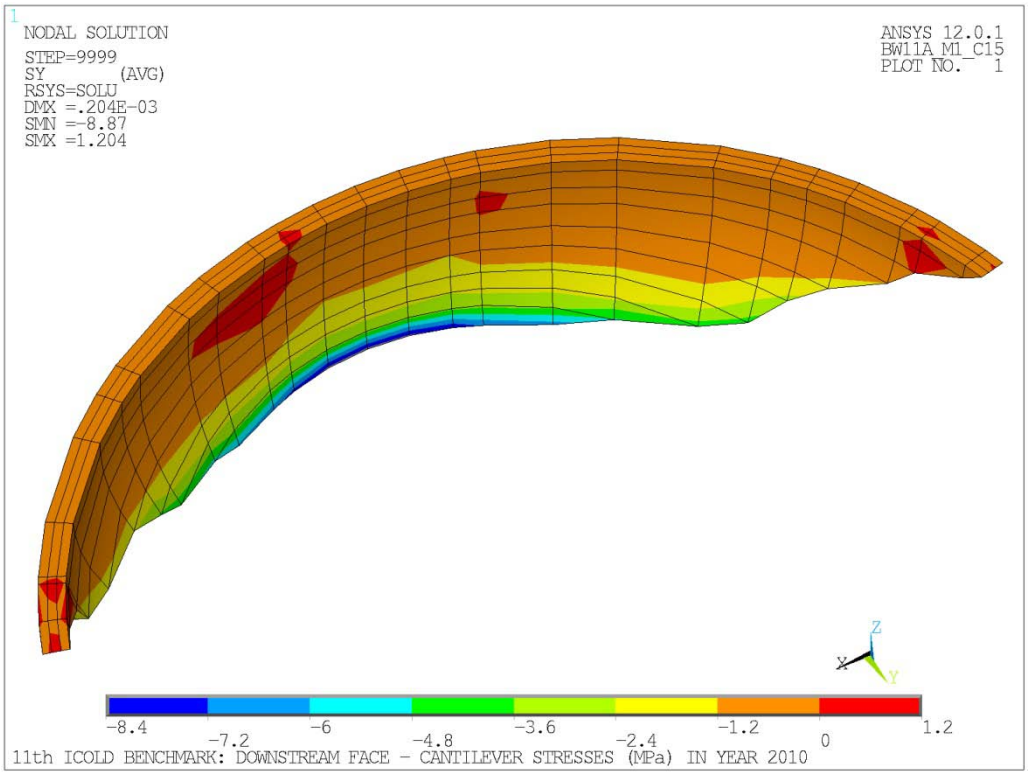

Figure 6 Downstream Face Cantilever Stresses (MPa) in Year 2010

Displacement contours are presented in Figures 7 and 8. Figure 7 presents the computed vertical displacements in 2010. As noted previously, the computed vertical displacements in the central portion of the dam are expected to be under predicted by the model because relative vertical at the contractions joints is not modeled. It should be noted that we typically do include the contraction joints in our ANSYS models on dams, but time constraints did not allow this to be done for this benchmark analysis. Figure 8 presents the global y-displacements contours on the deformed shape of the dam. It is noted from Figure 8 that the global y-axis points downstream. The maximum y-displacement occurs below the crest of dam just below the spillway which was not included in the model.

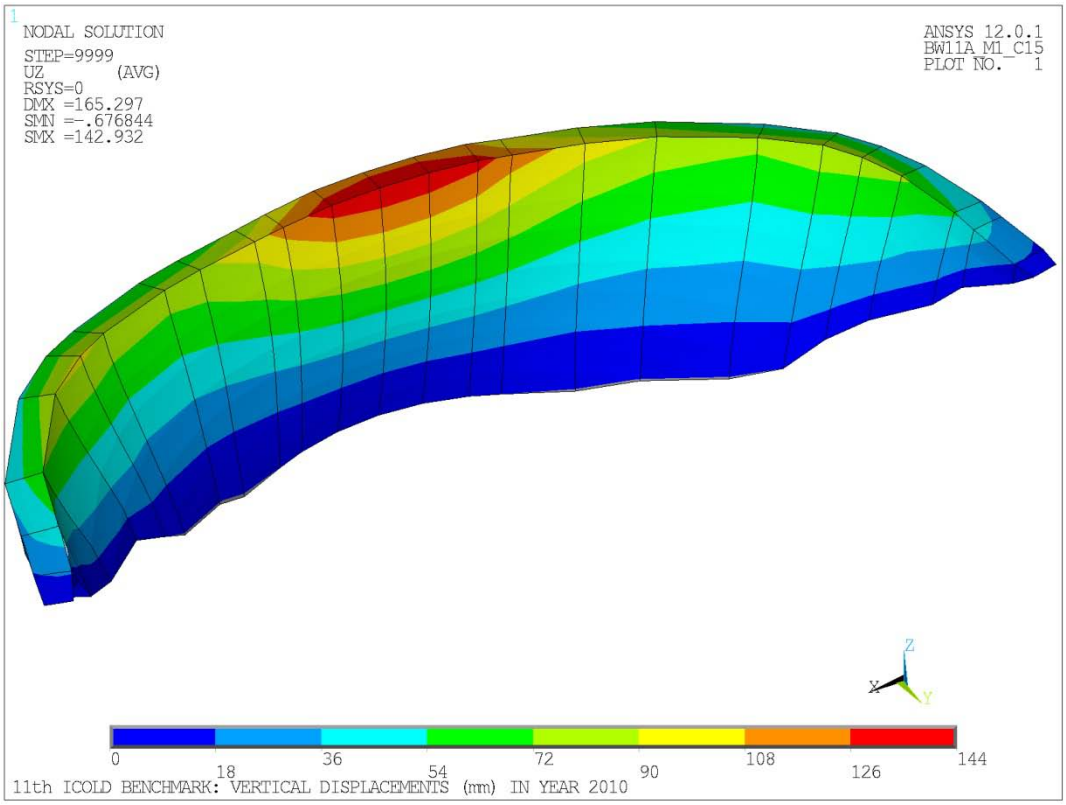

Figure 7 Vertical Displacements (mm) in Year 2010

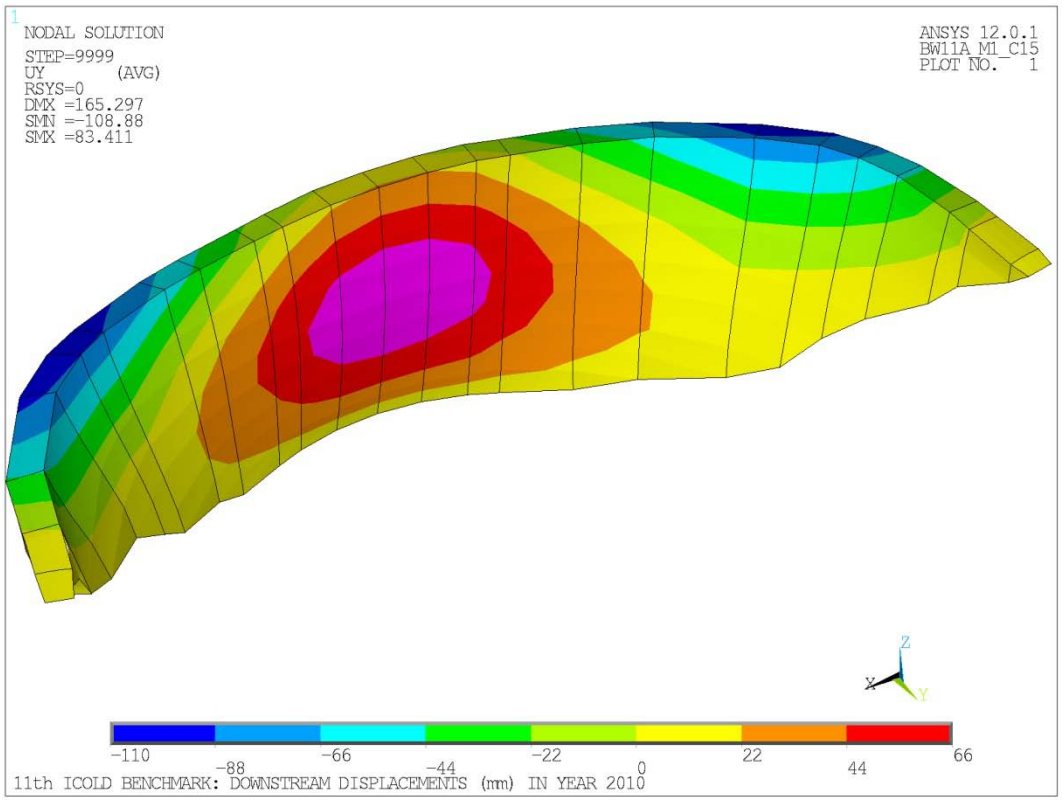

Figure 8 Downstream Displacements (mm) in Year 2010

The orientations of minimum principal stresses (maximum compressive stresses) near the upstream and downstream faces are shown in Figures 9 and 10. ANSYS plots the principal stress orientations at the element Gauss points.

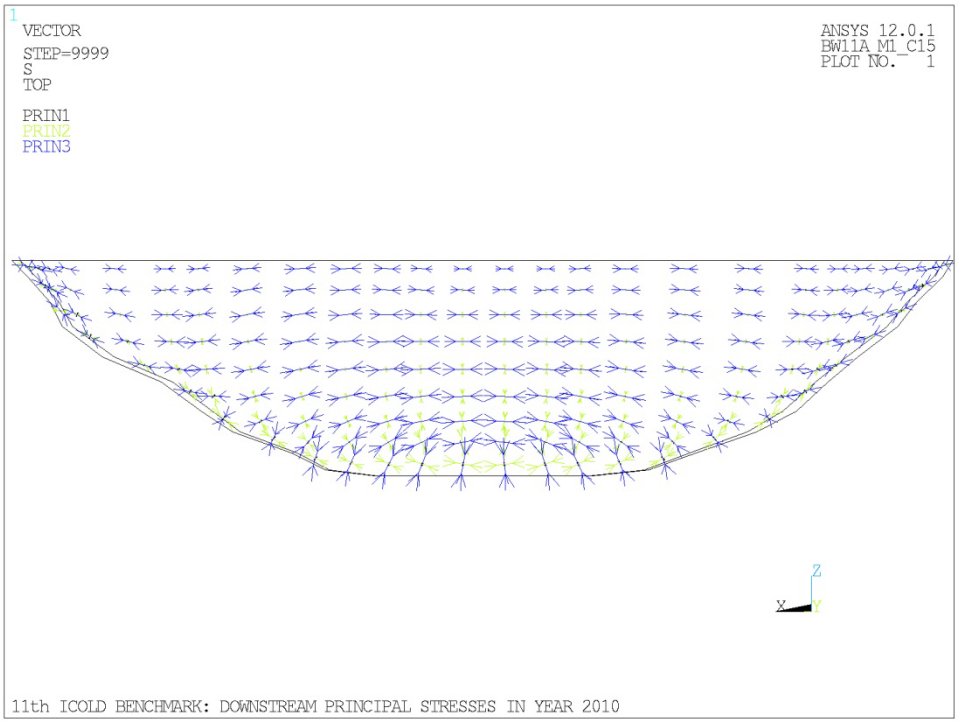

Figure 9 Downstream Principal Stresses in Year 2010

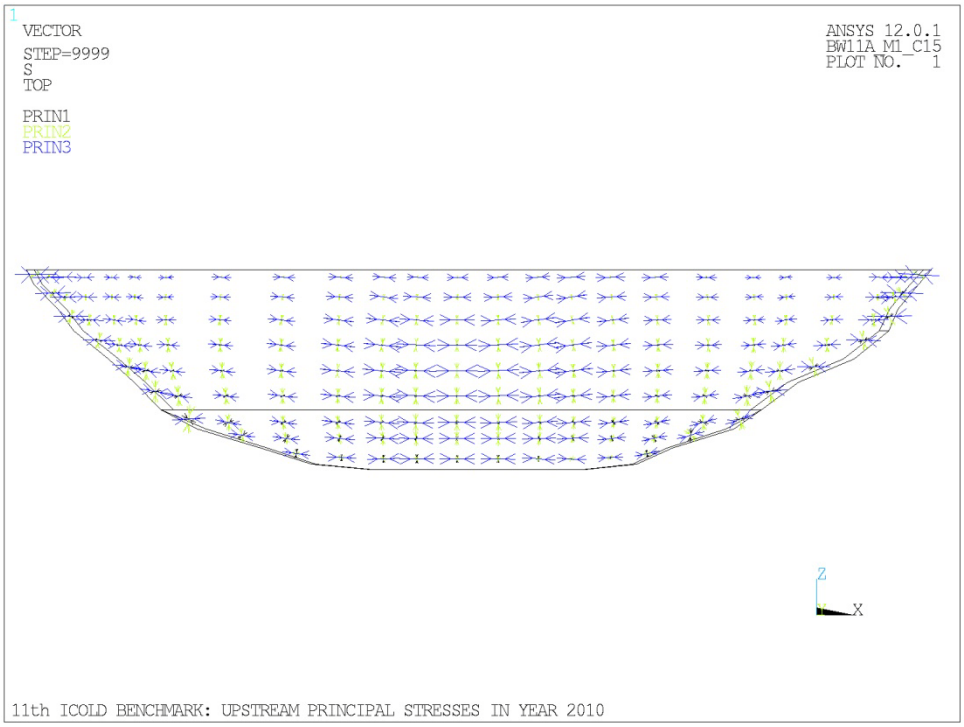

Figure 10 Upstream Principal Stresses in Year 2010

4.2 Computed Stress and Displacement Changes Caused BY AAR

The change in computed selected stresses and displacements caused by AAR was calculated by subtracting the ANSYS results at 1963 from the 2010 results. Figure 11 presents the computed change in arch stress on the upstream face from 1963 to 2010. It is noted that the reservoir level is slightly higher in 2010 compared to 1963 but this effect is small compared to AAR-induced changes in stress. From Figure 11, it is observed that AAR-induced stresses are maximum near the abutments and actually relatively small changes in stress occur in the central portion of the dam. We found a similar result while analyzing Seminoe dam and this was confirmed by stress measurements. The change in arch stress on the downstream face of the dam is contoured in Figure 12. Figures 13 and 14 show the computed change in cantilevers on the upstream and downstream faces from 1963 to 2010. It is interesting to note that AAR induces a compressive cantilever stress at the upstream face at the base of the dam i.e., a beneficial effect! On the downstream face of the dam the cantilever compressive stress is reduced slightly by AAR but from Figure 6 the total stress is compressive as a result of hydrostatic loading.

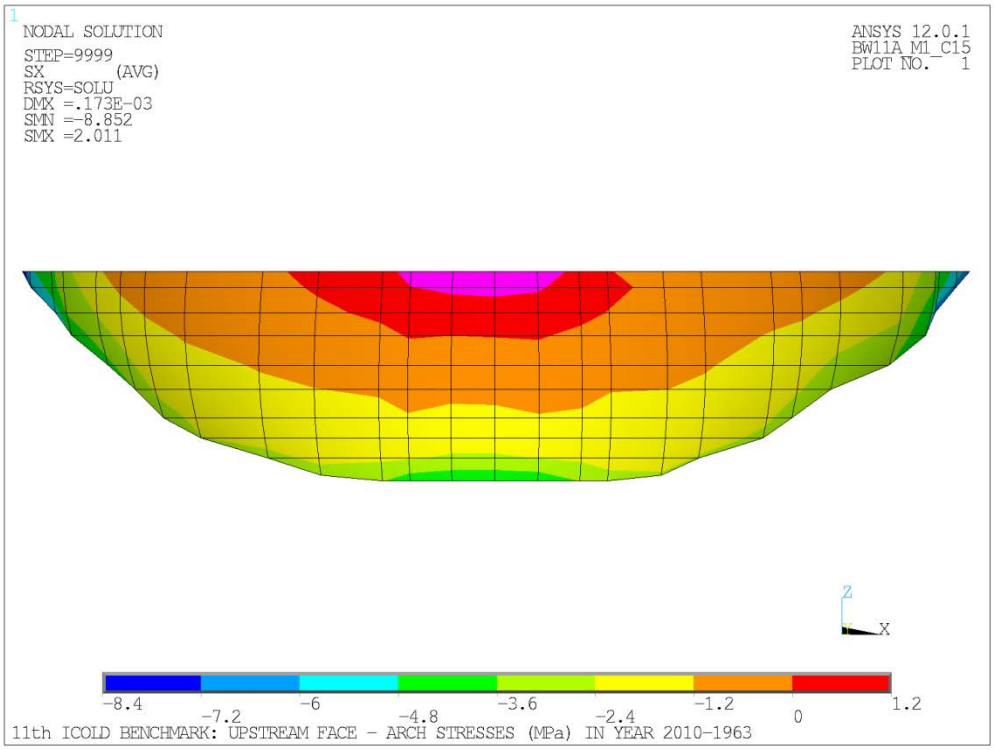

Figure 11 Upstream Face Arch Stresses (MPa) in Year 2010-1963

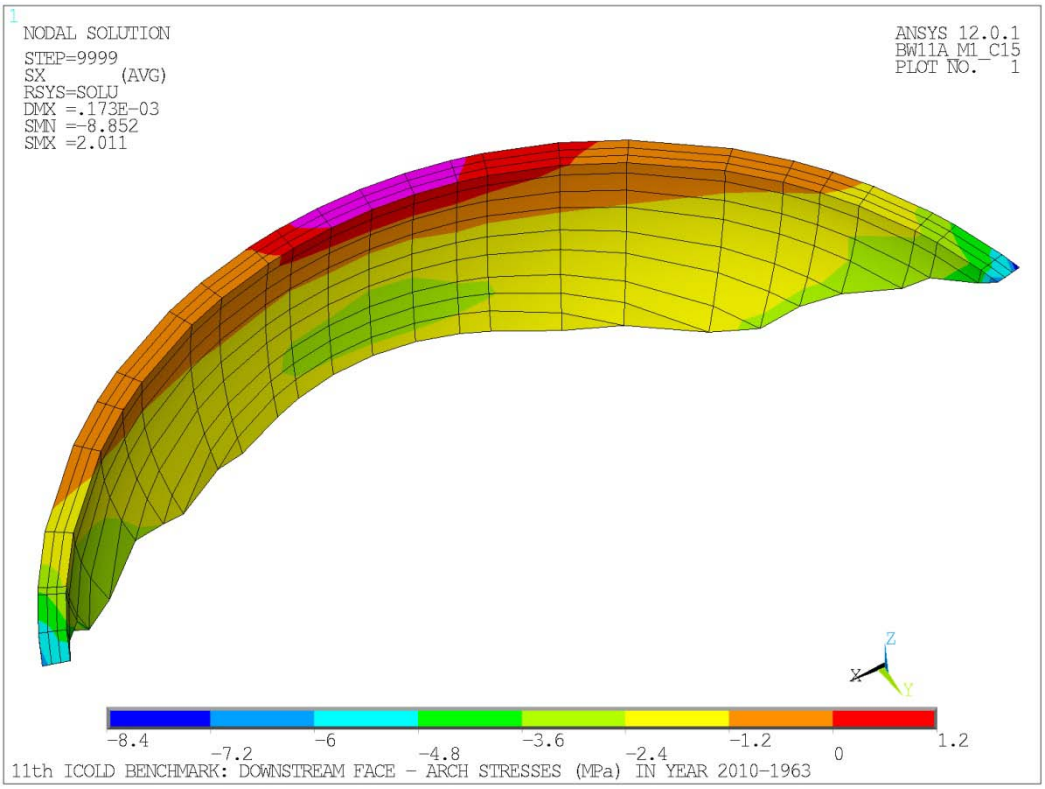

Figure 12 Downstream Face Arch Stresses (MPa) in Year 2010-1963

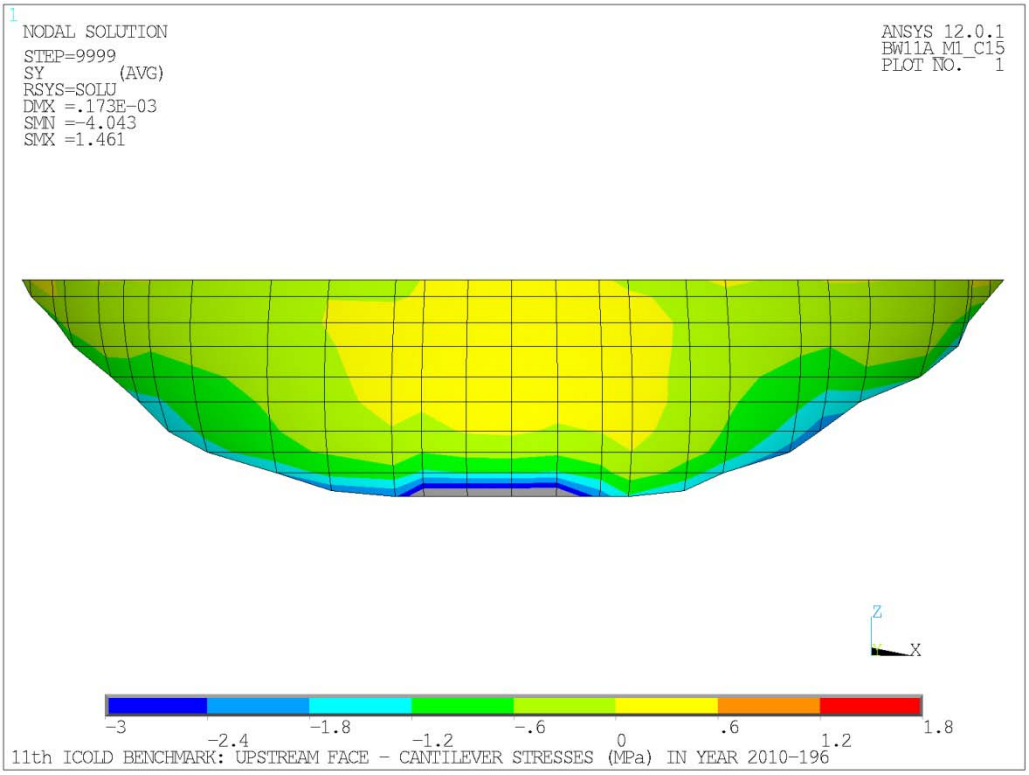

Figure 13 Upstream Face Cantilever Stresses (MPa) in Year 2010-1963

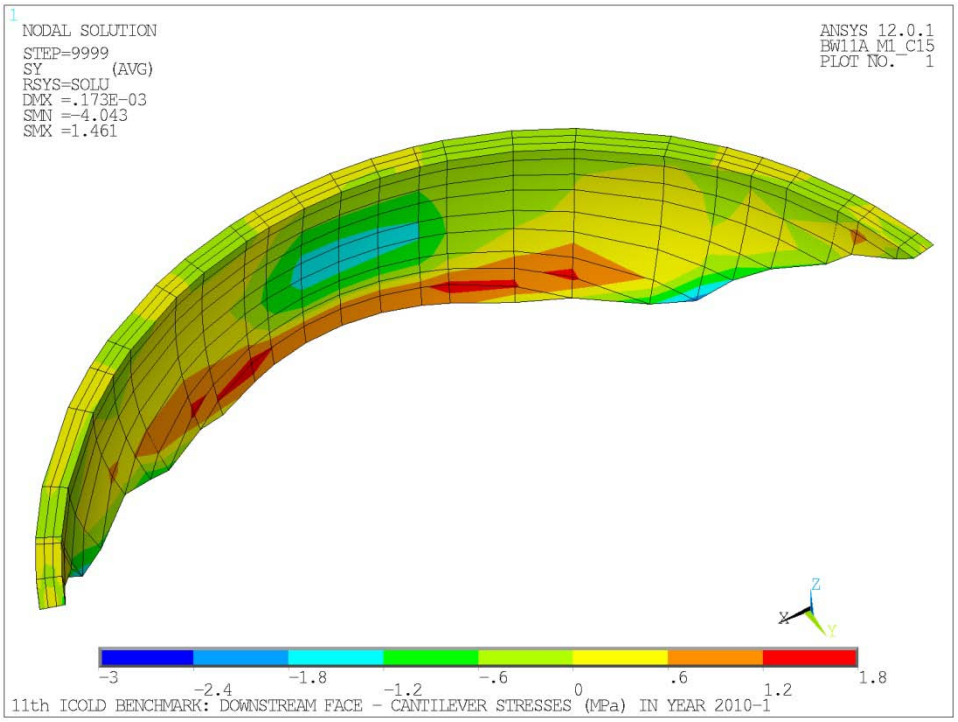

Figure 14 Downstream Face Cantilever Stresses (MPa) in Year 2010-1963

Figure 15 presents the global y-displacement contours as a result of AAR loading from 1963 to 2010. The difference in reservoir level in 1963 and 2010 affects the contours to some degree, but overall effect of AAR loading is clearly seen in Figure 15.

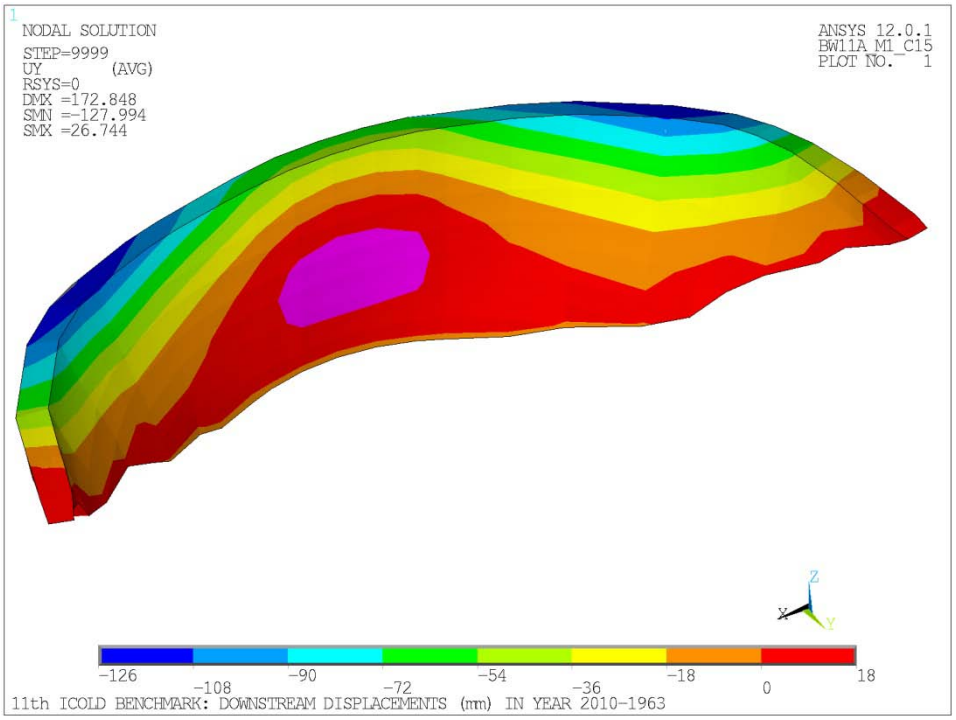

Figure 15 Downstream Displacements (mm) in Year 2010-1963

4.3 Benchmark Solution

Tables providing the benchmark solution are given in Appendix A.

5. Conclusions

The following conclusions are drawn:

- A reasonable calibration to available measurements has been achieved
- An improved calibration could be made by modeling the vertical contraction joints with surface contact elements. Contact elements could also be used at the concrete/ rock interface joint
- The AAR-induced loading causes the dam to tilt upstream. This has the beneficial effect of inducing a compressive stress at the base of the dam at the upstream face where typically tensile cantilever stresses are of concern.
- The change in arch stresses near the dam abutments is quite large and the forces generated by the stresses should be taken into consideration for abutment stability analysis.
- The effect of a potential slow-down of the reaction has not been considered due to a lack of expansion characteristics of this concrete.

References

[1] Curtis, D.D. (1995). Modeling of AAR Affected Structures Using the GROW3D FEA Program, USCOLD Second International Conference on Alkali-Aggregate Reaction in Hydroelectric Plants and Dams, Chattanooga, TN, pp. 457-477.

[2] Curtis, D.D. (2002). Preliminary Structural Analysis of Seminoe Dam for AAR Loading. Workshop on Non-linear Structural Analysis of Concrete Dams, Denver Colorado.

[3] Curtis, D.D., Davis, B., Rahman, S., Powell, R., Updated Assessment of Concrete Growth Effects on a TVA Dam, 25th USSD Conference, Salt Lake City, Utah, USA, 2005

[4] Curtis, D.D. (2000), A Review and Analysis of AAR-Effects in Arch Dams, Proceedings of the 11th ICAAR, Quebec City, Quebec, Canada, pp 1283-1282.

Appendix A

Table 1 Definition of Reference Points

POINT	LOCATION	ELEVATION	NODES MODEL1.MESH
R1	Block 20	488	1256
R2	Block 20	480	1267
R3	Block 20	463	1283
R4	Block 20	438	1300
R5	Block 20	418	1316
R6	Block 0	480	2806
R7	Block 0	438	2839
R8	Block 0	418	2855
R9	Block 19	488	5416
R10	Block 19	480	5427
R11	Block 19	463	5443
R12	Block 19	438	5460
R13	Block 19	418	5476
R14	Crest Block 20	489	1735
R15	Crest Block 14	489	2135
R16	Crest Block 6	489	2706
R17	Crest Block 0	489	3366
R18	Crest Block 5	489	4026
R19	Crest Block 11	489	4686
R20	Crest Block 17	489	5105
R21	Crest Block 23	489	5416
R22	Crest Block 4	489	3127

THEME A - EFFECT OF CONCRETE SWELLING ON THE EQUILIBRIUM OF AN ARCH DAM

Organization Hatch **Name** Curtis

Solution 1A : End of construction

Point	Location	Elevation	STRESSES		
			Horizontal	Vertical	Major Principal
R1	Block 20	488	0.687	-0.043	-0.048
R2	Block 20	480	0.625	-0.230	-0.244
R3	Block 20	463	0.484	-0.693	-0.702
R4	Block 20	438	0.359	-0.984	-1.014
R5	Block 20	418	0.210	-0.780	-0.793
R6	Block 0	480	0.357	-0.212	-0.226
R7	Block 0	438	0.343	-1.189	-1.202
R8	Block 0	418	0.178	-1.584	-1.589
R9	Block 19	488	0.433	-0.043	-0.048
R10	Block 19	480	0.445	-0.227	-0.240
R11	Block 19	463	0.416	-0.681	-0.686
R12	Block 19	438	0.326	-1.000	-1.012
R13	Block 19	418	0.239	-0.907	-0.992
R14	Crest Block 20	489	0.469	-0.042	-0.049
R15	Crest Block 14	489	0.335	-0.042	-0.051
R16	Crest Block 6	489	0.323	-0.041	-0.045
R17	Crest Block 0	489	0.371	-0.041	-0.043
R18	Crest Block 5	489	0.429	-0.041	-0.044
R19	Crest Block 11	489	0.459	-0.042	-0.050
R20	Crest Block 17	489	0.439	-0.043	-0.053
R21	Crest Block 23	489	0.433	-0.043	-0.048
R22	Crest Block 4	489	0.469	-0.040	-0.041

Solution 1B : RWL = 483,80

Point	Location	Elevation	STRESSES			DISPLACEMENTS		
			Horizontal	Vertical	Major Principal	Radial	Vertical	Tangential
R1	Block 20	488	-2.165	-0.039	-2.169	15.73	5.44	13.63
R2	Block 20	480	-2.110	-0.172	-2.127	14.84	5.23	12.79
R3	Block 20	463	-2.031	-0.424	-2.143	12.90	4.53	11.00
R4	Block 20	438	-1.961	-0.766	-2.266	10.68	2.95	9.23
R5	Block 20	418	-1.498	-1.135	-1.938	8.57	0.55	7.78
R6	Block 0	480	-3.015	-0.144	-3.020	68.02	12.43	8.92
R7	Block 0	438	-2.889	-0.375	-2.956	56.31	11.11	6.01
R8	Block 0	418	-2.421	-0.744	-2.603	44.89	9.49	4.67
R9	Block 19	488	-2.195	-0.039	-2.203	16.51	7.93	-13.83
R10	Block 19	480	-2.155	-0.171	-2.170	15.49	7.76	-12.89
R11	Block 19	463	-2.079	-0.419	-2.176	13.31	7.04	-10.94
R12	Block 19	438	-1.989	-0.743	-2.280	10.95	5.22	-9.08
R13	Block 19	418	-1.803	-1.244	-2.423	8.77	2.14	-7.62
R14	Crest Block 20	489	-2.593	-0.039	-2.602	28.91	8.35	15.59
R15	Crest Block 14	489	-2.864	-0.039	-2.878	48.90	10.91	14.60
R16	Crest Block 6	489	-2.976	-0.040	-2.982	66.84	12.28	10.60
R17	Crest Block 0	489	-3.051	-0.040	-3.052	78.01	12.98	3.93
R18	Crest Block 5	489	-3.038	-0.040	-3.041	74.50	13.23	-4.07
R19	Crest Block 11	489	-2.904	-0.040	-2.912	57.61	12.82	-10.33
R20	Crest Block 17	489	-2.619	-0.039	-2.627	33.81	11.02	-13.86
R21	Crest Block 23	489	-2.195	-0.039	-2.203	16.51	7.93	-13.83
R22	Crest Block 4	489	-2.554	-0.040	-2.555	76.44	11.95	6.56

THEME A - EFFECT OF CONCRETE SWELLING ON THE EQUILIBRIUM OF AN ARCH DAM

Organization Hatch **Name** Curtis

Solution 1C : RWL = 486,10

Point	Location	Elevation	STRESSES			DISPLACEMENTS		
			Horizontal	Vertical	Major Principal	Radial	Vertical	Tangential
R1	Block 20	488	-2.391	-0.040	-2.395	16.79	5.81	14.40
R2	Block 20	480	-2.322	-0.168	-2.339	15.83	5.60	13.52
R3	Block 20	463	-2.207	-0.424	-2.322	13.72	4.83	11.63
R4	Block 20	438	-2.101	-0.793	-2.423	11.31	3.10	9.75
R5	Block 20	418	-1.589	-1.180	-2.051	9.04	0.53	8.20
R6	Block 0	480	-3.317	-0.140	-3.323	72.64	12.84	9.33
R7	Block 0	438	-3.084	-0.362	-3.153	59.38	11.53	6.30
R8	Block 0	418	-2.551	-0.746	-2.741	47.05	9.85	4.91
R9	Block 19	488	-2.406	-0.039	-2.414	17.60	8.45	-14.61
R10	Block 19	480	-2.357	-0.168	-2.373	16.50	8.28	-13.63
R11	Block 19	463	-2.254	-0.419	-2.357	14.14	7.49	-11.56
R12	Block 19	438	-2.130	-0.768	-2.440	11.59	5.50	-9.59
R13	Block 19	418	-1.912	-1.299	-2.572	9.26	2.20	-8.04
R14	Crest Block 20	489	-2.855	-0.040	-2.865	31.08	8.77	16.38
R15	Crest Block 14	489	-3.161	-0.040	-3.174	52.46	11.33	15.28
R16	Crest Block 6	489	-3.293	-0.041	-3.298	71.56	12.68	11.09
R17	Crest Block 0	489	-3.382	-0.041	-3.382	83.41	13.36	4.10
R18	Crest Block 5	489	-3.369	-0.041	-3.372	79.67	13.64	-4.26
R19	Crest Block 11	489	-3.217	-0.041	-3.224	61.69	13.30	-10.80
R20	Crest Block 17	489	-2.888	-0.040	-2.895	36.27	11.55	-14.54
R21	Crest Block 23	489	-2.406	-0.039	-2.414	17.60	8.45	-14.62
R22	Crest Block 4	489	-2.867	-0.041	-2.868	81.75	12.18	6.86

Solution 1D : RWL = 479,90

Point	Location	Elevation	STRESSES			DISPLACEMENTS		
			Horizontal	Vertical	Major Principal	Radial	Vertical	Tangential
R1	Block 20	488	-1.589	-0.040	-1.593	13.17	4.53	11.90
R2	Block 20	480	-1.579	-0.184	-1.595	12.48	4.33	11.16
R3	Block 20	463	-1.610	-0.401	-1.713	11.00	3.80	9.62
R4	Block 20	438	-1.652	-0.661	-1.909	9.27	2.61	8.09
R5	Block 20	418	-1.305	-1.015	-1.687	7.54	0.61	6.85
R6	Block 0	480	-2.242	-0.159	-2.248	57.19	11.72	8.12
R7	Block 0	438	-2.460	-0.366	-2.522	49.80	10.27	5.42
R8	Block 0	418	-2.163	-0.727	-2.327	40.53	8.74	4.20
R9	Block 19	488	-1.656	-0.039	-1.663	13.95	6.69	-12.08
R10	Block 19	480	-1.647	-0.184	-1.660	13.12	6.53	-11.25
R11	Block 19	463	-1.662	-0.397	-1.744	11.40	5.99	-9.56
R12	Block 19	438	-1.678	-0.645	-1.915	9.52	4.60	-7.96
R13	Block 19	418	-1.574	-1.102	-2.094	7.72	2.01	-6.71
R14	Crest Block 20	489	-1.920	-0.039	-1.932	23.56	7.46	13.95
R15	Crest Block 14	489	-2.098	-0.040	-2.116	40.22	10.12	13.24
R16	Crest Block 6	489	-2.153	-0.040	-2.161	55.60	11.61	9.67
R17	Crest Block 0	489	-2.190	-0.040	-2.191	65.30	12.37	3.58
R18	Crest Block 5	489	-2.178	-0.040	-2.182	62.31	12.54	-3.74
R19	Crest Block 11	489	-2.097	-0.040	-2.109	47.80	11.94	-9.42
R20	Crest Block 17	489	-1.929	-0.040	-1.941	27.79	9.89	-12.46
R21	Crest Block 23	489	-1.656	-0.039	-1.663	13.95	6.69	-12.08
R22	Crest Block 4	489	-1.721	-0.041	-1.722	63.92	11.76	5.99

THEME A - EFFECT OF CONCRETE SWELLING ON THE EQUILIBRIUM OF AN ARCH DAM

Organization Hatch **Name** Curtis

Solution 2A : RWL = 483,80 - 30 July 1973

Point	Location	Elevation	STRESSES			DISPLACEMENTS		
			Horizontal	Vertical	Major Principal	Radial	Vertical	Tangential
R1	Block 20	488	-2.062	-0.020	-2.063	11.74	20.43	12.94
R2	Block 20	480	-2.219	-0.180	-2.222	11.70	17.29	12.40
R3	Block 20	463	-2.426	-0.481	-2.442	11.21	11.80	10.80
R4	Block 20	438	-2.504	-0.829	-2.503	9.67	7.22	8.74
R5	Block 20	418	-1.915	-1.191	-1.895	8.00	2.51	7.24
R6	Block 0	480	-2.767	-0.126	-2.769	56.99	29.93	13.72
R7	Block 0	438	-3.195	-0.445	-3.208	56.79	19.51	8.11
R8	Block 0	418	-2.880	-0.804	-2.947	46.24	14.73	6.10
R9	Block 19	488	-2.331	-0.063	-2.337	12.09	20.06	-12.36
R10	Block 19	480	-2.334	-0.188	-2.355	12.57	17.45	-12.47
R11	Block 19	463	-2.406	-0.419	-2.457	11.56	13.20	-10.65
R12	Block 19	438	-2.442	-0.716	-2.527	9.53	9.05	-8.26
R13	Block 19	418	-2.323	-1.267	-2.502	7.51	4.43	-6.47
R14	Crest Block 20	489	-2.622	-0.046	-2.630	17.85	20.79	16.08
R15	Crest Block 14	489	-2.947	-0.052	-2.958	35.05	24.23	18.47
R16	Crest Block 6	489	-2.778	-0.040	-2.780	52.57	30.17	17.04
R17	Crest Block 0	489	-2.357	-0.025	-2.357	63.78	37.93	6.45
R18	Crest Block 5	489	-2.361	-0.027	-2.362	60.91	37.91	-7.31
R19	Crest Block 11	489	-2.705	-0.064	-2.710	44.69	29.68	-15.93
R20	Crest Block 17	489	-2.630	-0.043	-2.634	24.87	24.83	-18.00
R21	Crest Block 23	489	-2.331	-0.063	-2.337	12.09	20.06	-12.36
R22	Crest Block 4	489	-1.917	-0.030	-1.917	63.41	38.39	10.79

Solution 2B : RWL = 486,10 - 30 May 1981

Point	Location	Elevation	STRESSES			DISPLACEMENTS		
			Horizontal	Vertical	Major Principal	Radial	Vertical	Tangential
R1	Block 20	488	-2.259	-0.021	-2.260	9.58	34.48	13.36
R2	Block 20	480	-2.535	-0.187	-2.535	10.24	28.54	13.07
R3	Block 20	463	-2.890	-0.505	-2.876	10.88	18.66	11.56
R4	Block 20	438	-3.038	-0.869	-2.935	9.74	11.20	9.11
R5	Block 20	418	-2.299	-1.243	-2.073	8.16	4.18	7.39
R6	Block 0	480	-2.896	-0.102	-2.909	53.50	45.57	18.33
R7	Block 0	438	-3.621	-0.505	-3.614	60.49	27.23	10.15
R8	Block 0	418	-3.359	-0.859	-3.372	49.56	19.71	7.47
R9	Block 19	488	-2.661	-0.071	-2.667	9.74	31.57	-12.25
R10	Block 19	480	-2.676	-0.191	-2.700	11.37	26.84	-13.14
R11	Block 19	463	-2.828	-0.423	-2.859	11.24	19.36	-11.35
R12	Block 19	438	-2.915	-0.709	-2.928	9.33	12.89	-8.42
R13	Block 19	418	-2.805	-1.311	-2.800	7.21	6.61	-6.20
R14	Crest Block 20	489	-2.908	-0.043	-2.915	10.81	32.64	17.60
R15	Crest Block 14	489	-3.297	-0.061	-3.306	27.38	36.69	22.72
R16	Crest Block 6	489	-2.969	-0.042	-2.972	46.50	46.26	23.12
R17	Crest Block 0	489	-2.227	-0.027	-2.227	58.78	60.42	8.93
R18	Crest Block 5	489	-2.253	-0.031	-2.254	56.28	60.11	-10.33
R19	Crest Block 11	489	-2.888	-0.071	-2.892	39.00	45.19	-21.27
R20	Crest Block 17	489	-2.915	-0.045	-2.918	20.12	37.77	-22.39
R21	Crest Block 23	489	-2.661	-0.071	-2.667	9.74	31.57	-12.24
R22	Crest Block 4	489	-1.826	-0.023	-1.826	59.56	61.70	14.86

THEME A - EFFECT OF CONCRETE SWELLING ON THE EQUILIBRIUM OF AN ARCH DAM

Organization Hatch **Name** Curtis

Solution 2C : RWL = 479,90 - 30 May 1994

Point	Location	Elevation	STRESSES			DISPLACEMENTS		
			Horizontal	Vertical	Major Principal	Radial	Vertical	Tangential
R1	Block 20	488	-1.479	-0.025	-1.482	-2.62	54.66	8.56
R2	Block 20	480	-1.906	-0.213	-1.902	-0.11	44.18	9.04
R3	Block 20	463	-2.639	-0.476	-2.597	4.34	27.87	8.68
R4	Block 20	438	-3.112	-0.677	-2.979	6.01	17.05	6.66
R5	Block 20	418	-2.392	-1.032	-2.202	6.07	7.04	5.48
R6	Block 0	480	-1.642	-0.113	-1.686	16.98	67.15	23.98
R7	Block 0	438	-3.254	-0.608	-3.232	46.14	36.46	11.82
R8	Block 0	418	-3.408	-0.913	-3.356	41.55	24.99	8.26
R9	Block 19	488	-2.045	-0.074	-2.052	-2.71	46.14	-6.37
R10	Block 19	480	-2.110	-0.202	-2.134	1.40	38.04	-8.84
R11	Block 19	463	-2.527	-0.389	-2.520	4.61	26.04	-8.26
R12	Block 19	438	-2.907	-0.542	-2.834	5.02	17.40	-5.67
R13	Block 19	418	-2.955	-1.047	-2.766	4.19	9.92	-3.58
R14	Crest Block 20	489	-1.950	-0.040	-1.961	-17.62	49.02	15.20
R15	Crest Block 14	489	-2.236	-0.073	-2.248	-10.37	53.82	25.78
R16	Crest Block 6	489	-1.721	-0.043	-1.728	5.38	68.77	30.57
R17	Crest Block 0	489	-0.793	-0.029	-0.793	16.84	92.64	11.92
R18	Crest Block 5	489	-0.831	-0.035	-0.832	15.60	91.76	-14.63
R19	Crest Block 11	489	-1.646	-0.076	-1.654	1.17	66.43	-27.62
R20	Crest Block 17	489	-1.947	-0.049	-1.954	-6.36	54.55	-25.42
R21	Crest Block 23	489	-2.045	-0.074	-2.052	-2.71	46.14	-6.37
R22	Crest Block 4	489	-0.574	-0.021	-0.574	19.75	95.62	19.95

THEME A - EFFECT OF CONCRETE SWELLING ON THE EQUILIBRIUM OF AN ARCH DAM

Organization Hatch **Name** Curtis

Solution 3A : RWL = 486,06 - 30 April 2010

Point	Location	Elevation	STRESSES			DISPLACEMENTS		
			Horizontal	Vertical	Major Principal	Radial	Vertical	Tangential
R1	Block 20	488	-2.272	-0.028	-2.274	-6.46	82.27	9.68
R2	Block 20	480	-2.769	-0.202	-2.765	-2.52	66.19	10.70
R3	Block 20	463	-3.579	-0.512	-3.533	4.32	41.29	10.67
R4	Block 20	438	-4.061	-0.802	-3.887	6.97	24.87	8.05
R5	Block 20	418	-3.038	-1.167	-2.820	7.18	10.00	6.45
R6	Block 0	480	-2.531	-0.077	-2.569	15.79	95.33	32.68
R7	Block 0	438	-4.132	-0.676	-4.105	54.06	50.28	15.40
R8	Block 0	418	-4.217	-1.003	-4.147	48.31	33.90	10.48
R9	Block 19	488	-2.930	-0.076	-2.938	-6.57	68.48	-6.60
R10	Block 19	480	-2.965	-0.189	-2.991	-0.43	56.32	-10.42
R11	Block 19	463	-3.409	-0.420	-3.401	4.62	38.12	-10.12
R12	Block 19	438	-3.785	-0.636	-3.692	5.56	25.01	-6.79
R13	Block 19	418	-3.770	-1.213	-3.548	4.58	14.14	-3.94
R14	Crest Block 20	489	-2.878	-0.038	-2.887	-29.37	72.08	18.59
R15	Crest Block 14	489	-3.311	-0.073	-3.320	-21.14	77.41	34.01
R16	Crest Block 6	489	-2.729	-0.041	-2.735	0.07	98.10	41.84
R17	Crest Block 0	489	-1.602	-0.029	-1.602	16.25	133.13	16.47
R18	Crest Block 5	489	-1.656	-0.038	-1.657	14.84	131.83	-20.34
R19	Crest Block 11	489	-2.621	-0.076	-2.626	-5.04	95.13	-37.59
R20	Crest Block 17	489	-2.906	-0.049	-2.910	-13.77	79.16	-33.63
R21	Crest Block 23	489	-2.930	-0.076	-2.938	-6.56	68.48	-6.59
R22	Crest Block 4	489	-1.371	-0.025	-1.371	21.09	136.74	27.60

XI ICOLD BENCHMARK WORKSHOP ON NUMERICAL ANALYSIS OF DAMS

Valencia, October 20-21, 2011

THEME A

EFFECT OF CONCRETE SWELLING ON THE EQUILIBRIUM AND DISPLACEMENTS OF AN ARCH DAM

Meriot, Pierre-Yves[1]

Molin, Xavier[2]

Noret, Christine[3]

CONTACT

Christine Noret, TRACTEBEL ENGINEERING S.A., Dams and Hydroelectric Schemes, Le Delage – 5 rue du 19 mars 1962, 92622 Gennevilliers CEDEX, FRANCE, christine.noret@gdfsuez.com, +33 1 41 85 01 00.

Summary

Tractebel Engineering France has recently developed a swelling law named SCAS (Stress Controlled Anisotropic Swelling) in order to simulate the differential expansion caused by an alkali-aggregate reaction in a finite-element model. This law was applied to compute both horizontal and vertical movements of Kariba dam, from the first impounding in 1963 until 2010, as suggested by the formulator of the theme A [1]. The initial step (response of the dam structure without any swelling effect) has provided an early check of the model in normal conditions. The second step was devoted to the calibration of the swelling law and parameters which allow the best identification of the drift during the 1963-94 period. The anisotropic swelling law, well configured, has shown excellent results. Using the same swelling model as in previous step, the objective of the third step was to predict the stresses and displacements from 1995 to 2010. Results have highlighted the slowing down of the swelling rate these last years, due partially to the increasing compressive stresses and mainly to the chemical decrease of the alkali-aggregate reaction.

---

[1] TRACTEBEL ENGINEERING S.A., Dams and Hydroelectric Schemes, Gennevilliers, FRANCE

[2] TRACTEBEL ENGINEERING S.A., Hydraulics and Private Sector, Gennevilliers, FRANCE

[3] TRACTEBEL ENGINEERING S.A., Dams and Hydroelectric Schemes, Gennevilliers, FRANCE

1. INTRODUCTION

Kariba dam is a large arch dam built on the Zambezi River between Zambia and Zimbabwe in the late fifties. This dam has shown evident signs of swelling soon after the starting of its operation, identified in the eighties as being due to alkali-aggregate reaction. The theme A of this BW11 proposes to evaluate the ability of the different existing methods and software to consider anisotropic concrete swelling in a finite element model.

The solution proposed by Tractebel Engineering France – Coyne et Bellier used the COBEF software, and the anisotropic swelling law named SCAS (Stress Controlled Anisotropic Swelling), based on the Charlwood model. The computation consists of 3 steps, as indicated in the subject:

- step 1: response of the dam structure without any swelling effect;
- step 2: calibration of the swelling law with monitoring of the dam movements during the 1963-94 period;
- step 3: prediction of the stresses and the displacements fields during the 1995-2010 period.

2. PRESENTATION OF THE MODEL

The mesh corresponds to the BW11A_Model2.mesh file provided by the formulator. It consists of 7476 nodes for 1606 elements, divided in three groups: the dam; the foundation; the joint element between the dam and the foundation (to model a Coulomb friction).

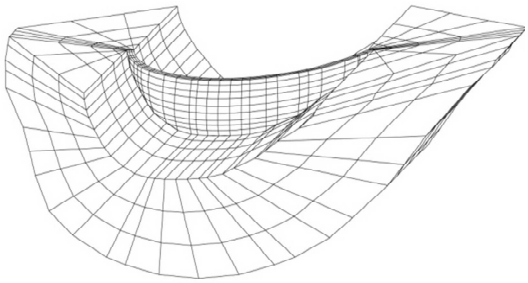

Figure 1: general view of the mesh

The computed dam is divided in 10 arches and 25 cantilever elements. As show figure 2, the mesh describes the dam with 3 or 4 elements in the thickness of the arches. The foundation is built with 4 layers of elements around the dam. Elements for the dam and the foundation are 3D quadratic. For the contact dam/foundation, they correspond to a joint surface.

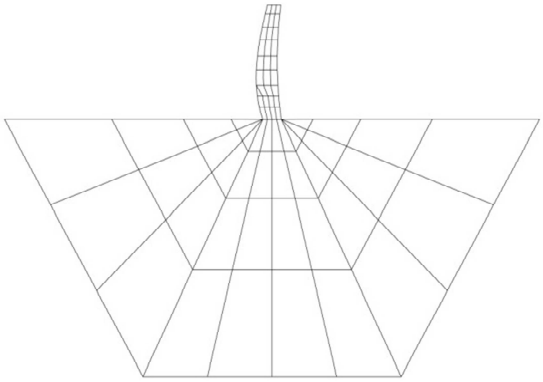

Figure 2: view of the crown cantilever

Material properties are as follows:

Table 1: material properties

Group	Unit weight	Young's modulus	Poisson's ratio
Dam	2.35 t/m3	22 000 MPa	0.2
Foundation	None	10 000 MPa	0.2

The normal and the tangential stiffness of the joint between the dam and the foundation are 50 000 MPa/m. The friction angle limit is $\phi = 45°$ and the maximal traction allowed is 0.01 MPa.

3. LOAD CASES

Ungrouted dead weight

The ungrouted dead weight, consequence of the way of construction of an arch dam - by independent blocks - is applied with a non-linear law (ORTHO non-linear law in COBEF): stresses through cantilever surfaces in the dam are cancelled from the monolithic dead weight, and vertically redistributed.

Hydraulic loads

As suggested for the exercise, the water level is considered constant on 3 successive periods from 1963 to 1994. From 1995 to 2010 (the prediction period of the exercise), the water level, substantially more variable, is computed at 4 different elevations. Assumptions of the water level are summarised in the following figure.

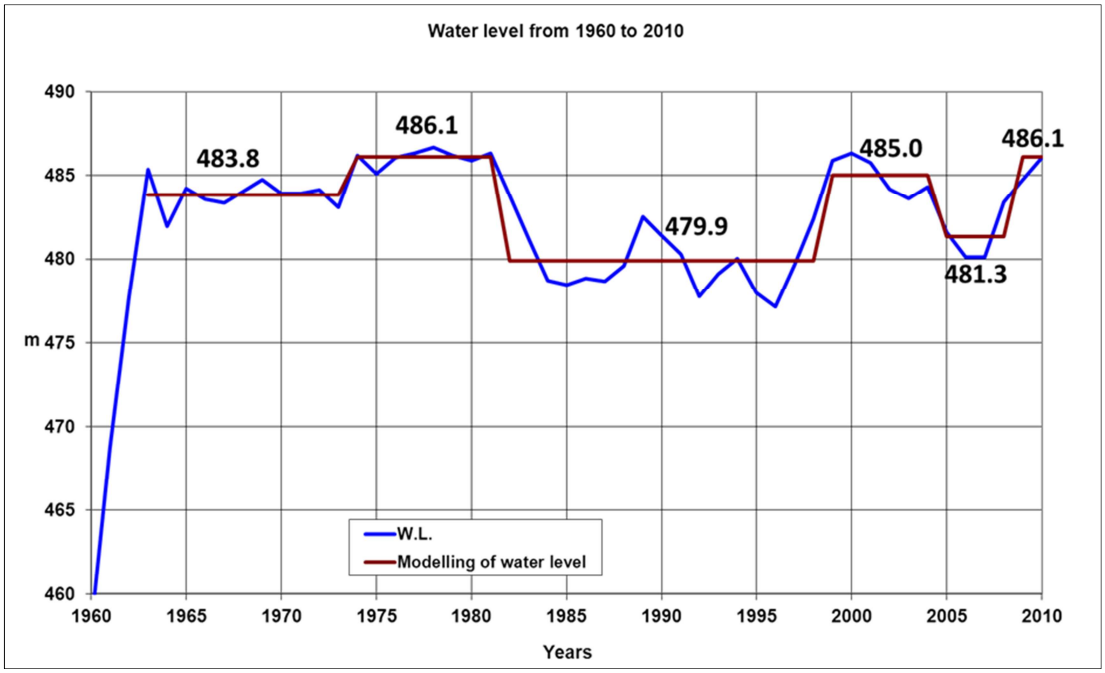

Figure 3: water level modelling

Hydraulics loads are applied on the upstream face and under the dam, to represent uplift pressures. As soon as the dam/foundation's joint is opened, uplift pressures are considered equal to the upstream water pressure.

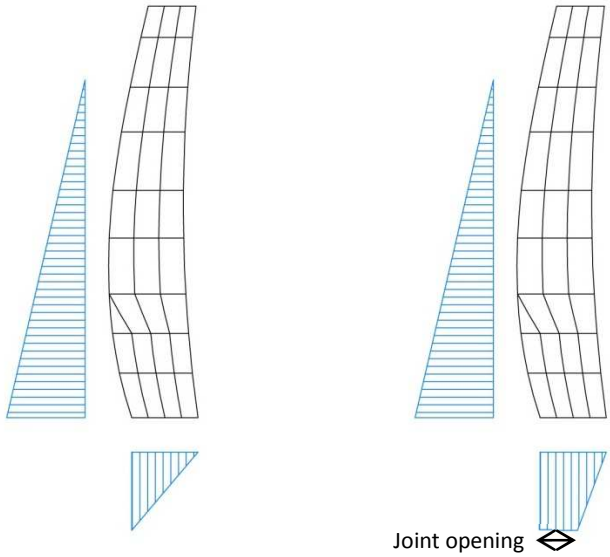

Figure 4: hydraulic loads

Isotropic concrete swelling

In a first approximation, the concrete swelling effects can be taken into account with an equivalent thermal expansion. The concrete is warmed with temperature Δθ adjusted to reproduce monitoring data:

$$\lambda \times \Delta\theta = \varepsilon_g = \dot{\varepsilon}_g \times \Delta t \quad (1)$$

With:

λ: thermal linear expansion coefficient of the concrete

$\dot{\varepsilon}_g$: expansion rate (m/m/year)

ε_g: deformation (m/m)

This approximation corresponds to an isotropic swelling, constant in all directions. However experimental studies show AAR swelling is stress dependent. Some theories (A. Sellier, INSA Toulouse, V. Saouma, University de Boulder) and swelling law (Charlwood [2]) have been proposed. As in Kariba dam arch stresses are higher than vertical stresses (see following results and also a previous study of Kariba swelling, Ozanam [4]), the expansion rate is more important vertically than horizontally. To compute observed displacements with an isotropic load, two modelling have been carried out: one with a thermal load fitted to the upstream drift and other one fitted to the crest rise, as shown in figure 5.

Stress Controlled Anisotropic Swelling (SCAS)

An anisotropic swelling law was developed to compute the concrete swelling due to AAR, named SCAS (Stress Controlled Anisotropic Swelling), similar to that proposed by Charlwood. This law has been developed by Coyne et Bellier and already tested on a computation of Bimont dam's swelling (Kyoto [3]). This law calculates the concrete expansion in each direction of the principal stresses throughout the structure. As a result, concrete swelling varies in magnitude and direction in the model.

Figure 5 compares the different computations with the observed displacements at the crown cantilever: unlike the isotropic computations, the anisotropic model fit both vertical and radial displacements.

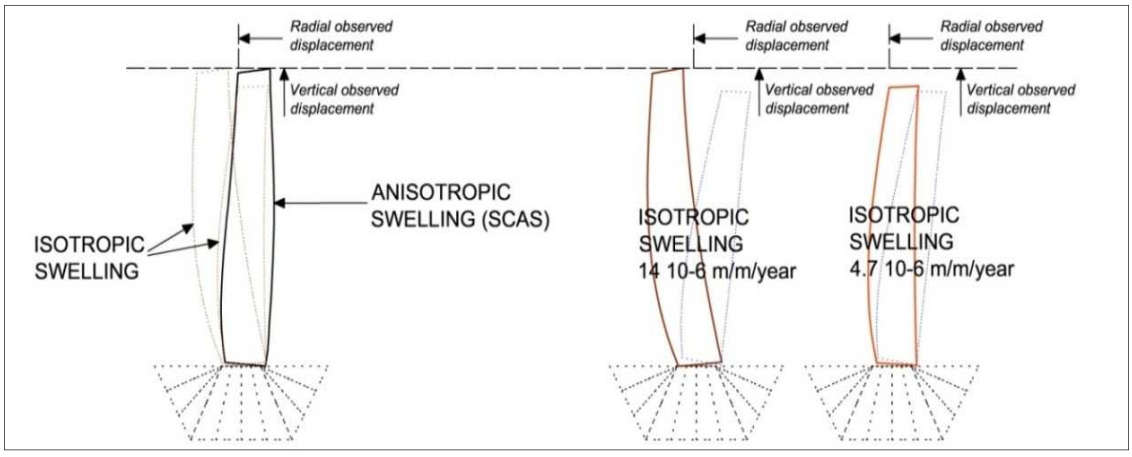

Figure 5: the two isotropic and the anisotropic computations at crown cantilever

Relationship between the rates of concrete expansion and concrete stresses is described below.

Expansion rate (µm/m/year); $\dot{\varepsilon}_g = F(\sigma_i)$, i = 1, 2, 3, with:

- $F(\sigma_i) = 0$ if $\sigma_i \geq \sigma_L$ (high compression), (2)
- $F(\sigma_i) = \dot{\varepsilon}_{gL}$ if $\sigma_i < 0$ (traction), (3)
- $F(\sigma_i) = \dot{\varepsilon}_{gL} \times \left(1 - \frac{\sigma_i}{\sigma_L}\right)$ if $0 \leq \sigma_i < \sigma_L$ (low compression). (4)

This swelling law depends only on two parameters:

- the unrestrained concrete growth strain rate at zero stress $(\dot{\varepsilon}_{gL})$;
- the stress for which the concrete expansion is cancelled (σ_L).

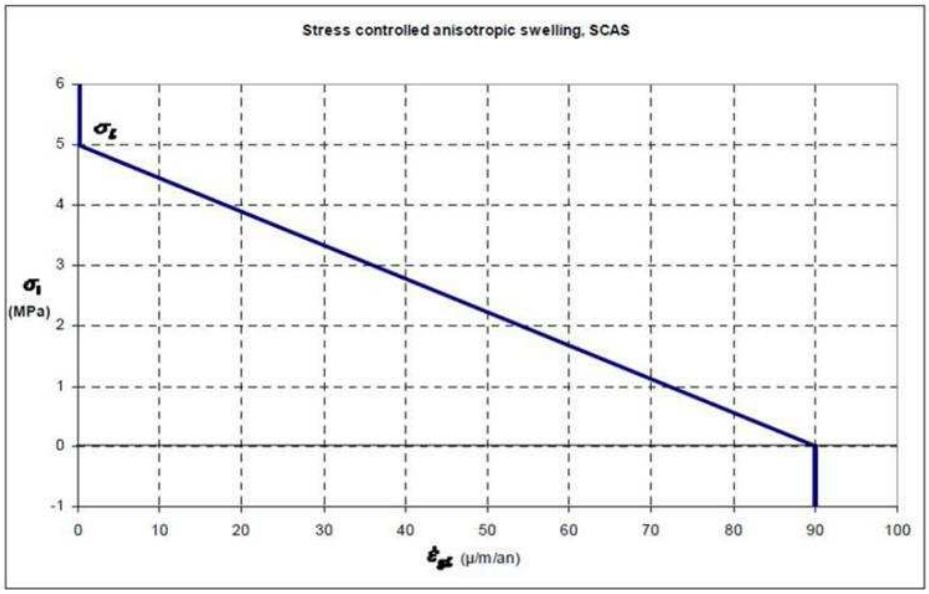

Figure 6: SCAS law

The swelling concrete law is encoding in COBEF as an explicit law. Instead of a rate of swelling, deformations are applied in the model, as indicated below:

$$\varepsilon_g = \int_t^{t+\Delta t} \dot{\varepsilon}_g(\tau).\, d\tau \text{ , in µm/m} \quad (5)$$

The duration Δt of each step of the computation has been chosen equal to 1 year for this study. Figure 7 describes the iterative process of the calculation.

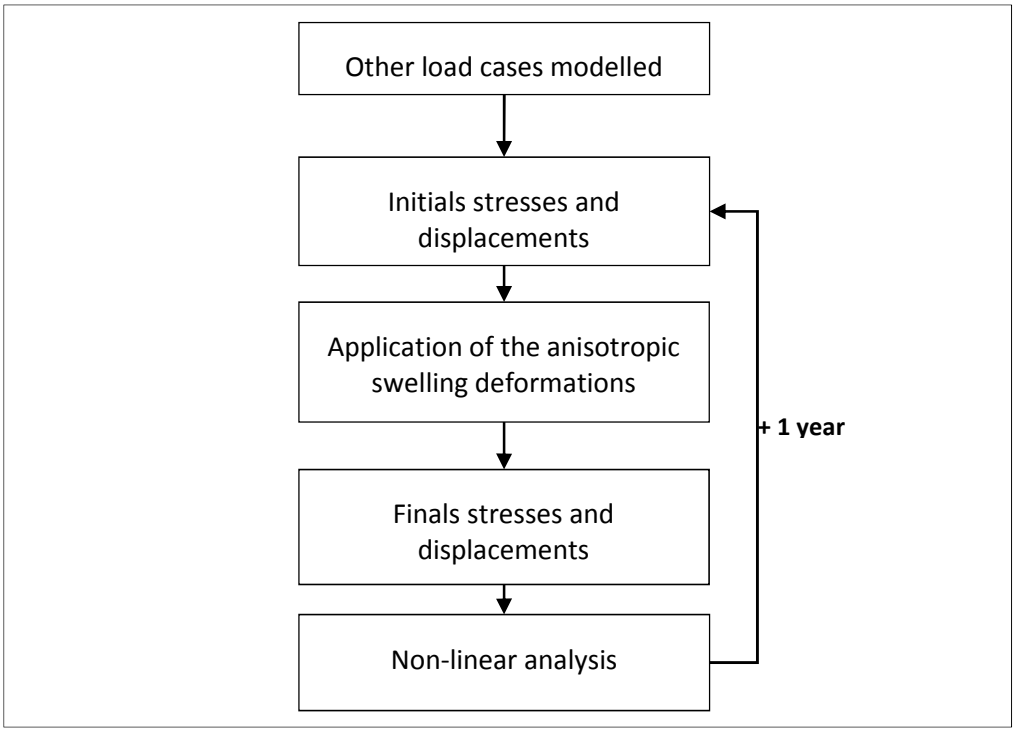

Figure 7: SCAS iterative process

Load combinations

To compute dam behaviour as real as possible, non-linear laws have been applied. A first one cancels all tensile stresses in any given element, in order to simulate the presence of cracks (grouted cracks) in concrete (NOTEN non-linear law in COBEF). Another one computes a Mohr-Coulomb law with no cohesion in the joint element at the dam/foundation contact (JNOT non-linear law in COBEF).

Since the computation process is non-linear, results are load path dependant and loads have to be applied following the true history of the dam, within limits imposed by the necessary simplification of the analysis. Ungrouted dead weight was first applied (displacements have been reset after this first load), and then the reservoir load has been applied. Finally the swelling has been applied together with the water level adjustment as necessary.

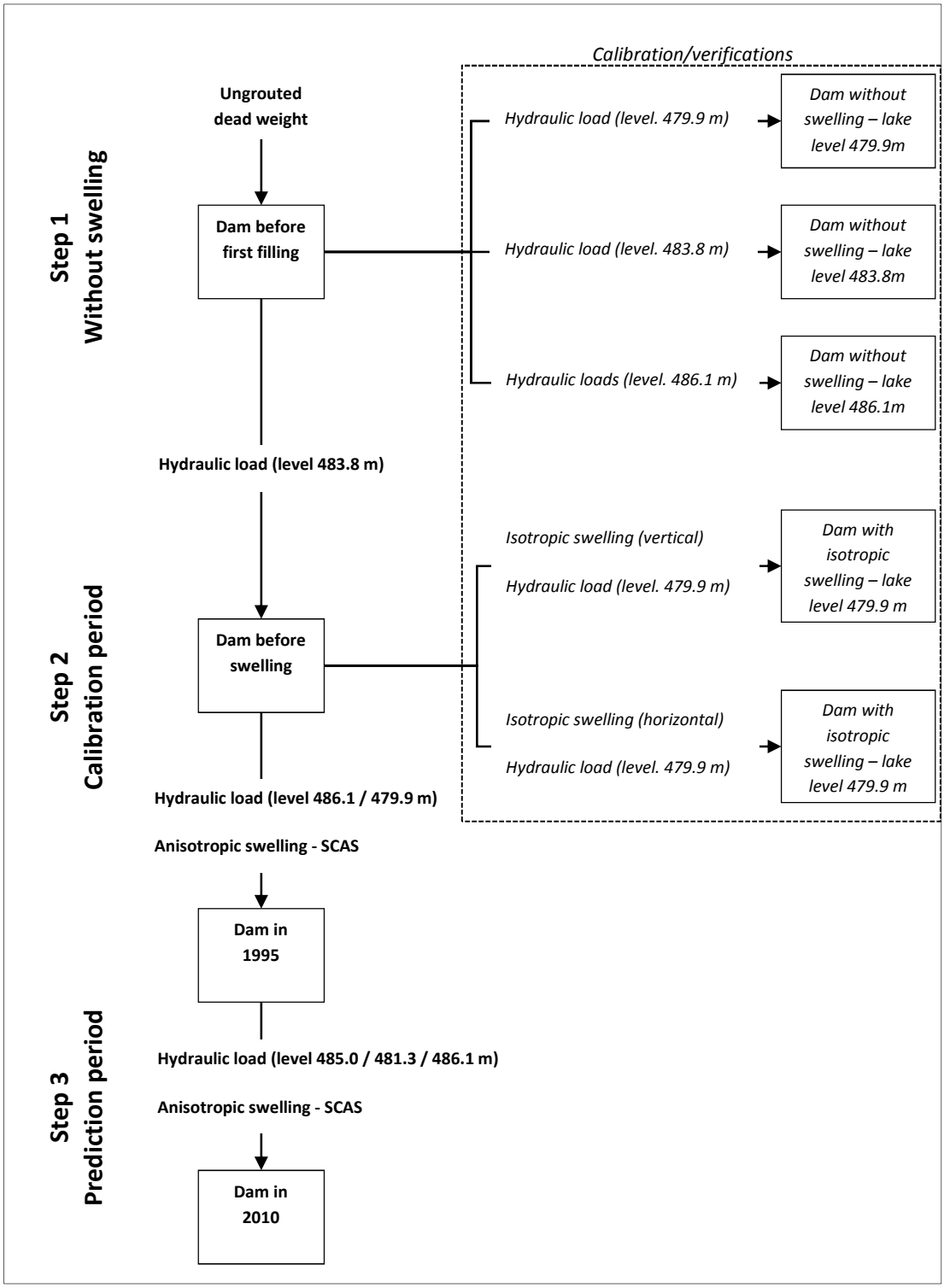

Figure 8: load combinations

4. FIRST STEP RESULTS - WITHOUT SWELLING

Radial displacements of the crown cantilever vary from 7.2 cm with the reservoir at elevation 479.9 m to 9.1 cm with the reservoir at elevation 486.1 m, in the downstream direction.

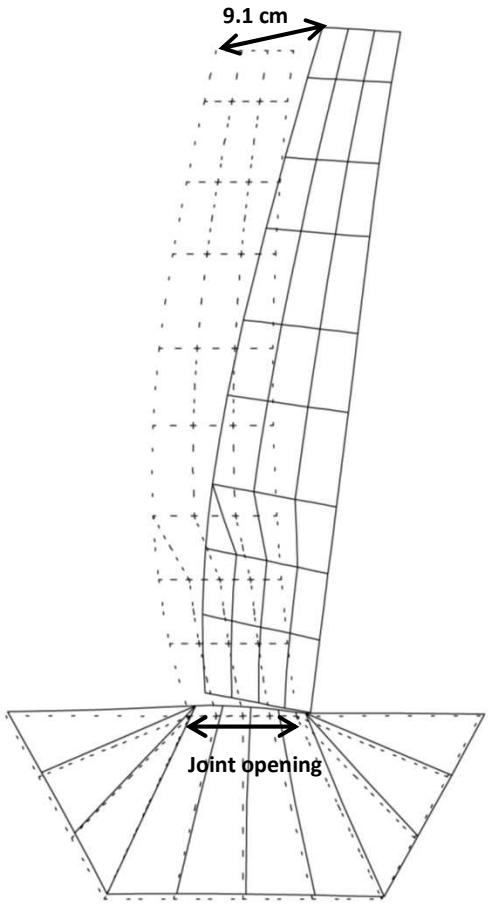

Figure 9: displacement (x by 200) at crown cantilever – lake level = 486.10 m

On the downstream face of the dam, arch stresses are globally predominant. Hydraulic loads lead to a concentration of high vertical stresses at the dam/foundation contact, increased by the joint opening (see figure 14). The arch compressive stress peak is horizontally and in the order of 6 MPa for the maximum computed water level.

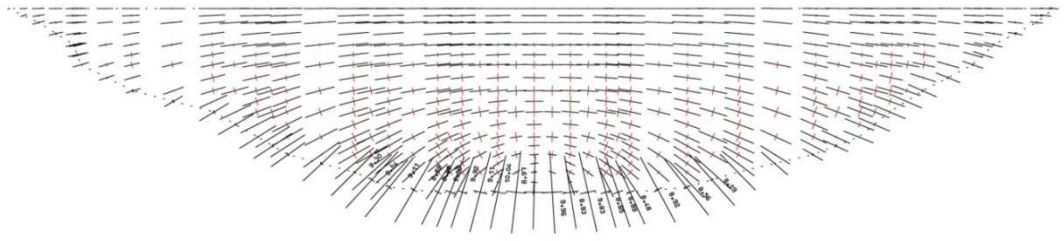

Figure 10: principal stresses at the downstream face, no swelling

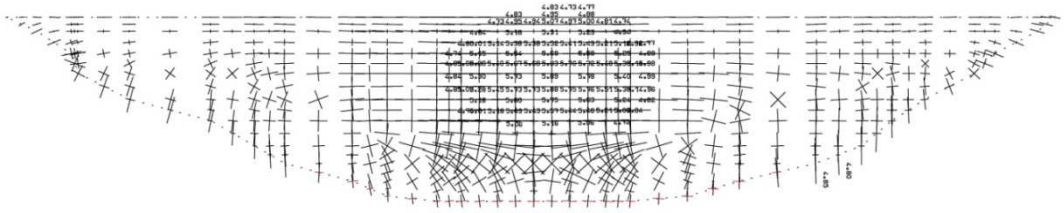

Figure 11: principal stresses at the upstream face, no swelling

Vertical compressive stresses in the crown cantilever are located at the upstream face, with maximal values around 3.5 MPa at mid-height (figure 12). Except at the dam/foundation joint where the compressions are at the downstream foot and reach 12 MPa. Low vertical tensile stresses, around 1 MPa, appear at the downstream face. The computed lake variations have few influences on the global state of stress in the cantilevers.

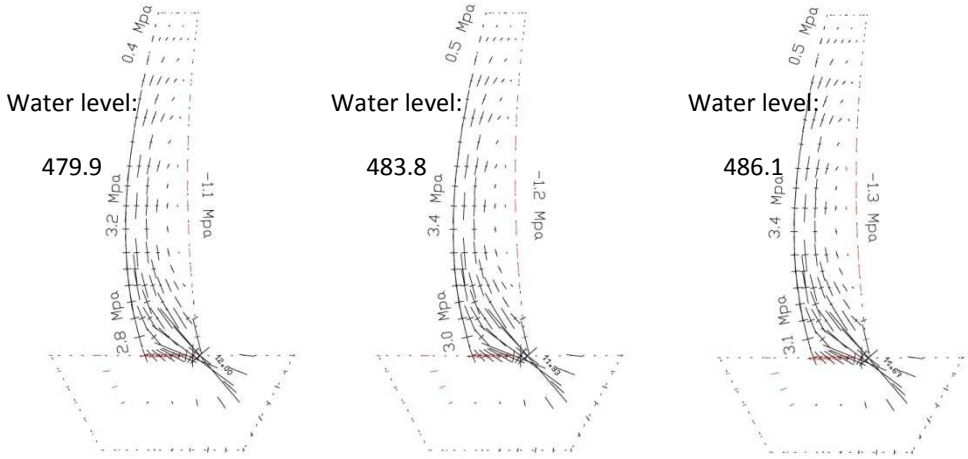

Figure 12: principal stresses in the crown cantilever

In the arch at mid-height, figure 13, main stresses are about twice higher than vertical stresses in the crown cantilever. It explains the strong anisotropy which exists between vertical and horizontal swelling rates, as shown in the second step. The lake level variation has a significant effect on the horizontal tangential stresses. They increase about 20% at the key when the level changes from 479.9 m to 486.1 m.

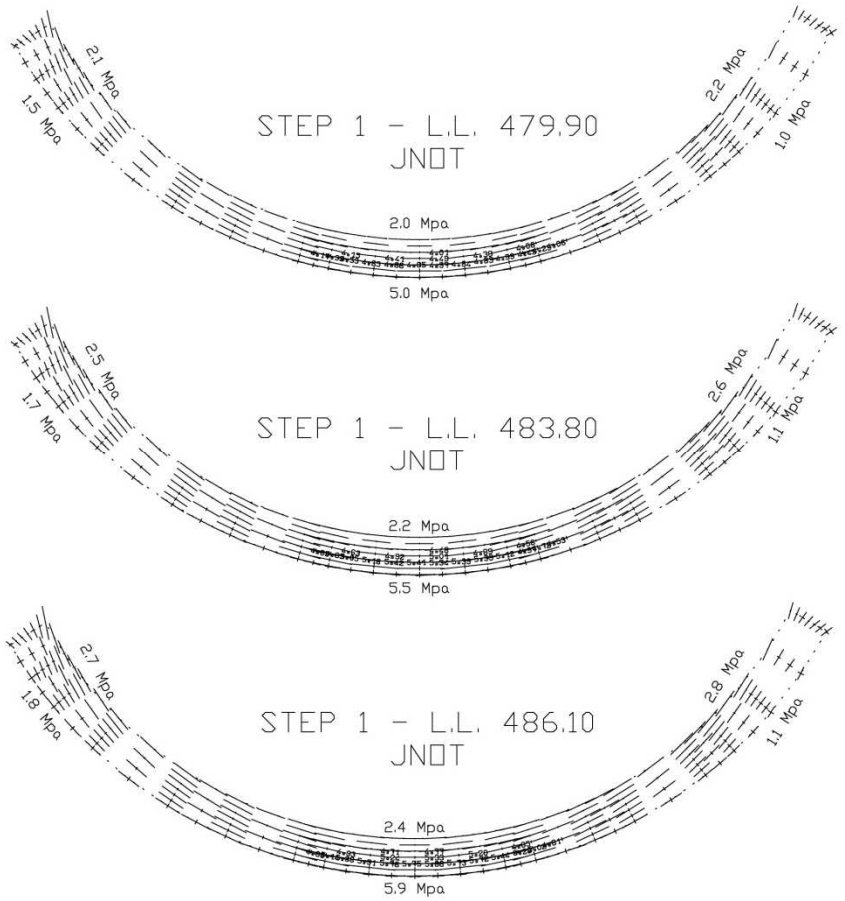

Figure 13: principal stresses in the mid-height arch

Hydraulic loads lead to an important opening of the joint dam/foundation. As shown figure 14, it is totally opened at the crown cantilever when the lake level reaches 483.80 m.

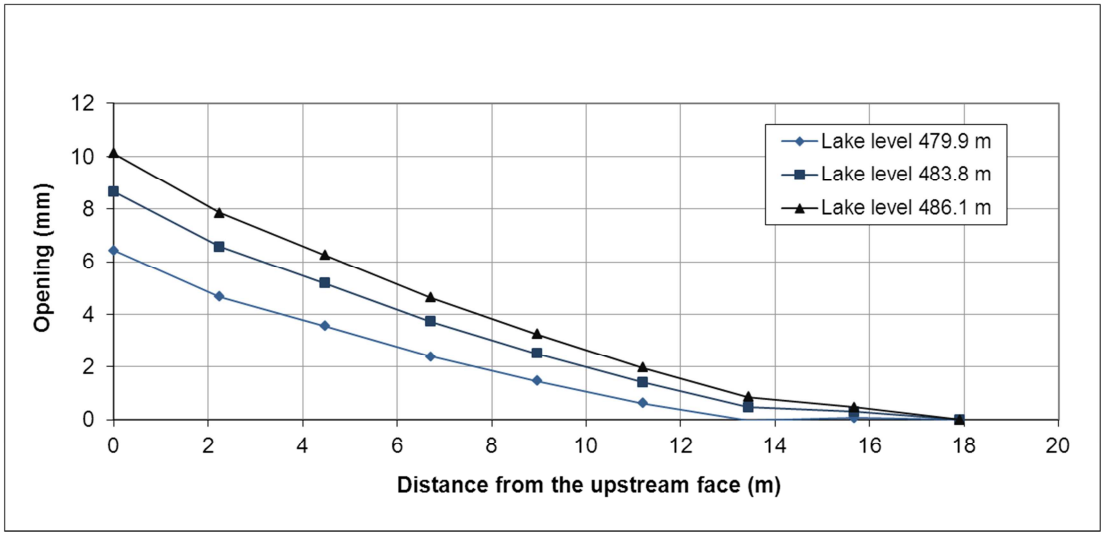

Figure 14: opening of the preformed joint

5. SECOND STEP RESULTS – WITH SWELLING

Analysis of the monitoring data

From 1963 to 1995, the T434 target radial drift reaches 60 mm. In the isotropic computation, this drift has been modelled constant.

For the anisotropic computation, different periods have been differenced: no swelling from 1963 to 1967 (time needed by the alkali-aggregates reaction to become apparent) and then displacement rate constant as soon as the lake level is considered constant.

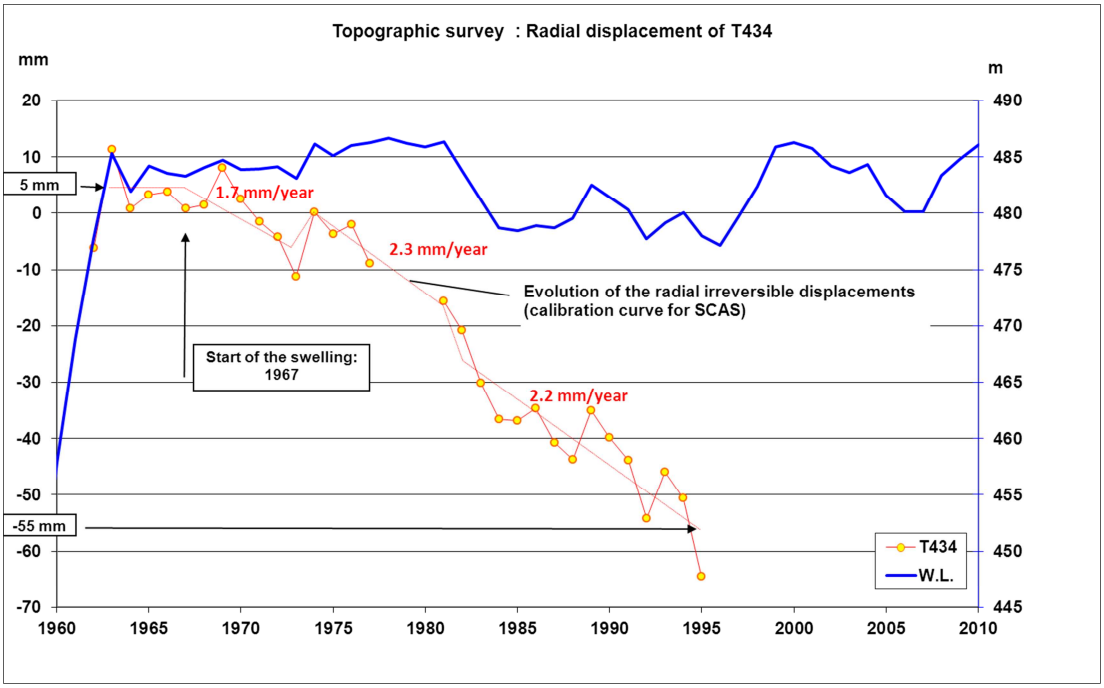

Figure 15: radial calibration data for the anisotropic swelling law

Unlike the radial displacement, the crest rise is roughly constant from 1963 to 1995. Average rise rates are indicated below:

Location	Crest block 20	Crest block 14	Crest block 6	Crest block 0	Crest block 5	Crest block 11	Crest block 17	Crest block 23
Rise rate from 1963 to 1995 (mm/year)	1.2	1.3	1.6	2.0	2.0	1.5	1.3	1.1

Anisotropic swelling

Results shows that observed displacements cannot be computed with an isotropic rate of swelling. This is due to the stress dependant of the concrete rate, highlighted in Kariba dam

with arch stresses higher than vertical stresses. An anisotropic swelling law appears essential to modelize correctly Kariba behaviour.

Isotropic computations gave a first assessment of the stresses/rate of swelling relation.

- In the vertical direction, stresses average inside the dam for both initial and final states is 1.6 MPa. It is correlated to an isotropic swelling rate fitting the crest rise equal to 14 10^{-6} m/m/year.
- In the horizontal tangential direction, stresses average inside the dam for both initial and final states is 4.1 MPa. It is correlated to an isotropic swelling rate fitting the radial drift equal to 4.7 10^{-6} m/m/year.

These two points provide a first couple of parameters $\dot{\varepsilon}_{gL}$, σ_L for SCAS. After different tests, the most appropriate parameters appear to be:

- $\dot{\varepsilon}_{gL}$ = 18.5 10^{-6} m/m/year
- σ_L = 4,8 MPa

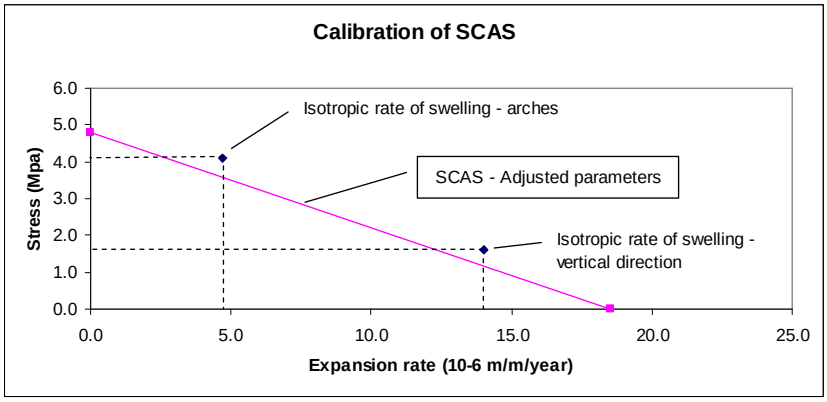

Figure 16: parameters for SCAS

Results of the computation with the anisotropic swelling law

Figure 17 compares the radial drift computed to the monitoring results: globally a good agreement is obtained. It shows the change in the rate of drift according to variation of the lake level. A rise of the lake level, entailing higher arches compression, leads to a slowing down of the radial drift rate.

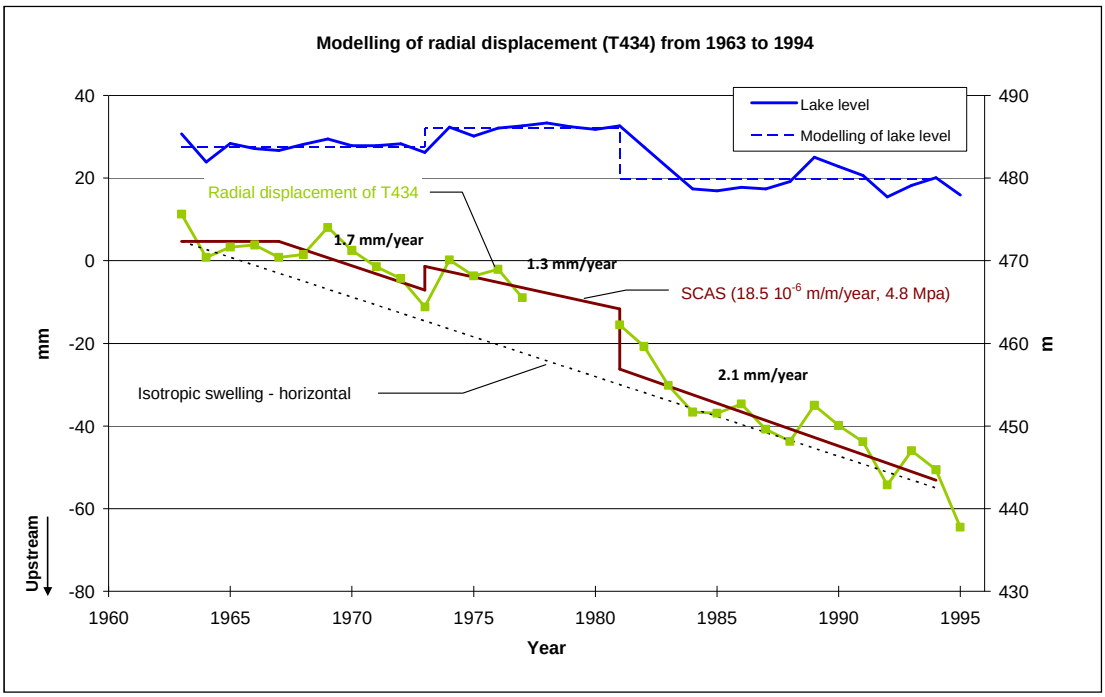

Figure 17: computed radial drift from 1963 to 1994 and monitoring data

The crest rise is also well computed by the anisotropic swelling law. Figure 18 corresponds to the crest shape at the beginning in 1963 and at the end of the calibration periods in 1994. The differences witch appear between the computation and the observation in the central part of the dam are due to the local effects of the spillways, not modelized in this exercise. The figure 19 shows the constancy of the vertical drift at one point of the crest (block 17), despite water level modification. This is due to the low influence of the water level fluctuation and of the swelling on the vertical stresses.

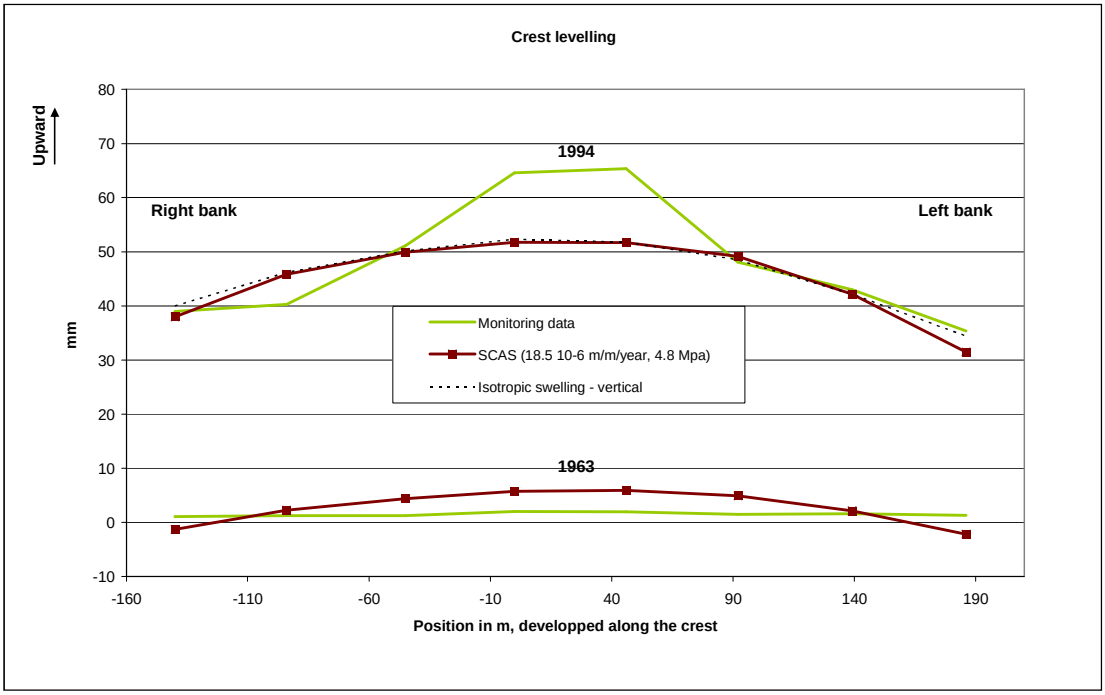

Figure 18: computed vertical drift at crest in 1963, 1994, and monitoring data

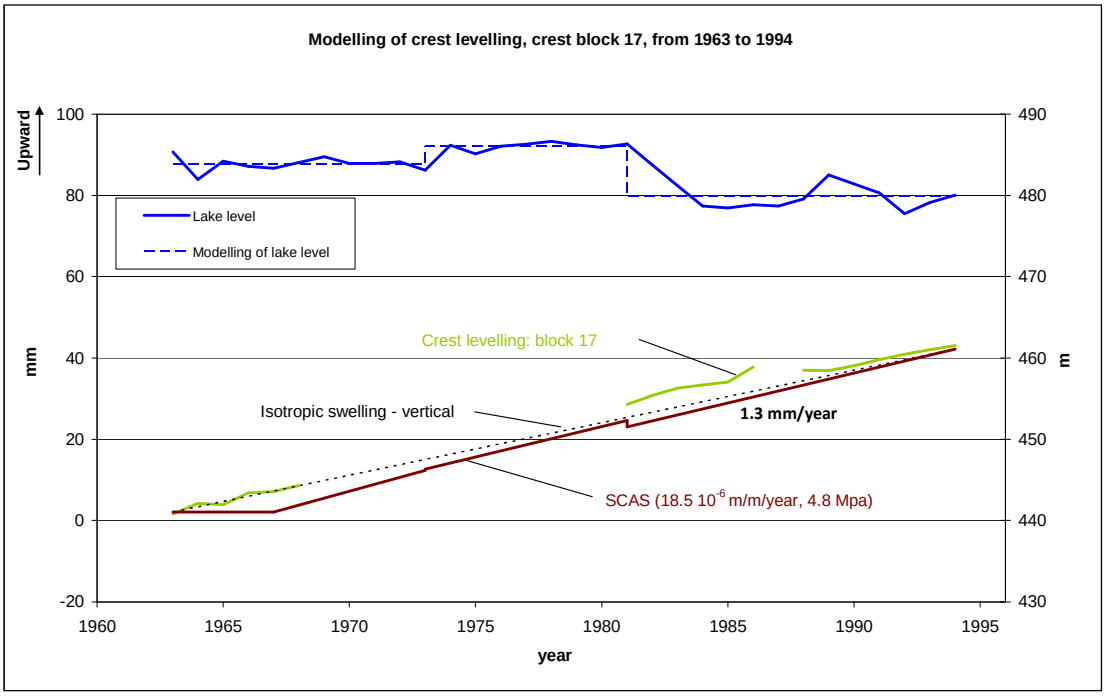

Figure 19: computed vertical drift from 1963 to 1994 at crest block 17 and monitoring data

Looking at the stresses, computed anisotropic swelling of concrete has different impacts on the dam:

- In the lower part of the dam, swelling increases arch stresses, because of their important confinement close to rock contact. Most values of these horizontal stresses reach 4.8 MPa, the limit which stops the concrete expansion.
- At mid-height, swelling tends to re-inverse the arch stress distribution from the one given by hydraulic loads, with an increase of compressive stresses on the downstream face and a reduction on the upstream face, as shown in figure 20.
- In the upper arches, due to the particular shape of the dam, swelling entails tension and leads to a slightly decrease in the arch stresses.
- In the cantilevers, there is no important modification of the vertical stresses. As previously, swelling tends to re-inverse the distribution of vertical stresses coming from hydraulic loads, with a reduction of the compressive ones on the upstream face.

The swelling also tends to reclose the joint elements at the dam/foundation contact.

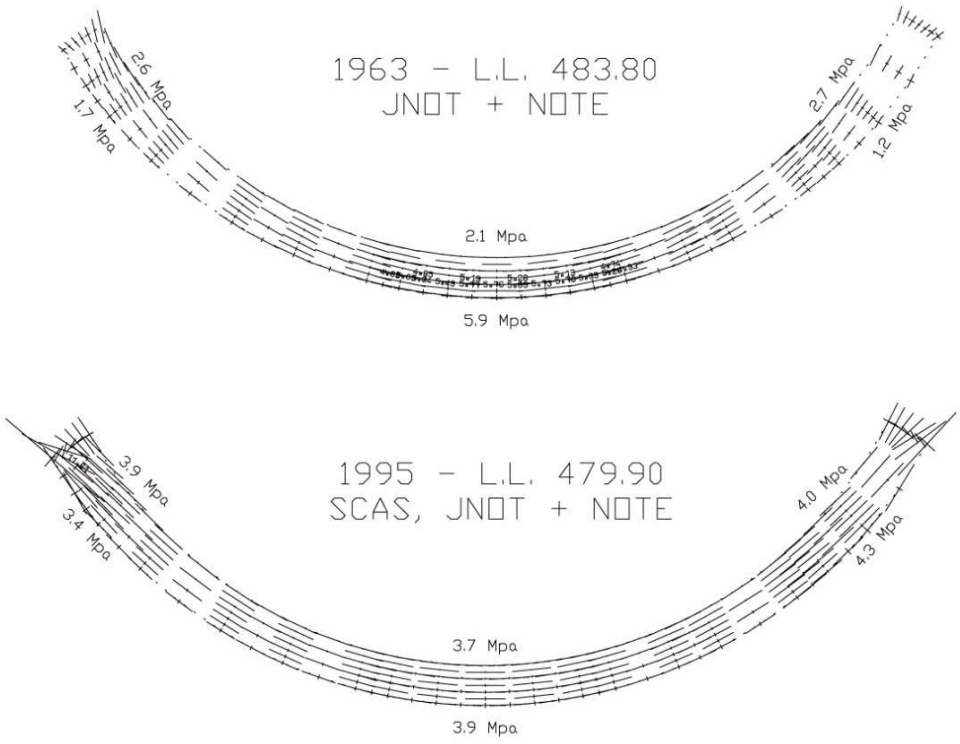

Figure 20: comparison of the arch stresses in 1963 and in 1995, mid-height of the dam

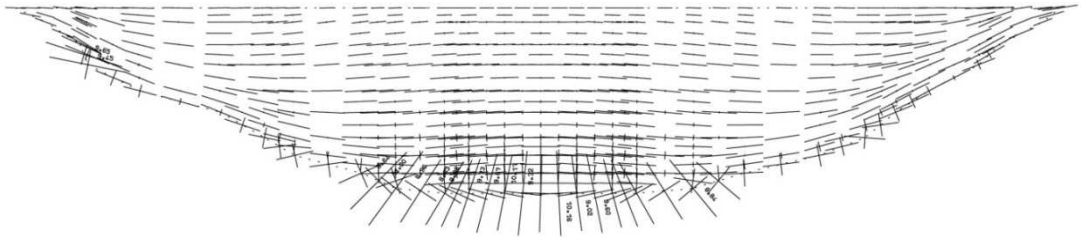

Figure 21: principal stresses on the downstream face in 1995

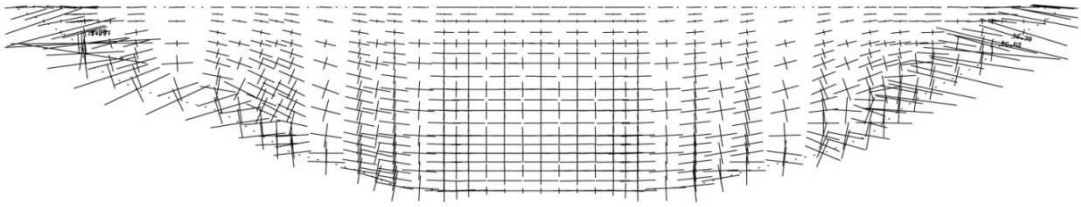

Figure 22: principal stresses on the upstream face in 1995

6. RESULTS OF THE PREDICTION

Using the same swelling model as in previous step, with parameters calibrated during this step, the computed displacement deviate from the monitoring results on the 1995-2010 period. As shown on figure 23, the computed radial movement of T434 is 2.5 cm far from the observation in the upstream direction in 2010. The overestimation of the vertical drift appears figure 24.

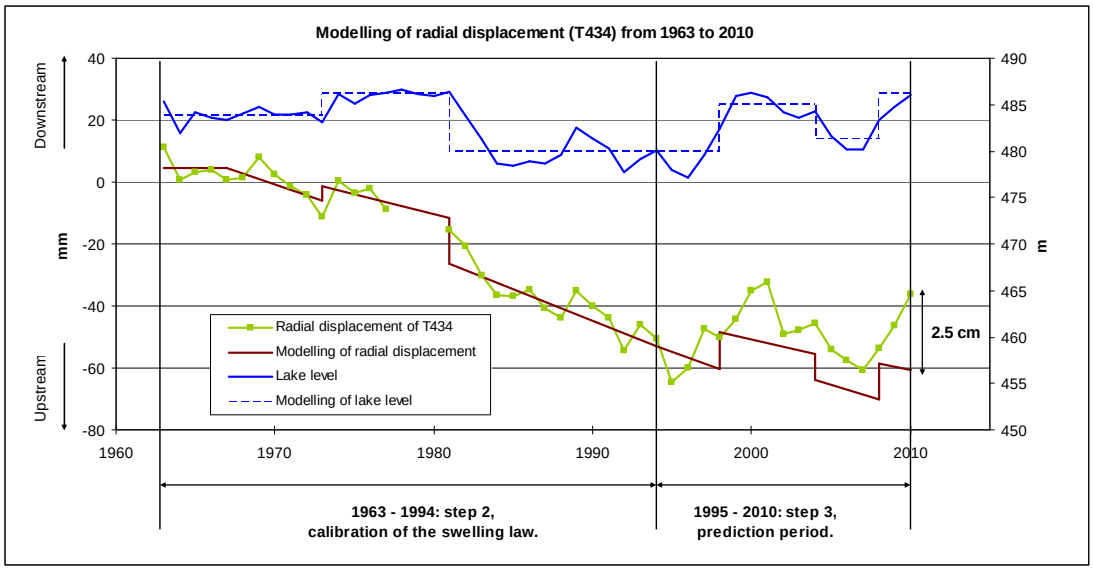

Figure 23: computed radial drift from 1963 to 2010

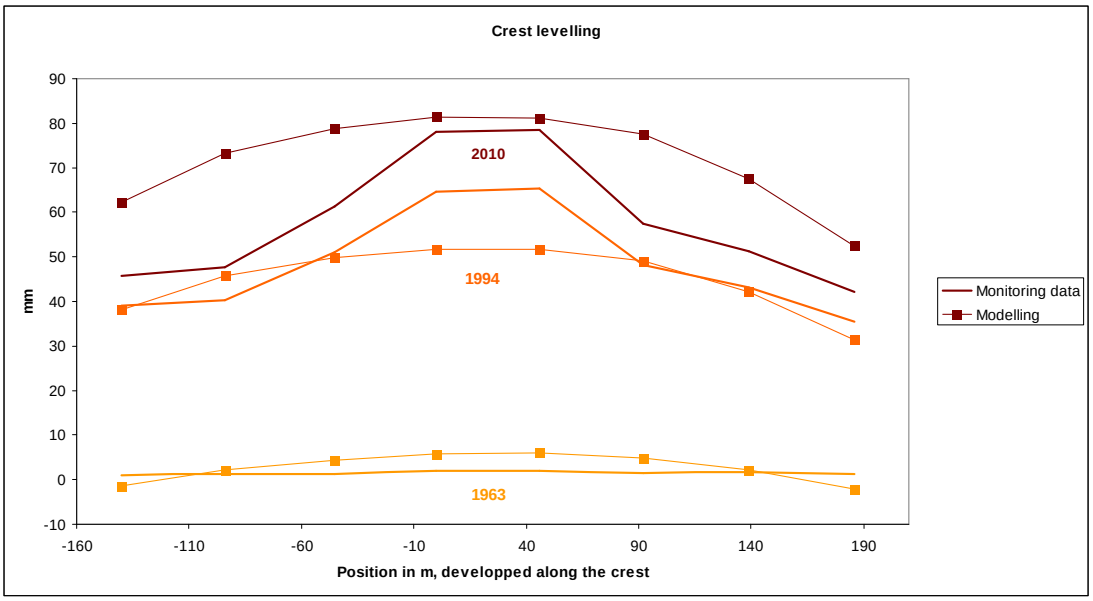

Figure 24: computed vertical drift in 1963, 1994 and 2010

It appears these last years a reduction of the rate of the irreversible displacements on Kariba dam, mentioned in the 2005 and the 2010 inspection report of Kariba dam (Goguel *and coll.* [5] and Noret *and coll*. [6]). According to the result of the second step, this diminution cannot be the consequence of an increase of the stress pattern throughout the dam: except for the arches in the lower part of the dam, stresses are not enough to stop the concrete expansion, particularly in the cantilevers where they remain relatively low along the years. The slowing down of the rise rate appears to be the consequence of a chemical diminution of the alkali-aggregates reaction, not computed in this model.

When comparing the stress patterns in 1995 and in 2010 calculated with the anisotropic swelling law, it does not appear any major evolution. Arch stresses arch slightly increase in the upper part of the dam, where the limit stress stopping the swelling is not reached. In the lower part, the arch expansion is stopped. Vertically, stresses in the cantilever are still stable. Consequently, despite the divergence in displacements, computed stresses in 2010 are reliable. They might overestimate some values, which is conservative in terms of security for the monitoring of the dam.

7. CONCLUSION

Theoretical model and experimental observations highlight that the concrete swelling rate generated by AAR is stress dependent. It varies in space depending on the stress tensor and in time depending on the stress evolution. Tractebel Engineering France has developed the SCAS model derived from the Charlwood law to take into account this behaviour in a numerical analysis.

Applied to Kariba Dam, where differences between vertical and arch stresses are important, this model provides a reliable description of the evolution of the dam in term of displacements and stresses. With only two parameters, the SCAS law is easily adjustable and usable for the many other dam which, as Kariba dam, are affected by the alkali-aggregates reaction.

8. REFERENCES

[1] C. NORET and X. MOLIN, *THEME A: Effect of concrete swelling on the equilibrium and displacements of an arch dam,* Eleventh International Benchmark Workshop on Numerical Analysis of Dams, 20p, 2011.

[2] R. G. CHARLWOOD, A review of alkali aggregate reaction in hydro plants and dams, *Hydropower and Dams*, p. 73 – 80, may 1994.

[3] C. NORET, X. MOLIN, A. CARRERE, *Combined contributions of investigations and modelling in the analysis of Bimont arch dam behaviour*, Q95.R45., ICOLD, Kyoto, 2012.

[4] O. OZANAM, B. GOGUEL, K. GURUKUMBA, *Effet du niveau d'exploitation de la retenue sur le taux de gonflement du béton : modélisation dans le cas de Kariba,* XIX^{ème} Congrès International des Grands Barrages – Communication / volume V, Q.74-9, International Commission On large Dam INTERNATIONAL, Florence, 1997.

[5] B. GOGUEL, G. MILESI, E. TEKIRDAGLIOGLU, *Report for 2005 – 5 yearly inspection,* 5 yearly inspection report of Kariba dam, COYNE ET BELLIER, PARIS – FRANCE, 226p, 2006.

[6] C. NORET, B. GOGUEL, N. ROSIN-CORRE, O. CLAVE, *2010 5 – yearly inspection report,* 5 yearly inspection report of Kariba dam, COYNE ET BELLIER, PARIS – FRANCE, 115p, 2011.

XI ICOLD BENCHMARK WORKSHOP ON NUMERICAL ANALYSIS OF DAMS

Valencia, October 20-21, 2011

THEME A: EFFECT OF CONCRETE SWELLING ON
THE EQUILIBRIUM AND DISPLACEMENTS OF AN ARCH DAM

Dr NORET, Christine

CARRERE, Alain

MOLIN, Xavier

MERIOT, Pierre-Yves

CONTACT
Dr NORET Christine, Tractebel Engineering – Coyne et Bellier, 5 rue du 19 mars 1962, 92622 Gennevilliers Cedex, France, +33 1 41 85 03 69, christine.noret@gdfsuez.com

SYNTHESIS REPORT

1. Introduction

The exercise presented for this theme A is described in the previous report N°A0. It consists to reproduce Kariba dam behavior which is swelling for 50 years by a numerical analysis.

A mesh and the basic material characteristics were given to the participant as well as some monitoring results representative of what is observed. The position of the reference points (given in Table 3 of A0) for the comparison between simulation and observations are located in a vertical plane parallel to the dam faces, situated at 1/3rd of the width from the downstream face.

During the workshop, some swelling tests performed on Kariba dam concrete in 1977 were presented. Following photography shows the laboratory implemented in SEIL, Coyne et Bellier.

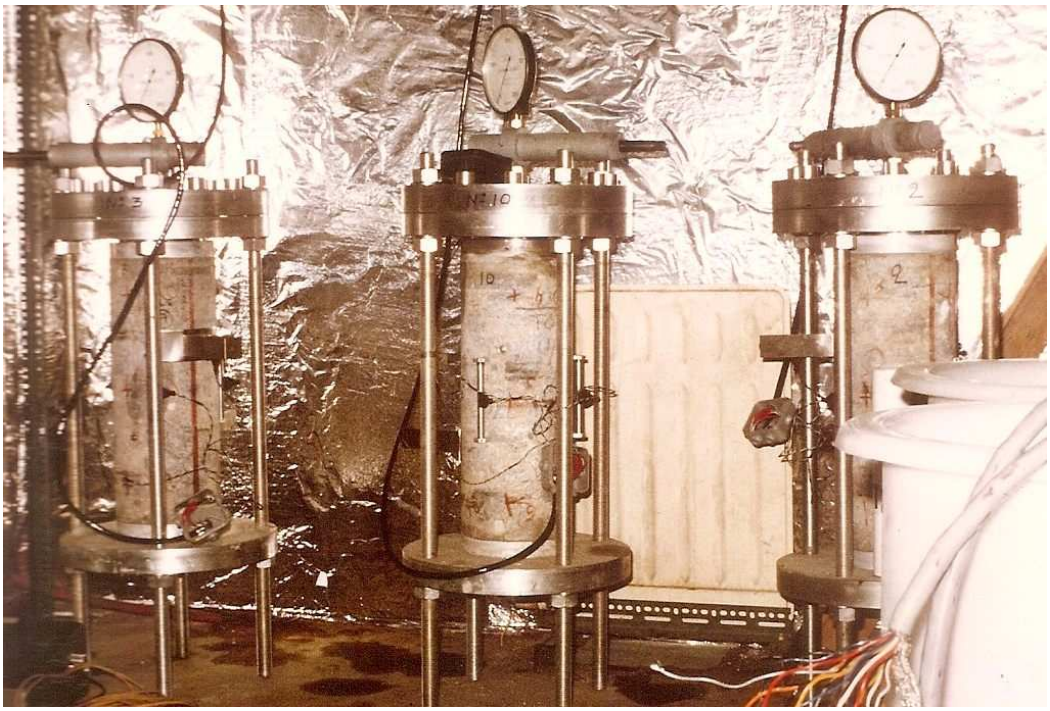

Main results provided by these tests are:

- Swelling is stopped at Hy=84%
- Rate of swelling depends on stress

  25-30 µ/m/year free

  12-21 µ/m/year with σ=1.3 MPa

  8-13 µ/m/year with σ=4 MPa

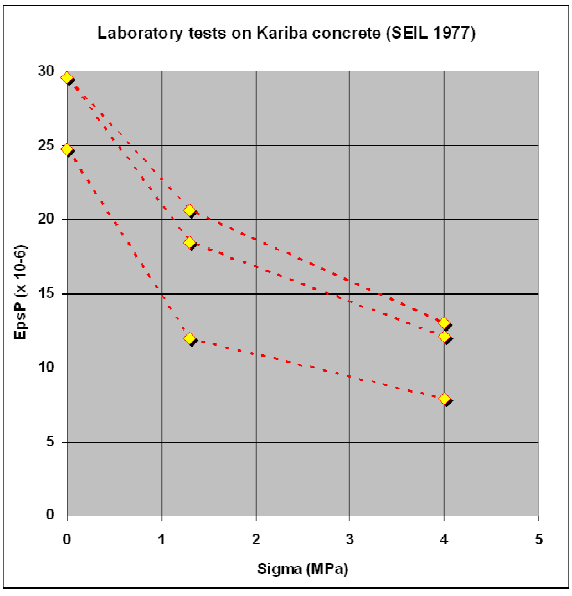

2. Participants to the exercise

Nine participants from 7 countries took part to this theme and sent their contributions two weeks before the workshop. Their institutions and Author names are given below in the order of reception of their contributions:

A1. Finite element modelling of concrete swelling effects on Kariba dam

By G. Faggiani, A. Frigerio, P. Masarati and M. Meghella (RSE, Milan, Italy)

A2. Effect of Concrete Swelling on the Equilibrium and Displacements of an Arch Dam

By J. Rodríguez, L. Lacoma, F. Martínez, F. and J. Martí, (Principia, Madrid, Spain)

A3. Kariba's dam behavior modeling

By E. Grimal and J. Moles-Dimartino (EDF-CIH, Le Bourget du Lac, France)

A4. A model of concrete swelling for describing the Kariba dam

By T. Menouillard, J.F. Seignol, L-I Boldea, P. Roure, A. Tzenkov, R. M Gunn (Stucky, Renens, Switzerland)

A5. Numerical Simulation of concrete structure affected by AAR: the case study of Kariba dam

By R. Esposito, M.A.N. Handriks, G. Lilliu and G-J M.A. Schreppers, (Delft University of Technology, Department of Structural Mechanics, Delft, The Nederland's)

A6. Prediction of swelling due to AAR in Kariba dam

By G-J Schreppers and G. Lilliu (TNO DIANA BV, Delft, The Nederland's)

A7. Effect of Concrete Swelling on the Equilibrium and Displacements of an Arch Dam

By V. Kostylev (The B. E. Vedeneev VNIIG, Inc. St Petersbourg, Russia)

A8. Analysis of AAR Loading on Kariba Dam Using Grow3D Routines

By D. D. Curtis, L. Feng, M. Lafreniere (Hatch, Niagara Falls, Canada)

A9. Effect of Concrete Swelling on the Equilibrium and Displacements of an Arch Dam

By P.Y. Meriot, X. Molin and C. Noret (Tractebel Engineering- Coyne et Bellier, Gennevilliers, France)

Four participants provided two solutions so that 13 solutions have been received in the framework of this Theme.

Different softwares were used, as well as different methodologies, from quite simple ones to very sophisticated ones. Tables below give a summary of their contributions:

N°	**A1**	**A2**	**A3**	**A4**	**A5**
Institution	**RSE**	**Principia**	**EDF-CIH**	**Stucky**	**TU Delft**
1st author	Meghella	Rodriguez	Moles	Menouillard	Esposito
Software	CANT-SD	Abaqus/St	ASTER	CESAR	DIANA
Model	Charlwood	Saouma	Grimal	Coussy-Larive	Larive/Saouma
Kinetics	***no***	***yes***	***yes***	***yes***	***yes/yes***
Stress effect	***yes***	***yes*** *(delay)*	***yes*** *(creep)*	***no***	yes *(delay)*

N°	**A6**	**A7**	**A8**	**A9**
Institution	**TNO DIANA**	**VNIIG**	**HATCH**	**TEF-COB**
1st author	Schreppers	Kostilev	Curtis	Mériot
Software	DIANA	ANSYS	ANSYS	COBEF
Model	Larive / cst	Larive	Growth3D	SCAS
Kinetics	***yes / no***	***yes***	***no***	***no***
Stress effect	***anisotropy***	***yes***	***yes*** *(+ creep)*	***yes***

Note: During the Workshop, participants were invited to propose minor amendments to their results if they found it useful, and to send them before the end of the year. This final version of the Synthesis on Theme A takes into consideration modifications to initial results received to date, as follows:

- Participant n°A4 made a correction in the post-treatment of the displacements fields,
- Participant n°A6 made a correction in the initial state displacements field,
- Participant n°A7 made just a minor correction in his paper,
- Participant n°A8 made several corrections to his initial calculation.
- Finally, only Participant n°A3 carried out a new analysis, whose results substantially differ from the original ones presented during the workshop.

3. Comparison of results with monitoring measurements

3.1. Step 1 : Reference conditions

The purpose of this initial step was to provide the response of the dam structure in normal conditions, i.e. without any swelling effect. This was used to detect possible discrepancies between different participants' solutions, independently from the swelling modelling.

Four load cases had to be submitted: End of construction and three reservoir water levels: 486.1, 483.8 and 479.9.

At the end of construction, usual assumptions are the cancellation of the displacements and the preservation of the stress field, mainly vertical stress due to the dam weight. Next figure shows the vertical stresses at different elevations. Results from all participants are very similar: differences are less than 5%.

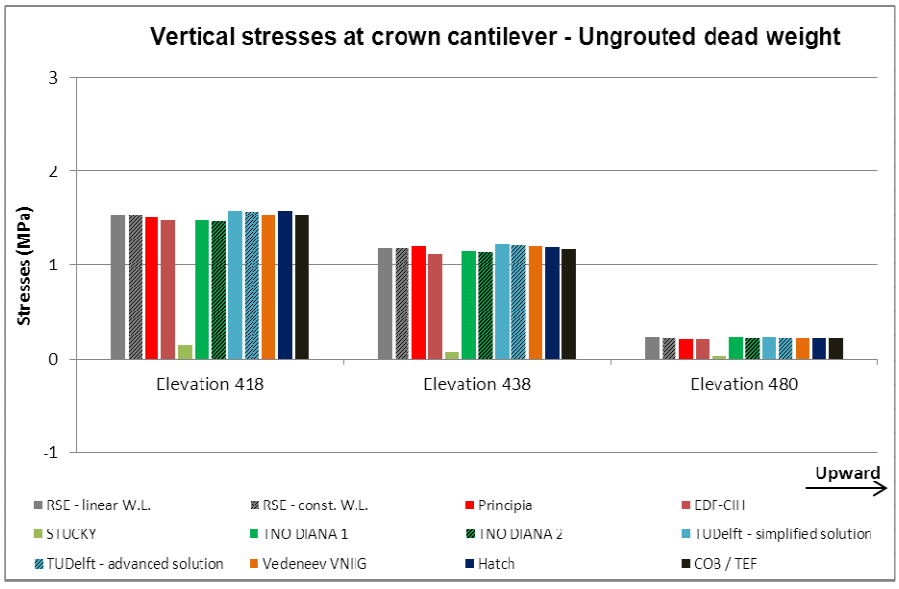

Figure 1: Vertical stresses at the end of construction

Following figure 2 shows the impact of the lake level variations on the arch and vertical stresses field. If arch stresses are similar in blocks 19 and 20, major differences appear in the cantilever block.

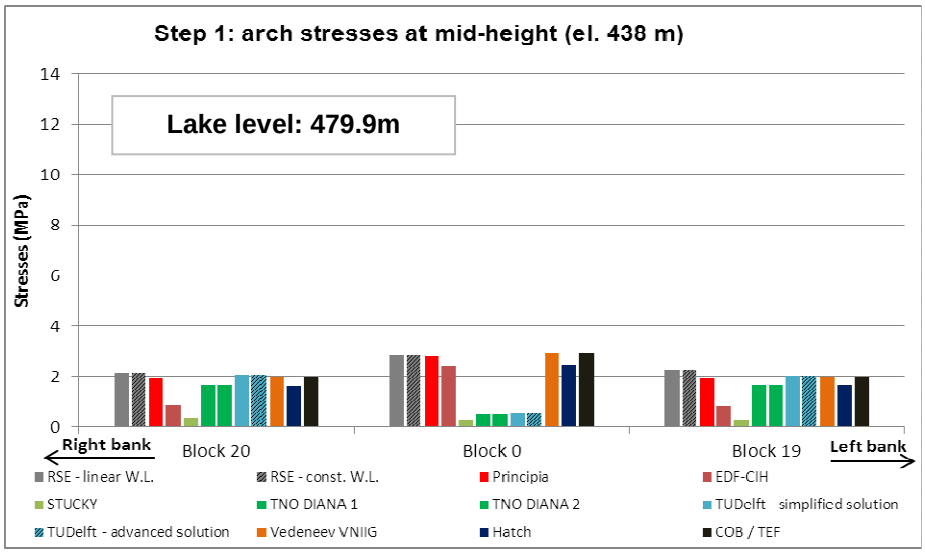

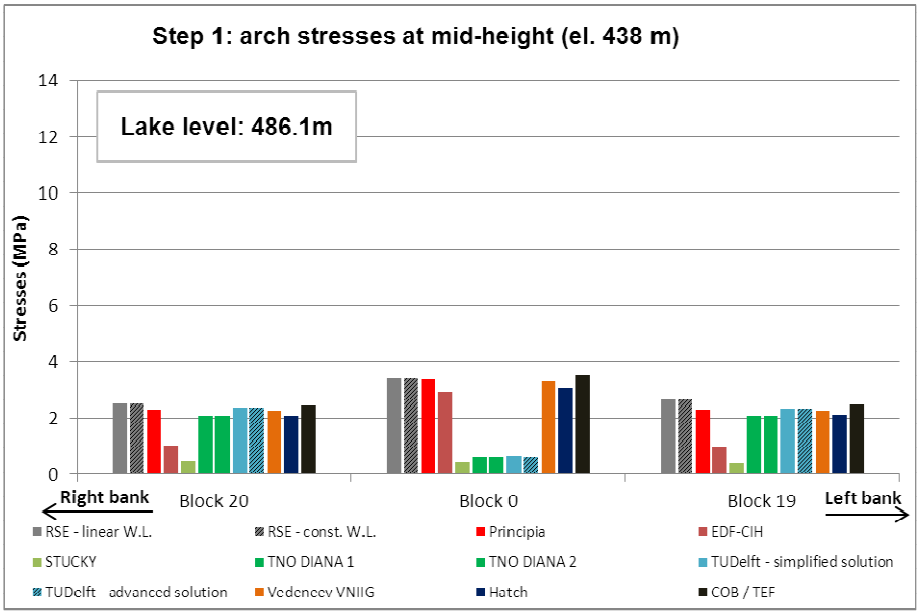

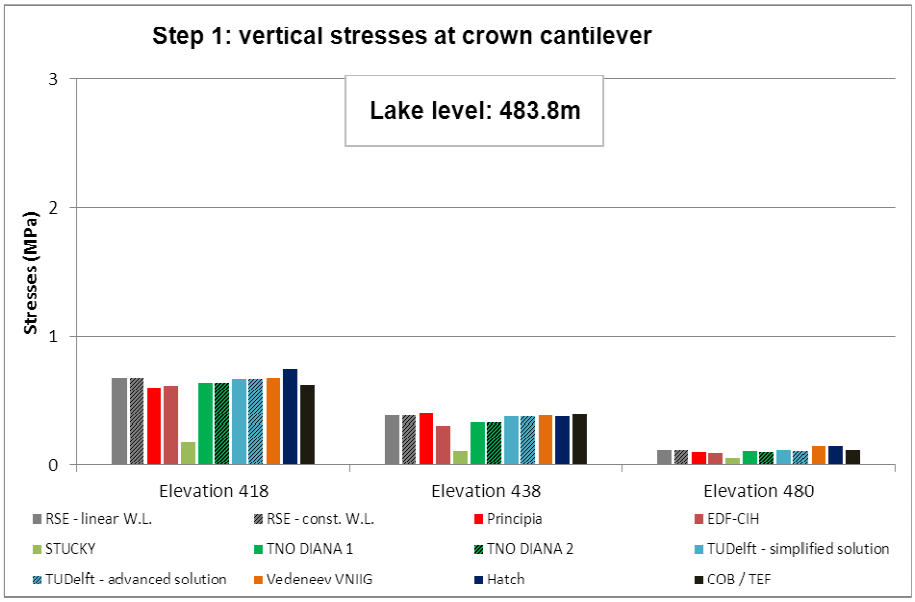

Figure 2: Arch and Vertical stresses for different lake levels.

Following figure 3 shows the impact of the lake level variations on the radial displacements at crest. Results are similar with a standard deviation equal to 15%.

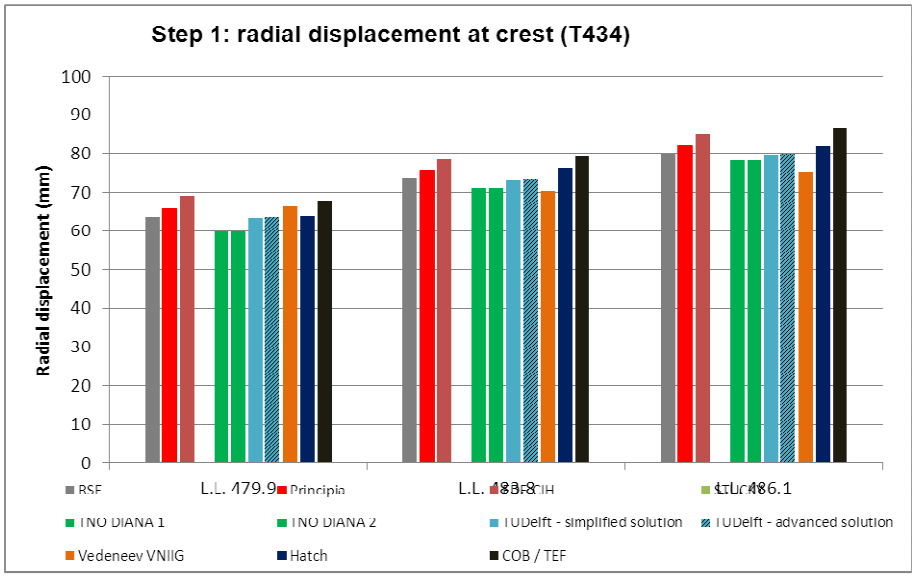

Figure 3: Radial displacement at crest for various lake levels

Next figure shows the vertical displacement of the dam crest in 1963 for a lake level equal to 483.80. We got two groups of models. Difference may be explained by the inclusion or not of the displacements at the end of construction: the dam weight induces crest lowering while hydrostatic pressure applied on the upstream dam face induces a rotation of the whole dam on its foundation bedrock, inducing a crest lift.

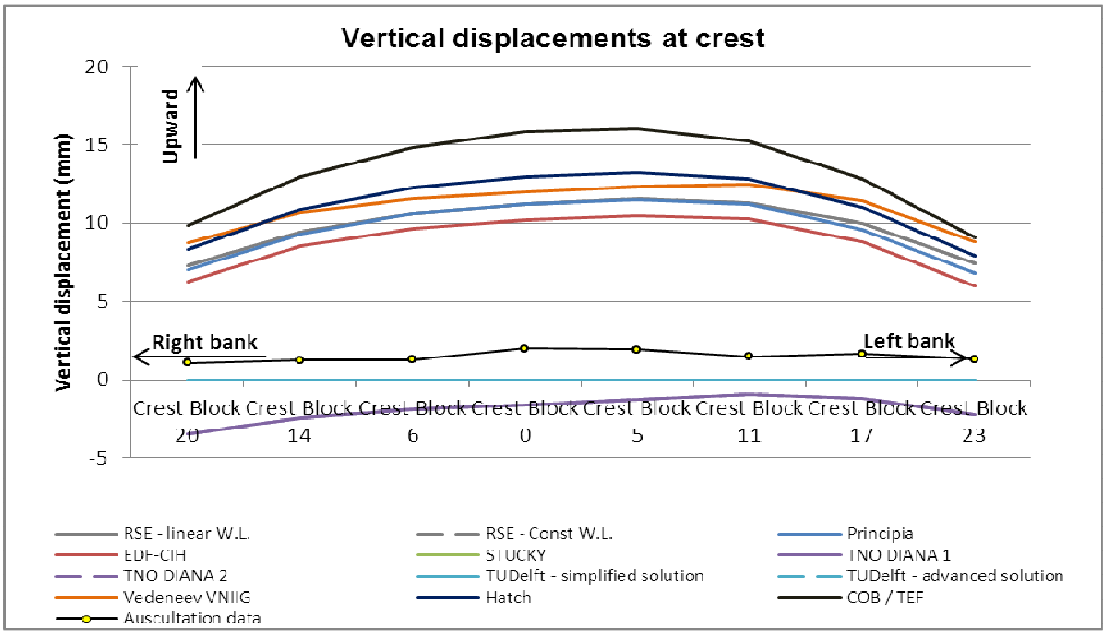

Figure 4: Vertical displacements in 1963 for WL=483.80.

In order to avoid such initial discrepancies, we decided to adjust the displacements as presented in figure 5.

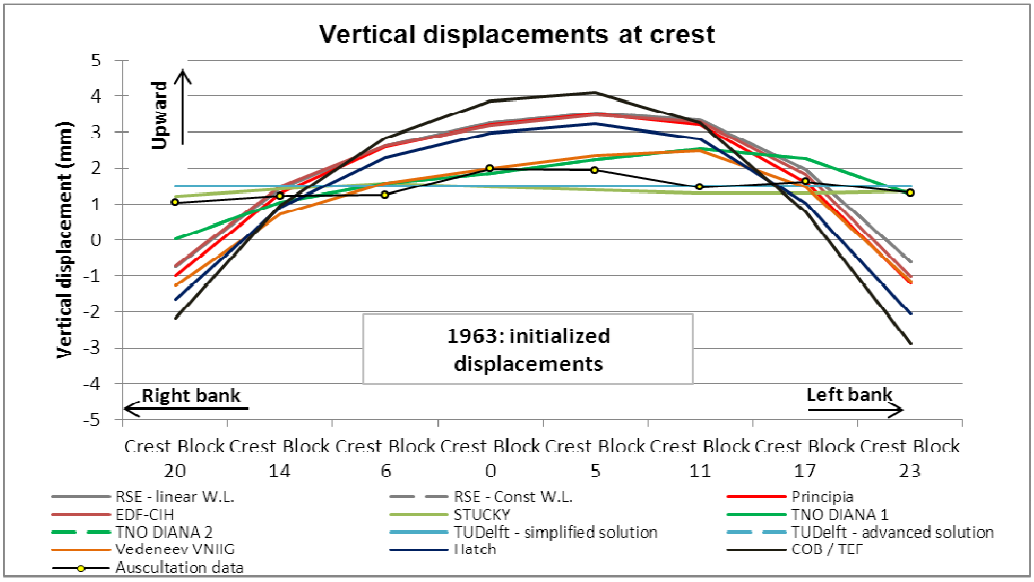

Figure 5: Adjusted vertical displacements in 1963 for WL=483.80.

3.2. Steps 2 and 3: Swelling during the period 1960-2010

Step 2 was devoted to the calibration of the swelling law and parameters which allowed the best identification of the drift shown by monitoring of both vertical and radial movements during the 1963-94 period.

Step 3 covered the prediction period 1995-2010. Using the same swelling model as in previous step, participants shall determine the stress and displacements fields predicted at the end of the prediction period, i.e. on April 30, 2010 with the water level being at El. 486.06.

Based on the swelling model description given in some participants' papers, we deduced the stress-dependent laws for the swelling expansion rate and the swelling kinetics. These laws are in fact very similar.

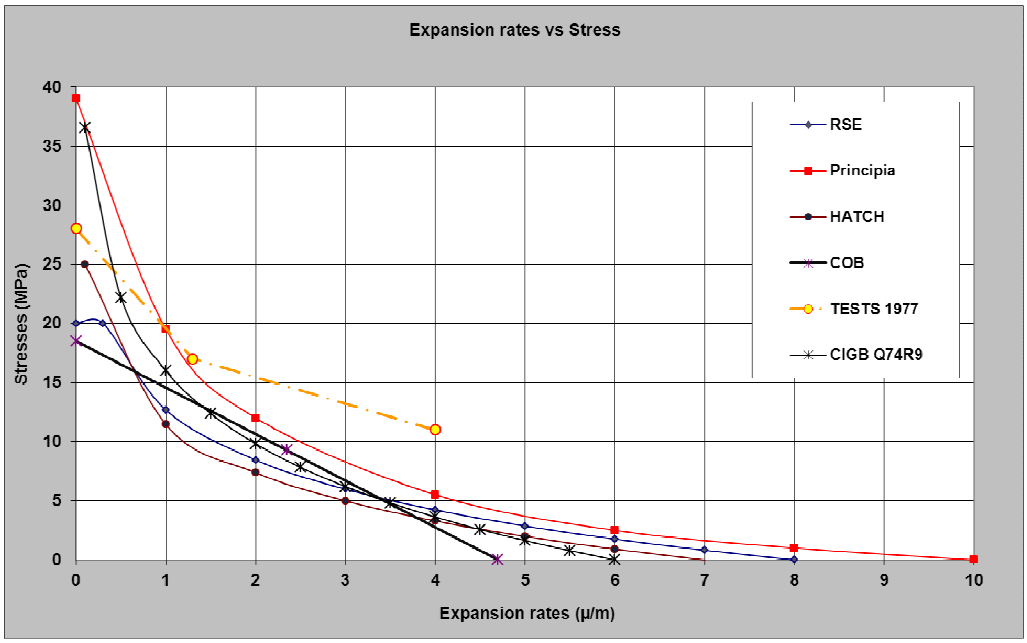

Figure 6: Expansion rate versus stress for stress dependant laws

2/3 of the participants adopted Larive law to take into account the swelling kinetics with various values for τl and τc.

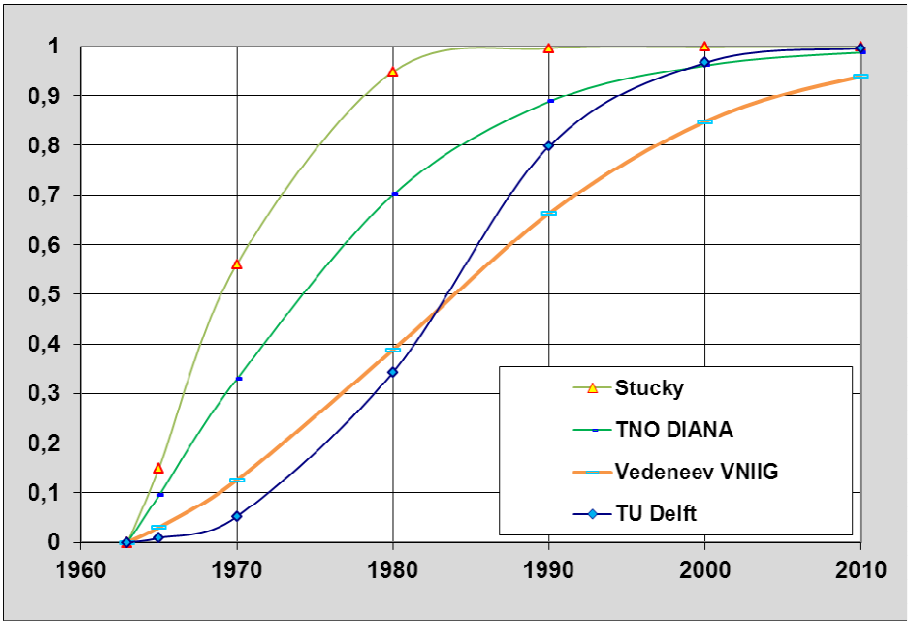

Figure 7: Swelling Kinetics (Larive law)

3.2.1.Radial displacements

On the next figure, are presented the monitoring results for the radial displacements at crest (T434). In the red rectangle (prediction period) a significant deceleration of the radial displacements is observed.

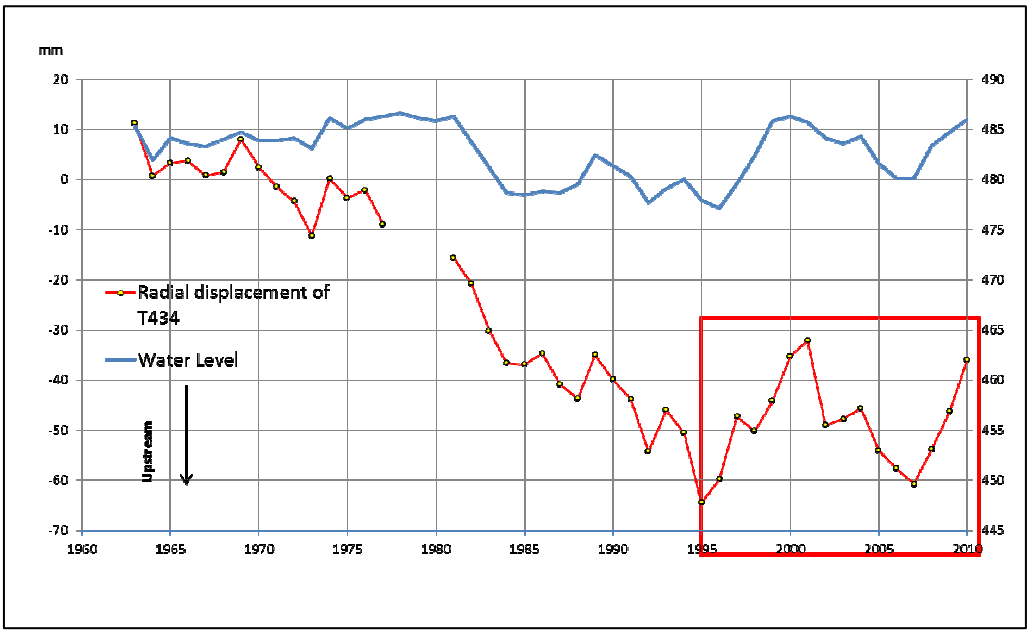

Figure 9: Observed radial displacements at crest (T434)

Following figure shows the radial displacements versus time simulated by all participants from 1963 to 2010. As for the vertical displacements, we adjusted them to cancel the initial differences in 1963. Corrections were quite small (as seen in Figure 3) except for the simulations presented by TU-Delft.

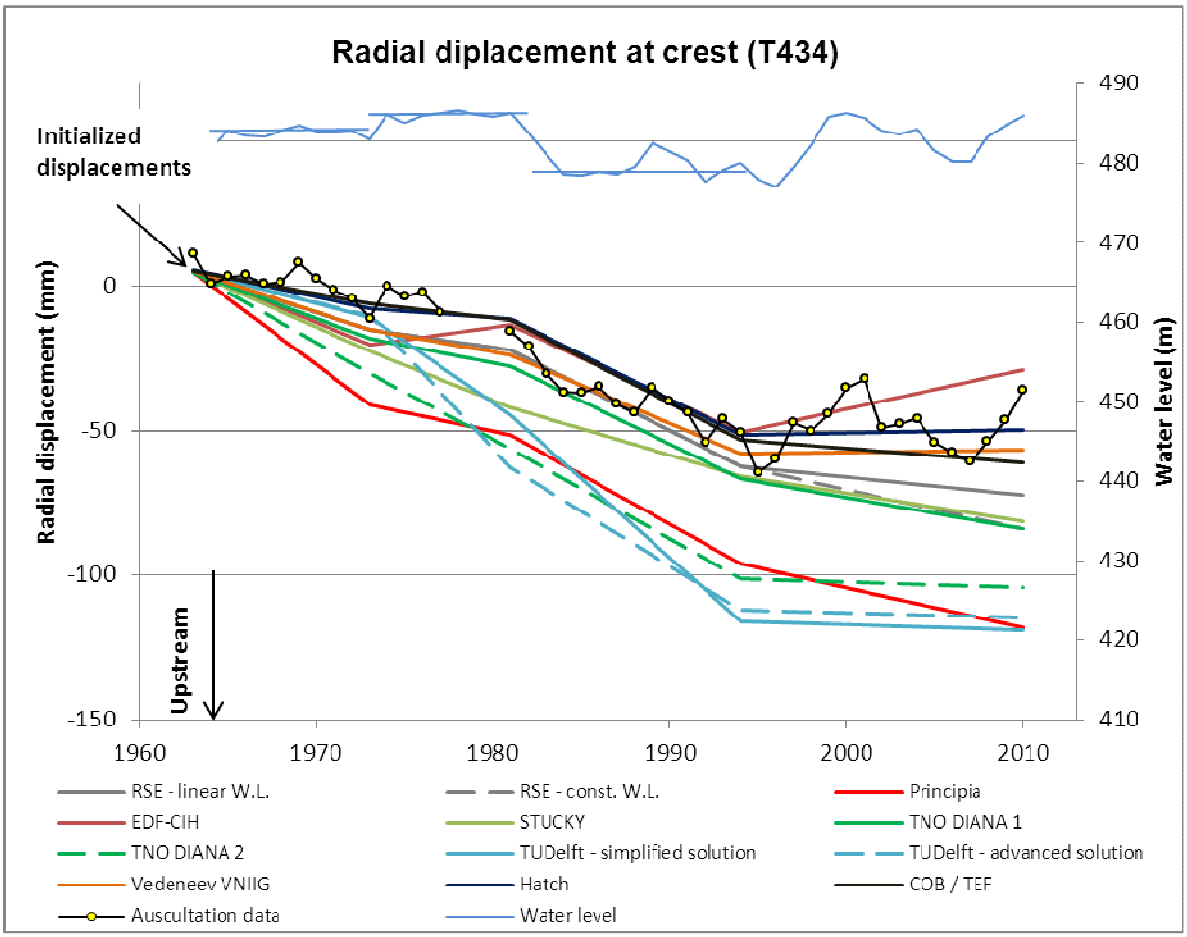

NB : displacements simulated by TU Delft and EDF-CIH were adjusted in 1963

Figure 10: Radial displacement at crest

Although most of the participants got quite good simulation results during the calibration period (+/- 15%), the quality of prediction on radial displacement in 2010 is quite variable (+/- 100%). Those models that do not take into account a swelling kinetic systematically overestimated the radial displacement.

3.2.2.Dam crest leveling

Results are examined successively in terms of time evolution and spatial distribution.

On the next figure, are presented the time evolution of the monitoring results for the vertical displacements at different points along the crest. Significant deceleration of the vertical displacements is also observed during the prediction period (red rectangle).

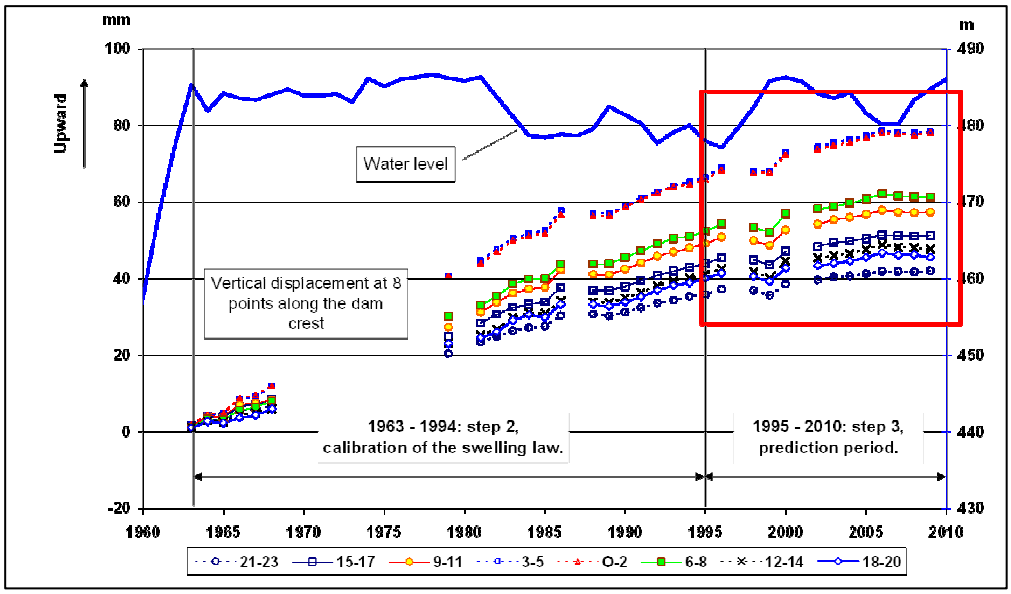

Figure 11: Observed vertical displacements along the crest

Following figure shows the vertical displacements versus time simulated by all participants from 1963 to 2010.

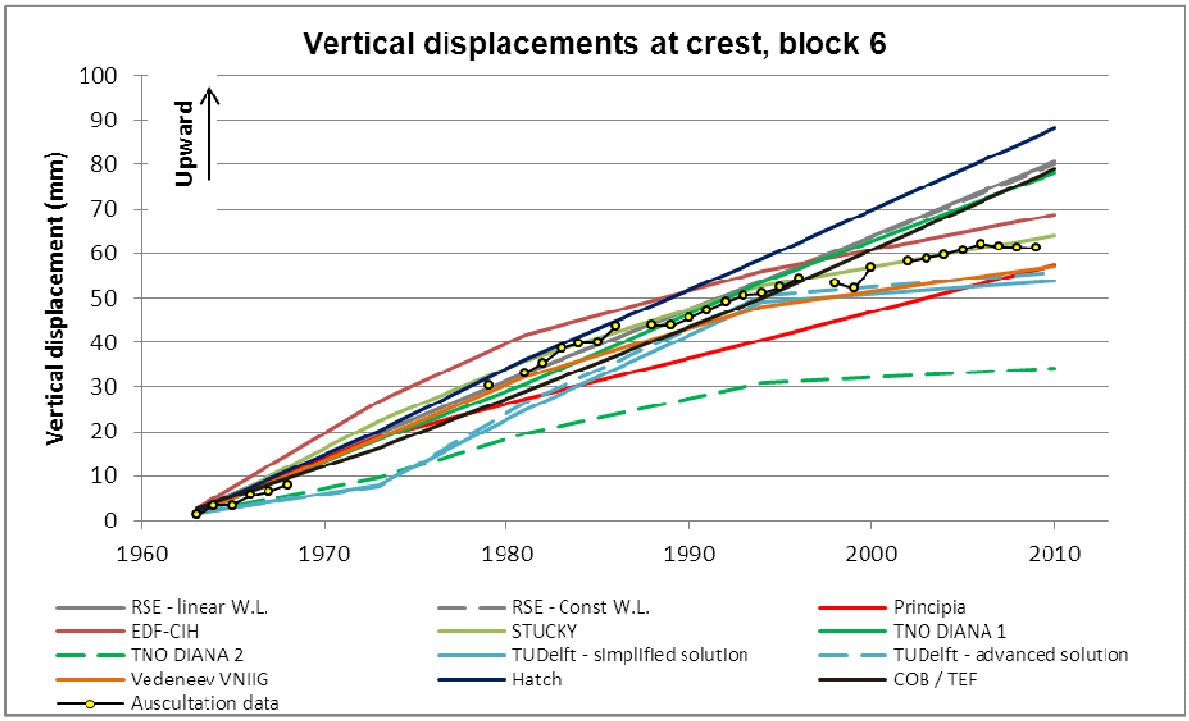

Figure 12: Simulated and vertical displacements at block 6

Simulations of vertical displacements are rather good and seem better than for radial displacements. Many participants calibrated indeed their model mainly on these displacements. The dispersion of the predicted vertical displacement in 2010 is thus much smaller.

Next figure shows the spatial distribution of the crest displacements for different years.

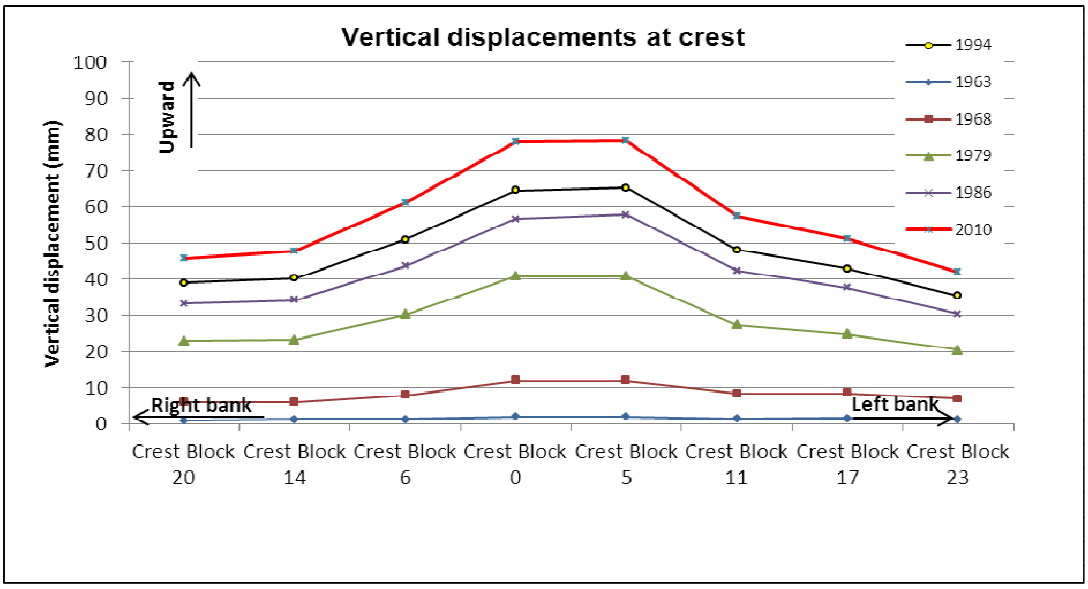

Figure 13: Observed vertical displacements along the crest

On this figure, the elevation rate at points n°0-2 and 3-5 is appreciably higher than their neighbours. This fact can be interpreted as being due to the presence of the spillway in the upper part of the corresponding dam blocks, through the many openings and the increased surface of contact between concrete and water..

Next figure presents the simulated displacements for year 1994 and 2010.

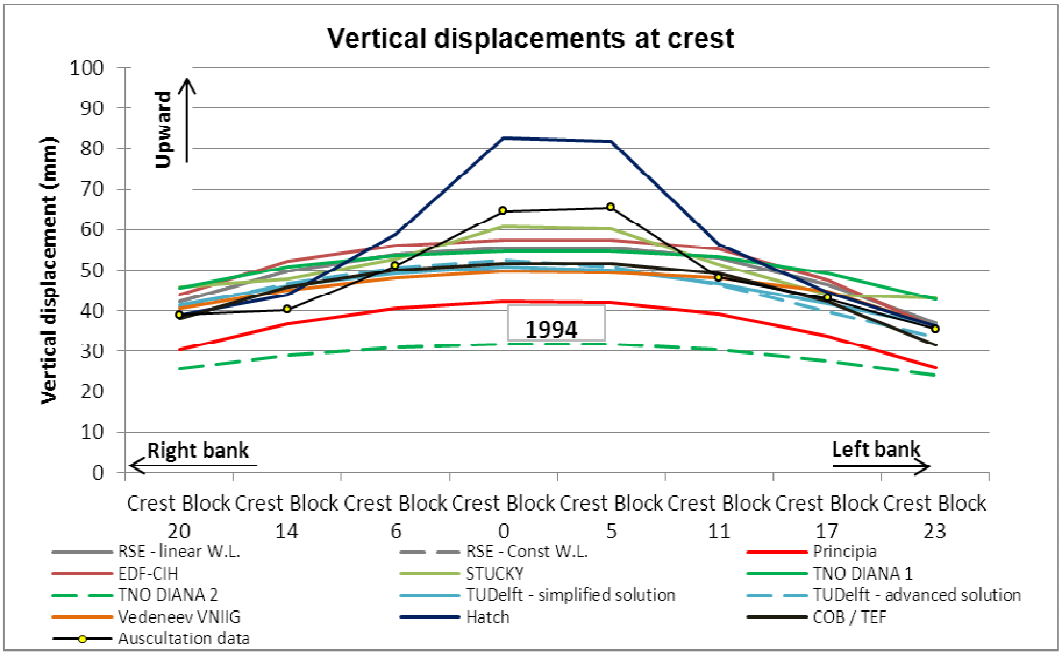

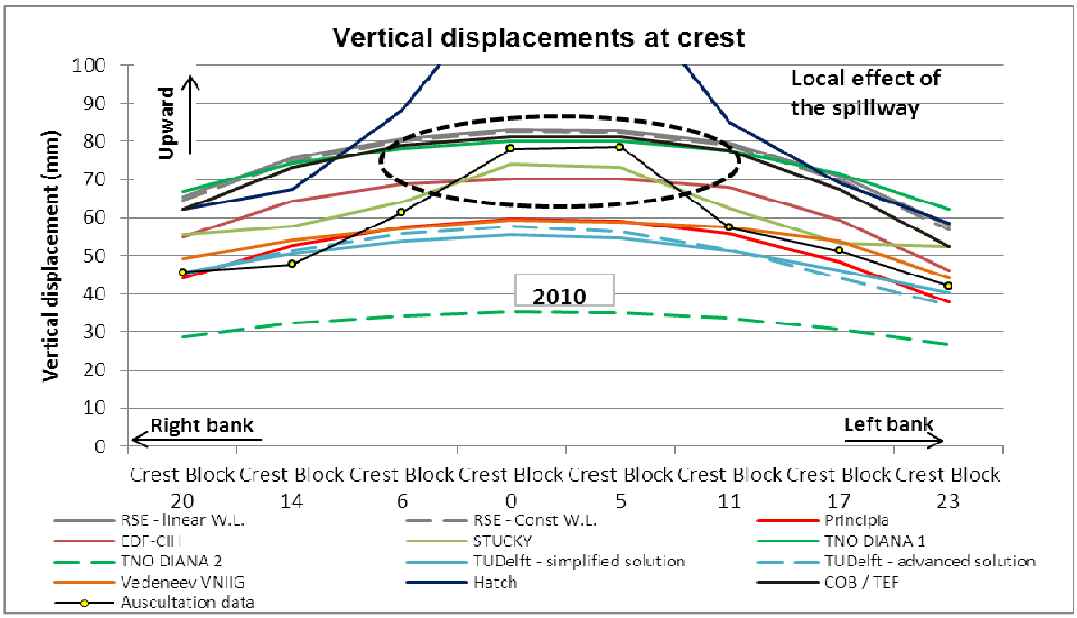

Figure 14: Simulated vertical displacements along the crest for years 1994 (above) and 2010 (below)

If the displacements are very similar at the end of the calibration period, the predicted ones are much dispersive. Hatch reproduced with its model the local increase of the vertical displacements, but with too big amplitude.

3.2.3. Comparison of results

The following figures 15 and 16 present the comparison of results in terms of displacements predicted for the 1994 and 2010 conditions.

Standard deviation for radial and vertical displacements is calculated by taking into account:

- For the calibration period : differences between observations and simulations in 1981 and 1994
- For the prediction: differences between observations and simulations in 2010

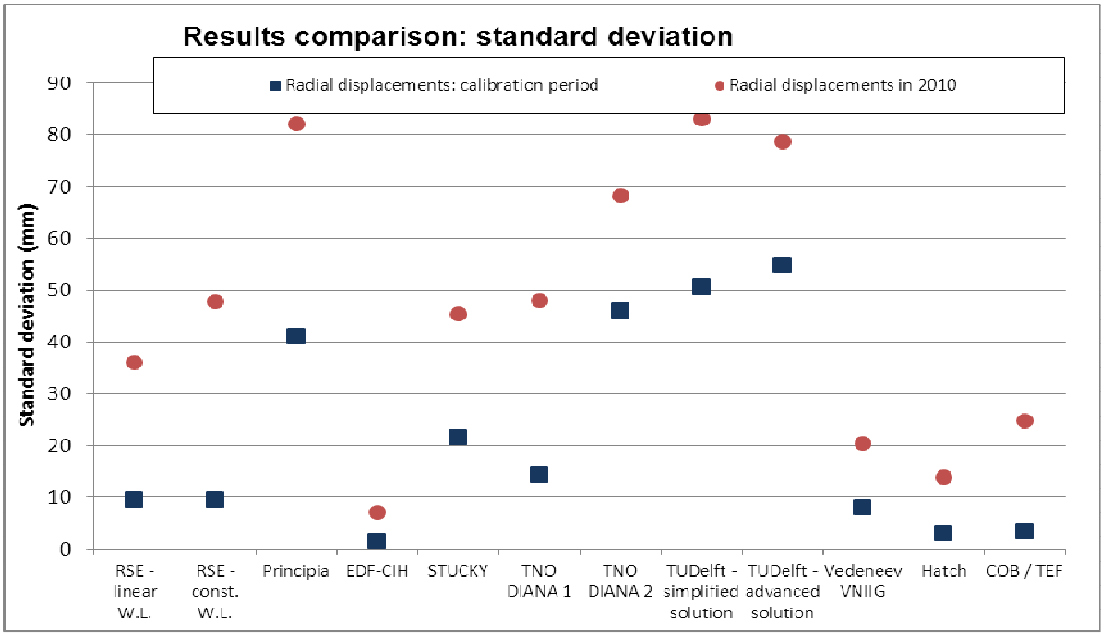

Figure 15: Comparison of predictions on radial displacements

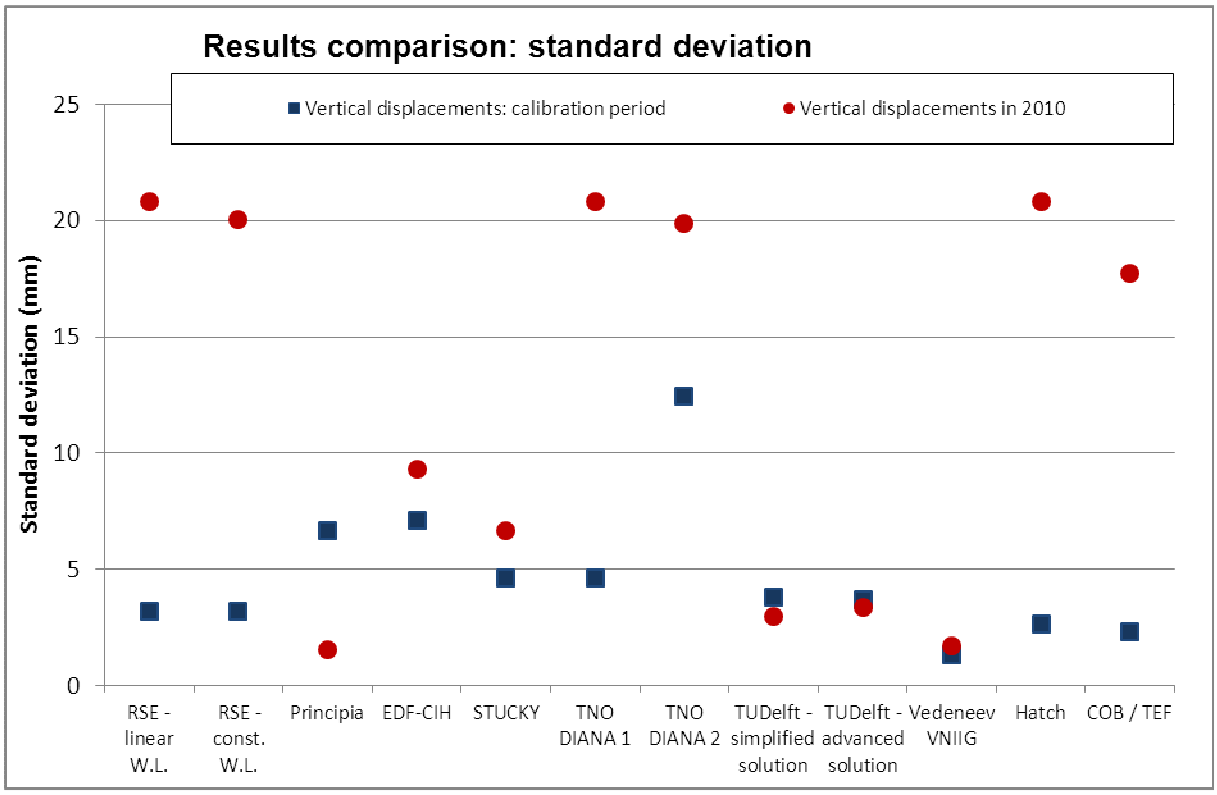

Figure 16: Comparison of predictions on vertical displacements

Stress results corresponding to these predicted displacements in 2010 are shown on next figures 17 and 18.

Some out layers appear, which cannot get any explanation; moreover no monitoring result of stresses inside the dam is available to validate or not the results.

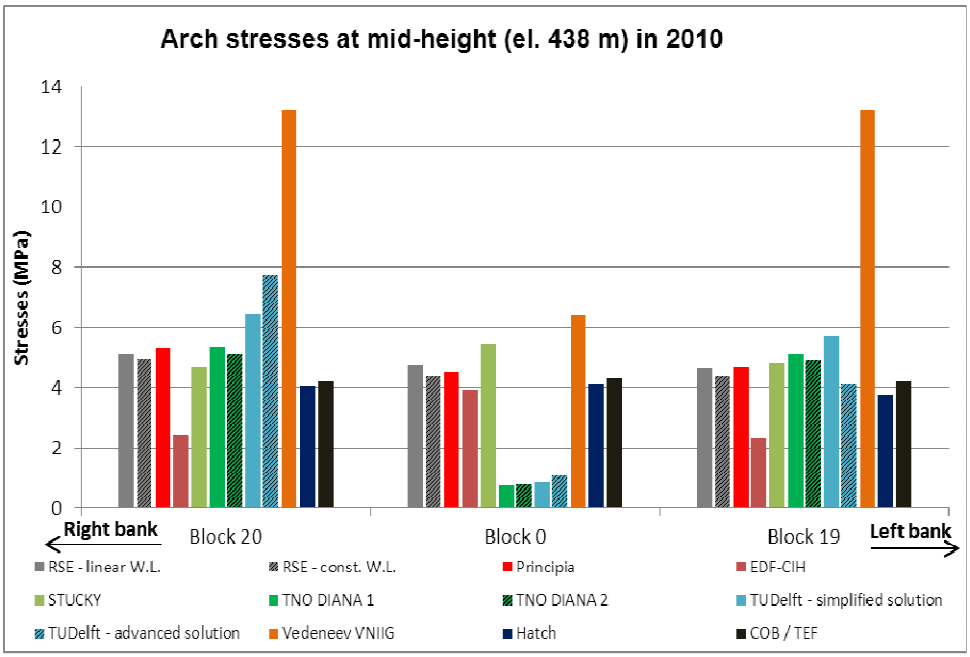

Figure 17: Comparison of arch stresses

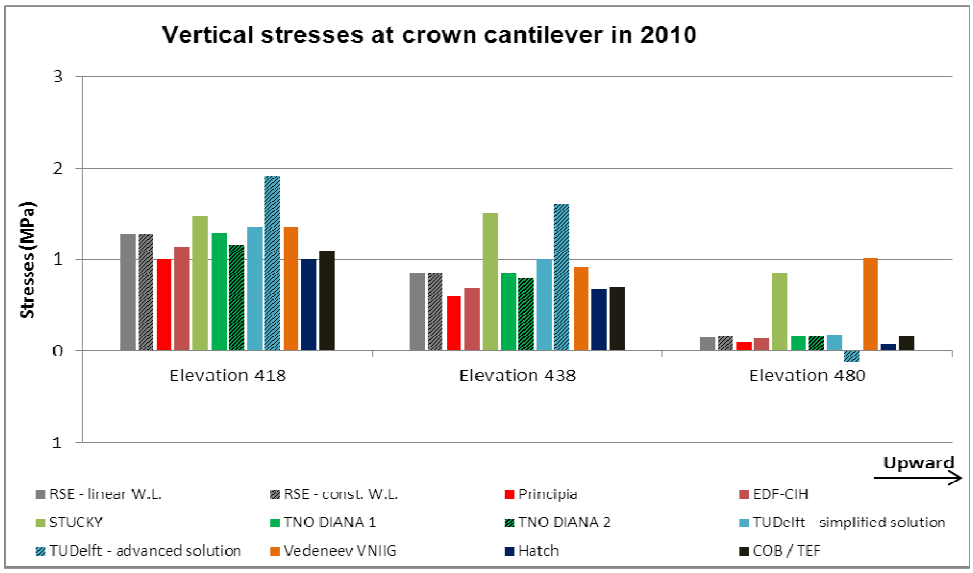

Figure 18: Simulated vertical and arch stress at different elevations for year 2010

4. Conclusion

The case of Kariba is especially well fitted to the exercise in the frame of a benchmark workshop, because it shows clearly the evolution with time of the swelling process, and its consequences on irrecoverable displacements. The quality of the dam monitoring is good. Another positive aspect is the nearly constant temperature and hygral conditions throughout the years and the low and slow lake level variations.

There are a number of differences among methods used by participants to the exercise, with different consideration of the two main aspects of the swelling process: stress dependence on the one hand, kinetics on the other. It is significant that the best prediction result in terms of displacements has been achieved with a method that takes into consideration kinetics as well as stress dependency, although in a very simplified way for the second.

Regarding the first important aspect which is stress dependency, the simplest way is just to adjust a special law such as Charlwood's, as was done rather successfully by several participants Another maybe more clever way is to refer to a constitutive law of concrete with a creep function, with the drawback that the calibration process is more difficult. All stress dependency relations provided by the participants are very near.

Kinetics can be considered through different ways. Methods referring to temperature or hygral conditions to determine the swelling rates have failed, because the information needed to calibrate them was not available. In fact this is always the case in the real world, except maybe in some laboratory conditions. Following the basic principle of numerical analysis that methods should be adjusted to information available, the best practical way to approach kinetical aspects is to consider as carefully as possible the time story of monitoring data which is not easy. The choice of the kinetic law parameters was quite different from one participant to one other.

Acknowledgements

We warmly thank all participants that took part to this exercise.